Universidad del País Vasco / Euskal Herriko Unibertsitatea

Facultad de Ciencia y Tecnología

Programa doctoral de Cuaternario: cambios ambientales y huella humana

Ph.D. Thesis

Climatic and Hydrological Perspectives on Climate Change in the Pyrenees: An Integrated Approach

Author: Nerea Bilbao Barrenetxea

Supervisors: Dr. Sérgio Henrique Faria
Dr. Javier Senent-Aparicio

Bilbao, May 2024

Universidad del País Vasco / Euskal Herriko Unibertsitatea

Facultad de Ciencia y Tecnología

Programa doctoral de Cuaternario: cambios ambientales y huella humana

Ph.D. Thesis

Climatic and Hydrological Perspectives on Climate Change in the Pyrenees: An Integrated Approach

Author: Nerea Bilbao Barrenetxea

Supervisors: Dr. Sérgio Henrique Faria

Dr. Javier Senent-Aparicio

Bilbao, May 2024

Years passed; centuries of centuries passed
Before soil and wood began to cloak
These bones of the ancient giants,
Before the outcrops bore moss; the meadows, flowers,
Before the woodlands were filled with birds;
The birds with song.

JACINT VERDAGUER
Canigó (1886)

Abstract

High mountain regions, characterized by their cryospheric elements such as snow, permafrost, and glaciers, are increasingly vulnerable to climate change. These areas, including the Pyrenees, face significant hydro-climatic challenges. The Pyrenees, a key focus of this thesis, exhibit unique climatic and hydrological characteristics that require detailed study to address the scientific gaps in understanding their hydro-climatic systems.

High mountain regions are critical from ecological, social, and economic perspectives, yet they are among the most affected by climate change. The increase in surface air temperature, particularly due to elevation-dependent warming, has significant implications for snowfall and glacier mass, which are projected to decrease substantially by the end of the century. This reduction in snow cover and glacier mass directly impacts water resources, ecosystems, and socio-economic structures in these regions .

This thesis aims to enhance our understanding of the Pyrenees region by exploring various critical aspects of its hydro-climatic system within the current environmental context. The research is structured to address several key objectives, beginning with an international overview of high mountain regions, focusing particularly on the Pyrenees, and progressing through detailed studies on climate variability, land-use changes, and the application of machine learning for improving climate and hydrological characterizations. Chapter 1 introduces the scope and methodologies of the thesis, emphasizing the integration of spatial scales to capture the complex dynamics of the Pyrenean region. The thesis is structured to examine both the entire Pyrenean mountain range and specific basin scales, offering a comprehensive perspective on the region's hydrology and climate interactions. Chapter 2 provides a global context for high mountain regions, underscoring the unique climatic and hydrological challenges they face due to climate change. It highlights the Pyrenees' specific characteristics, including its climate and hydrological dependencies, and sets the stage for subsequent chapters by identifying the primary vulnerabilities and challenges of these regions.

Chapter 3 delves into the impact of climate variability and land-use changes on the hydrological cycle of the Pyrenees. Through a quantitative analysis in a basin located in the western Pyrenees, the chapter examines the individual contributions of climate change and land-use changes to alterations in the hydrological cycle, with a focus on extreme values. The findings underscore the significant influence of these factors on streamflow patterns and hydrological processes, providing valuable insights into the current and future states of the region's water resources.

Chapter 4 delves into the capabilities and limitations of high-resolution climate simulation products in the Pyrenees region. This chapter employs a methodology that allows the identification and quantification of the weaknesses and strengths of these simulations with a special emphasis on the extreme events and the spatial distribution of the results, thus improving the current knowledge on the quality of these simulations in the region.

Chapter 5 introduces machine learning approaches to improve climate and hydrological characterizations. By developing and applying machine learning algorithms to climate model outputs, this chapter aims to refine the accuracy of hydrological predictions. The integration of these advanced techniques with traditional modeling approaches represents a significant methodological innovation in the field.

Finally, Chapter 6 synthesizes the findings from the previous chapters, offering a comprehensive discussion of the results and their implications. The chapter concludes with recommendations for future research and potential pathways to further enhance the understanding of climate change impacts on high mountain hydrology.

In summary, this thesis makes a contribution by providing a detailed and comprehensive analysis of the impacts of climate change on the hydrology of the Pyrenees. The use of advanced modeling techniques, high-resolution simulations, and machine learning approaches represents a methodological advancement that contribute to the predictive capabilities for water resource management in high mountain regions. The thesis successfully integrates multiple spatial scales and methodological approaches to help provide a holistic understanding of the complex dynamics of the Pyrenean region.

Resumen

Las regiones de alta montaña, caracterizadas por sus elementos criosféricos como la nieve, el permafrost y los glaciares, son cada vez más vulnerables al cambio climático. Estas zonas, incluidos los Pirineos, se enfrentan a importantes retos hidroclimáticos. Los Pirineos, foco clave de esta tesis, exhiben características climáticas e hidrológicas únicas que requieren un estudio detallado para abordar las lagunas científicas en la comprensión de sus sistemas hidroclimáticos.

Las regiones de alta montaña son críticas desde el punto de vista ecológico, social y económico, y sin embargo se encuentran entre las más afectadas por el cambio climático. El aumento de la temperatura del aire en superficie, debido sobre todo al calentamiento dependiente de la altitud, tiene importantes repercusiones en las nevadas y la masa glaciar, que, según las previsiones, disminuirán sustancialmente de aquí a finales de siglo. Esta reducción de la capa de nieve y de la masa glaciar repercute directamente en los recursos hídricos, los ecosistemas y las estructuras socioeconómicas de estas regiones.

Esta tesis pretende mejorar nuestra comprensión de la región pirenaica explorando diversos aspectos críticos de su sistema hidroclimático en el contexto medioambiental actual. La investigación está estructurada para abordar varios objetivos clave, comenzando con una visión general internacional de las regiones de alta montaña, centrándose particularmente en los Pirineos, y avanzando a través de estudios detallados sobre la variabilidad climática, los cambios en el uso del suelo y la aplicación del Machine Learning para mejorar las caracterizaciones climáticas e hidrológicas. El Capítulo 1 introduce el alcance y las metodologías de la tesis, haciendo hincapié en la integración de escalas espaciales para captar la compleja dinámica de la región pirenaica. La tesis está estructurada para examinar tanto el conjunto de la cordillera pirenaica como escalas específicas de cuenca, ofreciendo una perspectiva global de las interacciones hidrológicas y climáticas de la región. El Capítulo 2 proporciona un contexto global para las regiones de alta montaña, subrayando los desafíos climáticos e hidrológicos únicos a los que se enfrentan debido al cambio climático. Destaca las características específicas de los Pirineos, incluidas sus dependencias climáticas e hidrológicas, y sienta las bases para los capítulos siguientes al identificar las principales vulnerabilidades y retos de estas regiones.

El Capítulo 3 profundiza en el impacto de la variabilidad climática y los cambios en el uso del suelo sobre el ciclo hidrológico de los Pirineos. Mediante un análisis cuantitativo en una cuenca situada en los Pirineos occidentales, el capítulo examina las contribuciones individuales del cambio

climático y de los cambios en el uso del suelo a las alteraciones del ciclo hidrológico, centrándose en los valores extremos. Los resultados subrayan la influencia significativa de estos factores en los patrones de los caudales y en los procesos hidrológicos, proporcionando valiosas perspectivas sobre el estado actual y futuro de los recursos hídricos de la región.

El Capítulo 4 profundiza en las habilidades y limitaciones de los productos de simulacion climatica de alta resolución en la región de Pirineos. Este capítulo emplea una metodología que permite la identificacion y cuantificacion de los puntos debiles y fuertes de estas simulaciones con un especial enfasis en los eventos extremos y en la distribucion espacial de los resultados, mejorando así el conocmiento actual sobre la calidad de estas simulaciones en la región.

El Capítulo 5 introduce enfoques de aprendizaje automático para mejorar las caracterizaciones climáticas e hidrológicas. Mediante el desarrollo y la aplicación de algoritmos de aprendizaje automático a los resultados de los modelos climáticos, este capítulo pretende refinar la precisión de las predicciones hidrológicas. La integración de estas técnicas avanzadas con los enfoques tradicionales de modelización representa una importante innovación metodológica en este campo.

Por último, el Capítulo 6 sintetiza las conclusiones de los capítulos anteriores, ofreciendo un amplio debate sobre los resultados y sus implicaciones. El capítulo concluye con recomendaciones para futuras investigaciones y posibles vías para seguir mejorando la comprensión de los impactos del cambio climático en la hidrología de alta montaña.

En definitiva, esta tesis supone una contribución al proporcionar un análisis detallado y exhaustivo de los impactos del cambio climático sobre la hidrología de los Pirineos. El uso de técnicas avanzadas de modelización, simulaciones de alta resolución y enfoques de aprendizaje automático representa un avance metodológico que contribuye a las capacidades predictivas para la gestión de los recursos hídricos en regiones de alta montaña. La tesis integra con éxito múltiples escalas espaciales y enfoques metodológicos para ayudar a proporcionar una comprensión holística de la compleja dinámica de la región pirenaica.

Contents

List of Figures

List of Tables

Chapter 1

Introduction

1.1 Background and Motivation

High mountain regions, with their unique environmental characteristics and sensitivity to climatic shifts, are inherently vulnerable to the impacts of climate change (Diaz et al., 2003; IPCC, 2022). These environments, due to their altitude and topography, face particular challenges affecting the ecosystems stability and evolution. In this context, the **Pyrenees** stand out as a notable example, acting as a critical provider of ecosystem services OPCC-CTP, 2018) (Amblar-Francés et al., 2020; Catalan et al., 2006), especially **water resources** (Moreno et al., 2021). These play a pivotal role in sustaining various economic and social structures within the Pyrenees and surrounding territories, underpinning agricultural activities, urban development, and ecological balance (López-Moreno et al., 2008; Boix-Fayos et al., 2020). Currently, the hydro–climatic system of the Pyrenees is undergoing significant changes, which are exacerbated by other environmental changes such as land-use changes. These alterations have had a considerable impact on the region, notably affecting flow regimes and ecosystem's capacity to adapt to climatic variations (Bilbao-Barrenetxea et al., 2024; López-Moreno et al., 2011).

Understanding the **hydro-climatic system of the Pyrenees** is paramount for developing effective strategies to mitigate and adapt to climate change in the region. However, the intricate topography and climatic variability of the Pyrenees present challenges in accurately characterizing its climate and hydrology, as well as projecting future trends. The complex interplay of factors such as altitude, complex orography, and local weather phenomena complicates efforts to model and predict the region's hydro-climatic dynamics with precision (Zamora et al., 2017). The significance of comprehending the Pyrenees' hydro-climatic system extends beyond scientific inquiry; it directly impacts the resilience of vulnerable economic and social structures in the region (Palomo and

Palomo, 2020). As climate change intensifies, the **need for robust tools and methodologies** to assess and manage hydrological risks becomes increasingly urgent (IPCC, 2022). Addressing these challenges requires interdisciplinary collaboration and innovative approaches to leverage existing data and models effectively in the face of uncertain future conditions.

Monitoring and characterizing hydro-climatic systems have seen significant development in recent decades. Among the great mountain ranges of Europe, the Pyrenees stand out not only for their natural value but also for their extensive network of environmental monitoring stations, making them one of the most densely instrumented regions globally. This dense network (CEDEX, AEMET, HydroPortail), coupled with the favorable geographical location of the Pyrenees, facilitates the monitoring of climate change effects and their temporal evolution. Furthermore, this mountain range features several agents that actively participate in the process of monitoring, researching, adapting, mitigating, and communicating climate change, including the IPE-CSIC (Pyrenean Institute of Ecology) and the CBNPMP (Conservatoire Botanique National des Pyrénées et de Midi-Pyrénées). In addition, the cross-border initiative (Spain–Andorra–France) of the Pyrenean Climate Change Observatory (OPCC), which launched in 2010, aims to promote territorial collaboration on climate change. However, there remains a substantial gap in scientific knowledge regarding the biophysical impacts on the Pyrenees and its surrounding territories (OPCC-CTP, 2018).

In this context, a niche of opportunity emerges, highlighting the need to shed light on the reliability and performance of techniques used to understand the hydro-climatic system. The tools and data at our disposal can be broadly categorized into two groups: observational data and simulations.

Firstly, observational data, encompassing meteorological and hydrological observations, play a crucial role. The Pyrenees region boasts a high density of measurement stations, overseen by various state and sub-state entities, yet publicly accessible. Moreover, recent scientific efforts have led to the generation of high-resolution databases for key climate variables (Cuadrat et al., 2020b), significantly facilitating comprehensive analyses of the region's climate dynamics.

On the other hand, **simulations**, including climate simulations from joint projects such as CMIP (Taylor et al., 2012) and CORDEX (Jacob et al., 2014, 2020), offer valuable insights. These projects provide simulation products derived from numerous models for both historical periods and future climate projections under various emission scenarios. However, it is paramount to apply best practices when utilizing these products as decision-making tools; Evaluating the models' ability to represent specific climate variables in a given region is crucial. Another type of simulation pertains to hydrology. **Hydrological models** aim to simulate the characteristics and dynamics of rivers, enabling us to observe the potential impact of system modifications on the hydrological regime. Likewise, in recent years, there has been a notable surge in the development of novel techniques rooted in Artificial Intelligence (AI), such us those based on Machine Learning (ML). When paired with above mentioned established physically-based models, these **emerging ML-driven methodologies** synergize to enhance simulation outcomes significantly.

Integrating **observational** data with **simulation products** and employing rigorous evaluation methodologies, alongside the application of **novel techniques**, are essential for enhancing our understanding of the hydro-climatic system in the **Pyrenees** region. This integrated approach allows for a more comprehensive analysis of current conditions and future scenarios, providing valuable insights into the environmental changes that this region faces in relation to **climate and land-use changes** and their impact on the dynamics of **water resources**. By generating these insights, this approach ultimately enables more informed decision-making, ensuring that strategies to manage and adapt to these changes are based on the best available scientific knowledge.

1.2 Objectives

This work aims to narrow the knowledge gap existing in the Pyrenees region regarding the understanding of its dynamics and evolution within the context of climate change. To achieve this, the issue will be approached from two perspectives. Firstly, we will delve into the current situation of this mountainous region, with a particular focus on identifying its vulnerabilities in the context of climate change and understanding how hydro-climatic systems evolve and interact. Secondly, we will delve into the methodologies and tools available for predicting the future evolution of these systems, assessing their capabilities and limitations. Ultimately, the goal is to push the boundaries of our comprehension regarding the Pyrenees region. Additionally, this research endeavors to lay the groundwork for advancing our insights into other high mountain regions. With this purpose, the thesis is organized around the following milestones and objectives:

- **Milestone 1**: Gain a deeper understanding of the Pyrenees region by exploring the interactions between climate, hydrology and other environmental changes, along with their vulnerabilities in the context of climate change.
  - **Objective 1**: Investigate the potential vulnerabilities of mountain regions while highlighting the specific characteristics of the Pyrenees.
  - **Objective 2**: Delve into the impact of climate variability and land use change on the hydrological cycle of a Pyrenean basin, elucidating their contributions.
- **Milestone 2**: Enhance understanding of forecasting tools, with a specific emphasis on their capacity to accurately replicate hydro–climatic dynamics.
  - **Objective 3**: Evaluate the strengths and limitations of current climate simulations in a region characterized by complex topography, with specific attention to extreme events.
  - **Objective 4**: Explore and propose Machine Learning-based techniques to enhance the characterization of climate and hydrology, aiding in more effective prediction of changes.

1.3 Structure and Methodologies

The dissertation's structure is depicted in Figure 1.1. Chapter 2 offers an overview of the Pyrenees region's characteristics, focusing on its vulnerabilities, particularities, and identified knowledge gaps (Objective 1). In Chapter 3, the current scenario in the Pyrenees region is examined using a hydrological basin as a case study, elucidating the interactions between climate, land use, and water resources (Objective 2). Chapters 2 and 3 thus contribute to completing Milestone 1 of the thesis. Chapter 4 assesses the high-resolution climate simulations of the EURO-CORDEX project for the Pyrenees region, comparing them to the observations of studied climate variables (Objective 3). Chapter 5 proposes and designs a Machine Learning-based technique, enhancing the characterization of climate and hydrology in a Pyrenean basin when combined with high-resolution simulations (Objective 4). Chapters 4 and 5 address Milestone 2. Finally, Chapter 6 deliberates on the obtained results and outlines potential future pathways to advance the understanding of the Pyrenees region.

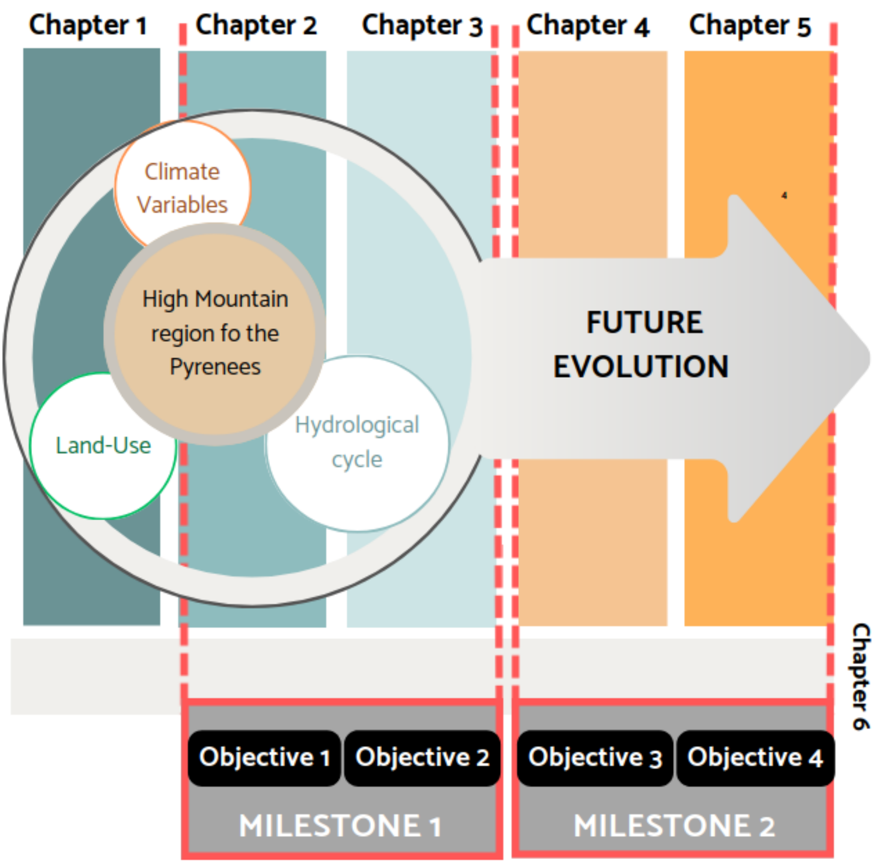

FIGURE 1.1: Scheme of the Thesis' structure

We have employed various methodological approaches to address the posed milestones and objectives, which will be elaborated upon in each of the subsequent chapters. However, a pivotal aspect of this dissertation lies in its integration of spatial scales across different chapters. On one hand, we examine the Pyrenean mountain range as a whole (Chapters 2 and 4), recognizing it as a complex system comprising smaller components, each contributing to the overall definition of the system itself. Therefore, we have introduced an additional scale—the basin scale—in this study to further elucidate its intricacies. Through basin-scale analysis, we derive significant findings and conclusions (Chapters 3 and 5), offering a comprehensive understanding of the Pyrenees region's functioning and dynamics. This integration of scales provides a broader and holistic perspective, aimed at addressing the region's inherent complexities.

Chapter 2

High Mountain Regions: An International Overview with a Focus on the Pyrenees

We often imagine mountains as remote, wild, and untouched places, the last corners of our planet not impacted by human activities. But the reality is vastly different: high mountains are suffering the impact of climate change in a particularly intense way. Among other factors, the complex network of interactions between high-mountain habitats and the species they harbour is being altered by the effects of climate change.

This chapter provides an introduction to the High Mountain regions (Section 2.1) and delves into the contemporary challenges confronting these distinctive areas today (Section 2.2). Among these challenges this Chapter highlights climate change and the complex nature of these terrains, which present difficulties in understanding their mechanisms and the evolution of their hydro-climatic systems. Subsequently, it introduces the Pyrenees region, providing detailed insights into its unique features (Section 2.3), with a particular focus on its climatic and hydrological aspects. As part of **Objective 1**, this chapter aims to deepen our understanding of the Pyrenees contributing thereby to the accomplishment of **Milestone 1**.

2.1 High–Mountains

High–mountain regions are geological structures in which cryospheric elements such as snow, permafrost, and glaciers play a leading role. Similarly, additional features, especially regarding extreme weather and

FIGURE 2.1: Key characteristics of high-mountain regions.

terrain complexity are also required. We must also consider the importance of spatial and institutional remoteness. These characteristics lead us to perceive high mountains as remote, alien spaces, detached from our lives and societies. But nothing could be further from the truth: mountains are the source and refuge of resources and goods that are essential in our everyday lives. In this sense, these regions are unquestionably important from an ecological, social, and economic point of view (Figure 2.1).

2.2 Challenges and Opportunities

The geographic and environmental conditions described above mean that high mountains are valuable and unique regions, thereby making them some of the territories most vulnerable to climate change. Their abrupt relief and steep slopes hide an intrinsic fragility. This vulnerability is related to a faster and more intense response to changes than non-mountainous regions (Diaz et al., 2003), and is understood by many experts as a potential early warning system. In other words, the impacts we are starting to observe in high mountains today might be warning us of the worst consequences we may suffer in the not-too-distant future.

2.2.1 Climate change

High-mountain regions are (and will continue to be) among those most affected by climate change. According to the conclusions of the Special Report on the Ocean and Cryosphere in a Changing Climate (SROCC; Intergovernmental Panel on Climate Change [IPCC], 2019), the increase in surface air temperature predicted in 21st century climate models may be more intense in high mountains because of regional dynamics and an effect called elevation-dependent warming (EDW). This process refers to the observation that the rate of warming (expressed in °C per decade, for instance) is not the same for all elevation ranges (Pepin et al., 2015). The increase in temperature directly impacts the rainfall/snowfall rates in high-mountain areas. Snowfall is projected to dwindle in most mountain areas, especially at lower elevations. The IPCC (2019) considers it probable that, by the end of the century (2081–2100), the snow cover at lower elevations in regions such as the European Alps, Himalayas, and Subtropical Andes will be reduced by 30 % in the best-case scenario and 80 % in the worst, compared to our near past (1986–2005).

The mass loss of glaciers is also accelerating (Hugonnet et al., 2021). Although the loss in glacier mass greatly varies between regions, best-case and worst-case scenario projections (depending on the concentration of CO2 in the atmosphere) indicate that globally, polar and mountain glaciers will lose between 18 % and 36 % of their masses, respectively, during the 21st century, compared to 2015 (IPCC, 2019). This loss of ice and snow in high-mountain areas stems from the increase in the Earth's average temperature due to the constant anthropogenic emission of greenhouse effect gases since the Industrial Revolution. Several examples of these changes have been documented. For example, in the Cordillera Blanca (Peruvian Andes), more than 30 % of the glacier mass disappeared between 1930 and 2014 (Schauwecker et al., 2014). Another illustrative example is that of Mount Kilimanjaro, whose glacier area suffered a severe loss of 85 % between 1912 and 2011 (Cullen et al., 2013). However, looking for such remote places is not necessary to observe the effects of climate change. In regions dominated by smaller glaciers, including the European Alps, Caucasus, and Pyrenees, among others, glaciers are predicted to lose more than 80 % of their masses (IPCC, 2019) by 2100, according to the IPCC's worst-case scenario (RCP8.5). Indeed, many of the glaciers in these mountain ranges will completely disappear in the future with the current increase in global temperature.

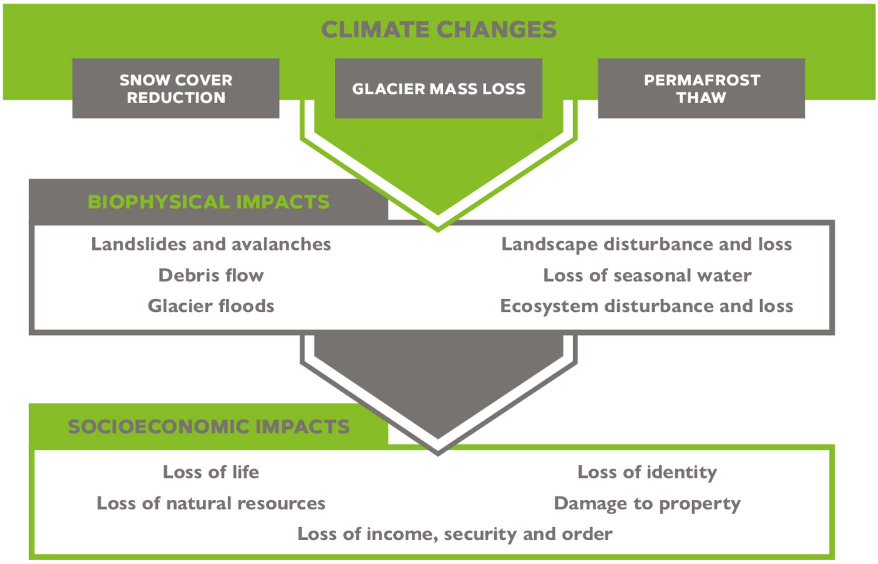

FIGURE 2.2: Climate changes in high-mountain areas and their associated biophysical and socio-economic impacts.

These cryospheric changes caused by climate change generate biophysical impacts such as the loss of seasonal water, which directly affects ecosystems and has socio-economic impacts on the inhabitants of these regions (Figure 2.2). Biophysical impacts materialise in a wide variety of forms: from landslides and avalanches to the disappearance of species.

Glacial lake outburst floods (GLOFs) are some of the most dangerous of these phenomena. These are defined as violent floods occurring when the containment elements of a glacial lake (i.e., glacier ice) collapse. In 2010, more than 200 lakes were identified as potentially affected by this danger in the Hindu-Kush–Himalaya alone (Ives et al., 2010). Another hazard derived from these climate changes is the transformation of areas that were already sensitive to wildfires, such as California's coastal mountain ranges or the Blue Mountains in Australia, regions facing a continued risk of wildfires, or the transformation of areas such as Tibet or Mongolia into regions prone to desertification (IPCC, 2019).In addition to some of the biophysical impacts mentioned above, climate changes produce significant imbalances in the ecological, social, and economic structures of high-mountain areas, which can sometimes result in the loss of human lives. A clear example of this are cases related to avalanches and landslides or droughts and flooding.

Although some initiatives to help adaptation to these new circumstances are already under way, many communities will not be able to adapt, which could lead to conflicts related to access to water and other resources. In fact, economic losses associated with these impacts (related to hydroelectric production and climate disasters) amount to billions of dollars. Indeed, between 1985 and 2014, the economic losses derived from hydrometeorological disasters are estimated to have amounted to 45 billion dollars in the Hindu-Kush–Himalaya and 7 billion dollars in the European Alps region (Beer, 2018).

However, beyond the economic cost, together with high-mountain ecosystems, we would also lose heritage that belongs to all of us. Traditional mountain communities are already experiencing changes in their livelihoods (e.g., shepherding and agriculture) associated with changes in the water supply. In remote high-mountain areas, indigenous communities are losing both their property and their cultural identity. For instance, in the vicinity of the Ausangate Mountain in Peru, the Quechua community has stopped celebrating traditional rites related to the deity of a now-disappeared glacier. The landscape is also being altered. It is intricately connected not only to cultural identity, but also to the economy of mountain societies, because tourism often represents the most important economic activity in these regions (Palomo and Palomo, 2020).

2.2.2 Knowledge Gaps in High–Mountains

Despite evidence of the harmful (sometimes even catastrophic) effects of climate change on high-mountain areas, the current lack of knowledge of these dynamics can negatively affect the adoption of measures aimed at alleviating their effects. This is because, in the context of climate change, mountains continue to be poorly understood. Two of the main reasons for our ignorance are the inaccessibility of the terrain and the fragmentation of stakeholders, which is evident, for example, in the lack of cross-border initiatives. Observational data are often scarce, too recent, or sometimes just low quality. This means that our current information is biased and inaccurate and tends to be useless when trying to correctly capture small scale changes (IPCC, 2019). However, it is important to highlight that there are specific cases with different realities in many mountain areas. In mountain ranges from rich and developed regions with a long history of mountain research, more and better climate data are available which cover a sufficient timescale to allow us to conduct robust climate studies.

Future changes are also predicted by global and regional climate models (GCMs and RCMs) which are still show limitations on precisely reproducing the details of meso- and sub-kilometre-scale dynamics in complex terrain areas. Mesoscale convective systems, for example, play a critical role in mountain areas and control weather variables such as rainfall (Gutowski et al., 2016). Thanks to advances in computational techniques and the efforts of the scientific community, great progress is already being made towards the incorporation of these processes into models. However, especially in understudied regions, the tools currently available are sometimes insufficient when it comes to comprehensively evaluating the impacts of climate change.

Another complication for the research of high- mountain areas in the context of climate change is the fact that, traditionally, efforts have focused on understanding the dynamics of each mountain range separately and independently. This is because each region will be affected in diverse ways depending on characteristics such as geographical location, area, elevation, and climate pattern. However, these unique regions also share common elements that are key to understanding them globally. Thus, the scientific community has focused on studying not only the singularities of each high-mountain region but are also grouping them together as closely related regions with common characteristics. This comprehensive approach implies a transdisciplinary perspective that allows us to jointly analyse the causes and effects of climate change on high-mountain regions.

Although some mountain regions have been assigned great importance in particular local and regional contexts for decades, the situation is different at the global level. In 2015, the foundations were set for an innovative global action plan for a combined response to the problems faced in high-mountain regions. Three key programmes were adopted that year: the Paris Agreement, which specifically mentions the protection of early warning areas, the United Nations Sustainable Development Agenda with its sustainable development goals (SDGs), and the Sendai Framework for disaster risk reduction. However, even though the foundations are there, according to the SROCC report (IPCC, 2019), experts state that there is little evidence available to allow us to systematically evaluate the effectiveness of international programmes when addressing specific challenges related to changes in high-mountain ecosystems and their cryosphere.

Hence, in order to avert the neglect of high mountain regions within the sphere of international policy, it is imperative to realign the objectives of relevant programs towards a contextualized understanding of the challenges inherent to mountainous terrains. (Bracher et al., 2018). In this sense, some initiatives such as defining specific key considerations to improve the conditions under which the SDGs can have a purpose in mountain regions, are already being developed.

2.3 A especial look at the Pyrenees

In the specific case of the Pyrenees, the effects of climate change have been noted over the last century. Indeed, in this region, the average temperature has increased markedly over the last 50 years. In addition, precipitation is decreasing by 2.5 % per decade (Amblar-Francés et al., 2020). According to climate model estimates, the annual maximum temperature in the Pyrenees for the 2030 horizon will increase by 1.0 to 2.7 °C compared to 1961–1990 levels in the RCP8.5 scenario (Amblar-Francés et al., 2020). Furthermore, by 2050, warming would be higher, ranging from 2.0 to 4.0 °C (Amblar-Francés et al., 2020). Glaciers are also at risk. More specifically, over the last 150 years, the Monte Perdido Glacier (Huesca, Spanish Pyrenees) has experienced more pronounced melting than in the last 2,000 years and data suggests that, under these climatic conditions, it will eventually disappear (Moreno et al., 2021). Because of these climate changes, many species' annual life cycles are starting earlier, thus affecting the interactions between different species (Charmantier and Gienapp, 2014). Lakes and peatlands, iconic ecosystems of the Pyrenees, are also at risk of disappearing because of their particular vulnerability (Catalan et al., 2006). In this context of rapid changes, The Pyrenees are also facing the challenges mentioned above, especially concerning climatic and hydrological aspects.

2.3.1 Climate System

The Pyrenees' climate is influenced by its positioning along its west-to-east axis, near the Atlantic Ocean and the Mediterranean Sea. However, the mountain range's rugged terrain leads to significant spatial variations in precipitation and temperature distribution. Close to the main divide and the Pyrenean summits, annual precipitation exceeds 1000 mm and can surpass 2000 mm in certain areas (Cuadrat et al., 2007). Nevertheless, precipitation typically diminishes from west to east and from north to south (Buisan et al., 2016). In regions under Atlantic Ocean influence (approximately up to the headwaters of the Gállego and Ara rivers), most precipitation occurs from December to March. Conversely, in eastern areas influenced by a Mediterranean climate, precipitation peaks during spring and autumn (April-June, September-November) (López-Moreno et al., 2009). Generally, precipitation falls as ice or snow above 1500-1600 m above sea level from late autumn to early spring (López-Moreno and García-Ruíz, 2004). Temperature variations in the region primarily follow an altitudinal gradient of approximately 0.63°C per 100 m (López-Moreno, 2006). In colder months, the 0°C isotherm typically lies around 1600 m above sea level (García-Ruiz et al., 1986), marking the general limit for persistent snow cover. Below this threshold, a snowpack is present only during the coldest winter months (December to February). Snow cover below 1300 m above sea level is typically ephemeral, despite frequent snowfall events during winter (adapted from López-Moreno, cited in Zamora, 2017).

Characterizing and predicting the evolution of climate dynamics is particularly complex in mountainous regions, where representing local orography poses a significant challenge for climate models (GCMs and RCMs) in reproducing both mean climate and extremes, especially for short-duration precipitation associated with convective instability. Convective precipitation occurs over a small area with varying intensity, attributable to the limited horizontal extent of convective clouds (cumulonimbus or cumulus congestus). In mid-latitudes, it is an intermittent phenomenon, often linked to baroclinic boundaries and orographic barriers. From a numerical standpoint, simulating convective processes is challenging due to the multitude of processes occurring at a very local scale (< 4 km). Consequently, they are typically parameterized, although this parameterization and associated assumptions may introduce systematic errors in convective precipitation simulation. Considering these limitations, it is essential to understand the performance of the tools we employ to use them responsibly and robustly (Reder et al., 2020).

2.3.2 Hydrological System

One of the most critical factors in this region is water availability. Among the many contributions of the Pyrenees, one of the most important is the fundamental function of supplying water to the surrounding territories. This is because a large part of the surface and underground affluents that feed the basins of the rivers Ebro, Bidasoa, Adour, Garonne, and Aude, among others, originate in this mountain range. More specifically, the Pyrenees account for 70% of the total inflow to the river Ebro. Therefore, these mountains are a key element in the supply of water not only for agriculture and electricity production, but also for industry and domestic consumption. The combined effect of the change in climate and land use will significantly alter the patterns and quality of water resources both in the Pyrenees and in a much wider territory that affects millions of inhabitants. This effect will have a special impact on the low-lying northern regions of the peninsular Mediterranean slope, which are major water consumers, including water-scarce and densely populated coastal regions (Observatorio Pirenaico para el Cambio Climático – Comunidad de Trabajo de los Pirineos [OPCC-CTP], 2018).

Snow plays a fundamental role in the hydrological system of the Pyrenees (Zamora et al., 2017). Indeed, the winter snowpack serves as a natural water reservoir, providing sustained water supply during spring and summer. The southern slopes of the Pyrenees feed into the Ebro River, which traverses a region with semi-arid climatic conditions characterized by low precipitation levels (approximately 350 mm per year) and high rates of potential evapotranspiration (PET) (around 1200 mm per year). Despite these conditions, the region boasts a large irrigation area (9800 km2), significant agricultural production, and populous cities such as Zaragoza and Lleida. Consequently, the meltwater from the Pyrenees plays a strategic role in the economy and development of the downstream region. Furthermore, the social and ecological significance of the Pyrenees is closely tied to solid water. The persistent winter snowpack serves as a vital source of income for Pyrenean communities through the tourism industry, driven by activities such as skiing and other winter sports (Lasanta et al., 2007; Pons et al., 2015).

2.4 Conlusions and connections

The Pyrenees, being a high mountain region, are inherently associated with specific vulnerabilities related to their topography, climate, and hydrological dependencies. Particularly influenced by the Mediterranean climate, the Pyrenees are poised to undergo significant changes in the coming decades, related to increased temperatures and changes in precipitation regimes, as well as alterations in the hydrological cycle and cryospheric elements, which will irremediably impact the socio–economical structures on the Pyrenees and surrounding territories.

The intrinsic vulnerabilities of high mountain regions, such as the orographical complexity or the inaccessibility of the terrain add layers of intricacy when simulating climatic and hydrological dynamics. Primarily, this challenge stems from the geological structures that define these regions' complex topography. This topography interacts with atmospheric currents, giving rise to mesoscale and microscale phenomena that are difficult to model accurately. Moreover, it hampers the simulation of hydrological processes, which are closely intertwined with snow dynamics in this region. By identifying the various challenges facing high mountain regions today and delving into the situation in the Pyrenees, we have successfully completed the **Objective 1** of the thesis.

Chapter 3

Climate Variability and Land–Use Change impacts on Water Resources in the Pyrenees

Mountains play a key role in freshwater storage, providing half of the world's population with water resources (Viviroli et al., 2007; Immerzeel et al., 2020). However, in recent decades, major changes have been observed in the variables and processes that shape the hydrological cycle, such as climate variables, land cover, snow cover, and soil properties, which irremediably impact the availability of water resources downstream (Arnell, 1999; Beguería et al., 2003; Stewart et al., 2005).

This chapter builds upon the concepts introduced in Chapter 2 concerning the Pyrenees region's situation in this global context. It further explores the relationships between the hydrological cycle, climate change, and land use changes (Section 3.1). To achieve this, it conducts a quantitative analysis in a basin located in the western Pyrenees, aiming to ascertain the individual contributions of these factors to the alteration of the hydrological cycle, with particular focus on extreme values (Sections 3.3 and 3.4). This chapter, thus, sheds light (**Objective 2**) on the interactions between the hydrological regime, climate change, and land use, thereby enhancing our understanding of these dynamics. This endeavor seeks to offer valuable insights into the present condition and evolution of the hydrological regime in the Pyrenees region, thereby advancing the achievement of **Milestone 1**.

3.1 Factors influencing the hydrological cycle of the Pyrenees

The hydrological cycle is particularly vulnerable in the Pyrenees region, located between the Mediterranean and Atlantic climates, which are experiencing significant increases in temperature and changes in precipitation regimes (Amblar-Francés et al., 2020). Similarly, snow cover and its melting and accumulation, closely interconnected with streamflow in the Pyrenees region (López-Moreno and García-Ruiz, 2004), are also altered in the context of climate change. Climate variability over the years has resulted in changes in the timing and magnitude of the streamflow.

Land–use changes are a pivotal factor influencing hydrological processes. Since the 1950s mountain regions such as the Pyrenees (Poyatos et al., 2003) and the Alps (Ranzi et al., 2002; Tasser et al., 2007) have experienced significant changes in land–use consisting of arable land abandonment and subsequent reforestation, especially in the mid-altitude regions, (i.e. those below 1600 m (García-Ruiz et al., 1995)).This progressive greening process has spread worldwide in the last three decades (Zeng et al., 2016; FAO, 2014). Afforestation and agricultural land abandonment notably impact evapotranspiration (Haria and Price, 2000; Rasouli et al., 2019a), interception, and other hydrological processes (Beguería et al., 2003). Numerous studies have explored the implications of these changes for the hydrological cycle, revealing significant reductions in streamflow as a consequence of revegetation (Rasouli et al., 2019b; Guo et al., 2024; Ranzi et al., 2017), with potential repercussions on mountain ecosystem services (Boix-Fayos et al., 2020). Furthermore, alterations in land–use influence flood and drought regimes (Ranzi et al., 2002). Several studies indicate potential flood mitigation effect resulting from revegetation-based management practices (Nadal-Romero et al., 2021; Valente et al., 2021).

The influence of these factors on hydrological cycle alterations in the Pyrenees has been extensively studied. López-Moreno et al. (2008) observed a negative discharge trend in certain Pyrenean basins, accompanied by increased potential evapotranspiration (PET), suggesting a reduction in runoff generation capacity due to climate factors. However, climate drivers alone do not fully account for the observed decrease in water discharges (López-Moreno et al., 2011). Additionally, reductions in snow cover resulting from global warming have notably impacted hydrological regimes (López-Moreno and García-Ruiz, 2004; Sanmiguel-Vallelado et al., 2017). However, numerous researchers primarily attribute the negative water yield trend in Pyrenean watersheds to land-use changes (Juez et al., 2022; Lorenzo-Lacruz et al., 2012; Martínez-Fernández et al., 2013).

Hence, this chapter endeavours to isolate and quantify the influence of climate variability and land-use changes on the hydrological cycle. This analytical approach has been frequently employed, leveraging the SWAT model, a physically-based distributed hydrological model (Senent-Aparicio et al., 2018a; Zhang et al., 2017; Yin et al., 2017). This methodology has been applied to several basins within the Iberian Peninsula (Molina-Navarro et al., 2014; Senent-Aparicio et al., 2018a). For example, Senent-Aparicio et al. (2018a) evaluated the impacts of climate variability and reforestation efforts on water resources in the headwaters of the Segura River Basin. Similarly, Molina-Navarro et al. (2014) investigated the effects of climate change and land-use management scenarios on water discharge and quality in the Pareja Reservoir, situated within the upper Tagus River Basin.

The indicators included in the Indicators of Hydrological Alteration in Rivers (IAHRIS, (Martinez and Fernández, 2010)) software have been used to analyse the impact of land abandonment on water resources. This software assesses 22 indices concerning the magnitude, variability, seasonality and duration of the three main elements of the flow regime: usual values, floods and droughts (Mellado-Díaz et al., 2019). The tool was developed in Spain to address the requirements of the European Water Framework Directive. Its purpose is to identify water bodies that can be categorised as heavily modified, particularly in response to significant dam construction throughout Spain over the past century (Fernández et al., 2012; Liu et al., 2022). Beyond its original use, some authors have used IAHRIS to assess the impact of climate change on water resources (Aznarez et al., 2021; Jiménez-Navarro et al., 2021; López-Ballesteros et al., 2020; Pérez-Sánchez et al., 2020). This study is the first to apply these indicators to evaluate the impact of land abandonment on river hydrological regimes. Furthermore, our aim is to assess and quantify the influence of climate variability and land–use changes on alterations to the hydrological regime.

3.2 A case study of the Anduña River Basin in Western Pyrenees

The Anduña River Basin (Figure 3.1) is located in the western area of the Pyrenees mountain range in Spain and covers an area of 4,728.61 ha. The terrain is orographically complex and is characterised by steep slopes,

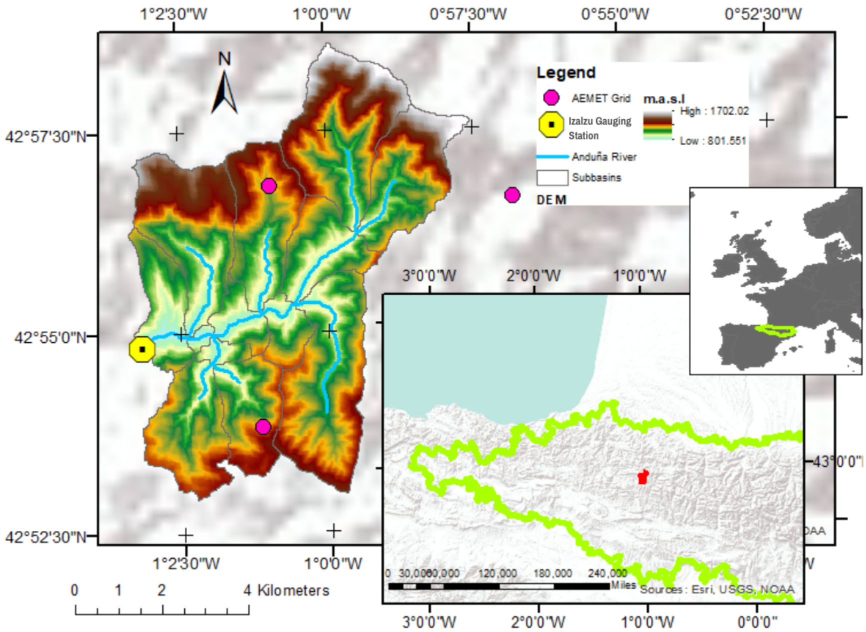

FIGURE 3.1: a) Location map of the Pyrenean region in Europe. b) Situation map of the Anduña River Basin in the Pyrenees. c) Digital elevation model (DEM) of the Anduña River basin and the location of Anduña gauging station.

giving the study basin a wide elevation range from 801 m to 1,702 m. The climate is predominantly Atlantic, with two distinct peaks in precipitation occurring in autumn and spring (Amblar-Francés et al., 2020). On average, the area receives approximately 1,750 mm of annual precipitation. Due to its high altitude, the region experiences lower temperatures compared to its surroundings. The gauging station of Izalzu records a streamflow of 46.2 hm^3 per year annually, and the hydrological regime is characterised by minimum streamflow in the summer months and two maximum discharge peaks in January and March, which are driven by the precipitation regime, with a substantial constribution by snowmelt component in spring.

Since 1956, land-use evolution in this region has been remarkable. In the 1950s, the region's population was primarily agrarian and rural, land-use mainly focused on agricultural and livestock activities with little mechanisation. Rain fed crops and large extensions of pastures and scrublands originating from extensive livestock farming predominated (Pardo et al., 2008). However, in subsequent decades, a massive abandonment of the countryside of the Pyrenees resulted in reforestation. Consequently, the land became predominantly occupied by forest (García-Ruiz et al., 1995), largely comprising conifers and hardwoods.

3.3 Accounting for the contribution of climate variability and land use–changes on water resources

Figure 3.2 presents a flowchart of the methodology employed in this study. The first step was to perform a Mann–Kendall trend analysis of the climatic variables for the historical period. Subsequently, a SWAT model was developed, calibrated and validated using observed daily flow data. The resulting SWAT model of the Anduña River basin was used to simulate Scenarios A, B and C. These scenarios simulated the effects of land–use change and climate variability on streamflow for the periods: 1956–1985 and 1986–2021. Scenario A was based on climate data for the period 1951-1985 and the 1956 land–use map, associated with the state before the region's transformation. Therefore, scenario A was the baseline scenario. Scenario B retained the land–use map before the massive reforestation process and incorporated climate data for the period 1986–2021, thus scenario B provided information on the change in hydrological variables caused by climate variability. Finally, scenario C, in addition to considering climate data for the period 1986–2021, updated the land–use map corresponding to the year 2000, thus this scenario accounted for changes produced by the combined effects of land–use change and climate variability.

The analysis examined changes in the hydrological cycle, focusing on runoff and PET, while utilising indicators of hydrological alteration (IHAs) to assess the extent of river modification(Fernández et al., 2012).

3.3.1 Trend analysis of climate variables

This study employed the Mann–Kendall test to identify trends in maximum and minimum temperatures, and precipitation during the historical period. The objective was to determine whether the time series exhibited consistent upward or downward trends, commonly referred to as monotonic trends. As a non-parametric test, it works with any distributions

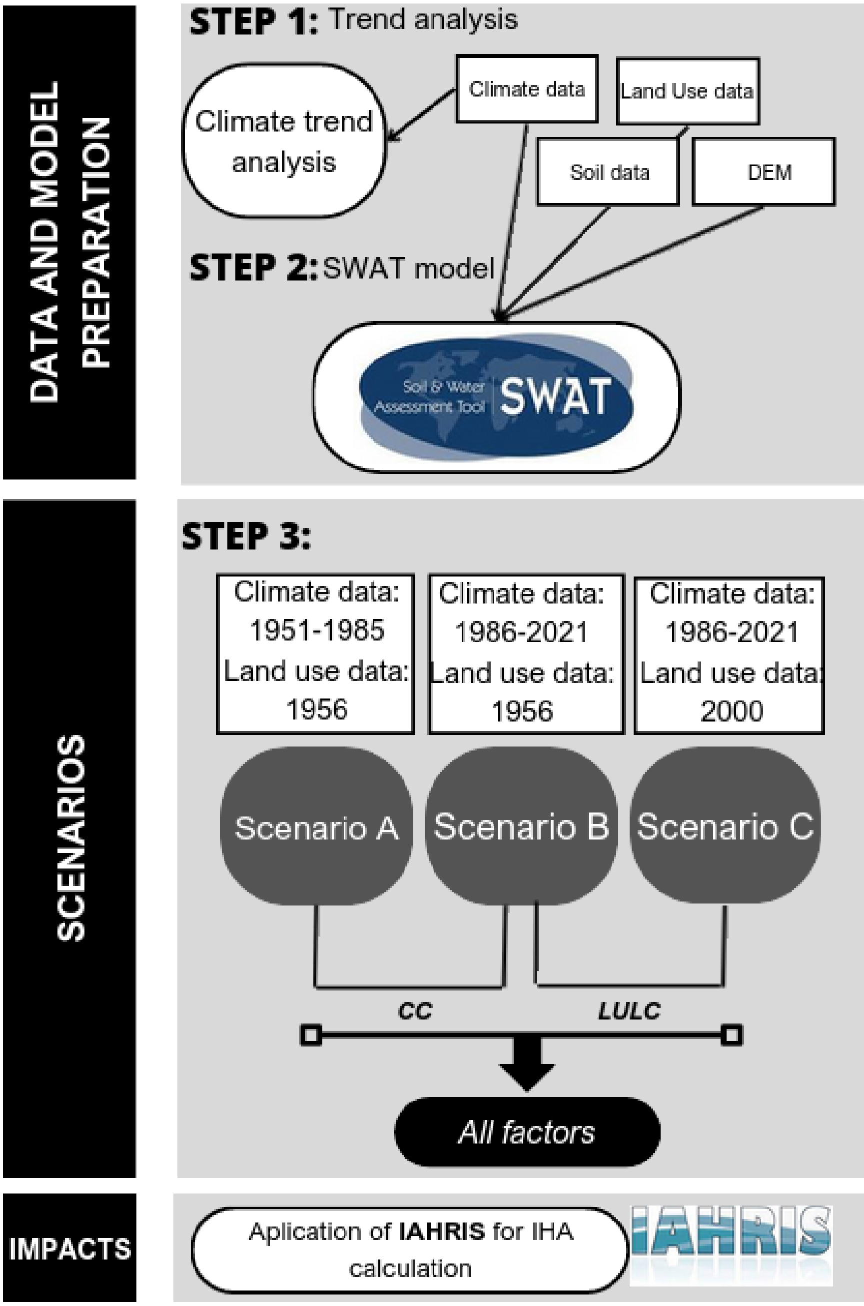

FIGURE 3.2: Flowchart of the methodology applied in the study conducted in Chapter 3.

(i.e., the variable does not have to meet the assumption of normal distribution). The Mann–Kendall test has frequently been used to quantify the significance of trends in meteorological time series (Gocic and Trajkovic, 2013; Soltani and Mofidi, 2013). The Z-test is used to asses the presence or absence of significant trends; a negative (positive) Z-value refers to a negative (positive) trend. Moreover, Sens' slope (Sen, 1968) estimates the slope of linear trends providing information on the magnitude of the trends, and is less sensitive to outliers than other metrics. It is given for N pairs of data using the following expression:

$$Q_i = median(\frac{x_j - x_k}{j - k}) \;\; for\ i = 1, ..., N \quad (1)$$

where x_j and x_k are the data values at time j and k (j $\geq$ k), respectively. Both methods have been applied using the Python package for the non-parametric Mann–Kendall family of trend tests.

3.3.2 SWAT model description

SWAT is a semi-distributed hydrological model that divided the basins of the study region into many sub-basins, further partitioned into hydrological response units (HRUs). Thus, the model considers the river network and its spatial heterogeneity (Arnold et al., 2012). Each HRU includes a combination of land cover, soil class, and slope. The SWAT model has been widely and successfully applied in watersheds with varying characteristics worldwide (Krysanova and White, 2015).

3.3.2.1 Input data for the hydrological modelling

The DEM data used as input for the SWAT model had a spatial resolution of 25 m x 25 m, obtained from the Spanish Geographical Institute (IGN, 2017). The soil dataset used in this study was the Harmonized World Soil Map, with a spatial resolution of 1 km x 1 km (Nachtergaele et al., 2012). The climate and land-use data varied depending on the scenario. The climate data, comprising maximum temperature, minimum temperature, and precipitation data for 1951–1985 and 1986—2020, was obtained from the Spanish Meteorological Agency (AEMET) with a spatial resolution of 5 km x 5 km and a daily temporal frequency. Land-use maps from 1956 and 2000 were used as reference data for both historical periods. These were downloaded from the Government of Navarra regional sources. The six land-use types in the Anduña River Basin included bare soil, broad-leaved forest, coniferous forest evergreen, mixed forest, pasture, and shrub. Finally, discharge observations in the study catchment outlet (Izalzu, Figure 1) were acquired from the Government of Spain's Centre for Public Works Studies and Experimentation (CEDEX) website.

3.3.2.2 Calibration, validation, and evaluation of model performance

Sensitivity analysis and calibration of the SWAT model were developed using the SWAT-CUP program (Abbaspour et al., 2007) and its sequential uncertainty fitting algorithm SUFI-2. This tool allows SWAT users to perform automatic calibrations more efficiently and has been widely used by the SWAT community (Arnold et al., 2012). First, a global sensitivity analysis was conducted to identify the parameters with the most influence on streamflow. Of the parameters analysed in 500 iterations, those obtaining p-values lower than 0.005 were selected. Moreover, five snow-related parameters were considered in the calibration, due to the influence of snow dynamics on the hydrological cycle in the study area (Palazón and Navas, 2014). Automatic calibration was then applied to determine the values of the parameters that best reproduced the discharge considering the Kling–Gupta efficiency (KGE) as the objective function. In total, 1,000 simulations were run, initially 500 and then a further 500 using the adjusted parameter ranges.

The following five metrics were used to quantitatively evaluate the model's performance in the calibration and validation stages: the Nash–Sutcliffe efficiency (NSE), the root mean square Error (RMSE), the percent bias (PBIAS), the coefficient of determination (R^2), and the KGE, according to the recommended evaluation procedure established in Moriasi et al. (2015). The results of the model statistics were evaluated using the criteria proposed by (Kalin et al., 2010), which classify the results as very good, good, satisfactory, and unsatisfactory.

3.3.3 IAHRIS Software

One of the most common and complete methods of assessing riverine changes is calculating IHAs (Papadaki et al., 2016; López-Ballesteros et al., 2020). This method provides information on the degree of alteration between simulated and baseline scenarios. In this case, we evaluated the degree of alteration of the Anduña River Basin caused by climate variability and land-use change, allowing us to determine the contribution to the IHAs. This method was applied using IAHRIS version 2.2 software, which includes the 24 IHAs described in Table 3.1. Based on the most significant aspects of the flow regime (magnitude, frequency, variability, seasonality, and duration), IAHRIS establishes the IHA related to the maximum extreme (floods), minimum extreme (droughts), and usual values.

TABLE 3.1: List of IHAs using IAHRIS.

Components of the regime	Aspect	Indicator	Description
Usual values	Magnitude	M1	Magnitude of annual volume Magnitude of monthly volume
		M2	Magnitude of volume of the month: 12 values
		M3	Variability of annual volume
	Variability	V1	Variability of monthly volume
		V2	Variability of volume of the month: 12 values
		V3	Extreme variability
	Stationarity	E1	Seasonality of maximums
		E2	Seasonality of minimums
Maximum extreme values (floods)	Magnitude	IHA7	Magnitude of maximum floods
		IHA8	Magnitude of effective discharge
		IHA9	Magnitude of connectivity flow
		IHA10	Magnitude of usual floods
	Variability	IHA11	Variability of maximum floods
		IHA12	Variability of usual floods
	Duration	IHA13	Floods duration
	Seasonality	IHA14	Seasonality of floods (1 for each month)
Minimum extreme values (droughts)	Magnitude	IHA15	Magnitude of extreme droughts
		IHA16	Magnitude of usual droughts
	Variability	IHA17	Variability of extreme droughts
		IHA18	Variability of usual droughts
	Duration	IHA19	Duration of droughts
		IHA20	Number of days of null flow (1 for each month)
	Seasonality	IHA21	Seasonality of droughts (1 for each month)

IAHRIS uses 25 parameters to calculate the 24 IHA indicators, (Table 3.2) that quantitatively characterize the flow regime of a river: four for usual values, eight for floods, and seven for droughts. Within the scope of these 25 parameters, our study investigated those pertinent to flood characterisation. Our analysis focused on the following parameters: the average of the maximum daily flows throughout the year (Q_c), effective discharge (ED), conductivity discharge (CD), and flushing floods (FF). The ED is a geomorphic concept representing the flow, or range of flows that transport the most sediment over the long term, while the CD is a key indicator that enables the transport of aquatic life, organic matter, nutrients, and sediments to the floodplain and riparian system. Likewise, the FF is the flow corresponding to the mean curve of flows classified at the 5% exceedance percentile.

Additionally, each IHA represented a parameter change between the baseline and altered scenarios. In the case study, the alteration associated with the change from Scenario A to Scenario B was related to climate variability and from Scenario A to Scenario C to the combined effect of climate variability and land-use change. These alterations are hereafter referred to hereafter as 'Impact A-B' and 'Impact A-C', respectively. Indicators were calculated for each disturbance with values ranging from 0 to 1, where 1 indicated no disturbance and 0 indicated maximum disturbance (Swanson, 2002).

TABLE 3.2: List of parameters for calculating IHAs.

Components of the regime	Aspect	Parameter	Description	Resulting
Usual values	Magnitude and variability	H1	Mean (hm3)	M1
		H2	Median (hm3)	
		H3	Coefficient of variation	V1
		H4	Mean of the month (hm3): 12 values	M2
		H5	Median of the month (hm3): 12 values	M3
		H6	Coefficient of variation of the month: 12 values	V2
				V3
		H7	Extreme variability (hm3)	V4
	Seasonality	H8	Maximum relative frequency of the month: 12 values	E1
		H9	Minimum relative frequency of the month: 12 values	E2
	Variability	P4	Difference between the average flows associated with 10% and 90% percentiles	IHA3
Maximum extreme values (floods)	Magnitude and frequency	P5	Average of the maximum daily flows throughout the year	IHA7
		P6	Effective discharge	IHA8
		P7	Connectivity discharge	IHA9
		P8	Flushing flood (5% percentile)	IHA10
		P9	Coefficient of variation of the maximum daily flows throughout the year	IHA11
		P10	Coefficient of variation of the flushing flood series	IHA12
		P11	Consecutive days in a year with percentile below 5%	IHA13
		P12	Average number of days per month with percentile above 5%	IHA14
Minimum extreme values (droughts)	Magnitude and frequency	P13	Average of the minimum daily flows throughout the year	IHA15
		P14	Ordinary drought discharge (95% percentile)	IHA16
	Variability	P15	Coefficient of variation of the minimum daily flows throughout the year	IHA17
	Duration	P16	Coefficient of variation of the ordinary droughts series	IHA18
		P17	Consecutive days in a year with percentile below 95%	IHA19
		P18	Average number of days in the month with null flow	IHA20
	Seasonality	P19	Average number of days per month with percentile below 95%	IHA21

IAHRIS presented the results in three spider charts: one for usual values, one for floods, and one for droughts. IAHRIS obtained another indicator that provides information on global alteration (IGA) from the ratio between the areas of natural and altered scenarios depicted in the spider charts.

3.4 Results

3.4.1 Climate Variability

The results of the Mann–Kendall test and the Sen's slope are given in Table 3.3. Regarding the maximum and minimum temperatures during the historical period, we observed a positive trend throughout all the months of the year with a confidence level of 0.001 in the summer months (June, July, and August). The significance level is also maintained in the annual trend. However, no clear trend was observed for precipitation, consistent with those obtained in previous studies in the Pyrenees region, indicating to trends close to 0 and statistically non-significant in most cases (Juez et al., 2022; Lemus-Canovas et al., 2019). Lemus-Canovas et al. (2019), also obtained a slightly positive non-significant trend in the western region of the mountain range, where our study area is located.

TABLE 3.3: Trend analysis results. Test Z is the Mann–Kendall (MK) test statistic; Qi is the Sen's slope estimator. ** Indicates a significance level of 0.01, and *** indicates a significance level of 0.001

	Precipitation			Maximum Temperature			Minimum Temperature		
	Test Z	Sig.	Q_i	Test Z	Sig.	Q_i	Test Z	Sig.	Q_i
jan	1.350		0.028	2.134		0.019	2.809	**	0.028
feb	0.715		0.012	1.107		0.018	1.817		0.022
mar	0.745		0.012	1.191		0.016	1.995		0.015
apr	0.645		0.008	2.144		0.028	1.936		0.014
may	0.735		0.008	1.698		0.024	1.886		0.016
jun	-0.139		-0.002	3.743	***	0.046	4.070	***	0.027
jul	1.489		0.009	3.703	**	0.041	3.946	***	0.025
aug	0.010		0.000	3.345	***	0.041	4.358	***	0.028
sep	-0.199		-0.002	0.893		0.012	0.655		0.006
oct	0.705		0.012	2.144		0.026	3.018	**	0.025
nov	1.201		0.024	1.152		0.013	2.422		0.022
dec	0.000		0.000	1.102		0.012	1.648		0.015
annual	1.896	**	0.009	4.735	***	0.028	5.490	***	0.021

3.4.2 Land-use Change

LULC data for the past and baseline periods are given in Table 3.4. According to data for the year 1956, more than 43 % of the area was covered by pasture and more than 12 % was covered by scrubs, while the area occupied by the three forest types was 44 %. In contrast, the 2000 land-use map reveal a radically different picture, with forests extending over 73 % of the region and pastures and scrubs representing less than 30 %. This transformation is representative of socio–economic changes that occurred throughout the final decades of the 20th century in the region, which consisted of the abandonment of ploughed lands and subsequent plant succession which resulted in a reforested landscape (García-Ruiz et al., 1995; Poyatos et al., 2003; Lasanta et al., 2015, 2017).

TABLE 3.4: Surface area and percentage of cover of the six land-use types for the years 1956 and 2000.

Land Cover Type	Area Coverage km^2 (%)		Change (%)
	1956	2000	1956–2000
Bare Soil	15 (0.3%)	23 (0.5%)	0.23
Broad-leaved Forest	1604 (33.2%)	1872 (38.8%)	6.71
Coniferous Forest Evergreen	334 (6.9%)	1331 (27.5%)	19.62
Mixed Forest	171 (3.5%)	347 (7.2%)	5.61
Pasture	2101 (43.5%)	1075 (22.3%)	-22.60
Shrub	607 (12.6%)	183 (3.8%)	-9.88

3.4.3 Model Calibration and Validation

As discussed in the Section 3.3, the sensitivity analysis did not consider snow-related parameters. The selected parameters are consistent with those identified in previous studies. Crucial similarities between sensitive parameters can be observed in Stratton et al. (2009), who explored sensitivity in a basin influenced by snow is explored, and Grusson et al. (2015), who studied a basin on the French side of the Pyrenees. Based on these and other studies of basins with similar characteristics (Palazón and Navas, 2014), the snow parameters given in Table 3.5 were incorporated into the calibration.

The NSE values for calibration and validation on a daily basis (Table 3.6) are considered satisfactory according to the criteria described by Kalin et al. (2010). Similarly, the PBIAS values, present very good results, since they remain below ± 25 % and indicate only a slight tendency to overestimate the actual values. The remaining indices used to evaluate of the model's performance also gave satisfactory values: the R^2 is above

TABLE 3.5: Calibration parameters codes, descriptions, initial calibration range and final optimal values.

Parameter	Description	Calibration Range	Adjusted Value
Esco	Soil evaporation compensation factor	0 – 1	0,7543
Epco	Plant uptake compensation factor	0 – 1	0,7325
Cn_2	Initial SCS runoff curve number condition II	±20 %	-19.88
Awc	Available water capacity	±20 %	12.04
Snofall tmp	Snowfall temperature (ºC)	-5 – 5	0,491
Snomelt tmp	Snowmelt base temperature (○C)	-5 – 5	2,465
Snomelt max	Maximum melt rate of snow during a year (mm ºC-1 day -1)	0 – 10	5,206
Snomelt min	Minimum melt rate of snow during a year (mm ºC-1 day -1)	0 – 10	1,276
Snomelt lag	Snow pack temperature lag factor	0 – 1	0,973

TABLE 3.6: Calibration and validation statistical values on a daily basis.

Period	R^2	NSE	PBIAS	KGE
Calibration (1992-2004)	0.72	0.51	-12.67	0.55
Validation (2005-2018)	0.75	0.55	-16.49	0.62

0.70 in both cases, while the KGE is above 0.55. These favourable results validate the SWAT model of the Anduña River Basin for simulating daily flow in the scenarios described in the Section 3.3.

Figure 3.3 gives the monthly time series of simulated and observed streamflow for the calibration and validation periods, observed monthly precipitation, and the values of the model performance evaluation statistics. The negative PBIAS indicate an overestimation of low flows (Figure 3.3). Despite this, Moriasi et al. (2015) propose that a PBIAS of less than 25% is acceptable for evaluating hydrological models. Recent reviews by Tan et al. (2021) support this criterion for SWAT model applications, while Mulligan (2013) suggests that physically based models, if accurately simulating current conditions, will likely perform well under scenario conditions. Moreover, Arabi et al. (2007) find that relative comparisons for land use scenarios yield consistent results with lower uncertainty. Therefore, despite inherent model uncertainties, we consider that the calibrated model is suitable for achieving our study objectives.

3.4.4 Impacts of landuse change and climate variability on the hydrological cycle

Table 3.7 presents the annual precipitation, mean annual runoff and evapotranspiration (ET) simulated by the SWAT model under scenarios A, B,

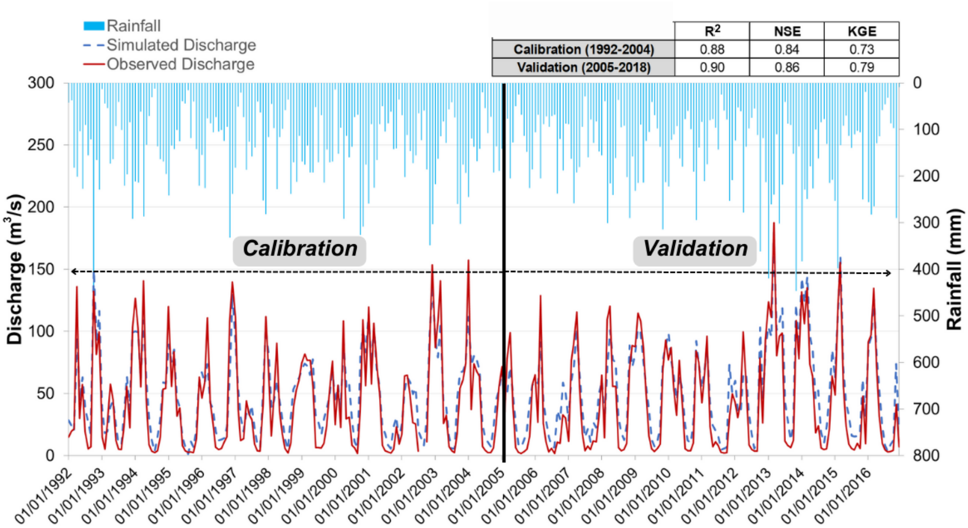

FIGURE 3.3: Monthly calibration and validation time-series and statistical values.

and C. From the comparison between scenarios A and B, we obtained information on the impact of climate variability on the hydrological cycle and observed that precipitation increases minimally, consistent with the trend analysis described in Section 4.1. Climate variability, also related to a rise in temperatures, increased ET by 15.5 mm and resulting in a decrease in runoff of 21.8 mm. The combined effect of climate variability and land-use change were obtained by comparing Scenarios A and C, which resulted in an increase in ET of 31 mm and a decrease in runoff of 36.12 mm. Therefore, the contribution of each factor in the increase of ET was 50 %. Concerning the decrease in runoff, the impacts of land-use change was almost as important as climate variability, contributing by 41.36 % while climate variability contributed by 58.64 %.

TABLE 3.7: Simulated average annual runoff, precipitation, PET, ET and percolation under scenarios A, B and C (mm).

Scenarios	P	PET	Percolation	ET	Runoff	Change ET	Change Runoff
A	1718.3	794.3	512.78	576.6	1100.2		
B	1722.2	836.7	481.71	592.1	1079.1	+15.5	-21.2
C	1722.2	836.7	467.23	607.6	1064.1	+31.0	-36.1

3.4.5 Impacts of land-use change and climate variability on the alterations hydrological regime

The results obtained using IAHRIS for the characterization of floods (Table 3.8) pointed to an increase in the magnitude of the maximum extreme events in the comparison of scenarios A and B. Overall, climate variability produced increases of more than 40 % in the variables Qc, ED and CD . The alteration of these variables is slightly mitigated by reforestation, leading to a decrease in values of 5 %, as observed in the results obtained for Scenario C, representing the combined effect of both factors on the hydrological regime.

TABLE 3.8: Flood parameters of IAHRIS over A, B and C scenarios. Q_c refers to the average of the maximum daily flows throughout the year, ED to effective discharge, CD to conductivity discharge, FF flushing floods and the CV expresses the variability of parameters

Scenarios	Q_c	ED	CD	FF	CV(Q_c)	CV(FF)
A	11.21	10.05	13.50	4.31	0.40	0.24
B	15.90	15.30	20.00	4.25	0.44	0.23
C	15.06	14.40	18.80	4.22	0.43	0.23

The changes in flood regimes translate into increases in the frequency and magnitude of flooding of the floodplain, directly influencing factors such as the availability of oxygen for plant roots, fundamental for the composition and productivity of riparian species and communities. Similarly, these changes can alter sediment erosion and deposition responsible for modulating the geomorphology of the floodplain surface, producing significant alterations in the successional dynamics of riparian ecosystems (Richter and Richter, 2000; LeRoy Poff and Allan, 1995).

3.4.6 Indicators of Hydrological Alteration

Figure 3.4 shows the results of IGA and spider-charts of IHA for the usual values, floods, and droughts, obtained using the IAHRIS method. The results are presented dissagregated into two different disturbances: impact A-B refers to the disturbance between scenarios A and B, while impact A-C describes the disturbance between scenarios A and C. Impact A-B reflects the contribution of climate variability in the alteration of the indicators, while impact A-C refers to the alteration caused by the combined effects of climate variability and land-use changes.

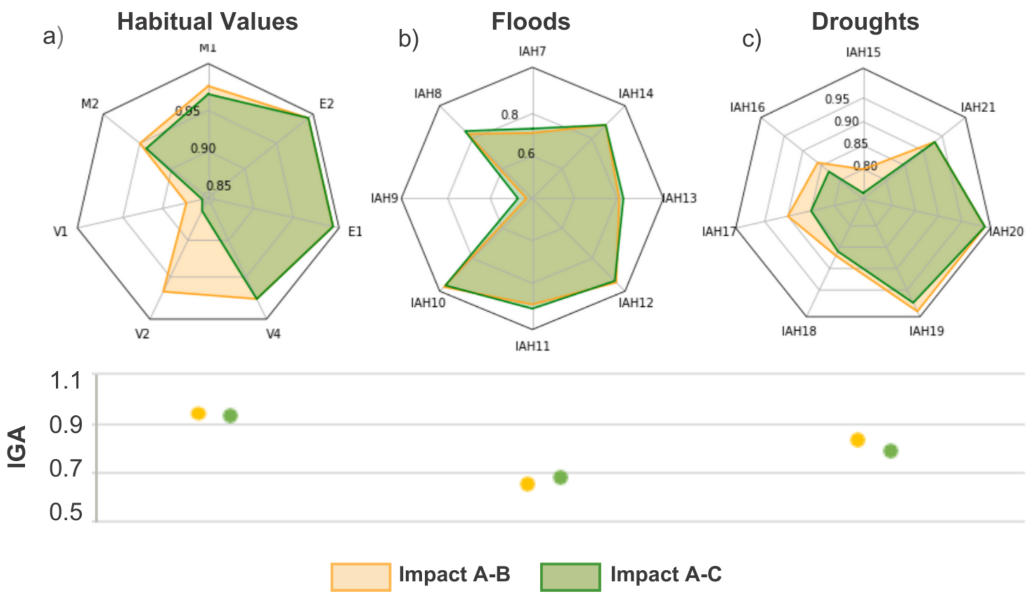

FIGURE 3.4: Spider charts of the IHAs and IGA values for habitual values, floods and droughts under impacts A–B and impact A–C.

Concerning the IGA indicators (Figure 3.4.b), a decrease in the quality of the water regime was observed, especially for floods: the IGA decreased to 0.65 due to climate variability, although this was slightly mitigated by the reforestation process, reaching 0.67. For the usual values and droughts, the IGA revealed higher values, above 0.8, indicating that the alteration was more subtle. Similarly, the results indicate that the combined effects of the climate and reforestation slightly increased the alteration in the usual values and droughts, contrasting with the results for floods.

The spider-charts (Figure 3.4.a) present the results of the indicators of hydrological alteration. Regarding the usual values, no indicator excessively influence the water regime, since all gave values higher than 0.80. We observed the greatest change in the variability of annual volume (V1) derived from climatic causes and accentuated by changes in land-use. However, the determining factor in the monthly volume variability (V2), was land-use change, causing the indicator's value to drop to 0.86. Changes in annual and interannual variability could influence the structure of ecosystem communities (Bêche et al., 2006). The indicators concerning to annual and monthly magnitude decreased slightly and the seasonality maxima and minima presented values close to 1, indicating minimal disturbance conditions. These conditions would be favourable for developing processes vital for habitat diversity and for stimulating germination and dispersal (Bêche et al., 2006).

The flood regime was the most altered of the analysed regimens, as the IGA indicates (Figure 3.4.b), the alteration was entirely due to climatic influences. This changes was slightly alleviated by reforestation. The most affected indicator was the frequency of connectivity flow (IHA9; Table 3.2), which is fundamental for enabling the transport of aquatic life, organic matter, nutrients, and sediments to the floodplain and riparian river system, as well as in maintaining adequate moisture conditions for species growth stages (Larsen et al., 2019). In addition, it is closely linked to successional dynamics, for example, by stimulating the rejuvenation of secondary channels and creating pond features that help maintain local plant and animal diversity in floodplains (Richter and Richter, 2000). The loss of connectivity with floodplains implies continuous ageing of the riparian habitat, endangering species renewal (Nilsson and Svedmark, 2002). The magnitude of maximum floods (IHA7) was the second most altered factor and the magnitude of effective discharge (IHA8) was also affected by climatic causes. Hence, the regeneration and flushing cycles of the usual flows would be affected along with the and sediment mobilisation transport processes responsible for riverbed geomorphology (Wohl

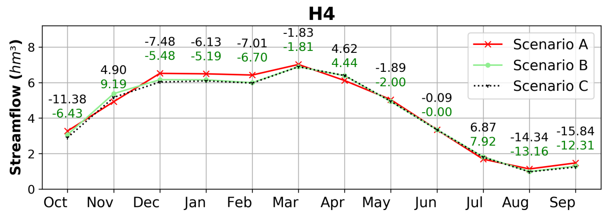

FIGURE 3.5: Monthly streamflow mean simulations under scenarios A, B and C with the changes expressed in percentages for scenario A–B (green) and for scenario A–C (black).

et al., 2015).

Concerning droughts (Figure 3.4.c), the major alterations occurred in magnitude and frequency, which became more evident with the combined effects of climatic causes and reforestation. These predominantly affected the magnitude of extreme droughts (IHA15), the magnitude of usual droughts (IHA16), and the variability of extreme droughts (IHA17).

Figure 3.5 presents the mean monthly streamflow values under scenarios A, B, and C. The most significant decreases were observed in the winter, summer, and early autumn months. The decrease in winter was predominantly associated with climate variability accentuated by the influence of revegetation. The same trend occurred in summer and early autumn. This decrease would be associated with temperatures rise, illustrated in Table 3.3, which would cause an increase in ET. The greening process would accentuate this increase in ET by reducing streamflow.

The variability in streamflow for each month (H6) is displayed in Figure 3.6. We observed greater variability in the months with more precipitation for all scenarios. Increases were observed in March, June, and October due to the influence of climate variability, while a decrease in variability was observed during the winter months. Parameters H8 and H9 (Figure 3.6) provide information on the seasonality of maximum and minimum streamflow values, respectively, obtained for each month as the relative frequency or probability that the annual maximum and minimum monthly contribution occurs in that month (Martínez Santa-María and Fernández Yuste J.A., 2008). We observed that the probability of the annual maximum streamflow occurring in April increased almost two-fold due to the impact of climate variability. Similarly,

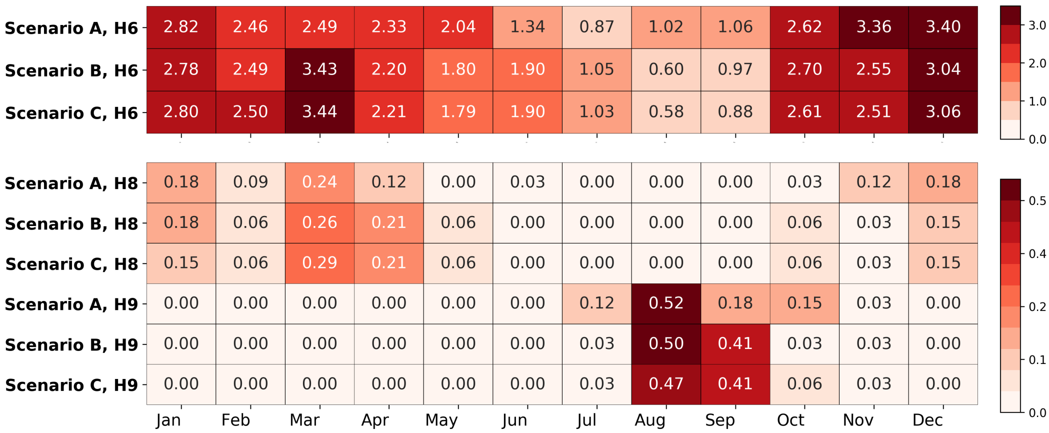

FIGURE 3.6: Monthly values for IAHRIS parameters under scenarios A, B and C

climate variability altered the seasonality of the minimums. Therefore, the probability of the minimum occurring in September increased from 0.18 to 0.41. Climate variability caused a delay in the maximum and minimum for the hydrological regime in the Anduña River Basin. These alterations in the natural seasonal patterns of the water regime could produce distortions in the river functioning as an ecosystem due to the loss of synchrony with species' life cycles, affecting, among other things, reproductive patterns, migration, growth, and development, (Naiman et al., 2002) and favoring the progression of foreign species resulting in a biodiversity loss (Richter and Richter, 2000; Growns and Reinfelds, 2014).

3.5 Discussion

Examining the long-term time series data revealed a notable decline in runoff within the Anduña River Basin from 1951 to 2020. This trend aligns with similar observations documented for multiple catchments within the Pyrenees mountain region, as noted by Juez et al. (2022); Vicente-Serrano et al. (2021); López-Moreno et al. (2008). Additionally, analogous runoff reductions have been observed in other natural, non-managed catchments across the Iberian Peninsula, particularly those undergoing significant land–use transformations (Lorenzo-Lacruz et al., 2012; Vicente-Serrano et al., 2020).

Additionally, our analysis further quantifies the respective contributions of key factors underlying this decline in runoff, specifically climate variability and land-use change. Notably, our findings attribute nearly equal importance attributed to both factors, with contributions of 58.6% and 41.4%, respectively. These results substantiate the hypothesis posited by López-Moreno et al. (2008), supported by subsequent studies such as Juez et al. (2022), highlighting that the decline in streamflow magnitude cannot be solely ascribed to climate factors but is partially linked to greening processes in the Pyrenees. Our findings align with those of Vicente-Serrano et al. (2021). While the authors observed a more pronounced downward trend in streamflow that could be attributed to differing climatic conditions between the Mediterranean and Atlantic regions, they estimate that non-climate-related streamflow decline accounts for between 46% and 65% of the total reduction.

The peak flows analysis indicates an increase attributed to climate factors, in terms of magnitude and frequency, consistent with the findings of other studies conducted in mountainous basins (Roy et al., 2001; Stoffel et al., 2016). Braun et al. (2000) emphasized that flooding in mountain watersheds is frequently linked to intense precipitation and snowmelt during winter. However, this surge in stream flow is mitigated by the process of revegetation, which modulates the hydrological cycle's response to precipitation, not only in mean annual values but also in peak flows (Minang et al., 2015; Ranzi et al., 2002). Reforestation plays a crucial role in reducing flood risks by enhancing soil permeability through increased infiltration due to tree roots (Keeler et al., 2019) and heightened interception by forest canopies. These factors collectively contribute to minimising the hazards associated with flooding (Gallart and Llorens, 2004; Andréassian, 2004; Valente et al., 2021). Conversely, in cases of usual and extreme minimum streamflow (droughts), the reforestation process exacerbates alterations to the water regime, together with climatic causes.

Changes in these two determinants of water regime dynamics are expected to persist in the future. Specifically, rising temperatures and alterations in precipitation patterns are likely to significantly contribute to exacerbating changes in the water regime. Additionally, the process of land abandonment and the subsequent reforestation of agricultural lands could continue to spread. Coupled with the upward migration of forest boundaries due to increasing temperatures (López-Moreno et al., 2008; Beniston, 2003), this effect will likely enhance forest cover, intensifying impacts on the water regime. Given that climate variability is beyond the control of regional actors, developing land management plans aimed at reducing water consumption by vegetation is key to mitigating future impacts on the hydrological cycle. Llena et al. (2024) propose scrub cleaning as an effective measure with positive effects on surface runoff and hydrological connectivity in a Mediterranean basin in the Pyrenees. This practice would be useful for enhancing soil quality (Nadal-Romero et al., 2018) and help prevent forest fires (Lasanta et al., 2019). Furthermore, alternative silviculture practices such as thinning (Manrique-Alba et al., 2020), should be considered to adapt dense pine reforestation to new conditions in the context of climate change and protect hydrological regime.

3.6 Conclusions and connections

This chapter used the SWAT model to quantify the contributions of climate variability and land–use change to alterations in the hydrological regime of a natural catchment in the Pyrenees region.

The SWAT model satisfactorily reproduced the hydrological dynamics of the Anduña River Basin obtaining the following statistics for the validation period: an R^2 of 0.75, an NSE of 0.55, a PBIAS of -16.49 and KGE of 0.62. These results indicate a good performance of the model.

The climate trend analysis revealed a significant positive trend in the summer months for the maximum and minimum temperatures and in January and October for the minimum temperature. This significant trend is maintained on an annual scale. Regarding precipitation, no clear trend was identified on a monthly scale. However, a slight increase in precipitation was observed on an annual scale. Furthermore, a radical transformation in the distribution of land–use in the basin, from a land dominated by pastures and shrubs to a basin were forests predominate, was observed.

These environmental changes have an impact on water resources. Specifically, climate variability and greening process have decreased the mean annual streamflow in the Anduña River Basin, with the contribution of climate variability being 58.6 %, while the contribution attributed to the greenness process is 41.1 %. Likewise, the results obtained by IAHRIS highlight an increase in the magnitude of maximum extreme events (floods) since an increase of 40 % in the variables Qc, ED, and CD due to climate variability was observed. Reforestation mitigated the alteration of these variables by approximately 5 %. According to the IHAs, a degradation in the water regime was observed, especially in the case of floods. The degradation in the case of floods is caused by climate variability and alleviated as a consequence of the greening process. In the case of the usual values and droughts, the combination of climate and land-use change generated a greater alteration. On a monthly scale, a modification in the magnitude, variability, and seasonality of the streamflow was observed, predominantly caused by climate variability.

This chapter offers novel and relevant insights into the repercussions of climate change and land use changes on the hydrological regime of the Pyrenees, thereby contributing to **Objective 2** and advancing scientific comprehension of these dynamics in the region. Moreover, it contributes, together with Chapter 2, to address the **Milestone 1** by providing valuable information to understand the hydro–climatic dynamics of the Pyrenees.

Chapter 4

High–Resolution Climate Simulations: Advantages and Limitations in a Complex Orography Region

Climate simulations, such as Global Climate Models (GCMs) and Regional Climate Models (RCMs), play a pivotal role in both characterizing present climate conditions and projecting future climate scenarios (Taylor et al., 2012; Jacob et al., 2014; Vautard et al., 2021). GCMs, with their broad global perspective, capture large-scale atmospheric and oceanic processes, while RCMs provide finer spatial resolution, which is particularly valuable for regional-scale assessments. Through these simulations, insights into current climate patterns, variability, and trends are gained, facilitating the assessment of climate risks and vulnerabilities. Furthermore, by simulating various scenarios of greenhouse gas emissions and other forcing factors, GCMs and RCMs allow for the anticipation of potential climate changes and their impacts on different regions and sectors (IPCC, 2022).

Understanding the performance and ability of climate simulations to accurately represent climate dynamics is essential for their effective use, particularly in challenging environments like mountainous regions (Torma et al., 2015; Reder et al., 2020; Careto et al., 2022c). Here, the complex mesoscale and sub-kilometer climatic dynamics governing the climate pose unique obstacles. In such areas, where accurate representation is crucial, the insights provided by climate models like GCMs and RCMs become even more valuable, aiding decision-makers in devising adaptation strategies and informed policy decisions at doverse spatial scales.

In this Chapter, we undertake the evaluation of GCM and RCM simulations over the Pyrenees region, considering the spatial distribution of results and extreme events of climate variables. The Chapter will include an introduction to the Added Value concept (Section 4.2), a definition of the variables and databases considered (Section 4.3), a description of the applied methodology (Section 4.4), presentation of results (Section 4.5), and their subsequent discussion (Section 4.6).This comprehensive analysis addresses **Objective 3**, assessing the advantages and limitations of the climate simulations in characterizing the region's climate, thereby contributing to the accomplishment of **Milestone 2** aiming to thoroughly understand prediction tools including climate models.

4.1 The Concept of Added Value

Regional Climate Models (RCMs), have been developed in the recent decades to address the challenge of downscaling low-resolutiontion Models (GCMs) into high-resolution information. This approach overcomes the practical limitations of employing high-resolution models on a global scale. Over the past years, RCMs have gained increasing significance, primarily due to the growing demand for high-resolution simulations to conduct impact assessment studies for climate change adaptation strategies. However, despite the advantages of these models, there are limitations that must also be taken into account (Kotlarski et al., 2014, 2015; Vautard et al., 2021)

In this scenario of the proliferation of RCMs, the Coordinated Regional climate Downscaling Experiment, CORDEX (Giorgi et al., 2009; Jones et al., 2011; Gutowski et al., 2016), was created. In particular, for the European region, more than 70 RCM simulations have currently been conducted within the framework of the EURO-CORDEX initiative. However, downscaling the information derived from GCMs is computationally very expensive. Therefore, it is a prior need to assess the added value (AV) of using RCMs against GCMs in simulating the climate system.

For this aim, previous studies have proposed different methods to compute the AV depending on multiple factors such as the variable, the region of interest and the spatial and temporal scale. Di Luca et al. (2016) proposed the potential added value metric, which delves into the increased spatial-scale variability not present in the simulations at lower resolutions. This approach involves analyzing the discrepancies in high-ranking percentiles at the scale of individual grid-cells. The results showed potential added value values in regions of complex topography and short time scales, especially less than 3 hours. Perkins et al. (2007) proposed a metric to measure the ability of a model to simulate the full observational distribution of a climate variable. This methodology enables us to direct our analysis towards a specific segment of the PDF, for example, its tails, making possible to study low-probability events that are not reflected in the mean. Soares and Cardoso (2018) combined the definition of AV proposed by Di Luca et al. (2016) and the definition of model skill proposed by Perkins et al. (2007) to create a new metric called DAV (Distributed Added Value) that provides a normalized measure of the added value in relation to the gain associated with downscaled simulations, comparing the PDFs of the RCMs and GCMs with observations. The results showed positive AVs for precipitation throughout the European region, specifically where convective processes are relevant, such as the Alps or Iberian Peninsula. In that line, Ciarlo et al. (2021) applies a point-by-point analysis of PDFs to spatially assess the added value of a RCM, including both a comprehensive representation of the characteristics of a variable and its geographical variation. Quantifications of the PDF-based AV indicate that higher AV values are obtained at the tails ends of the distribution for the precipitation variable.

Common outcomes are reported in the literature (Feser, 2006; Prein et al., 2016; Fantini et al., 2018; Di Luca et al., 2016; Torma et al., 2015; Ciarlo et al., 2021; Qiu et al., 2020). First, the increase of AV with spatial resolution is associated with a better representation of topographic features. This results in a significant increase in AV in regions with complex topography, such as mountainous or coastal areas. Secondly, it is emphasized that there is a substantial improvement in AV even when the RCMs have been upscaled to the GCM grid. This means that the better performance of the RCM is due to a better representation of the physical processes and not to the disaggregation of the large-scale forcing. In addition, they all point out the importance of having high-quality observational data due to the impact they have when computing the AV index, especially significant in the tails of the distribution (Ciarlo et al., 2021) which makes accurate analysis limited in many regions of the globe.

The high-mountain region of the Pyrenees is a particularly vulnerable region to climate change (Chapter 2 and Chapter 3) with impacts on essential sectors such as water management or tourism (Amblar-Francés et al., 2020). Until present, the Pyrenees have not been considered separately when evaluating the benefits or losses of using high versus low resolution models. In this work, the assessment of AV in the Pyrenees is performed, considering the entire mountain region as the area of interest and focusing on the performance of RCMs versus GCMs.

4.2 Climate observations and simulations

In this study, the added value method proposed by Ciarlo et al. (2021) was applied to quantify the gain or loss representing a variable when using RCMs or GCMs in the Pyrenees region (41°N–44°N, 2.5°W–3.5°E). This metric is based on the probability distribution function (PDF) of each grid point providing a spatial distribution of the added value over the study area. It combines the spatial downscaling signal described by Giorgi et al. (2009) and the spatial correlation skill mentioned in Rummukainen (2016) allowing a spatial analysis over the whole PDFs. Daily precipitation ('pr'), maximum temperature ('tmax'), and minimum temperature ('tmin') were analyzed using a high-resolution observational dataset against a set of RCMs and GCMs. Furthermore, the orography ('orog') variable from model simulations was considered to further investigate the relationship between the added valued and the elevation.

CLIMPY observational dataset covering the Pyrenees (Cuadrat et al., 2020b) was used as reference with a spatial resolution of 1 km $\times$ 1 km on a daily basis covering the period 1981–2015. It is a reconstruction (Serrano-Notivoli et al., 2017) of the variables based on the information from 1,343 meteorological stations located in Spain, France, and Andorra. This dataset was created in the framework of the transboundary project CLIMPY and has already been validated in different studies (Amblar-Francés et al., 2020; Lemus-Canovas and Lopez-Bustins, 2021) .

We evaluated the EURO-CORDEX ensemble (Jacob et al., 2014, 2020), with a total of 72 RCM simulations (Table 4.1) and a spatial resolution of 0.11°. These simulations cover a time period of 130 years and are available for different Representative Concentration Pathways (RCP4.5, RCP8.5, and RCP2.6). This analysis focused on analyzing the historical simulation up to 2005 and the RCP8.5 simulation after 2005. These simulations consist of two models, the RCM and the driver model, the GCM (with a resolution of 1.00 °), forming an incomplete matrix of 12 RCMs and 8 GCMs.

In this study, the data will undergo interpolation onto two rectilinear grids with resolutions of 0.11° and 1.00°, corresponding to the

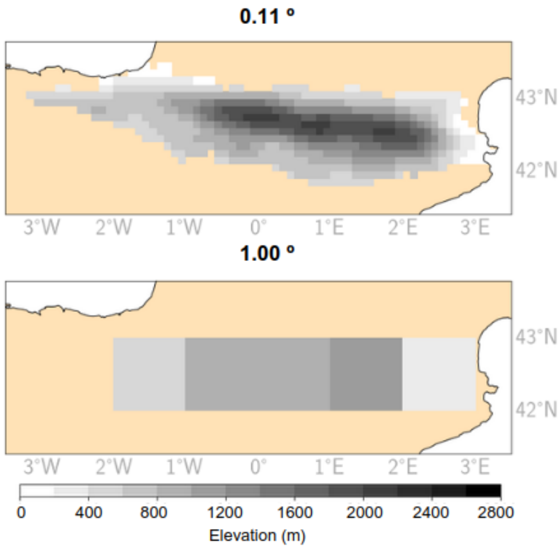

FIGURE 4.1: Topography for the Pyrenean analysis region at the two resolutions investigated in this work: top (0.11°) and bottom (1.00°)

RCM and GCM models, respectively. Interpolation to the finer resolution (0.11°) was accomplished using the distance-weighted average remapping method (Ciarlo et al., 2021; Fantini et al., 2018; Torma et al., 2015) implemented in the Climate Data Operators software (CDO, https://code.zmaw.de/projects/cdo). This method, as noted by Torma et al. (2015), yields the most consistent spatial patterns across different resolutions. Additionally, the analysis incorporates evaluation at the native resolution of the GCMs, where all data (including observations and RCMs) are upscaled to a 1.00° grid. This approach, as highlighted by Terzago et al. (2017) and Vautard et al. (2021), mitigates the impact of horizontal resolution on the performance of coarser-scale climate models. Spatial interpolation for this step utilize conservative remapping, also available within CDO.

4.3 Methodology: Added Value Index

For each grid point the PDF of the daily events (including dry events for precipitation) were computed, over the period 1981–2015 for each variable in the observations, RCMs, and GCMs. To ensure the consistency in the bin size across all three datasets and for each variable, a bin size of 1

TABLE 4.1: EURO-CORDEX RCM ensemble members and their corresponding driving GCMs used for this analysis. The column 'Variables' includes the variables that have been taken into account for each of the members.

Institution/Driving model	Member	Code	RCM	Variables
CCCma-CanESM2	r1i1p1	1	CLMcom-CCLM4-8-17	pr; tmin; tmax; orog
CCCma/CanESM2	r1i1p1	1	GERICS-REMO2015	pr; tmin; tmax; orog
CNRM-CERFACS/CNRM-CM5	r1i1p1	2	CLMcom-CCLM4-8-17	pr; tmin; tmax
CNRM-CERFACS/CNRM-CM5	r1i1p1	2	CLMcom-ETH	pr; tmin; tmax; orog
CNRM-CERFACS/CNRM-CM5	r1i1p1	2	CNRM-ALADIN63	pr; tmin; tmax; orog
CNRM-CERFACS/CNRM-CM5	r1i1p1	2	DMI-HIRHAM5	pr; tmin; tmax; orog
CNRM-CERFACS/CNRM-CM5	r1i1p1	2	GERICS-REMO2015	pr; tmin; tmax; orog
CNRM-CERFACS/CNRM-CM5	r1i1p1	2	IPSL-WRF381P	pr; tmin; tmax
CNRM-CERFACS/CNRM-CM5	r1i1p1	2	KNMI-RACMO22E	pr; tmin; tmax; orog
CNRM-CERFACS/CNRM-CM5	r1i1p1	2	MOHC-HadREM3-GA7-05	pr; tmin; tmax; orog
CNRM-CERFACS/CNRM-CM5	r1i1p1	2	RMIB-UGent-ALARO-0	pr
CNRM-CERFACS/CNRM-CM5	r1i1p1	2	SMHI-RCA4	pr; tmin; tmax; orog
ICHEC/EC-EARTH	r12i1p1	4	CLMcom-CCLM4-8-17	pr; tmin; tmax; orog
ICHEC/EC-EARTH	r12i1p1	4	CLMcom-ETH	pr; tmin; tmax
ICHEC/EC-EARTH	r12i1p1	4	DMI-HIRHAM5	pr; tmin; tmax; orog
ICHEC/EC-EARTH	r12i1p1	4	GERICS-REMO2015	pr; tmin; tmax; orog
ICHEC/EC-EARTH	r12i1p1	4	ICTP-RegCM4-6	pr; tmin; tmax; orog
ICHEC/EC-EARTH	r12i1p1	4	IPSL-WRF381P	tmin; tmax
ICHEC/EC-EARTH	r12i1p1	4	KNMI-RACMO22E	pr; tmin; tmax; orog
ICHEC/EC-EARTH	r12i1p1	4	MOHC-HadREM3-GA7-05	pr; tmin; tmax; orog
ICHEC/EC-EARTH	r12i1p1	4	SMHI-RCA4	pr; tmin; tmax; orog
ICHEC/EC-EARTH	r12i1p1	4	UHOH-WRF361H	pr; tmin; tmax
ICHEC/EC-EARTH	r1i1p1	3	CLMcom-ETH	pr; tmin; tmax
ICHEC/EC-EARTH	r1i1p1	3	DMI-HIRHAM5	pr; tmin; tmax; orog
ICHEC/EC-EARTH	r1i1p1	3	KNMI-RACMO22E	pr; tmin; tmax; orog
ICHEC/EC-EARTH	r1i1p1	3	SMHI-RCA4	pr; tmin; tmax; orog
IPSL/IPSL-CM5A-MR	r1i1p1	6	DMI-HIRHAM5	pr; tmin; tmax
IPSL/IPSL-CM5A-MR	r1i1p1	6	GERICS-REMO2015	pr; tmin; tmax; orog
IPSL/IPSL-CM5A-MR	r1i1p1	6	IPSL-WRF381P	pr; tmin; tmax
IPSL/IPSL-CM5A-MR	r1i1p1	6	KNMI-RACMO22E	pr; tmin; tmax; orog
IPSL/IPSL-CM5A-MR	r1i1p1	6	SMHI-RCA4	pr; tmin; tmax; orog
MIROC/MIROC5	r1i1p1	7	CLMcom-CCLM4-8-17	pr; tmin; tmax; orog
MIROC/MIROC5	r1i1p1	7	GERICS-REMO2015	pr; tmin; tmax; orog
MIROC/MIROC5	r1i1p1	7	UHOH-WRF361H	pr
MOHC/HadGEM2-ES	r1i1p1	5	CLMcom-CCLM4-8-17	pr; tmin; tmax; orog
MOHC/HadGEM2-ES	r1i1p1	5	CLMcom-ETH	pr; tmin; tmax
MOHC/HadGEM2-ES	r1i1p1	5	CNRM-ALADIN63	pr; tmin; tmax; orog
MOHC/HadGEM2-ES	r1i1p1	5	DMI-HIRHAM5	pr; tmin; tmax; orog
MOHC/HadGEM2-ES	r1i1p1	5	GERICS-REMO2015	pr; tmin; tmax; orog
MOHC/HadGEM2-ES	r1i1p1	5	ICTP-RegCM4-6	pr; tmin; tmax; orog
MOHC/HadGEM2-ES	r1i1p1	5	IPSL-WRF381P	pr; tmin; tmax
MOHC/HadGEM2-ES	r1i1p1	5	KNMI-RACMO22E	pr; tmin; tmax; orog
MOHC/HadGEM2-ES	r1i1p1	5	MOHC-HadREM3-GA7-05	pr; tmin; tmax; orog
MOHC/HadGEM2-ES	r1i1p1	5	SMHI-RCA4	pr; tmin; tmax; orog
MOHC/HadGEM2-ES	r1i1p1	5	UHOH-WRF361H	pr; tmin; tmax
MPI-M/MPI-ESM-LR	r1i1p1	8	CLMcom-CCLM4-8-17	pr; tmin; tmax; orog
MPI-M/MPI-ESM-LR	r1i1p1	8	CLMcom-ETH	pr; tmin; tmax
MPI-M/MPI-ESM-LR	r1i1p1	8	CNRM-ALADIN63	pr; tmin; tmax; orog
MPI-M/MPI-ESM-LR	r1i1p1	8	DMI-HIRHAM5	pr; tmin; tmax; orog
MPI-M/MPI-ESM-LR	r1i1p1	8	ICTP-RegCM4-6	pr; tmin; tmax; orog
MPI-M/MPI-ESM-LR	r1i1p1	8	IPSL-WRF381P	pr; tmin; tmax
MPI-M/MPI-ESM-LR	r1i1p1	8	KNMI-RACMO22E	pr; tmin; tmax; orog
MPI-M/MPI-ESM-LR	r1i1p1	8	MOHC-HadREM3-GA7-05	pr; tmin; tmax; orog
MPI-M/MPI-ESM-LR	r1i1p1	8	MPI-CSC-REMO2009	pr; tmin; tmax
MPI-M/MPI-ESM-LR	r1i1p1	8	SMHI-RCA4	pr; tmin; tmax; orog
MPI-M/MPI-ESM-LR	r1i1p1	8	UHOH-WRF361H	pr; tmin; tmax; orog
MPI-M/MPI-ESM-LR	r2i1p1	9	CLMcom-ETH	pr; tmin; tmax
MPI-M/MPI-ESM-LR	r2i1p1	9	MPI-CSC-REMO2009	pr; tmin; tmax; orog
MPI-M/MPI-ESM-LR	r2i1p1	9	SMHI-RCA4	pr; tmin; tmax; orog
MPI-M/MPI-ESM-LR	r3i1p1	10	CLMcom-ETH	pr; tmin; tmax
MPI-M/MPI-ESM-LR	r3i1p1	10	GERICS-REMO2015	pr; tmin; tmax; orog
MPI-M/MPI-ESM-LR	r3i1p1	10	SMHI-RCA4	tmin; tmax; orog
NCC/NorESM1-M	r1i1p1	11	CLMcom-ETH	pr; tmin; tmax
NCC/NorESM1-M	r1i1p1	11	CNRM-ALADIN63	pr; tmin; tmax; orog
NCC/NorESM1-M	r1i1p1	11	DMI-HIRHAM5	pr; tmin; tmax; orog
NCC/NorESM1-M	r1i1p1	11	GERICS-REMO2015	pr; tmin; tmax; orog
NCC/NorESM1-M	r1i1p1	11	ICTP-RegCM4-6	pr; tmin; tmax; orog
NCC/NorESM1-M	r1i1p1	11	IPSL-WRF381P	pr; tmin; tmax
NCC/NorESM1-M	r1i1p1	11	KNMI-RACMO22E	pr; tmin; tmax; orog
NCC/NorESM1-M	r1i1p1	11	MOHC-HadREM3-GA7-05	pr; tmin; tmax; orog
NCC/NorESM1-M	r1i1p1	11	SMHI-RCA4	pr; tmin; tmax; orog

mm/day for the precipitation variable as in Ciarlo et al. (2021) and a 0.5 °C for the minimum and maximum temperature variables as in Perkins et al. (2007), were selected.

Then, the Relative Probability Difference (D_M) was computed following the methodology defined in Ciarlo et al. (2021) by (4.1), which provides information about the discrepancies that exist between the distributions of the observations and the models, whether GCM or RCM. That is, a higher (lower) value of D_M means a worse (better) performance of the model

$$D_M = \frac{\sum_{v=1}^{v_t} |(N_M - N_O)| \Delta v}{\sum_{v=1}^{v_t} (N_O \Delta v)}, \tag{4.1}$$

where N_M and N_O are, respectively, the number of events for the GCM or RCM and observations per bin, and Δv is the bin size of the variable. Two values for D_M, namely D_{RCM} and D_{GCM}, for the RCM and GCM simulations, respectively, were obtained.

Hence, the Added Value (AV) index is defined as the difference between both estimates of D_M as shown in (4.2), previously defined in Ciarlo et al. (2021). A positive (negative) AV value represents an improvement (worsening) in the results of the RCM in relation to the GCM when representing the probability distribution of the variable

$$AV = D_{GCM} - D_{RCM}. \tag{4.2}$$

Note that, for the exceptional case when the GCM does not simulate events for a specific bin (for instance, at the tails of the distribution, i.e., extreme values), N_{GCM} will be zero, while the value of N_O and N_{RCM} may not. In this situation, the value of D_{GCM} will always be equal to 1, while D_{RCM} could exceed this value, which significantly disturbs the AV calculation by obtaining misleading negative AV values. Hence, a conditional assumption is applied. In this scenario, if N_{GCM} is equal to zero for a particular bin, yet N_{RCM} and N_O are both non-zero, the D_{RCM} value for that bin is zero. This approach guarantees a positive contribution to the AV index in these cases. The inverse condition, namely, the cases where both N_{GCM} and N_O are non-zero while N_{RCM} equals zero, has not been considered. This omission arises from the negligible number of instances relative to the total number of events, accounting for less than 0.01 %.

To shed light on the relationships between AV and elevation, the linear relationship was calculated with the Pearson correlation coefficient. A 95% level of significance, corresponding to a p value equal to 0.05 was considered and computed as follows: For a given sample with correlation coefficient r, the p-value is the probability that abs(r′) of a random sample x′ and y′ drawn from the population with zero correlation would be greater than or equal to abs(r). (https://docs.scipy.org/doc/scipy/reference/generated/scipy.stats.pearsonr.html). For this calculation, we considered the AV and orography matrix of each RCM member. Consequently, those members lacking orography information (Table 4.1) were excluded from the analysis.

4.4 Results

4.4.1 Added Value for the entire PDFs

Figure 4.2 illustrates the relative probability difference (D_M; (4.1)) of the RCM and GCM ensemble means, and the resulting added value index (AV in (4.1)) for the three analyzed variables. Regarding precipitation, the D_{RCM} exhibits values between 0.2 to 0.4 uniformly distributed across the region. In contrast, D_{GCM} displays a latitudinal gradient with higher values on the southern slope of the mountain range ($\sim$0.7) and lower values on the northern part ($\sim$0.3). Consequently, the resulting AV index indicates better performance of the RCMs with notable improvement in the central zone of the southern slope where the GCM ensemble-mean performs poorly.

In terms of minimum temperature, homogeneous values of the D_{RCM} ensemble mean across almost the entire mountain range were observed. This contrasts with the values of D_{GCM}, which exceed 0.8 in the highest regions as well as on the eastern area of the southern slope. Consequently, a significantly high AV is observed in these areas, where the GCM ensemble mean exhibits inadequate performance. The results for maximum temperature demonstrate a similar pattern, but with some distinctions. Although the D_{GCM} is also higher in high-elevation regions, it is more localized compared to the case of minimum temperature, suggesting that, overall, the GCM ensemble mean represents maximum temperatures more accurately than minimum temperatures. The AV for maximum temperature reaches its highest values in the central region, surrounded by values close to 0.

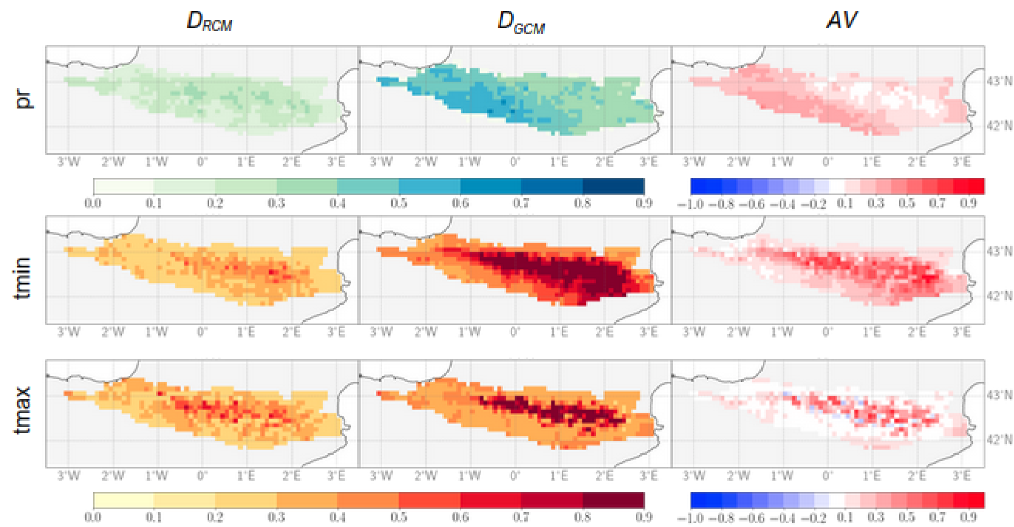

FIGURE 4.2: Relative probability difference (D_M in (4.1)) of the RCM (left column) and the GCM (middle column) and the added value (AV in (4.2); right column) of the ensemble means at 0.11° resolution, for precipitation (top row), minimum temperature (middle row) and maximum temperature (bottom row) using CLIMPY as reference over the period 1981–2015.

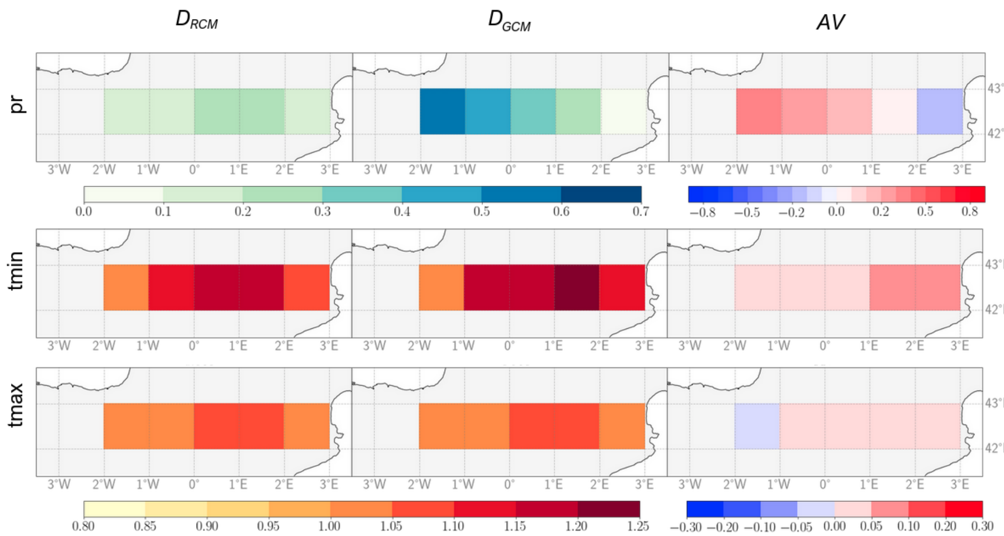

FIGURE 4.3: Relative probability difference (D_M in (4.1)) of the RCM (left column) and the GCM (middle column) and the added value (AV in (4.2); right column) of the ensemble means at 1.00° resolution, for precipitation (top row), minimum temperature (middle row) and maximum temperature (bottom row) using CLIMPY as reference over the period 1981–2015.

Figure 4.3 exhibits a parallel structure to Figure 4.2, albeit with data upscaled to the native resolution of the GCM (1.00°). Remarkably, the findings for both D and AV remain consistent across the two resolutions. However, due to the coarse spatial resolution and the relatively small coverage area of the Pyrenees, our analysis is confined to a grid of only five cells. Despite this limitation, the obtained information aligns with the spatial distribution depicted in Figure 4.2. In the case of precipitation, the AV at 1.00° resolution shows maximal values in the western sector of the mountain range. This phenomenon is related with a poor GCM performance, as evidenced by high D_{GCM} values. Conversely, for tmin, the highest AV is observed in the central–eastern area of the Pyrenees, corresponding to the region of highest elevation (Figure 4.1). Finally, for tmax, AV values are notably lower, with instances of negative values occurring in the lower altitude zones of the mountain range.

The conclusions derived from analyzing the ensemble mean overlook the signals provided by each individual member. Figures B.1–B.3 present the AV a 0.11° for the individual members in a matrix format, where the rows represent the GCM driver and the columns represent the RCM. Similarly, Figures B.4–B.6 present this same information but for the calculation performed at a resolution of 1.00°. The results are consistent for both fine and coarse resolution. Concerning precipitation, the AV demonstrates a stronger dependence on the GCM rather than the RCM, aligning with the findings of Ciarlo et al. (2021) and Di Luca et al. (2016). The groups of models driven by CanESM (Code 1), CNRM (Code 2), and NCC (Code 11) exhibit the highest AV, while the models driven by MPI (Codes 8 and 9) yield lower AVs, occasionally even showing negative values, meaning that MPI GCMs (Codes 8 and 9) have an excellent performance over the Pyrenees. The spatial distribution of the AV in all members follows a consistent pattern observed in Figure 4.2, with lower AV values in higher-elevation areas of the mountain range. Regarding temperatures, the predominance of the GCMs in the AV result is less evident. However, for both minimum and maximum temperatures, the models driven by CNRM (Code 2) show lower AVs at both resolutions, which in the case of coarse resolution is also evident for the EC-EARTH GCM (Codes 3 and 4). In the case of minimum temperature, the contribution of the RCMs to the AV signal is especially noticeable, particularly with the RCM models RCA4 and RACMO22E, which have a negative influence on representing the variable's mean. Conversely, in the case of maximum temperature, the RCM model REMO2019 positively shapes the AV signal, particularly at 0.11° resolution.

4.4.2 Added Value for percentile intervals

It is particularly important to focus on specific intervals of the PDF to gain insights into how the models perform in the tails of the distribution, which are associated with unusual events. Figure 4.4 provides a visual representation of the AV index at 0.11° resolution as a function of percentile intervals. Two approaches are considered: one with 0 percentile as the lower limit of the interval (0–x) and another with 100 percentile as the upper limit (x–100). The percentiles are varied from 1 to 100 in the first case and from 99 to 0 in the second case. Figure 4.4 displays two curves: the orange line represents the average AV index of all members as a function of percentile, while the orange shading represents inter-member variability; the blue curve, on the other hand, illustrates the evolution of the AV index of the ensemble mean shown in Figure 4.2 as a function of percentile. The blue line represents the spatial average for the entire region, while the blue shading represents spatial variability.

In terms of precipitation, the AV index gradually increases for the 0–x case, indicating a lower AV at the left end of the distribution, which corresponds to minimum precipitation values ($<$ 1mm/day), including dry events. This observation is corroborated when considering the x–100 case, where overall, the AV values are higher compared to the 0–x case. Furthermore, as the 100th percentile was approached, the AV index increases. These results suggest that RCMs struggle to accurately represent events located in the left extreme of the precipitations PDF. In the 90–100 interval, a minimum in the AV index is observed, followed by a slight increase. To gain a better understanding of this trend, Figure 4.4c includes the probability density functions (PDFs) of all members and observations. The PDFs demonstrate that all members (RCMs and GCMs) overestimate low-intensity events, a characteristic linked to the well-known drizzle phenomenon: both RCMs and GCMs exhibit a pattern of background light rain events persisting throughout the year, yet they inadequately capture episodes of zero rainfall (Coppola et al., 2021; Kämäräinen et al., 2018; van Meijgaard and Crewell, 2005). From 10 mm/day values and onwards, which corresponds to the 90th percentile, the GCMs start to underestimate precipitation, while the RCMs remarkably reproduce the PDF of the observations. The inflection point occurs around the 90th percentile, where the curve of the observations intersects with the curves of the GCMs. This intersection explains the existence of the minimum in Figure 4.4b at the 90th percentile.

Both maximum and minimum temperatures exhibit similar behavior.

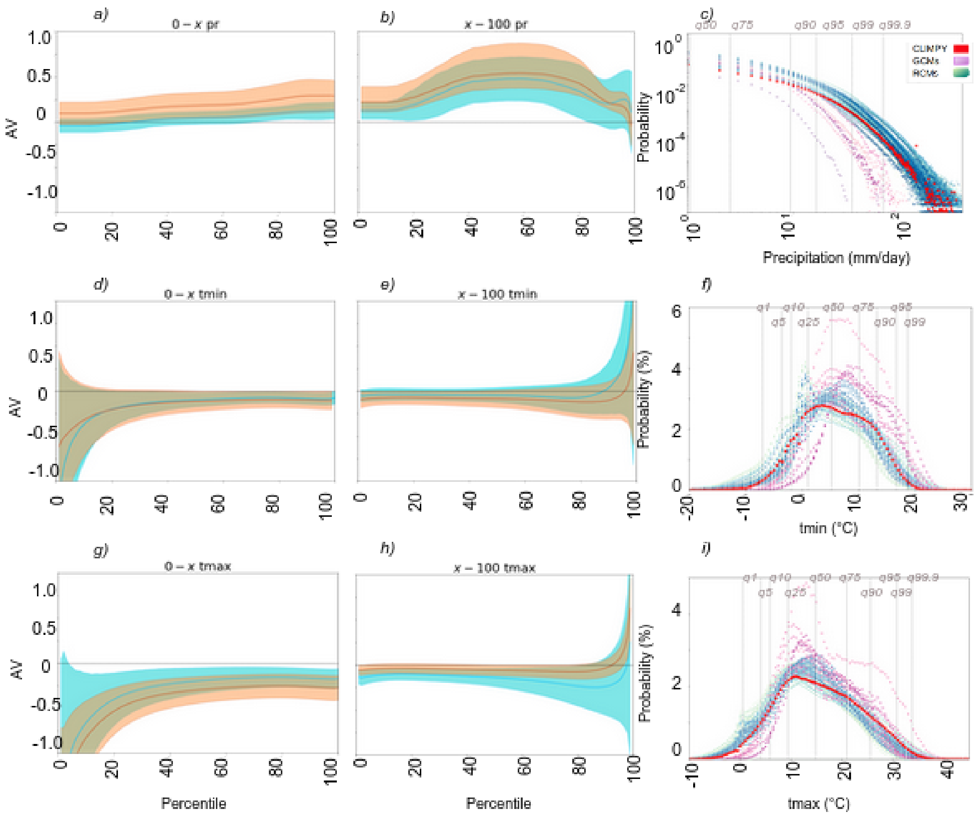

FIGURE 4.4: Evolution of the mean and variability of the members (orange) and the ensemble and its spatial variability (blue) of the added value index (AV in (4.2)) as a function of the percentile intervals on the first and second columns for the variables ‘pr’ (a,b), ‘tmin’ (d,e) and ‘tmax’ (g,h). The third column shows the PDFs of the observations (red), RCM members (blue), and GCM members (pink) and the CLIMPY percentiles for ‘pr’ (c), ‘tmin’ (f) and ‘tmax’ (i).

In the 0–x interval, the AV index reaches very low values, stabilizing around -0.2 when x is below the 20th percentile in both cases. The orange shaded areas represent the variability among members, which is considerable in intervals with $x < 20$. This indicates that the members considered present diverse AV values, ranging from positive to negative values. The spatial variability (shaded in blue) follows the same pattern. In the 0–x intervals where $x < 20$, the shaded area exhibits significant amplitude. In summary, this suggests that the AV index will vary considerably depending on the spatial location and RCM member in the lower tails of the temperature distribution.

Conversely, in the x–100 interval, the AV index increases in the right tail of the distribution when the 100th percentile is included. These results indicate that dynamical downscaling provides added value in the right tail of the maximum and minimum temperature distribution, corresponding to the warm events of both temperatures. However, it diminishes the quality of the simulation in the left tail of the distribution, which represents the minimum temperature values, associated with cold events.

In terms of the temperature PDFs (Figure 4.4f; Figure 4.4i), it is worth noting that they exhibit a similar shape to the observations, with improvements observed in the fit for the RCMs. The GCMs consistently overestimate the maxima and underestimate the minima of both temperatures, although the dynamic downscaling corrects the overestimation for the maxima. In the lower tail of the distribution, however, the RCMs overestimate the number of minimum events for both temperatures, resulting in negative AV values (Figure 4.4d; Figure 4.4g).

Figures 4.5, 4.6 and 4.7 provide insights into the spatial distribution of the AV of the ensemble mean for specific intervals, and these results align with the trends observed in Figure 4.4. In the case of precipitation (Figure 4.5), there is a gradual increase in AV for the 0–x interval, as depicted in Figure 4.4a. Furthermore, the x–100 interval exhibits higher AV values compared to the 0–x interval, confirming the observations in Figure 4.4b and indicating a very low AV near the zero percentile. When considering the spatial distribution of AVs, lower values are observed in the higher regions of the mountain range. As x increases, these regions expand and decrease in value, occasionally reaching negative values in certain areas. Consequently, a minimum AV occurs at the 90th percentile, which corresponds to the intersection between the PDFs of the GCMs and RCMs (Figure 4.4c).

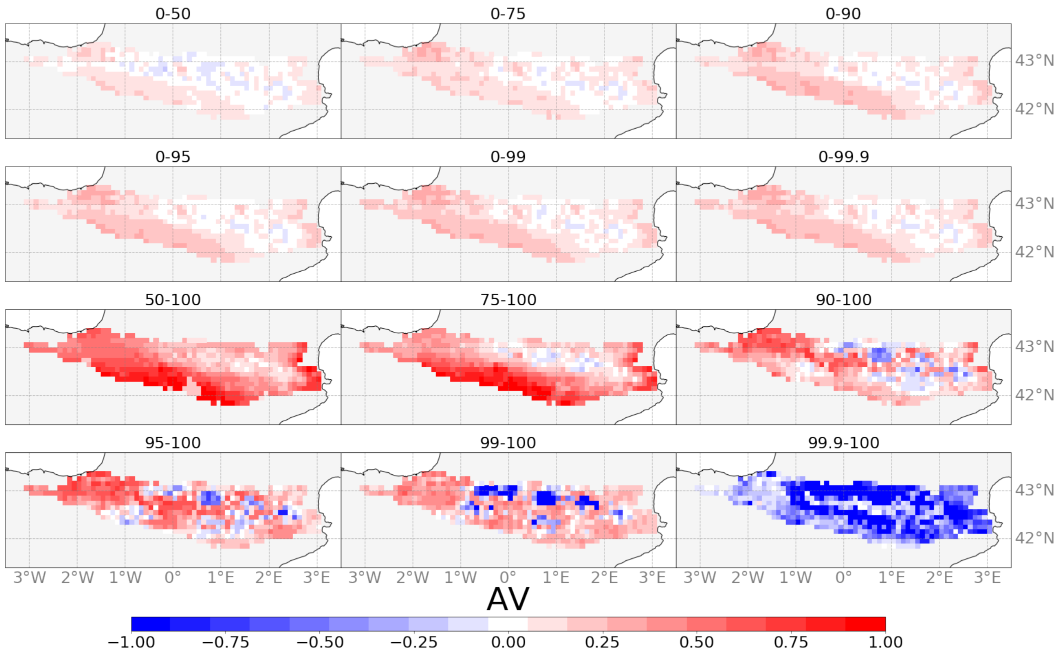

FIGURE 4.5: Added value index (AV in (4.2)) for RCM ensemble mean at different percentile intervals at $0.11° \times 0.11°$ for precipitation variable using CLIMPY as reference over the period 1981–2015.

The detection of low AV at high elevations may be linked to deficiencies in precipitation observations within these areas. In high-mountain regions, such as the Pyrenees, lower station density is prevalent due to their remote locations (Isotta et al., 2014). Coupled with the lack of calibration for under-catch gauges, which can lead to underestimation of precipitation, particularly in windy and snowy conditions, the observations may not accurately represent the precipitation patterns in higher elevation regions (Adam and Lettenmaier, 2003; Torma et al., 2015). These observation biases have the potential to influence the AV index, thereby limiting the reliability of the results at high altitudes.

Figure 4.5 also reveals an interesting feature of the AV index within the 99.9–100 interval, where a decrease in AV across the entire region is observed. This phenomenon occurs due to the small number of events within this interval, each event being classified into bins based on its magnitude. Although dynamical downscaling improves the representation of the upper tail of the distribution, it struggles to accurately predict the magnitude of these rare events, causing them to be placed in different bins compared to the observations. Consequently, when comparing the frequency of events in each bin, the AV decreases. Given the minimal number of events, this does not significantly impact the overall AV index of the PDF.

The results for minimum and maximum temperatures in Figures 4.6 and 4.7 also exhibit consistency with Figure 4.4b,c. The right tail of the distribution, which corresponds to minimum events, demonstrates a very low AV. The AV remains consistently low throughout the evolution of the interval, but when reaching the 90–100 range, it experiences an exponential increase, yielding considerably high values in the central region of the mountain range. This positive AV signal aligns with the mean spatial distribution depicted in Figure 4.2. In essence, the presence of positive mean AV values for both maximum and minimum temperatures is influenced by the AV of the upper end tail of the distribution.

The most notable distinction between the evolution of the AVs for minimum and maximum temperatures lies in their spatial extent. In the case of minimum temperature, the positive AVs cover a larger area and reach higher values. Conversely, the positive AVs associated with maximum temperature remain more localized within the higher elevations of the mountain range, surrounded by negative AVs.

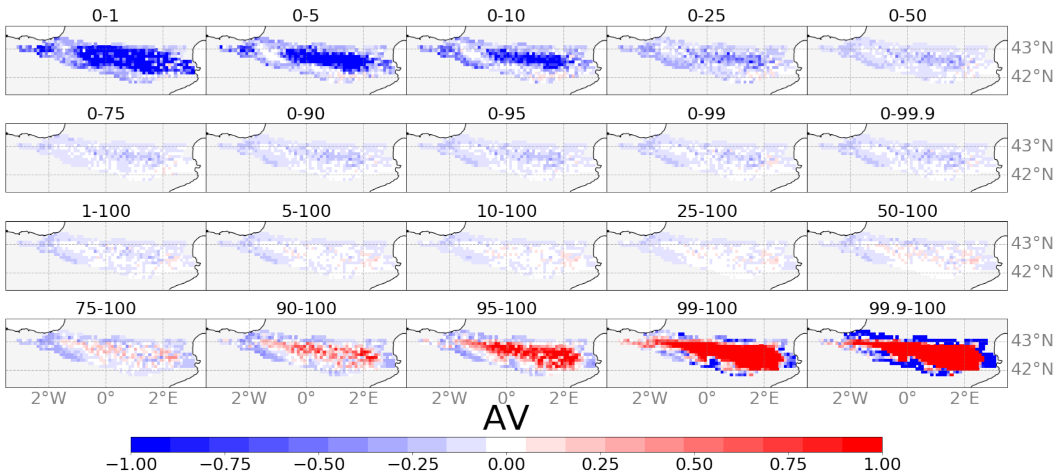

FIGURE 4.6: Added value index (AV in (4.2)) for RCM ensemble mean at different percentile intervals at $0.11° \times 0.11°$ for minimum temperature variable using CLIMPY as reference over the period 1981–2015.

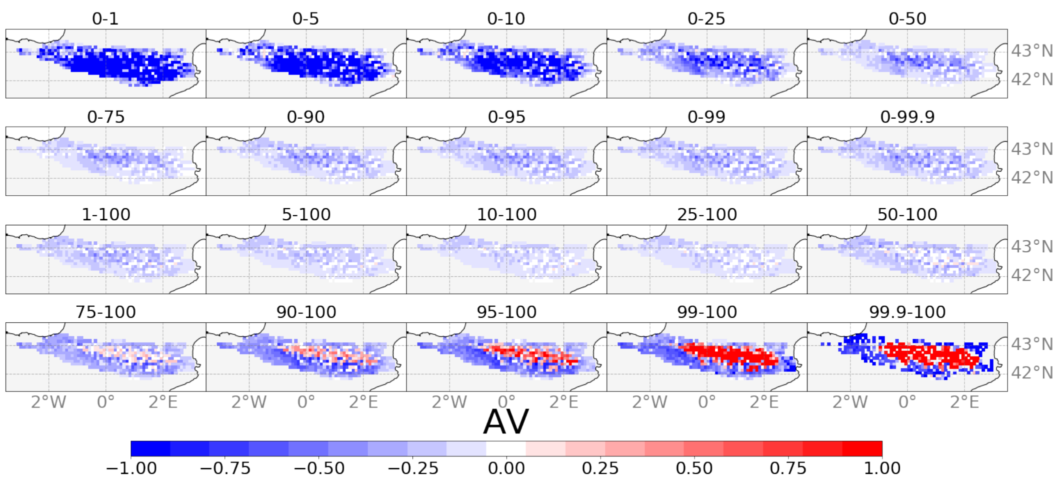

FIGURE 4.7: Added value index (AV in (4.2)) for RCM ensemble mean at different percentile intervals at $0.11° \times 0.11°$ for maximum temperature variable using CLIMPY as reference over the period 1981–2015.

4.4.3 Added Value evolution with orography

Considering the apparent correlation between the AV index and elevation, Figure 4.8 provides insight into the correlations between the AV mean and elevation for the Pyreneean region, allowing for a more comprehensive exploration of their spatial relationships. The scatter plot of precipitation (Figure 4.8.a) shows a negative relationship between ensemble mean AV and elevation, although the AV remains positive for the entire elevation range, consistent with Figure 4.2. Likewise, precipitation demonstrates a widespread negative correlation across nearly all members (Figure 4.8.b), implying that as elevation increases, the AV index tends to decrease. This findings aligns with the outcomes obtained in Sections 3.1 and 3.2, suggesting that while remains positive across the entire region there is a limitation of AV at higher elevations potentially related to constraints within the observational dataset at these altitudes. The set of models driven by CanESM2 (Code 1) exhibits notable positive correlation values, which can potentially be attributed to the widespread misrepresentation of precipitation by this GCM that is significantly improved through the dynamical downscaling process across the entire region.

Conversely, the relationship between AV and elevation for both temperatures demonstrate positive values, implying higher AV in the elevated regions. However, there are some distinctions in the scatter plots of tmax and tmin (Figure 4.8.a): while the AV for the tmax ensemble mean does not show a clear increase with elevation from 0 m to 1500 m, beyond 1500 m, there is a significant rise. In the case of tmin the positive relationship of AV and elevation is constant for the whole elevation range. Similarly, the correlation coefficients of the individual members are also generally positive (Figure 4.8.b). This observations align with the findings illustrated in Figure 4.6 and Figure 4.7. However, it is worth noting that there are some exceptions where negative correlation coefficients are observed. Specifically, in the model group driven by CNRM (Code 2) and by EC-EARTH (Codes 3 and 4), these negative correlations can be attributed to the excellent performance of the GCM, which limits the RCM's ability to improve the representation of the variable AV in those cases.

Figure 4.9 shows the evolution of the correlation coefficients between AV and elevation as a function of the percentile intervals, following a similar approach of Figure 4.4. The evolution of the AV of precipitation remains constant. However, the temperature results lead us to the conclusion that

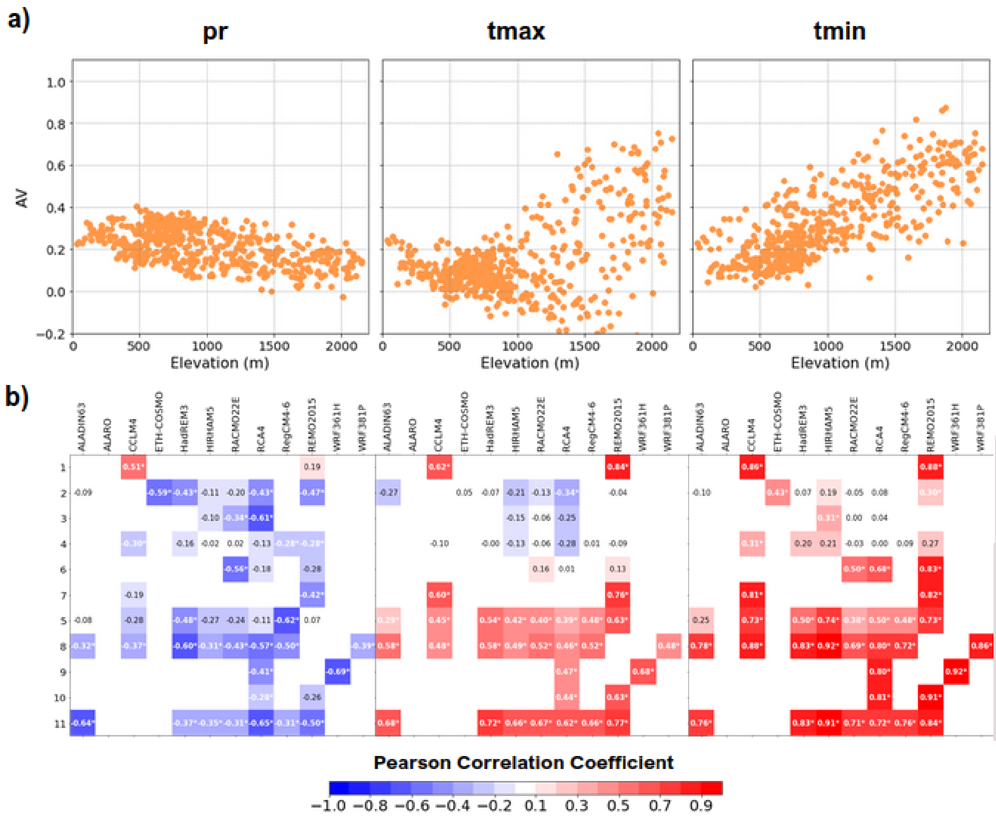

FIGURE 4.8: a) AV vs. elevation scatter plots for the ensemble mean for the variables precipitation, maximum temperature and minimum temperature b) Correlation coefficients between AV and elevation for all members of the variables precipitation, maximum temperature and minimum temperature. The matrix is formed by the RCMs (x axis) and the GCMs (y axis) expressed as the codes defined in Table 4.1. Asterisk (*) indicates a statistically significant correlation at 95 % from t-Student test.e and minimum temperature. Asterisk (*) indicates a statistically significant correlation at 95 % from t-Student test.

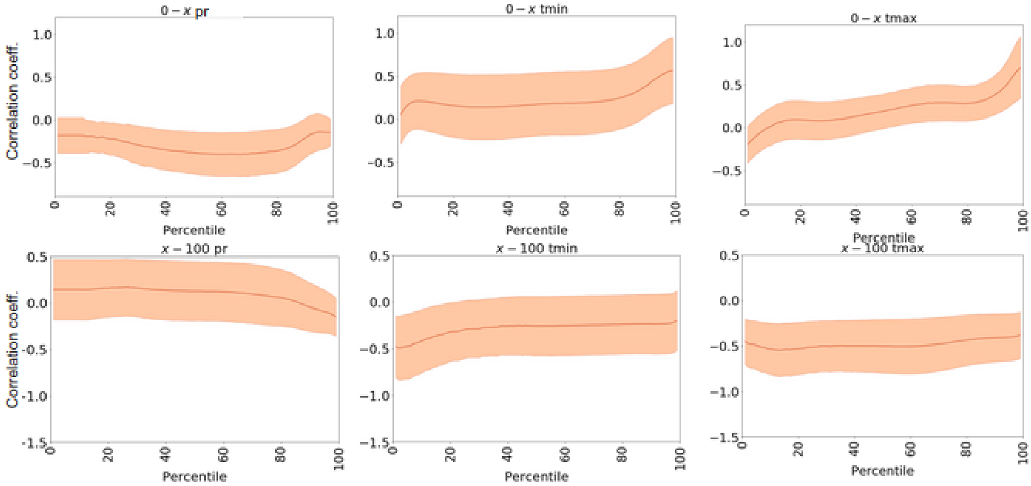

FIGURE 4.9: The variability of the correlation coefficients between AV index (AV in (4.2)) compared to CLIMPY, and elevation at different percentile intervals for 'pr', 'tmin' and 'tmax'. Each point x describes the correlation coefficient of the percentile interval '0–x' (up), and 'x–100' (down). The shaded area shows the standard deviation of the members.

the positive correlations observed for the entire PDF (Figure 4.8) are influenced by the upper tail of the distribution. This indicates that dynamic downscaling enhances the representation of warm events in the higher regions. However, negative correlation values were noted in the lower end of the temperature distributions. This, combined with the low AV values of the temperatures in the lower tails (Figure 4.4d,g; Figure 4.6 and Figure 4.7), suggests that the inadequacy of the lowest tails of representation of the temperatures by the RCMs is primarily located in the high altitude regions.

4.5 Discussion

There is a clear positive added value of using high-resolution RCMs derived from a dynamically downscaling of low-resolution GCMs, rather than using the latter, particularly in relation to precipitation at both resolutions: at 0.11○ (Figure 4.2) and at 1.00° (Figure 4.3). This finding aligns with previous studies analyzing precipitation at European scale, including topographically complex regions such as the Alpine Range and the Iberian Peninsula, among others (Careto et al., 2022c; Terzago et al., 2017). The improvement of simulating precipitation in the RCMs can be attributed to a better representation of topographically induced local circulation due to an increase in the spatial resolution (Careto et al., 2022c). Also, Prein et al. (2016) suggested that this positive AV stems from a more accurate depiction of precipitation in areas influenced by prevailing westerly winds, particularly evident during winter months when synoptic-scale flow plays a dominant role in the European sector. This is consistent with our results showing an increase in the AV index, particularly in the western part of the Pyrenees where westerly disturbances coming from the Atlantic Ocean contribute the most to winter precipitation.

Similarly, in the case of maximum and minimum temperatures, a positive AV is identified when using RCMs, particularly in higher elevation areas of the Pyrenees in both resolutions (Figures 4.2 and 4.3). Specifically, a more extensive positive AV is observed for minimum temperatures compared to the maximum temperatures which is consistent with the conclusions drawn by Cardoso and Soares (2022), who found larger positive AVs for the minimum temperature than for the maximum temperature in Europe. The high AV values for minimum temperatures can be attributed to the GCMs' potential misrepresentation of orographically induced minimum temperatures, which are automatically rectified by considering topographic features more accurately through resolution refinement (Perkins et al., 2007). In fact, Di and Ramo (2013) established that the potential added value of 2–m temperature provided by RCMs in the North American region, particularly in areas with complex topography, could be directly attributed to more than 65% of orographically induced simple interactions. Specifically, this pertains to the general correlation between temperature and terrain elevation. Thus, a more detailed representation of elevation gradients would significantly enhance the temperature portrayal of GCMs, even in the absence of fine-scale atmospheric processes. Consequently, it remains to be determined the extent to which the achieved AV might be mitigated by considering the simple relationships between high-resolution surface forcing and the low-resolution maximum and minimum temperatures. Additionally, Cardoso and Soares (2022) suggest that positive AV values for maximum temperatures over the Iberian Peninsula are associated with improved representations of precipitation and snow, mainly regarding the better representation of snow free surfaces.

It is important to note that significant variations exist in the signals of individual members (Figures B.1–B.6) at both resolutions, indicating substantial dependence of the AV on the driving GCM. This behavior underscores the notion that the quality of the GCM driver may limit the RCM's ability to enhance the representation of the variable. In the case of precipitation, the excellent performance of the MPI-ESM-LR model (Codes 8 and 9; Brands et al. (2013)) leads to lower AV values. However, for the EC-EARTH GCM (Codes 3 and 4), characterized by good precipitation representations (D_{GCM}=0.32 and 0.29 respectively for 0.11° resolution), the downscalling continues to yield significant AV values. This observation suggests the presence of other influential factors shaping the relationships between the AV and the models. One such factor may involve the accurate or deficient positioning of storm tracks by the GCMs. Dynamic downscaling holds promise for enhancing precipitation characterization, provided the GCM accurately identifies the positioning of storm tracks. However, if the GCM fails to do so, the potential AV of the RCM may be limited. Indeed, Zappa et al. (2013) highlight the importance of correct storm track positioning for the EC-EARTH GCM (Codes 3 and 4). Conversely, the HadGEM GCM (Code 5) exhibits similar D_{GCM} values (0.27) to EC-EARTH, yet dynamic downscaling does not lead to an improved variable characterization, resulting in a lower AV. This discrepancy could be attributed to the model's poor positioning of storm tracks during the summer months at the longitudes of the study area (Zappa et al., 2013). Likewise, for both minimum and maximum temperature, GCMs with better performance, such as CNRM-CM5 (Code 2; McSweeney et al. (2015)), restrict the AV achieved through dynamic downscaling using RCMs. In other words, a low D_{GCM}, indicating a better variable representation by the GCM, constrains the RCMs' capacity to improve upon that representation, resulting in diminished AVs. Despite the nuanced character of the improvements brought about by downscaling in this context, they remain pertinent in certain instances. For instance for the 0.11° resolution, in the CNRM+CLMcom-ETH model, low and comparable D_{GCM} values are observed for both tmax and tmin, standing at 0.31 and 0.33, respectively. However, while the AV of downscaling for tmax is nearly zero (-0.007), for tmin it stands at 0.12, signifying a noteworthy enhancement in variable representation. Similarly, the EC-EARTH driver exhibits Dgcm values around 0.41 for both temperature variables and the RCM RCA4 manages to improve tmax representation by 0.03, while the AV for tmin approaches zero.

The employed methodology allows for a more in-depth examination of AV through different intervals of the probability density function (PDF). It is observed that all GCMs consistently underestimate high rainfall events, while exhibiting an overrepresentation of light rainfall events (Figure 4.4c), as also been highlighted by Perkins et al. (2007). RCMs succeed in significantly improving the representation of events above the 90th percentile, as reflected in the AV's evolution relative to the percentile, particularly evident in the x–100 case (Figure 4.4b). However, for precipitation rates below 10 mm/day, RCMs record higher precipitation values than observations, resulting in an intersection between the PDF of observations and the PDFs of RCMs. This intersection is also evident in Figure 4.4b, manifesting a minimum in the AV (Ciarlo et al., 2021). Consequently, RCMs face challenges in representing light rainfall events and dry events (Boberg et al., 2009, 2010; Soares and Cardoso, 2018; Careto et al., 2022c). It is important to acknowledge that while these limitations in reproducing minimum precipitation events exist, they are unlikely to significantly influence the characterization of total precipitation. This is because such events typically contribute minimally to the overall precipitation amount (Dai, 2001).

At the spatial level (Figure 4.5), the lowest AV values within percentile intervals (0–50, 0–75, 0–90) are concentrated in the easternmost extremity of the mountain range, characterized by a Mediterranean climate (Lemus-Canovas et al., 2019), where water recycling through soil moisture-atmosphere feedback plays a critical role (Rios-Entenza et al., 2014; Careto et al., 2022c), due to the importance of the contribution of evapotranspiration in the precipitation regime, especially in the summer months, which could lead to an overrepresentation of light precipitation events.

Further exploration of the contributions of PDF intervals to temperature AV reveals that while the AV remains close to zero around the mean values of the PDF, it is the tails ends of the temperature PDFs that shape the signal. GCMs tend to overestimate higher percentile events while underestimating the lower tail events (Figure 4.4f, Figure 4.4i), in line with the findings of Perkins et al. (2007). Dynamical downscaling significantly improves the representation of upper tail extremes in both maximum and minimum temperatures, primarily over the central region of the Pyrenees characterized by higher elevations. Moreover, greater benefits are observed for minimum temperatures compared to maximum temperatures (Cardoso and Soares, 2022). Conversely, there is a general decline in the representation of lower tails for both temperatures, indicating that dynamical downscaling has a negative effect on simulating cold extremes. Additionally, difficulties arise in representing accurately near-freezing temperatures (Figure 4.4f, Figure 4.4i), leading to an overestimation of maximum and minimum temperatures close to 0 $^{\circ}C$, as also noted by Careto et al. (2022a). These deficiencies in RCMs are associated with problems in simulating snow dynamics and its interactions, influencing snow-albedo feedback and surface flux partitioning. Terzago et al. (2017) reported thicker snowpack over the alpine ridge and shallower snowpack in lower elevation regions simulated by RCMs compared to observational datasets. Such biases in snowpack representation likely contribute to biases in simulated snow-albedo feedback and surface temperatures (Minder et al., 2016). These biases in extreme minimum temperatures manifest as negative AV values at the left extreme of the PDF for both temperatures, spreading across the entire Pyrenees area. An additional significant aspect of the added value regarding maximum and minimum temperatures is the presence of inter-member variability within the extreme tails of the distribution. This variability is closely linked to the GCMs' ability to simulate temperature patterns.

The findings additionally reveal significant correlations between AV values and orography in the Pyrenees region, emphasizing the significance of elevation when assessing the performance of climate simulations (Reder et al., 2020). The negative correlation values point to a negative AV in high-altitude regions specially in high precipitation rates, potentially indicating the limited quality of observations at these points (Torma et al., 2015). Concerning temperatures, there exists a positive correlation at the right tail of the distribution, indicating that high AV values are concentrated in high-elevation regions in warm events. Conversely, a negative correlation in the left tail suggests that, for cold events, higher-altitude regions yield lower AV values.

4.6 Conclusions and connections

This chapter presents a comprehensive assessment of the added value provided by Regional Climate Models (RCMs) compared to Global Climate Models (GCMs) in the high mountain region of the Pyrenees for the variables precipitation, minimum temperature, and maximum temperature. To conduct this analysis, the CLIMPY observational database as a reference was employed. The assessment delves into both the spatial distribution of added value as well as the contribution of Probability Distribution Function (PDF) intervals of the analyzed variables to the overall added value. This chapter facilitates the achievement of **Objective 3**, which entails identifying both the strengths and limitations present in climate simulations. Furthermore, it contributes to the **Milestone 2** by conducting an in-depth analysis of the predictive tools employed in forecasting future climate changes.

The results obtained highlight a significant enhancement achieved through dynamical downscaling in accurately reproducing mean precipitation across the central and southwestern parts of the mountain range. Notably, these regions are influenced by westerly disturbances that play a key role in shaping the precipitation regime. The mean maximum and minimum temperatures also exhibit positive added values, particularly evident in the higher elevations of the Pyrenees and are potentially related to the spatial resolution refinement.

Examining the contributions of individual model members to the added value reveals a significant dependence on the quality of the GCM simulation. This dependency implies that the GCMs limits the RCMs capacity to enhance the representation of these variables effectively.

Analyzing the precipitation through PDF intervals uncovers that dynamical downscaling enhances precipitation events exceeding the 90th percentile, while hampers to adequately represent lower precipitation rates, notably in the eastern region where a Mediterranean climate prevails. The overestimation of low precipitation rates likely stems from an inadequate representation of water recycling through moisture–atmosphere feedback by RCM models. Negative added value values are registered in the higher Pyrenean regions, potentially attributed to observational data deficiencies.

Regarding the temperature percentile intervals, the impact of downscaling becomes particularly apparent at the extremes. These extreme events also exhibit amplified spatial and inter-member variability. RCMs showcase an improved ability to capture warm events in the highest regions compared to GCMs. Conversely, dynamical downscaling's effectiveness in representing cold extremes is compromised, especially in the elevated areas where snow dynamics wield more influence.

These findings underscore the significant contributions of RCMs in accurately characterizing precipitation, minimum temperature, and maximum temperature variables. Nevertheless, it remains imperative to recognize their limitations, thereby facilitating the responsible utilization of RCM data for both historical periods. In addition, this information obtained from a historical period analysis is valuable when applying future projections of climate models. Liang et al. (2008) claim that the main biases present in the historical simulation of both RCMs and GCMs are systematically propagated into the projected future climate at regional scales, suggesting that the strengths and weaknesses of RCMs pointed out by this study will also be reproduced for future scenarios. Therefore, being aware of these advantages/limitations is essential for a more informed application of such data in the development and implementation of adaptation plans and risk management strategies for the future. Notably, these limitations manifest themselves in the sparse portrayal of dry and cold events by RCMs. The former could be linked to the misinterpretation of evapotranspiration's impact on precipitation patterns in Mediterranean regions within the Pyrenees. The latter could be primarily attributed to the models' deficiency in effectively simulating snow dynamics. This challenge assumes particular significance in the elevated regions of the Pyrenees, where snow dynamics have a substantial influence.

Chapter 5

Machine Learning Approaches for Improvement of Climate and Hydrological Characterization

Accurately characterising future climate is of cucial importance for medium and long-term water resource planning and management within the context of climate change (IPCC, 2022). While General Circulation Models (GCMs) and Regional Climate Models (RCMs) (Jacob et al., 2014; Giorgi et al., 2009) have emerged as powerful tools for climate prediction (Semenov and Stratonovitch, 2010), they still exhibit certain limitations when it comes to representing regional climates affected by small-scale processes as discussed in Chapter 4 (Torma et al., 2015). Hence, the development of new techniques to mitigate these deficiencies and uncertainties becomes imperative. In this chapter, a novel approach rooted in Machine Learning is explored for constructing Multi-Model Ensembles, aligning with **Objective 4**. This chapter, together with Chapter 4, completes the **Milestone 2** of the thesis.

Firstly, the chapter introduces us to the concepts of Multi-Model Ensembles (Section 5.1). It then proceeds to delineate the study basin, along with the variables and databases utilized (Section 5.2). Subsequently, it elucidates the methodology, rooted in the development of Machine Learning algorithms and the application of the hydrological model (Section 5.3), before concluding with an analysis and discussion of the results (Section 5.4).

5.1 Multi Model Ensembles of climate simulations

Despite the clear advantages of RCMs over GCMs in capturing the primary features of regional climate (Chapter 4) (Kotlarski et al., 2014; Ciarlo et al., 2021), inherent uncertainties persist, extending beyond the scope of downscaling. These uncertainties encompass structural disparities in both GCM and RCM models (Knutti et al., 2008), the downscaling technique itself (Zhu et al., 2019), model parametrizations in reference to physical processes (Chen et al., 2011), and initial conditions, among other factors (Knutti et al., 2008; Dey et al., 2022). Furthermore, in studies conducted at the catchment scale, such as those examining the impacts of climate change on water resources, a scale mismatch remains, at times leading to unresolved climatic dynamics beyond the capabilities of RCM resolutions (Crawford et al., 2019). Consequently, these uncertainties can result in significant discrepancies in climate change projections between different RCMs, even when considering identical emission scenarios (Ruane and McDermid, 2017). This, coupled with the scale mismatch that introduces limitations in climate representation, hampers the effective utilisation of this data for catchment-scale planning and water resource management (Venkataraman et al., 2016).

Impact modellers employ a wide array of methods to tackle these uncertainties and errors, encompassing a broad spectrum of complexities. These methods span from identifying the best-performing simulations within the study area (Crawford et al., 2019; Xu et al., 2020) to the utilisation of bias correction techniques with observational data (Dobor and Hlásny, 2019; Teng et al., 2015; Piani et al., 2010), and extend to the development of Multi-Model Ensembles (MMEs)(Calì Quaglia et al., 2022; Salman et al., 2018). Bias correction methods have been instrumental in rectifying the systematic biases inherent in simulations (Piani et al., 2010). Nevertheless, they often prove less efficient in addressing non-stationary biases (White and Toumi, 2013; Wang et al., 2018). A promising avenue for addressing the uncertainty of climate models lies in the development of MMEs, which have the potential to mitigate uncertainties and enhance the confidence in climate projections (Pavan and Doblas-Reyes, 2000; Lutz et al., 2016; Sanderson et al., 2015; Keller et al., 2019). MMEs are categorised into two distinct groups: SEM (Simple Ensemble Mean) and WEM (Weighted Ensemble Mean). In the former approach, all ensemble members are uniformly assigned equal weights, whereas in the Weighted Ensemble Method (WEM), each member is allocated a distinct weight determined by its proficiency in replicating past climate conditions (Oh and Suh, 2017; Ahmed et al., 2020). SEM, known for its simplicity, is a commonly employed method, which provides an overall better performance than individual members (Lambert and Boer, 2001). However, it comes with certain limitations. Many of the models share model parameterizations and components, which can lead to interdependencies between different climate simulations (Sanderson et al., 2015). Failing to account for this interdependence may result in misleading model consensus, reduced accuracy, and a flawed estimation of uncertainty (Herger et al., 2018). Moreover, SEM may not be suitable for all applications, as it significantly diminishes the spatial and temporal variability of information when compared to individual members and observational data (Wang et al., 2018).

In contrast, WEM methods have demonstrated their capacity to mitigate the impact of systematic biases within individual members and even enhance the ensemble's predictive capabilities (Krishnamurti et al., 1999, 2000). The use of Machine Learning algorithms to generate a Multi-Model Ensemble (ML–MME) is an emerging technique in climate simulation (Zhu et al., 2023; Sand et al., 2023). These algorithms have a significant potential to enhance the outcomes of climate simulations, especially in relation to its potential advantages in dealing with non-linearity between response variables and predictors (Ahmed et al., 2020; Sachindra et al., 2018; Xu et al., 2020). Krishnamurti et al. (1999) established a precedent of an MME based on multiple regression techniques to improve the 850 hPa meridional wind speed and precipitation simulations of eight general circulation models, obtaining superior results over the ensemble mean. Wang et al. (2018) employed four Machine Learning (ML) techniques to develop MMEs for mean monthly temperature and mean monthly precipitation by considering 33 CMIP5 GCMs over Australia and reported that Random Forest (RF) and Support vector machine (SVM) demonstrated a significant improvement over the ensemble mean, which is in agreement with the results reported by Sa'adi et al. (2017) who employed a Generalised Linear Model (GLM) to construct their MMEs obtaining better results for the MMEs than for the 20 individual members of the CMIP5 GCMs over Borneo Island, Malaysia. Results along these lines have been reported in studies in Iraq for monthly mean temperature (Salman et al., 2018), in Pakistan for monthly precipitation (Ahmed et al., 2020), or in the Gulf Basin and North America for both (Crawford et al., 2019). Daily scale studies also show favourable results for ML–MME techniques (Jose et al., 2022). Likewise, Dey et al. (2022) obtained significant improvements in the characterisation of these climate variables with data from CMIP6 GCMs.

In our study, we ventured into a novel approach by applying various

ML–MME methods to RCMs for the first time. These methods were then further applied to a hydrological model. We subjected them to a comparative analysis against the SEM (Simple Ensemble Mean) approach, focusing on monthly precipitation (pr), the monthly average of daily maximum temperature (tmax), and the monthly average of daily minimum temperature (tmin). Specifically, the ML–MME techniques encompassed Linear Regression (LR), Gradient Boosting (GB), and Random Forest (RF). This investigation is particularly noteworthy as we apply it to a complex topography region, which adds a layer of novelty to our research given the challenges it presents for simulation (Torma et al., 2015; Reder et al., 2020). First, a ranking of the RCMs has been developed based on their skill to characterize the past climate and the optimal number of RCMs to be included in the ML-MMEs has been determined. Once the final ML–MMEs for the three variables have been defined, the monthly series were analysed in detail by comparing them with the climate observations. To illustrate the practical utility of the ML–MMEs in the application of impact studies at the watershed scale, we employed them as input data for the Temez hydrological model, both for historical periods and future climate projections within the study area.

5.2 Data and study area

We considered the EURO-CORDEX ensemble (Jacob et al., 2014, 2020), with a total of 72 RCM simulations (Table C.1) with a spatial resolution of $0.11^\circ \times 0.11^\circ$ (explained in Section 5.4.2) . CLIMPY observational dataset (Cuadrat et al., 2020a; Serrano-Notivoli et al., 2017) is used as reference, with a spatial resolution of 1 km $\times$ 1 km on a daily basis covering the period 1980–2015 (further explanation can be found in Section 5.4.2). For the proper comparison between the data from simulations and observations, both must be on the same grid. Thus, an bilinear interpolation to a the rectilinear grid o the RCMs of $0.11^\circ \times 0.11^\circ$ resolution of CLIMPY has been performed.

The Esca River basin is located in the western Pyrenees, northeastern Spain, and covers an area of 425 km^2, which corresponds to four grid-cells of the climate datasets. Characterised by a large altitudinal gradient, the elevation of the highest point of the basin is 2,100 m, while its lowest point is 595 m above sea level. Orographic characteristics make this type of basin remarkably difficult to simulate its climate dynamics (Kotlarski et al., 2014; Smiatek et al., 2016) Therefore, they are particularly problematic areas for accurately predicting the future climate and its related impacts in hydrology (Fatichi et al., 2016). It is important to make efforts to overcome these difficulties, particularly in cases such as the Esca river basin, since it is a key tributary feeding the Yesa reservoir, the primary reservoir in the western Pyrenees. Data on streamflows of the Esca river were available from the website of the Spanish Centre for Hydrographic Studies (CEDEX) (https://ceh.cedex.es/anuarioaforos/default.asp), where data are updated to September 2017.

The selection of the variables pr, tmax and tmin is motivated by two primary considerations. Firstly, their availability within the CLIMPY database (Cuadrat et al., 2020a). Secondly, these variables are pivotal for characterizing the climate system, as emphasized in prior studies (Meehl et al., 2000; Perkins et al., 2007; Careto et al., 2022d,b), and play a crucial role in influencing diverse hydrological (Piani et al., 2010), biological, and industrial systems (Colombo et al., 1999; Coppola et al., 2021).

5.3 Methodology

This study follows a specific methodology, which progresses through several phases:(1) a ranking of the RCMs was developed according to the performance of the three analyzed variables—tmax, tmin, and pr—on a seasonal scale (Section 5.3.1), (2) the SEM and the ML–MMEs were constructed (Section 5.3.2) and (3) the optimal number of RCMs to form the MMEs was chosen (Section 5.3.3). (4) The definitive MMEs were evaluated (Section 5.3.4). Then, (5) to assess the impact of climate variables MMEs on flow characterization, we utilized these MMEs as input data for the Temez hydrological model (Section 5.3.5). Finally, (6) as an illustrative example of application of ML–MME results for climate change impact assessment, the definitive ML–MME algorithms were applied to the climate projections of the RCP8.5 emissions scenario.

The methodology proposed in the described 1, 2, 3 and 4 steps follows an outline of the data analysis processes (Berthold et al., 2010) presented in Figure 5.1. The methodology initiates with a feature selection process aimed at eliminating noise-inducing features (RCMs) from the dataset, thus ensuring the development of a stable and reliable prediction model. This involves conducting an RCM ranking followed by the application of a filter-wrapper technique to identify the most suitable features. Upon selecting the optimal RCMs, various ML models are generated by optimising their hyperparameters using cross-validation. Subsequently, MMEs

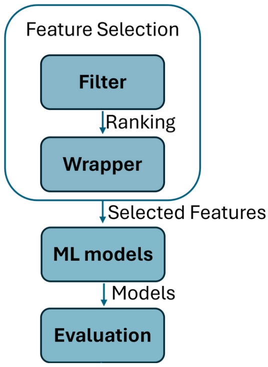

FIGURE 5.1: Outline of the stages of the data analysis process followed in the work conducted in Chapter 5.

of tmax, tmin and pr are generated using the developed ML algorithms. These MMEs were subjected to an statistical performance evaluation.

5.3.1 Ranking of RCMs

Within intelligent data analysis, one of the first phases is data pre–processing. In this instance, a selection of characteristics was applied to create an RCM ranking and to select those with the most relevant information for the attainment of a reliable predictive model. The procedure followed entails filter-wrapper processing, which consists of two parts: the filter part and the wrapper part. Initially, a ranking was created using a quantitative measure (filter part), and subsequently, the most relevant ones were selected (wrapper part– Section 5.3.3). Thus, the following procedure was applied to rank the RCMs according to their performance based on the observational data: The time series of pr, tmax, and tmin were divided into the four seasons representative of the Atlantic climate of the study area, namely, winter (DJF), spring (MAM), summer (JJA) y autumn (SON). For each variable and season the TSS (Taylor Skill Score, Taylor2001) was calculated (filter index). The TSS provides a quantitative measure of the ability of each RCM to simulate the variables pr, tmax, and tmin. It is based on the correlation and the ratio of the standard deviation of the RCMs against the observations of a given climate variable:

$$\mathrm{TSS} = \frac{4(1+R)^4}{(\sigma_f + 1/\sigma_f)^2 (1+R_0)^4}\,, \tag{5.1}$$

where σ_f refers to the ratio of the standard deviation of the RCMs versus the observations, R refers to the Pearson correlation coefficient, and R_0 represents the maximum value of the correlation, namely 1. TSS ranges from 0 to 1. A higher value indicates better simulation performance, while a lower value indicates worse performance. Based on the TSS results, twelve rankings were obtained, one per variable and season, which were taken into account to calculate the metric value rating RM (Ahmed et al., 2020):

$$\mathrm{RM} = 1 - \frac{1}{nm}\sum_{i=1}^{n} \mathrm{rank}_i \ , \tag{5.2}$$

where n and m represent the number of RCMs and seasons, respectively, while rank_i refers to the number of the ranking corresponding to the member at the i^{th} season. Finally, the RCM members were ordered according to the RM. As a result, we obtained a ranking of the RCM models ordered from best to worst according to their performance in relation to observational data in the studied basin.

5.3.2 Development of SEM and ML–MME algorithms

After developing the ranking of the RCMs, the MMEs structure and characteristics have been designed. In the first place, when formulating ML–MME algorithms, it is crucial to account for the seasonal dynamics inherent in the variables. This consideration enhances the algorithms' ability to discern patterns of variability. Due to the evident interannual temperature dynamics in out mid-latitude region, we have opted to consider the seasons independently, specifically for tmin and tmax when constructing the ML–MME algorithms (Morales-García et al., 2023; Ahmed et al., 2020). Conversely, with precipitation, we have pursued an alternative strategy: Given the complex nature of this variable and the alterations observed in the annual cycle over recent decades in European mid-latitudes (Christidis and Stott, 2022; Paluš et al., 2005), establishing clear seasonal patterns becomes a more intricate task. Designing ML algorithms solely based on the seasons might prove misguided, potentially hindering the algorithms from accurately capturing the variable's behaviour.

To address this complexity and unbalance of the data , we have chosen to consider monthly precipitation events categorising them into two subgroups Chao et al. (2018): those exceeding the 80^{th} percentile and those below it according to observational data. Through the separation of precipitation into two distinct databases, the range of the variable was reduced, leading to increased accuracy in the results obtained by the ML models. Following this rationale, each ML–MME technique has resulted in four algorithms for tmax and tmin, corresponding to each season. Additionally, two algorithms have been generated for precipitation: one for events within the 0–80 percentile interval and another for events in the 80–100 percentile interval.

Different methods were applied to construct the MME on a monthly scale, including, on the one hand, SEM, and on the other hand, three ML techniques: RF, GB and LR. The first MME development technique is the SEM, commonly and widely used for MME calculation (Clark, 2017). The remaining three techniques are more elaborate and are based on ML regression models. These three techniques are detailed below:

- Random Forest (RF). RF is a machine learning technique whose basis is a combination of predictor trees such that each tree depends on the values of a random vector tested independently and with the same distribution for each of them. It is a substantial modification of bagging that builds a large collection of uncorrelated trees and then averages them. The algorithm for inducing a random forest was developed by Breiman (2001). Bagging is the ensemble learning method typically used to reduce the variance within a noisy data set. The RF method combines the idea of bagging and random attribute selection to build a collection of decision trees with controlled variation. The selection of a random subset of attributes is an example of the random subspace method, a way to perform stochastic discrimination (Breiman, 2001).
- Gradient Boosting (GB). GB is a machine learning technique for regression analysis and statistical classification problems based on boosting. Boosting consists of combining the results of several weak classifiers to obtain a robust classifier. When these weak classifiers are added, they are added in such a way that they have different weights depending on the accuracy of their predictions. After a weak classifier is added, the data changes its weight structure: cases that are misclassified gain weight and those that are correctly classified lose weight. Thus, the strong classifiers focus more strongly on the cases that were misclassified by the weak classifiers. The GB technique creates a predictive model based on weak prediction models, usually decision trees. The GB is an ensemble that provides a set of prediction models, which conclude a satisfactory prediction outperforming in some cases the random forest ensemble (Bentéjac et al., 2021).

- Linear Regression (LR). LR is a supervised learning algorithm used in machine learning and statistics. In its simplest version, it calculates a line that will indicate the trend of a continuous data set. LR can be defined as an approach to model the relationship between a dependent scalar variable and one or more explanatory variables. The LR technique should minimise the cost of a quadratic error function and those coefficients will correspond to the optimal line. There are several methods to minimise the cost. The most common is to use a vector version and the so-called Normal Equation which will give a direct result (Weisberg, 2005).

For the selection of the hyperparameters of the machine learning techniques, a Grid has been used by means of cross-validation to sweep through all the parameters and thus select the most optimal ones.

5.3.3 Selection of RCMs

After the RCM ranking was completed and the MMEs characteristics defined, the process of selecting the optimal number of RCMs to be considered when creating the MMEs for each variable (tmax, tmin and pr) was initiated. This process is the wrapper part of feature selection presented in Figure 5.1. The MMEs were developed considering the RM-based rank of RCMs from 1 to 40 (Table C.1). Initially, only the outputs of the RCM with a rank of 1 were used to provide inputs to the MME. Subsequently, the outputs of the RCM with a rank of 2 were added to the input set, followed by the incremental introduction of RCMs with overall ranks 3, 4, 5 ... 40 into the input set, one RCM at a time. This approach, known as the top-ranked approach (Ahmed et al., 2020), started with the best-performing RCM (rank 1) and progressed with subsequent RCMs in ascending order of their RM-based rank.

The evaluation of the performance of the MME outputs, generated with varying numbers of RCMs, has been conducted on the reconstructed time series. This reconstruction of the results obtained by the MME has been carried out by transforming the data divided into seasons (tmax, tmin) or percentile intervals (pr) described in Section 5.3.2. into a time series.

The evaluation metric was the Modified Index of Agreement (*md*, (5.3)), which was initially proposed by Willmott (1981) and has been later widely applied (Ahmed et al., 2020). It ranges from 0 to 1, with higher values indicating a better fit of the model

$$md = 1 - \frac{\sum_{i=1}^{n}(x_{\text{obs},i} - x_{\text{sim},i})^j}{\sum_{i=1}^{n}(|x_{\text{sim},i} - \bar{x}_{\text{obs}}| + |x_{\text{obs},i} - \bar{x}_{\text{obs}}|)^j}\ , \tag{5.3}$$

where $x_{\text{sim},i}$ and $x_{\text{obs},i}$ are the i^{th} data point in the simulated RCM and the observed data series of a climate variable, respectively. It has been calculated for the four grid cells considered in this study.

With this procedure all RCMs are incoporated into the MMEs. Then the cut-off point is made just at the RCMs that start to worsen the *md* metric or when an overfitting issue is observed. This indicates that from that RCM onwards, the information provided by the other RCMs is more noisy than beneficial.

5.3.4 Evaluation of SEM and ML–MME algorthims

Once the selection phase was completed and the definitive MMEs were built, the evaluation was carried out. The data was divided in the training and testing phases, representing 80 % and 20 % of the data, respectively, divided chronologically. Therefore, the training phase covered the period of 1980–2006 while the test phase covered the period of 2007–2015. Notably, data from all four points in the mesh have been incorporated to feed the algorithms. Moreover, the evaluation was carried out with three additional metrics commonly used in the characterisation of time series similarities: the coefficient of determination (R^2), the root-mean-square error (RMSE), and the root mean square percentage error (RMSEPE).

5.3.5 Application of ML–MME data to Temez hydrological model

The Temez model (Témez, 1977), extensively applied in Spanish watersheds (Pérez-Sánchez et al., 2019; Escriva-Bou et al., 2017; Chavez-Jimenez et al., 2013; García-Barrón et al., 2015; Jódar et al., 2017; Marcos-Garcia et al., 2017; Senent-Aparicio et al., 2018b), falls within the category of aggregated watershed simulation models (Estrela, 1992). Operating from the onset of rainfall to the initiation of runoff and subsequent discharge into rivers, the Temez model manages moisture balances across interconnected processes within a hydrological system. Input variables for the Temez model encompass the spatial average monthly precipitation for the entire basin and Potential Evapotranspiration (ETP). In line with the current investigation's focus on monthly climate data, ETP was determined using the Thornthwaite method (Thornthwaite, 1948).

We assessed the hydrological model's outcomes based on four widely adopted evaluation criteria in hydrological research (Jimeno-Sáez et al., 2018). These criteria include the Nash–Sutcliffe Efficiency coefficient (NSE), the percent bias (PBIAS), the Pearson correlation coefficient (r), and the Kling–Gupta Efficiency coefficient (KGE).

After the evaluation of the four proposed ML–MME techniques, the algorithms were applied to future climate projections for the RCP8.5 emission scenario for long-term future and were utilized as input data for simulating future streamflow.

5.4 Results and discussion

5.4.1 Ranking of RCMs

Table C.1 presents the RCM rankings based on TSS across the DJF, MAM, JJA, and SON seasons for the variables tmin, tmax, and pr. Notably, substantial variations emerge among seasons and variables. In certain instances, an RCM that excels in simulating one variable and season finds itself at the lower end of the ranking when compared to other variables and seasons. A case in point is IPSL–RCA4 (Code 33), which stands out as the top performer in simulating precipitation during SON and JJA, as well as maximum temperature in SON. However, it exhibits inefficiencies in comparison to other RCM members when simulating precipitation in DJF and MAM (Kotlarski et al., 2014).

A notable observation is the high contribution of the GCM driver on the ranking position, which is in line with what is stated by Vautard et al. (2021), who established that some variables are conditioned by large-scale boundary conditions defined by the GCMs. For instance, RCM members driven by the MPI–ESM–LR GCM consistently achieve the highest RM values (Table C.1), indicating superior overall performance. This aligns with findings from Brands et al. (2013), underscoring the GCM's excellent ability to simulate precipitation over European mid-latitudes. A poor RCM performance, however, can also have a significant impact on the simulation, as in the case of the 60 and 48 models which, despite having the MPI as driver, occupy poor positions in the ranking. In the same way, RCMs with CNRM–CM5 as driver also rank high, because they are able to adequately characterise the temperatures (McSweeney et al., 2015).

Conversely, a GCM with deficiencies in simulating climate conditions adversely affects the ranking of RCMs that are driven by it. Such is the case with MOHC–HadGEM2, which exhibits notable biases in climate variables representation. Consequently, MOHC–HadGEM2 attains lower positions across all variables and seasons.

5.4.2 Selection of the optimal number of RCMs

To extract meaningful insights for determining the optimal number of RCMs to include in further analyses, we conducted an examination of the ML–MME learning curve. All machine learning techniques described previously have been used to select the number of RCMs. As depicted in Figure 5.2, the *md* values, relative to observations, are plotted against the number of RCMs utilised to construct the SEM and the ML–MMEs. The incorporation order of RCMs follows a top-ranked approach (Ahmed et al., 2020). Notably, for fewer than three RCMs, the *md* values exhibit a substantial increase initially, stabilising thereafter to an asymptotic trend for most ML techniques across all variables and periods. An exception is observed with GB, where, beyond a certain quantity of RCMs (for pr 16, for tmax 35 and for tmin 25), the *md* values approach 1. This indicates overfitting (Ying, 2019; Dietterich, 1995).

Upon closer examination of individual variables, precipitation stands out with notable differences between SEM and ML–MME. SEM records *md* values near 0.4, while ML–MME techniques yield values ranging from 0.6 to 0.8 (excluding the overfitting case of GB). For temperature variables, the initial *md* is higher, approximately 0.6, indicating that RCMs exhibit a greater capacity to replicate monthly temperature patterns compared to precipitation. This difference arises due to the higher complexity inherent in the dynamics of precipitation, which poses challenges for numerical models to simulate accurately (Perkins et al., 2007; Aghakhani Afshar et al., 2017), specifically affecting RCMs (Vautard et al., 2021; Herrera et al., 2020; Kotlarski et al., 2014). While improvements are observed in temperature variables with ML–MME, the contrast in *md* values is less pronounced, particularly for minimum temperature.

After reviewing the evolution of result improvements concerning the number of RCMs, and recognising a plateau after the initial progress, we opted to include a total of seven RCMs. This decision is motivated also to avoid instances of overfitting, as observed with GB for tmin variable, while maintaining a balance between model complexity and predictive performance. The number of models utilized aligns with the findings of

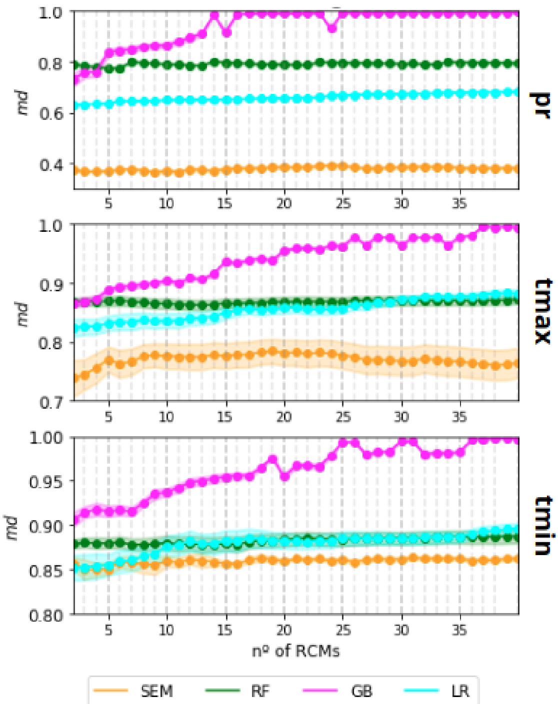

FIGURE 5.2: *md* vs. the number of RCMs for precipitation (pr), maximum temperature (tmax) and minimum temperature (tmin). The shaded area represents the standard deviation of the four grids of the mesh.

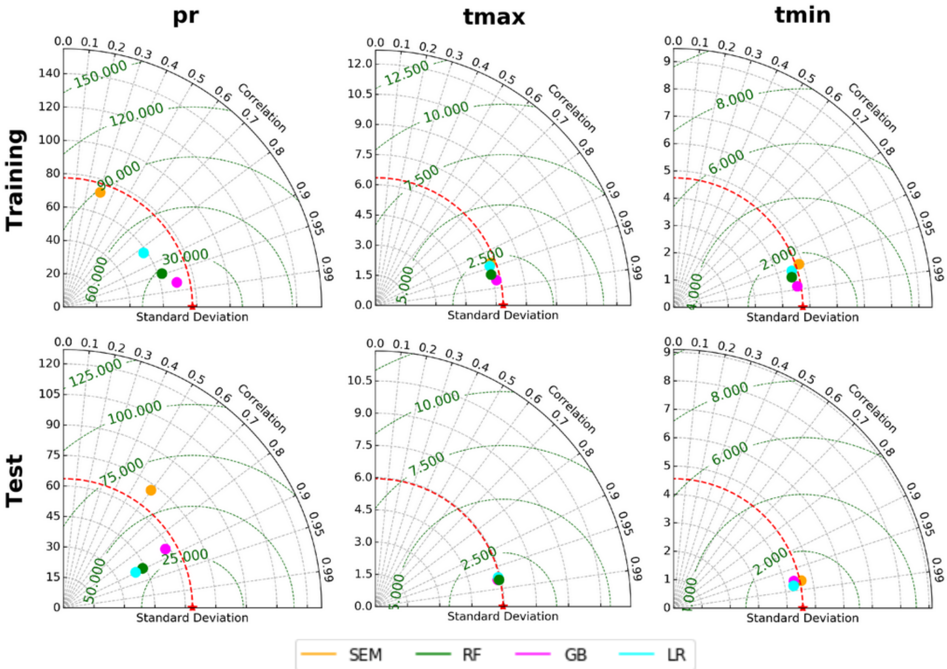

FIGURE 5.3: Taylor diagrams of the spatial average of the variables precipitation (pr), maximum temperature (tmax) and minimum temperature (tmin) for the training (1980–2006) and test (2007–2015) periods.

Dey et al. (2022), who, following a pre-selection process, incorporated 5 models into their analysis. Likewise, Ahmed et al. (2020) achieved comparable results in their precipitation analysis, drawing from data generated by 7-10 models exhibiting high performance.

5.4.3 Evaluation of SEM and ML–MMEs

Figures 5.3, 5.4, and 5.5 offer an assessment of the SEM and ML–MME results relative to CLIMPY observations for the variables pr, tmax, and tmin. To enhance result clarity, we focused on evaluating the spatial average of pr, tmax, and tmin within the study area. Notably, in the first column of Figure 5.3, the Taylor diagram for precipitation during both the training and test periods indicates substantial enhancements resulting from ML–MME application compared to SEM. Among the ML–MME methods, RF and LR yield comparable outcomes, while GB achieves the most favourable results at the annual scale for both training and test

FIGURE 5.4: Spatially averaged observed precipitation and simulated precipitation time series and evaluation metrics (SEM and ML–MME) for the training (1980–2006) and test (2007–2015) periods.

periods.

Concerning the spatial average of temperatures, Taylor diagrams do not reveal appreciable improvements. Both SEMs of tmin and tmax already exhibit statistics indicative of a robust representation of monthly temperatures in the study area, attributed to the high-quality simulations of the pre-selected RCMs (Table C.1). The exceptional starting point of RCMs' simulation quality may limit the potential enhancement capacity that ML–MMEs could offer.

For a more detailed analysis of precipitation performance, Figure 5.4 presents monthly time series plots of the spatial average results for SEM and ML–MME. The improvement across all ML–MMEs in comparison to SEM is evident. Whereas SEM exhibited a fit close to zero, high RMSE, and *md* below 0.5 in both periods, all ML–MME techniques demonstrate significantly improved performance, indicating their superior ability to simulate monthly precipitation patterns. Notably, GB achieves the best *md* results, with values of 0.88 and 0.75 for the training and test periods, respectively. RF, however, is not far behind, boasting an R^2 in the test period of 0.80, surpassing GB's 0.75. Despite LR showing higher RMSE values (around 44 mm/month) and a lower capacity to detect precipitation minima and maxima, the ML–MME based on LR markedly improves the representation of the study area's precipitation compared to SEM. These results are in line with those obtained in several studies (Acharya et al., 2014; Salman et al., 2018; Li et al., 2021). For instance, Dey et al. (2022) developed ML-based MME approaches for CMIP6 in an Indian River basin obtaining that the RF-based ML–MME showed improved performance compared to SEM. In the same vein, Jose et al. (2022) proposed RF as the best suitable ML model over India for creating MME and simulating the past observed climate variables, in a tropical river basin. In addition to studies conducted at basin scales, ML–MME approaches have also been applied at broader spatial scales. This is the case of Wang et al. (2018) who applied SEM, BMA (Bayesian Model Averaging technique), RF, and SVM with CMIP5 data over Australia, concluding that RF and SVM could generate better-performing MMEs compared to SEM and BMA.

Figure 5.5 provides a thorough evaluation of SEM, ML–MMEs, and the seven individual RCMs, both at the annual and seasonal scales during the test period. Notably, when comparing SEM with the ML–MME techniques, a widespread enhancement is observed, particularly in precipitation. For instance, the DJF season, which records the lowest *md* values (around 0.2) for individual RCMs, sees substantial improvement with ML–MME techniques, elevating *md* to approximately 0.55 for RF and LR, and surpassing 0.70 for GB. This improvement is consistent across all seasons and holds true for annual data as well. Similarly, R^2 and RMSE exhibit substantial enhancements across the board for precipitation. The coefficient R^2, which occasionally dips to 0 for certain RCMs and seasons, now consistently remains above 0.6 for all seasons and ML–MME techniques, reaching annual values of 0.8. The RMSEPE, expressed as a fraction, which exceeds 3 in some individual RCMs, is consistently below 1 for all ML–MME cases. This noticeable and significant improvement in the characterization of precipitation at both seasonal and annual levels, as evidenced by the three metrics analyzed in the study region, represents a significant qualitative advantage offered by ML-MMEs compared to the results obtained from individual

RCM members. This enhancement could potentially yield significant benefits for regional planning, including water and agricultural management, as well as climate risk preparedness, among others.

For temperatures, while no notable seasonal improvement is evident in *r* and *md*, annual values display enhancement for both tmax and tmin. However, the improvement in simulation quality, even at the seasonal scale, is manifested as a decrease in the RMSE values. Individual RCMs exhibit RMSE values ranging from 2.0 ºC to 5.2 ºC for tmax. Post-application of ML–MME techniques, RMSE is drastically reduced, with values between 0.8 ºC and 3 ºC. A parallel behaviour is observed for tmin. This improvement in temperature representation is of particular interest in an area like the analyzed study region, where the presence of snow and snowmelt processes are key factors directly dependent on temperatures, greatly influencing regional management.

In each examined case, MMEs consistently outperform individual members, even when represented by the least effective MME, SEM. This observation is supported by numerous studies that emphasise the MME's ability to enhance individual member performance and reduce climate output uncertainties. Notable analyses include regions such as India (Gusain et al., 2019), the USA (Srivastava et al., 2020), China (Zhuang et al., 2016), and Europe (Evin et al., 2021). Additionally, our results indicate that ML–MME exhibits superior performance to SEM, particularly for precipitation, as depicted in Figures 5.4 and 5.5. This finding underscores the ML–MME's relevance at the catchment scale. The enhanced performance of ML–MME over SEM may be attributed to ML approaches' capacity to address nonlinear, high-dimensional correlations between climate model outputs and observational datasets (Dey et al., 2022). Moreover, as highlighted by Li et al. (2021), ML–MME algorithms could be able to capture detailed information at local scales due to the incorporation of high-resolution observations on the construction of ML–MME algorithms.

In this study, we successfully integrate the EURO-CORDEX RCMs, the climatic simulations with higher spatial resolution for the study area, with the strengths of ML mathematical algorithms. This combination holds promise for reducing uncertainty in basin-scale climate projections. In the following section (Section 5.4.4), we utilise the outputs of the ML–MME algorithms to feed a hydrological model within the Esca River basin.

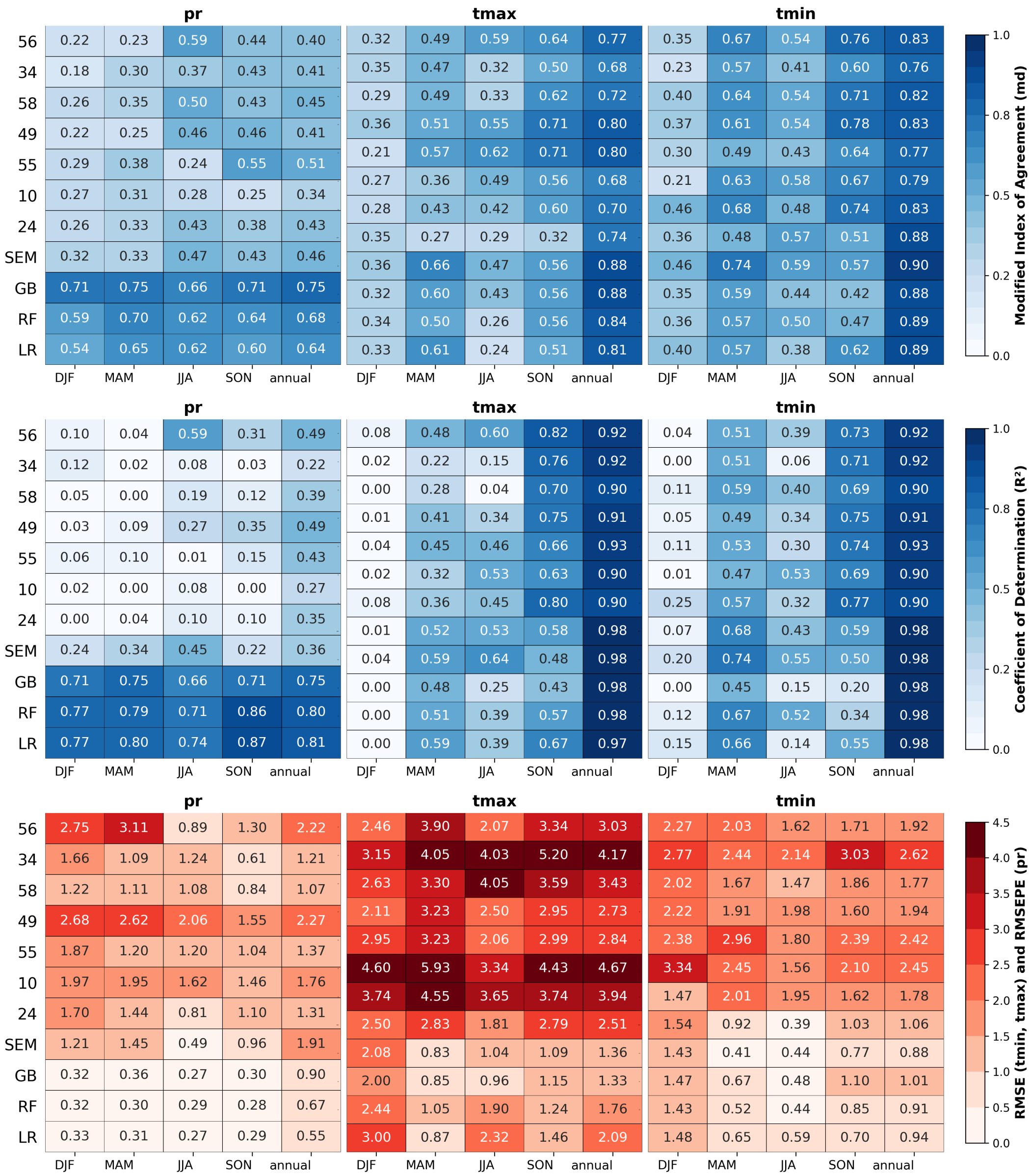

FIGURE 5.5: Heat maps representing the *md*, R^2, RMSE (tmax, tmin) and RMSEPE (pr) obtained from the comparison of the observations versus the SEM, the ML–MMEs and the individual RCMs for the test (2007–2015) period.

5.4.4 Application of SEM and ML–MME climate data to Temez hydrological model

5.4.4.1 Temez model setup

For the model setup development, the simulation period was divided into two distinct phases: the calibration period, spanning from 1981 to 2000, and the subsequent validation period, covering 2001 to 2014. A warm-up year was introduced to attain a stable state for the Temez model. Calibration focused on adjusting four key parameters: $H_{\max}$ (maximum soil storage capacity), C (surplus starting coefficient), $I_{\max}$ (maximum infiltration) and α (groundwater contribution coefficient). The first two parameters govern soil storage regulation, the third distinguishes surface runoff from groundwater runoff, and the fourth modulates subsurface drainage (Murillo and Navarro, 2011). Table 5.1 presents the metrics described in Section 5.3.4 for the comprehensive assessment of hydrological simulation.

TABLE 5.1: Calibration (1981–2000) and validation (2001–2014) results for the Temez hydrological model. The presented statistics are the Nash–Sutcliffe Efficiency coefficient (NSE), the Pearson correlation coefficient (r), the Root Mean Square Error (RMSE), the Kling–Gupta Efficiency coefficient (KGE), and the Percent Bias (PBIAS)

	NSE	r	RMSE	KGE	PBIAS
Calibration	0.63	0.85	13.27	0.78	-12.76
Validation	0.67	0.83	13.08	0.82	7.21

According to what was established by Moriasi et al. (2007) and Brighenti et al. (2019), the performance of the model both in the calibration and validation period is satisfactory since the results of NSE and KGE exceed 0.5 and the PBIAS reaches its maximum in the calibration period with -12.76 %, remaining below the ±25 %.

5.4.4.2 Evaluation of streamflow for SEM and ML–MME input data

Starting from the calibrated and validated Temez model, the simulations described bellow have been carried out in order to evaluate the impact of the climate-corrected data, which have been analysed in detail in section 5.4.3, on the characterisation of the flow variable. First, the monthly flow simulation has been developed by feeding the Temez model with data from precipitation observations and with the ETP derived from the tmax and tmin observations, denoted as $Q_{\text{sim-OBS}}$. Following the same approach, four additional flow simulations, subsequently identified as $Q_{\text{sim-SEM}}$, $Q_{\text{sim-GB}}$, $Q_{\text{sim-LR}}$ and $Q_{\text{sim-RF}}$, were developed. Each simulation incorporated input data derived from MME techniques: SEM, GB, LR, and RF, respectively. To facilitate the explanation, another term has been incorporated that refers to the group formed by the simulated flows using the climate data derived from the ML–MME, $Q_{\text{sim-ML–MME}}$.

Table 5.2 presents the statistics of the described simulations for the training period (1980–2006) and test period (2007–2015) of the ML–MME algorithms. The choice of these specific periods aligns with the study's focus on improving climate representation through ML–MME techniques and assessing the extent to which these improvements influence streamflow representation. The congruence in analysis periods for both climate variables and flow variables enhances the study's coherence. From the analysis of the statistics in Table 5.2 it is concluded that while the $Q_{\text{sim-SEM}}$ obtains unsatisfactory results for both periods, the ML–MMEs manages to enhance the representation of the flow significantly. Notably, both $Q_{\text{sim-RF}}$ and $Q_{\text{sim-GB}}$ exhibit statistics comparable to $Q_{\text{sim-OBS}}$, with NSE remaining above 0.60 for the training period and r achieving values exceeding 0.74 in both periods. The $Q_{\text{sim-LR}}$ simulation, although satisfactory, yields inferior results with higher PBIAS and lower NSE and KGE values. These outcomes signify that the improvements in climate variable representation by ML–MMEs propagate and significantly enhance flow characterisation in both the training and test periods.

TABLE 5.2: Statistics of simulated vs. observed streamflows for the training (1980–2006) and test (2007–2015) periods. The presented statistics are the Nash–Sutcliffe Efficiency coefficient (NSE), the Pearson correlation coefficient (r), the Root Mean Square Error (RMSE), and the Kling–Gupta Efficiency coefficient (KGE)

	Training				Test			
	NSE	r	RMSE	KGE	NSE	r	RMSE	KGE
$Q_{\text{sim-OBS}}$	0.67	0.85	12.55	0.81	0.60	0.82	15.00	0.78
$Q_{\text{sim-SEM}}$	-1.84	0.59	36.59	-0.27	-1.97	0.58	40.95	-0.36
$Q_{\text{sim-GB}}$	0.69	0.85	12.08	0.81	0.48	0.74	17.13	0.73
$Q_{\text{sim-LR}}$	0.56	0.77	14.48	0.69	0.52	0.74	16.42	0.61
$Q_{\text{sim-RF}}$	0.66	0.83	12.59	0.76	0.61	0.80	14.86	0.63

To further assess the performance of the hydrological simulations, the annual cycle for the four $Q_{\text{sim-ML–MME}}$ together with the $Q_{\text{sim-OBS}}$ and Q_{OBS} have been depicted in Figure 5.5. The latter refers to the observed flow rates. It is observed how in the training period (1980–2006) the annual cycle of the streamflow consists of two maxima in January and May and a minimum recorded in August and September. This interannual dynamics is captured by the calibrated and validated Temez model for the $Q_{\text{sim-OBS}}$ simulation. If we pay attention to the $Q_{\text{sim-MME}}$, we observe that while Q_{SEM} fails to characterise the annual cycle with a generalised overestimation of the flow that extends over most of the year, the other $Q_{\text{sim-MME}}$ accurately reproduce the hydrological cycle of the Esca river. The annual cycle of the test period (2007–2015) presents differences with respect to the training period, especially in the spring maximum, which is more accentuated and reaches 60 Hm^3. The Temez model with input data from climate observations ($Q_{\text{sim-OBS}}$) has more difficulty in simulating the hydrological cycle for this period, although it roughly succeeds in characterising it. The $Q_{\text{sim-ML–MME}}$ simulations accurately reproduce the $Q_{\text{sim-OBS}}$ cycle, especially $Q_{\text{sim-GB}}$, while $Q_{\text{sim-SEM}}$ demonstrates poor performance. In essence, the $Q_{\text{sim-ML–MME}}$ reproduce the interannual dynamics captured by the Temez model in the $Q_{\text{sim-OBS}}$ simulation, thus demonstrating that the improvements achieved in the climate representation derived from the application of ML–MME techniques have a positive impact on the characterisation of the hydrological cycle. On the other hand, it is important to highlight that the differences derived from the flow observations (Q_{OBS}) and the simulations are attributed to the errors provided by the Temez model, probably related to the misrepresentation of snow accumulation and melting processes by the hydrological model (Jimeno-Sáez et al., 2020).

5.4.5 Future projections of climate and hydrological variables

Thus far, it has been demonstrated that the utilization of ML-MME techniques has not only enhanced the representation of climate variables but has also significantly improved the accuracy of hydrological characterization during the historical period in the study area. Extending this methodology to future scenarios under the RCP8.5 emission scenario suggests that projections from trained ML–MME models may offer more realistic data than those from the SEM (Liang et al., 2008).

Figure 5.6. illustrates the annual cycles of the analysed variables—pr, tmax, tmin, and Q—for two distinct periods: historical (1986–2015), and long-term future (2065–2095). This figure juxtaposes simulation data from the ML–MME techniques with observational data from the historical

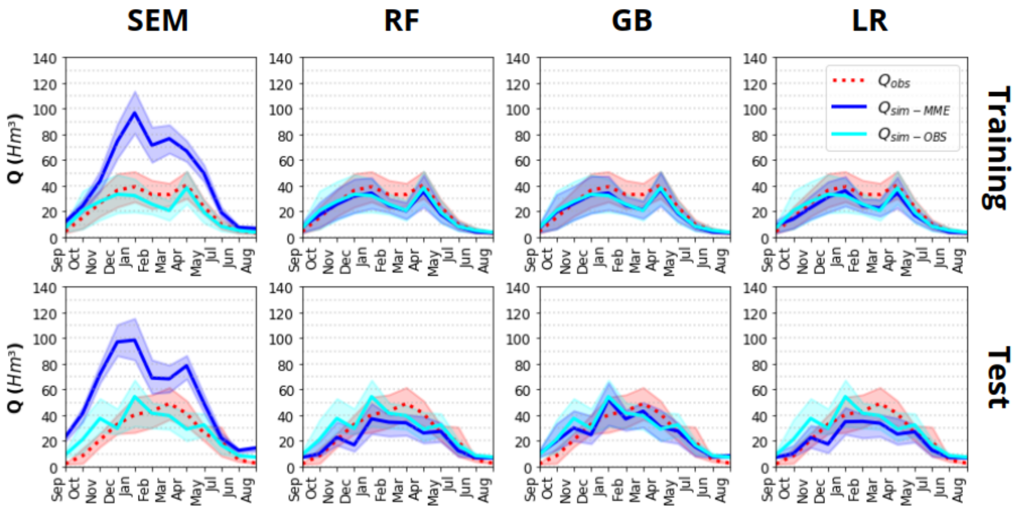

FIGURE 5.6: Annual cycle of streamflow for the training (1980–2006) and test (2007–2015) periods. Results are shown for observational flow data (Q_{OBS}), Temez-simulated flow with input data from CLIMPY climate observations ($Q_{\text{sim-OBS}}$) and Temez-simulated flow with input data from SEM and ML–MMEs ($Q_{\text{sim-MME}}$). The shaded area represents the annual variability of the streamflow results.

period. A comparative analysis reveals that ML–MME techniques better characterise climatic patterns compared to the SEM. Specifically, while the SEM tends to overestimate precipitation during DJF and MAM, the ML–MME captures the interannual dynamics more accurately, manifesting two peaks in April and November and a minimum that extends from June to August (Lemus-Canovas et al., 2019). Similarly, ML–MME techniques more precisely replicate interannual temperature variations. Further, the ML–MME techniques positively influence the streamflow annual cycle representation by the Temez model in the study area. Indeed, simulations driven by the SEM consistently exhibit overestimations, as discussed in Section 5.4.4, whereas RF–MME, GB–MME, and LR–MME demonstrate markedly superior performance.

These results and those analysed in sections 5.4.3. and 5.4.4. indicate that the ML–MME techniques provide more realistic information than SEM, also for the projections of the RCP8.5 emission scenario. If we focus on RF and GB we see that according to these projections, precipitation will decrease throughout the year except for DJF and MAM where will increase, thus modifying the interannual precipitation patterns. Concurrently, temperatures are expected to rise consistently (Amblar-Francés et al., 2020; Lemus-Canovas and Lopez-Bustins, 2021), with minimum temperatures notably increasing in March and April. These shifts in interannual dynamics will likely reshape the hydrological cycle, resulting in a more pronounced summer minima and intensified, albeit shorter-duration, maxima in February and March, as projected by RF and GB and in line with the results obtained in numerous Pyrenean Rivers (López-Moreno et al., 2014; García Ruiz et al., 2001; Stahl et al., 2010; Zabaleta et al., 2017; Boé et al., 2009; OPCC-CTP, 2018). While the simplicity of this hydrological modeling approach, coupled with monthly-scale analysis, limits our conclusions to informative insights, it also highlights the potential of integrating ML-MME techniques with more intricate hydrological models on a daily scale thus paving the way for the development of projections that can facilitate more precise resource–planning and adaptation strategies in the context of climate change.

5.5 Conclusions and connections

In this chapter, we effectively implemented machine learning algorithms to develop Multi Model Ensembles (MMEs) based on Regional Climate Models (RCMs) within the Esca River basin, situated in the high mountain

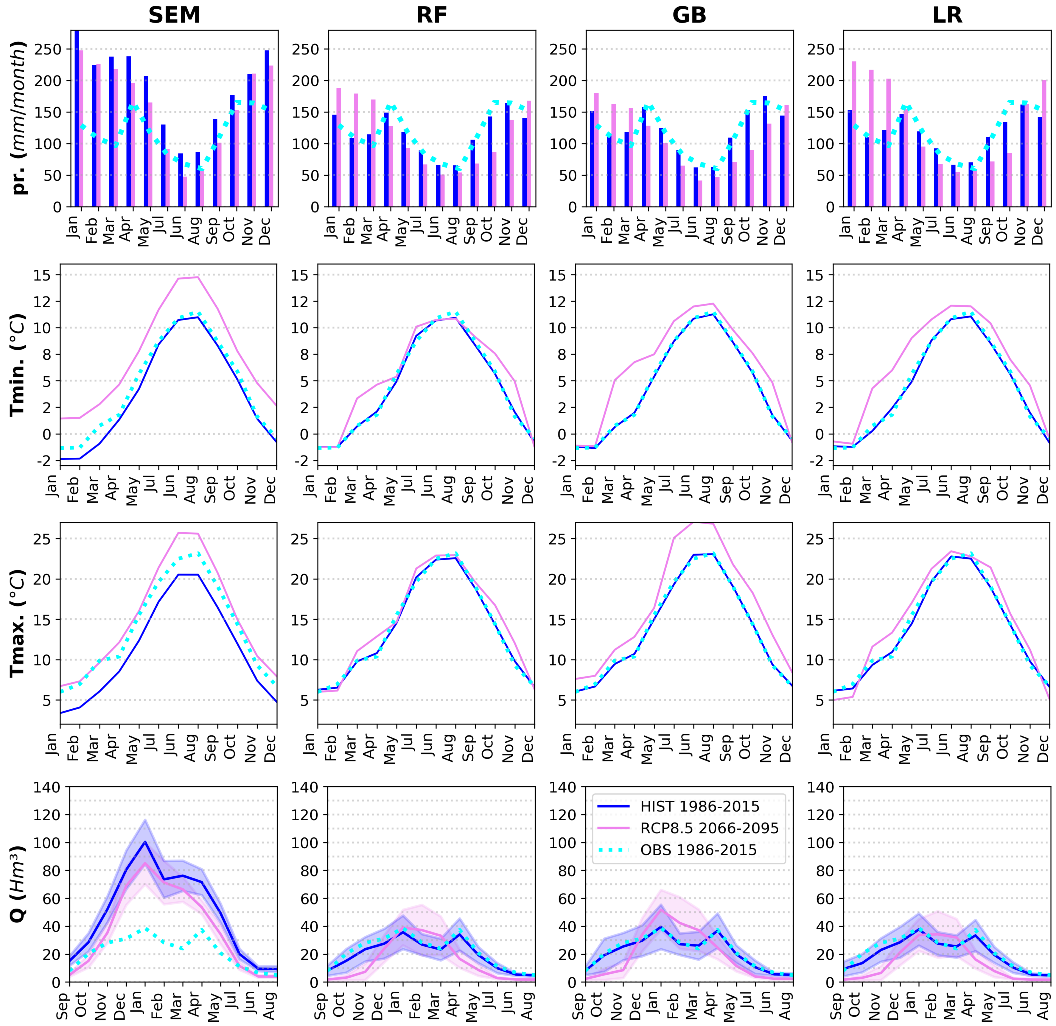

FIGURE 5.7: Annual cycles of pr, tmin, tmax and Q for historical and long-term future (RCP8.5 emission scenario) covering 1986–2015, 2066–2095 respectively. The shaded area for Q variable represents the annual variability of the results.

region of the Pyrenees. This approach enables the fulfillment of **Objective 4**, which aims to explore and propose novel techniques based on Machine Learning to enhance climate and hydrology characterization. Additionally, in conjunction with Chapter 4, it contributes to **Milestone 2** by conducting an analysis of the existing predictive tools for climate change forecasting.

Through the analysis conducted in Chapter 5 a comprehensive ranking of the RCMs was established, revealing substantial variability in performance across individual variables and seasons, with MPI-driven RCMs consistently outperforming others. To determine the optimal number of RCMs for MME construction, a top-ranked approach was adopted. Seven RCMs were selected based on performance curves analysis, forming the definitive MMEs.

Noteworthy enhancements were observed in precipitation representation on both annual and seasonal scales by the Machine–Learning (ML) based MMEs. Although the results obtained for temperatures using ML-based MMEs are more subtle at seasonal scale, a relevant improvement is observed in the annual RMSE values. Hydrological simulations employing MMES of climate variables based on Random Forest, Linear Regression and Gradient Boosting yielded outcomes comparable to those fed by climate observations, significantly outperforming simulations based on single RCMs and SEM. Our results showcase two key findings. Firstly, they highlight the potential of machine learning techniques in constructing MMEs to enhance the characterization of climate variables. Secondly, they underscore the advantages of utilizing these ML-MMEs as input data for hydrological models.

Additionally, our methodology showcased versatility by applying algorithms to climate projections under the RCP8.5 scenario, providing more realistic information than traditional methods and thereby offering opportunities for reducing uncertainty in climate outputs for adaptation planning and basin-scale impact analyses in the context of climate change. This contribution holds particular significance and novelty in a region characterized by complex topography, such as the high mountain region of the Pyrenees, where predicting future changes is not only a complex task but also essential for the climate change adaptation of the region.

Chapter 6

Conclusions and Future Work

6.1 Conclusions

Through the present work we have deepened in the existing knowledge gap in the Pyrenees region. Our research has been structured on the basis of two axes or **Milestones**, each consisting of two **Objectives**. In the following lines, there is a reflection on the different methodologies used in this dissertation. The provided contributions have been likewise here summarized.

El **Milestone 1** consisting of *"Gain a deeper understanding of the Pyrenees region by exploring the interactions between climate, hydrology and other environmental changes, along with their vulnerabilities in the context of climate change."* has been developed through **Objective 1 and Objective 2** oriented to (1) *"Investigate the potential vulnerabilities of mountain regions while highlighting the specific characteristics of the Pyrenees "* and (2) *"Delve into the impact of climate variability and land use change on the hydrological cycle of a Pyrenean basin, elucidating their contributions."*

Through Objective 1, we address the **challenges and opportunities of high mountain regions** in general, and specifically examine the Pyrenees. We delve into the region's climatic and hydrological systems, providing a general description of their functioning and characteristics while highlighting the complexities that hinder their analysis.

Objective 2 was subsequently addressed through an investigation into the interplay among land use changes, climate dynamics, and the hydrological regime at the basin scale in the western Pyrenees. The analysis underscores a significant **shift in land use patterns**. In the 1950s, pastures and shrubs dominated the landscape, with forests occupying a limited 44% of the area, and which extended to cover most of the study area (73%) in the 2000s (Section 3.2 and 3.4.2). Climatic variability was another focal point, revealing positive trends in both maximum and minimum temperatures (see Section 3.4.1). Regarding the hydrological regime, **a decline in runoff** was observed. Notably, our findings indicate that **land-use changes contribute to 41.4% of this decline**, nearly equaling the impact of climate variability on water resource reduction (see Section 3.4.4). Furthermore, we observed an increase in the frequency and magnitude of floods with an increase in flood parameters of about 40%. The alteration of these parameters is slightly mitigated by reforestation, leading to a decrease of 5% (Section 3.4.6).

The proposed framework to complete objective 2 is based on a methodology where scenarios simulated by a SWAT model are combined to quantify the impact and relative contribution of the change of these two factors in the hydrological cycle (Figure 3.2). Moreover, we have taken an additional step by analyzing the Indicator of Hydrological Alterations (IHA) for each scenario. This novel approach has enabled us not only to broadly examine the impact of each factor but also to delve deeply into various aspects of the hydrological regime, including **droughts and floods**, and to explore their implications for ecosystems and habitats.

The fulfillment of Objectives 1 and 2 has enabled us to effectively achieve **Milestone 1**, as we have expanded our understanding of the vulnerabilities and interactions within the Pyrenees region in the context of climate change.

El **Milestone 2** consisting of *"Enhance understanding of forecasting tools, with a specific emphasis on their capacity to accurately replicate hydro–climatic dynamics."* has been tackled by the **Objective 3 and Objective 4** directed to (3) *"Evaluate the strengths and limitations of current climate simulations in a region characterized by complex topography, with specific attention to extreme events."* and (4) *"Explore and propose Machine Learning-based techniques to enhance the characterization of climate and hydrology, aiding in more effective prediction of changes."*

In order to address **Objective 3** Chapter 4 presents an assessment of the added value of downscaling utilizing Regional Climate Models (RCMs) compared to Global Climate Models (GCMs) in the high mountain region of the Pyrenees, considering the **entire mountain range**. The EURO-CORDEX ensemble was investigated, employing CLIMPY, a gridded high-resolution observational database, as a reference. A recently proposed method (Ciarlo et al. (2021); Section 4.3) is applied to quantify the performance gains or losses associated with dynamic downscaling.

Specifically, the analysis focuses on calculating the added value by exploring the extremes of the Probability Density Function (PDF), spatial distribution patterns, and its relationship with elevation.

Overall, our findings reveal significant **improvements in the representation** and general characterization of precipitation, minimum temperature, and maximum temperature in the Pyreneean region by the RCMs (see Section 4.4.1). Furthermore, RCMs demonstrate enhanced performance in capturing maximum precipitation events; however, they struggle to represent low precipitation rates, particularly in the Mediterranean area of the mountain range. Regarding temperature extremes, dynamical downscaling exhibits improvements in capturing maximum events. Nevertheless, deficiencies are observed in the RCMs' representation of minimum temperature events for both minimum and maximum temperature variables, as well as in representing near-freezing temperatures (refer to Section 4.4.2). Likewise, the findings indicate a notable correlation between the AV and elevation. Specifically, for temperatures, this correlation is positive, implying a higher AV in highest altitude areas. This analysis holds particular significance for characterizing AV in mountains, and the conclusions drawn from our study would likely apply to other high mountain areas.

These findings highlight notable enhancements in simulating three key variables for climate characterization. Nonetheless, they also underscore their limitations. This insight gains significance when considering that the primary purpose of these models is to develop climate projections under emission scenarios related to climate change. Therefore, the thorough identification and quantification of their strengths and weaknesses, coupled with an exhaustive analysis encompassing various percentiles and their spatial distribution, is imperative when utilizing this data for designing and implementing adaptation and risk management strategies in the Pyrenees region over the coming decades.

Among the techniques and tools available for the knowledge of climate and hydrological systems, in addition to the traditional and effective physics-based models (such as the analyzed RCMs and GCMs), other approaches based on Machine Learning (ML) have been developed in the last decades for applications related to earth-sciences. This is the case of Machine Learning based Multi Model Ensembles (ML-MMEs). Through **Objective 4**, we address these new techniques by proposing (Chapter 5), the design of ML models for the improvement of climatic and hydrological characterization.

Chapter 5 employs machine learning algorithms to construct Multi Model Ensembles (MMEs) based on Regional Climate Models (RCMs) at **basin scale** (within the Esca River basin) in the Pyrenees. First, RCMs are ranked comprehensively based on their performance in simulating precipitation (pr), minimum temperature (tmin), and maximum temperature (tmax), revealing variability across seasons and influenced by the General Circulation Model (GCM) driving each RCM (see Table 5.1). The top-ranked approach is used to determine the optimal number of RCMs for MME construction, resulting in the selection of seven RCMs (Section 5.4.2).

The analysis of Machine Learning based Multi-Model Ensemble (ML–MME) results reveals substantial enhancements in precipitation, both on annual and seasonal scales, as well as in the accuracy of monthly time series fitting. An illustrative example of these enhancements can be observed through the R2 metric in the monthly time series: while the Simple Ensemble Mean (SEM) achieves an R2 of 0.36, machine learning algorithms attain values exceeding 0.75, with Random Forest (RF) and Linear Regression (LR) surpassing 0.80 (refer to Figure 5.4). In essence, **we have transitioned from a limited and unrealistic portrayal of monthly precipitation dynamics to a satisfactory performance in representing these dynamics** (see Section 5.4.3). Subtle yet qualitatively significant improvements are also notable at the seasonal scale for temperature variables. These enhancements in climate variables representation have **consequential implications for hydrological simulation quality** (see Table 5.2). Specifically, employing our ML-MMEs to input the Temez hydrologic model yields flow results comparable to those obtained using climate observation data, underscoring the effectiveness of employing ML-MMEs as input for basin-scale impact models to achieve more realistic and reliable outcomes.

Chapter 5 additionally includes an exercise centered on the application of RCM data algorithms under the RCP85 scenario for future projections (refer to Section 5.4.5). This methodology holds potential for providing more realistic data compared to traditional methods, thereby presenting opportunities to mitigate climate data uncertainty for adaptation planning within the context of climate change, especially when coupled with more complex impact models (such as SWAT). The study presented in Chapter 5 serves as a successful demonstration of the integration of both physics-based and ML-based models. Additionally, these promising outcomes have been achieved even in a region with complex topography such as the Pyrenees, characterized by challenging climate dynamics and significant spatial variations. This highlights the added value and versatility of our methodology.

With the successful attainment of **Objectives 3 and 4**, we have reached **Milestone 2**, which aims to enhance our comprehension of forecasting tools.

To conclude, this dissertation significantly advances our understanding of the Pyrenees region from a hydro-climatic perspective, while also contributing to the enhancement and development of tools and methodologies which enable the creation of knowledge. The comprehensive approach across the five chapters of the thesis offers a **holistic view of the mountain range, addressing regional, meso-scale, and basin-scale processes**. Furthermore, beyond enhancing our understanding of the Pyrenean region, this thesis illuminates knowledge applicable to high mountain regions more broadly, offering valuable insights and methodologies that can be applied to other mountainous areas. The conclusions drawn from this research are pertinent and, to some extent, **transferable to various mountain regions** within the context of climate change.

6.2 Future Work

The potential future directions of this research are both numerous and promising. One particularly valuable avenue, especially in the context of regional changes, involves leveraging advances in simulation techniques and methodologies to better characterize the impacts of climate change. This aligns with the objectives outlined in **Milestone 2**.

Exploring the framework proposed in Chapter 5 represents a promising path forward. The next logical step involves applying Machine Learning-based Multi-Model Ensembles (ML-MME) on a daily scale and integrating more complex hydrological models such as SWAT. This approach could provide reliable and accurate data on climatic and hydrological evolution at the basin level, which would be invaluable for designing realistic and effective climate change adaptation plans.

Another important direction is to focus on shorter-term processes, such as seasonal or monthly scales, for characterizing the hydro–climatic system. Applying similar methodologies to this framework could enhance our understanding of snow dynamics in the Pyrenees region, which is crucial for the socio-economic systems dependent on this area.

Both proposed pathways share the common goal of generating knowledge and data that can assist Pyrenean communities in adapting to forthcoming changes. However, for this information to be truly beneficial, it is essential to incorporate the needs of these communities into the design of climate services. By combining local stakeholders' knowledge with technical and scientific advances in climate change prediction, we can provide actionable insights that facilitate meaningful change in the Pyrenees region.

Appendix A

Publications and contributions

A.1 Journal Publications

Title: Climate change in high–mountain regions: An international perspective and a look at the Pyrenees.

- **Authors:** Nerea Bilbao–Barrenetxea, Sérgio Henrique Faria
- **Journal:** Metode Science Studies Jorunal: Annual Review
- **Publisher:** Metode
- **Year:** 2022
- **Summary:** High mountains are among the regions most affected by climate change. The complex network of interactions between climate, biological, and sociocultural structures in these regions is being altered by the changing climate. In this work, we try to explore the future challenges for these unique regions. We analyse why they are important and what problems they are facing in today's climate and political scenario, with a special focus on the Pyrenees.
- **Category:** History and Philosophy of Science
- **CiteScore (2022):** 0.6
- **Ranking in JCR:** 111/208
- **Quartile:** Q3

Title: Declining water resources in the Anduña River Basin of Western Pyrenees: Land abandonment or climate variability?

- **Authors:** Nerea Bilbao–Barrenetxea, Patricia Jimeno-Sáez, Francisco José Segura–Méndez, Gerardo Castellanos–Osorio, Adrián López–Ballesteros, Sérgio Henrique Faria, Javier Senent–Aparicio

- **Journal:** Journal of Hydrology: Regional Studies
- **Publisher:** Elsevier
- **Year:** 2024
- **Summary:**Study Region:Mountains play a crucial role in supplying water for consumption, irrigation, and hydroelectric power. However, they are highly vulnerable to climate change. The Pyrenees exemplify a mountainous region undergoing significant changes, notably in land-use practisces, with a significant shift towards forest cover. Study Focus: We use the SWAT model, to analyse in depth two factors that most influence the hydrological cycle: land-use change and climate variability. The model is calibrated and validated using daily streamflow for the periods 1992–2004 and 2005– 2018. The following results were obtained for both periods: an NSE of 0.51, an R2 of 0.72, and a PBIAS of –12.67 % for the calibration period and an NSE of 0.55, an R2 of 0.75, and a PBIAS of –16.49 % for the validation period, indicating that the model accurately represented the daily streamflow. Subsequently, we designed three scenarios based on combinations of historical data to quantify the contribution of each factor. New Hydrological Insights for the Region: Comparing the scenarios confirms the downward trend of streamflow in the region and provides quantitative information on the influence of each factor on this decline. Notably, that land-use changes account for 41.4 % almost as much as the climate variability. Furthermore, we observed an increase in the frequency and magnitude of floods with an increase in flood parameters of about 40%. The alteration of these parameters is slightly mitigated by reforestation, leading to a decrease of 5%.
- **Category:** Earth and Planetary Sciences (miscellaneous)
- **CiteScore (2022):** 5.8
- **Ranking in JCR:** 25/141
- **Quartile:** Q1

Title: Added Value of EURO–CORDEX downscaling over the complex orography region of the Pyrenees

- **Authors:** Nerea Bilbao–Barrenetxea, María Santolaria–Otín, Claas Teichmann, Sérgio Henrique Faria, María Máñez Costa
- **Journal:** Climate Dynamics

- **Publisher:** Springer
- **Year:** Under review
- **Summary:** This study presents an assessment of the added value of downscaling utilizing Regional Climate Models (RCMs) compared to Global Climate Models (GCMs) in the high mountain region of the Pyrenees, characterized by complex topography. The EURO-CORDEX ensemble was investigated, employing a gridded high-resolution observational database as a reference. A recently proposed method is applied to quantify the performance gains or losses associated with dynamic downscaling. Our analysis focuses on calculating the added value by exploring the extremes of the Probability Density Function (PDF), spatial distribution patterns, and its relationship with elevation. Overall, our findings reveal significant improvements in the representation and general characterization of precipitation, minimum temperature, and maximum temperature in the Pyreneean region. Furthermore, RCMs demonstrate enhanced performance in capturing maximum precipitation events; however, they struggle to represent low precipitation rates, particularly in the Mediterranean area of the mountain range. Regarding temperature extremes, dynamical downscaling exhibits improvements in capturing maximum events. Nevertheless, deficiencies are observed in the RCMs' representation of minimum temperature events for both minimum and maximum temperature variables, as well as in representing near-freezing temperatures.
- **Category:** Atmospheric Sciences
- **CiteScore (2022):** 10.2
- **Ranking in JCR:** 11/137
- **Quartile:** Q1

Title: Multi–model ensemble machine learning approaches to project climatic scenarios in a River Basin in the Pyrenees

- **Authors:** Nerea Bilbao–Barrenetxea, Raquel Martínez–España, Patricia Jimeno–Sáez, Sérgio Henrique Faria, Javier Senent–Aparicio
- **Journal:** Earth Systems and Environment
- **Publisher:** Springer
- **Year:** 2024

- **Summary:** This study employs machine learning algorithms to construct Multi Model Ensembles (MMEs) based on Regional Climate Models (RCMs) within the Esca River basin in the Pyrenees. RCMs are ranked comprehensively based on their performance in simulating precipitation (pr), minimum temperature (tmin), and maximum temperature (tmax), revealing variability across seasons and influenced by the General Circulation Model (GCM) driving each RCM. The top-ranked approach is used to determine the optimal number of RCMs for MME construction, resulting in the selection of seven RCMs. Analysis of MME results demonstrates significant improvements in precipitation on both annual and seasonal scales, while temperature-related enhancements are more subtle at the seasonal level. The effectiveness of the ML–MME technique is highlighted by its impact on hydrological representation using a Temez model, yielding outcomes comparable to climate observations and surpassing results from Simple Ensemble Means (SEMs). The methodology is extended to climate projections under the RCP8.5 scenario, generating more realistic information for precipitation, temperature, and streamflow compared to SEM, thus reducing uncertainty and aiding informed decision-making in hydrological modeling at the basin scale. This study underscores the potential of ML–MME techniques in advancing climate projection accuracy and enhancing the reliability of data for basin-scale impact analyses.

- **Category:** Geology

- **CiteScore (2022):** 11.8

- **Ranking in JCR:** 3/284

- **Quartile:** Q1

A.2 Conference Presentations

Title: MENdIA: Coupled hydro–climate model for high mountain regions integrated in ARIES

- **Authors:** Nerea Bilbao–Barrenetxea, Yuwei Wu, María Sanntolaria-Otín, Sérgio Henrique Faria

- **Conference:** International Symposium on Ice in a Sustainable Society (ISS). Bilbao,Basque Country, (Spain), 5–10 June 2022.

- **Organizer:** International Glaciological Society

- **Presentation:** Poster

Title: Quantifying the Effects of Land Use Change and Climate Variability on Water Resources in the Pyrenees.

- **Authors:** Nerea Bilbao–Barrenetxea, Javier Senent–Aparicio
- **Conference:** International SWAT Conference. Aarhus, Denmark, 28–30 June 2023.
- **Organizer:** SWAT community
- **Presentation:** Oral

A.3 Dissemination talks

- **Bilbao–Barrenetxea, N.** November 2022, Seminar at the University of Engineering of Bilbao (UPV/EHU). La ciencia del cambio climático ¿Qué sabemos sobre nuestro futuro?
- **Bilbao–Barrenetxea, N.** November 2024, Seminar at BC3 Symposium. Added Value of Euro–Cordex downscaling over the complex orography region of the Pyrenees

Appendix B

Supplementary Material of Chapter 4

This appendix contains supplementary information about the AV index of the ensemble mean for each of the members for precipitation, minimum temperature and maximum temperature for fine (0.11°) and coarse (1.00°) resolutions.

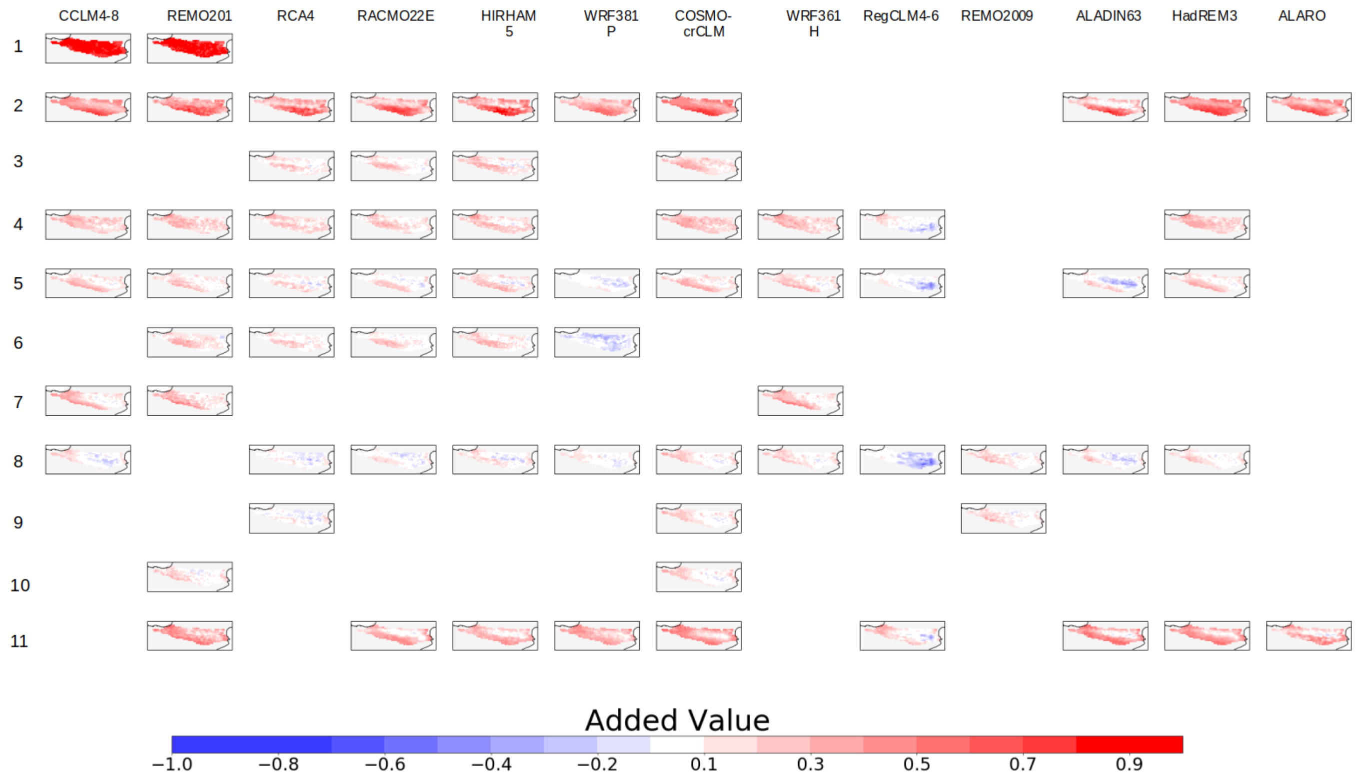

FIGURE B.1: Added value index (AV in 3 equation in Chapter 4) of precipitation for all the members at 0.11° resolution. Each row refers to the GCMs with their corresponding codes defined in Table 4.1 and each column refers to the RCM.

FIGURE B.2: Added value index (AV in 3 equation in Chapter 4) of maximum temperature for all the members at 0.11° resolution. Each row refers to the GCMs with their corresponding codes defined in Table 4.1 and each column refers to the RCM.

FIGURE B.3: Added value index (AV in 3 equation in Chapter 4) of minimum temperature for all the members at 0.11° resolution. Each row refers to the GCMs with their corresponding codes defined in Table 4.1 and each column refers to the RCM.

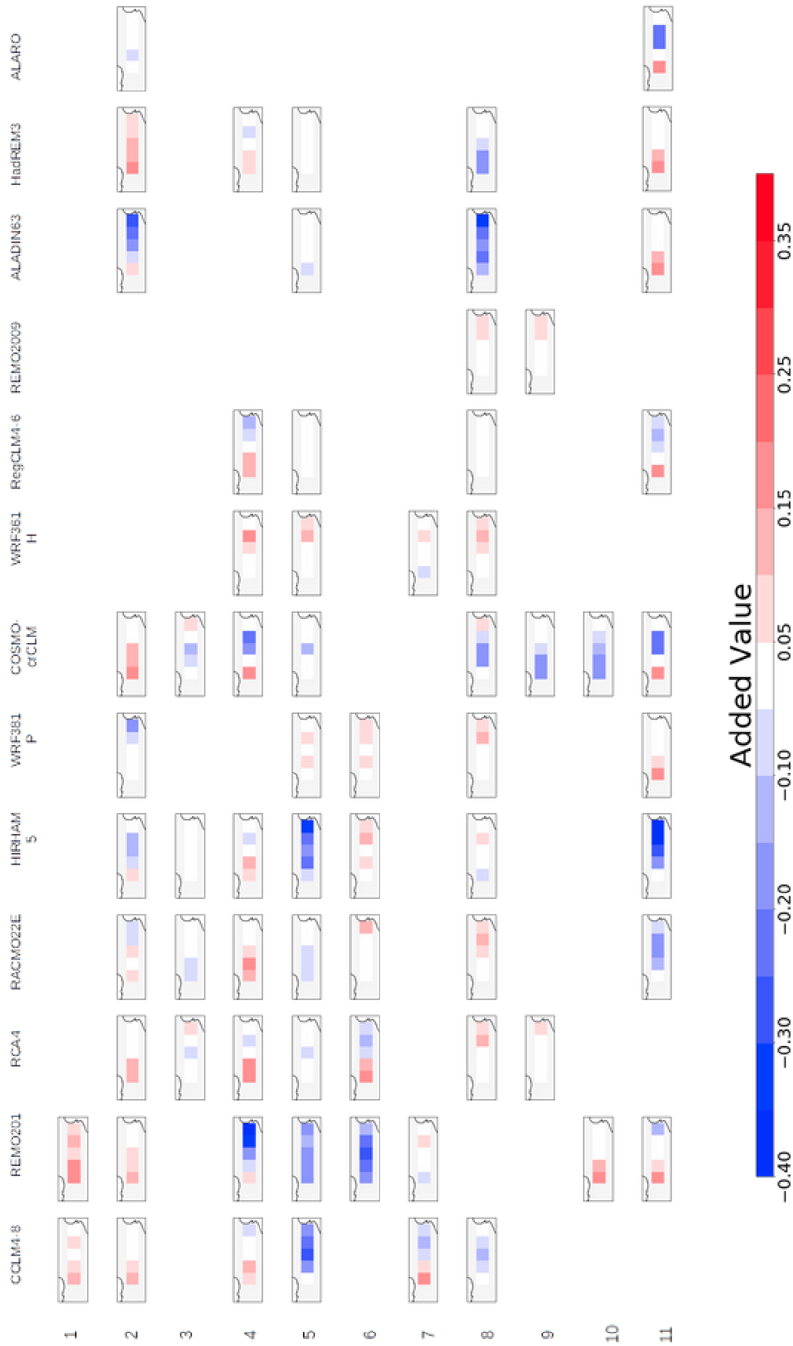

FIGURE B.4: Added value index (AV in 3 equation in Chapter 4) of precipitation for all the members at 1.00° resolution. Each row refers to the GCMs with their corresponding codes defined in Table 4.1 and each column refers to the RCM.

FIGURE B.5: Added value index (AV in 3 equation in Chapter 4) of maximum temperature for all the members at 1.00° resolution. Each row refers to the GCMs with their corresponding codes defined in Table 4.1 and each column refers to the RCM.

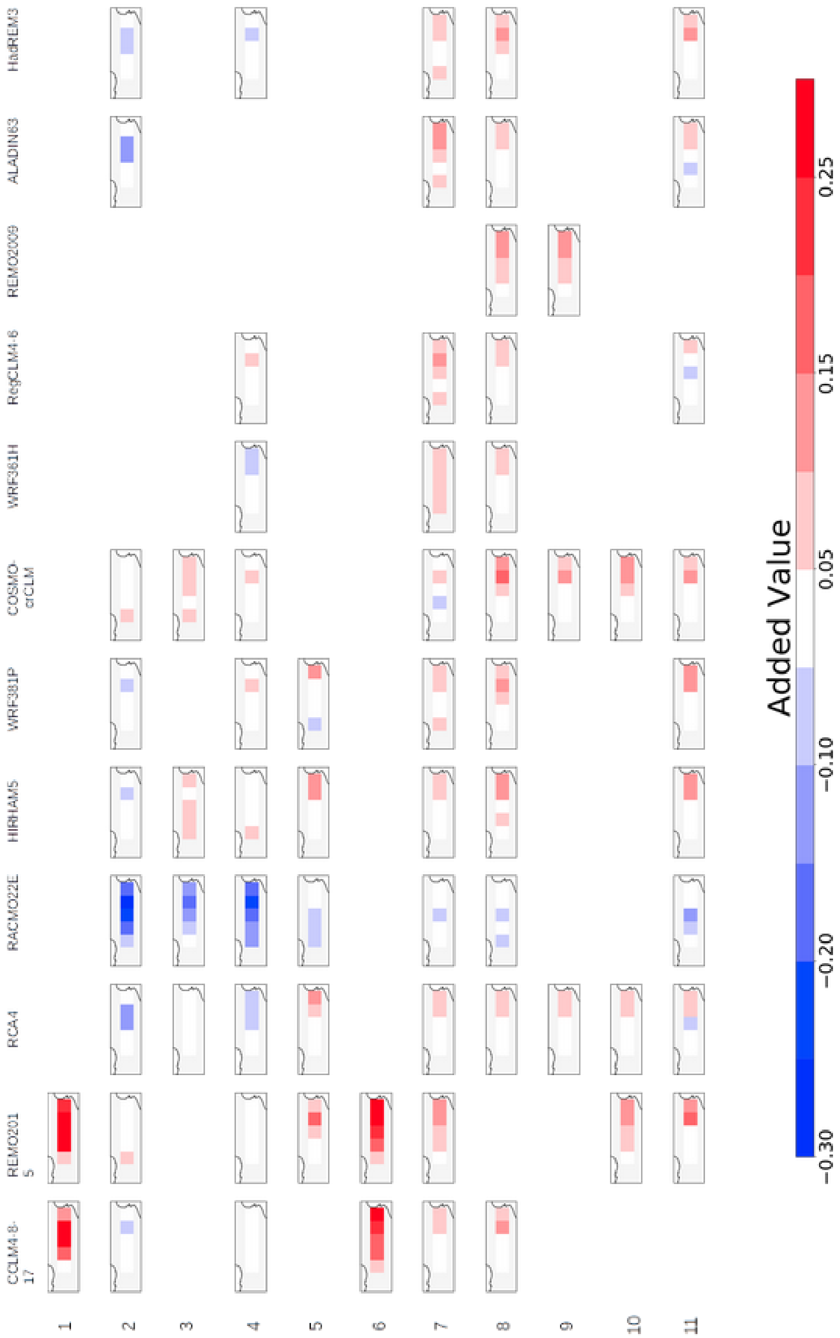

FIGURE B.6: Added value index (AV in 3 equation in Chapter 4) of minimum temperature for all the members at 1.00° resolution. Each row refers to the GCMs with their corresponding codes defined in Table 4.1 and each column refers to the RCM.

Appendix C

Supplementary Material of Chapter 5

This appendix contains supplementary information about the RCMs used in the analysis of Chapter 5, including individual ranks of RCMs for each variable and season (DJF, MAM, JJA and SON) based on TSS and overall ranks of RCMs based on RM values according to their ability to simulate CLIMPY monthly precipitation (pr), monthly average of daily maximum (tmax) and minimum temperature (tmin) over the study area over the period 1980–2015.

TABLE C.1: Ranking of RCMs

	RCM Names	pr				tmax				tmin				RM	Rank
		DJF	SON	JJA	MAM	DJF	SON	JJA	MAM	DJF	SON	JJA	MAM		
56	MPI-M-MPI-ESM-LR_SMHI-RCA4	42	41	2	42	3	1	26	11	9	14	51	3	0,7124	1
34	MIROC-MIROC5_CCLM4-8-17	7	11	33	49	6	46	2	16	48	13	25	4	0,6948	2
58	MPI-M-MPI-ESM-LR_ETH-COSMO-crCLIM-v1-1	2	12	5	12	35	43	50	58	2	4	47	13	0,6678	3
49	MPI-M-MPI-ESM-LR_CNRM-ALADIN63	33	20	18	16	20	3	33	30	11	21	55	31	0,6585	4
55	MPI-M-MPI-ESM-LR_MPI-CSC-REMO2009	45	27	19	41	13	13	36	37	3	7	52	5	0,6502	5
10	CNRM-CERFACS_SMHI-RCA4	32	53	21	39	38	2	1	27	55	15	12	17	0,6338	6
24	ICHEC-EC-EARTH_SMHI-RCA4	29	10	32	8	27	32	6	47	24	32	21	46	0,6315	7
52	MPI-M-MPI-ESM-LR_IPSL-WRF381P	38	23	29	24	17	16	60	24	6	6	58	14	0,6303	8
54	MPI-M-MPI-ESM-LR_MOHC-HadREM3-GA7-05	31	34	4	51	18	5	39	5	8	39	62	20	0,6291	9
51	MPI-M-MPI-ESM-LR_ICTP-RegCM4-6	46	15	53	58	25	9	42	2	13	11	45	6	0,6185	10
19	ICHEC-EC-EARTH_SMHI-RCA4	37	2	35	61	36	12	38	39	30	12	8	19	0,6138	11
53	MPI-M-MPI-ESM-LR_KNMI-RACMO22E	41	31	8	34	33	11	61	54	5	17	37	2	0,6080	12
1	CCCma-CanESM2_CCLM4-8-17	5	65	56	7	1	42	44	10	1	30	49	27	0,6045	13
57	MPI-M-MPI-ESM-LR_UHOH-WRF361H	50	46	20	38	12	14	52	20	7	33	48	9	0,5904	14
9	CNRM-CERFACS_MOHC-HadREM3-GA7-05	25	54	50	56	57	4	16	25	49	2	3	8	0,5904	15
29	IPSL-IPSL-CM5A-MR_DMI-HIRHAM5	69	66	15	2	42	27	37	4	31	46	2	10	0,5880	16
59	MPI-M-MPI-ESM-LR_MPI-CSC-REMO2009	3	8	28	44	30	35	58	62	4	23	61	7	0,5739	17
32	IPSL-IPSL-CM5A-MR_KNMI-RACMO22E	65	60	10	3	54	30	29	3	59	18	15	18	0,5728	18
2	CCCma-CanESM2_GERICS-REMO2015	10	62	6	35	26	44	21	34	16	38	33	42	0,5692	19
33	IPSL-IPSL-CM5A-MR_SMHI-RCA4	68	58	1	1	46	15	34	1	54	50	23	16	0,5692	20
25	ICHEC-EC-EARTH_ETH-COSMO-crCLIM-v1-1	62	55	49	9	31	62	10	19	18	8	9	40	0,5634	21
35	MIROC-MIROC5_GERICS-REMO2015	23	14	51	43	11	57	17	48	37	19	29	33	0,5516	22
21	ICHEC-EC-EARTH_ETH-COSMO-crCLIM-v1-1	19	9	39	15	39	37	24	61	39	25	28	49	0,5493	23
62	MPI-M-MPI-ESM-LR_SMHI-RCA4	12	38	52	29	21	22	35	9	22	47	46	53	0,5469	24
70	NCC-NorESM1-M_MOHC-HadREM3-GA7-05	30	3	9	10	41	28	59	7	47	60	39	55	0,5446	25
23	ICHEC-EC-EARTH_KNMI-RACMO22E	17	4	38	26	24	31	19	60	29	45	32	63	0,5446	26
5	CNRM-CERFACS_CNRM-ALADIN63	44	35	63	52	50	6	14	45	52	3	6	22	0,5399	27
31	IPSL-IPSL-CM5A-MR_IPSL-WRF381P	49	50	61	4	60	49	4	6	42	24	35	11	0,5364	28
18	ICHEC-EC-EARTH_MOHC-HadREM3-GA7-05	53	48	41	59	9	34	12	12	21	52	31	23	0,5364	29
11	ICHEC-EC-EARTH_CCLM4-8-17	8	25	45	48	7	45	30	51	57	27	10	43	0,5352	30
16	ICHEC-EC-EARTH_IPSL-WRF381P	64	29	24	54	2	29	28	32	19	56	34	29	0,5305	31
64	NCC-NorESM1-M_CNRM-ALADIN63	34	37	22	6	59	61	27	13	25	42	41	34	0,5293	32
30	IPSL-IPSL-CM5A-MR_GERICS-REMO2015	61	59	12	25	58	21	8	22	36	49	4	50	0,5246	33
4	CNRM-CERFACS_ETH-COSMO-crCLIM-...	16	43	43	67	48	19	13	41	44	28	18	26	0,5235	34
12	ICHEC-EC-EARTH_ETH-COSMO-crCLIM-v1-1	57	18	55	64	5	53	15	55	40	1	42	1	0,5235	35

Table 1: Ranking of RCMs (continued)

	RCM Names	pr				tmax				tmin				RM	Rank
		DJF	SON	JJA	MAM	DJF	SON	JJA	MAM	DJF	SON	JJA	MAM		
15	ICHEC-EC-EARTH_ICTP-RegCM4-6	56	32	30	69	8	20	45	33	32	31	30	21	0,5223	36
17	ICHEC-EC-EARTH_KNMI-RACMO22E	39	28	37	60	19	36	25	56	35	22	26	28	0,5176	37
3	CNRM-CERFACS_CCLM4-8-17	11	51	27	53	56	25	3	35	51	40	13	48	0,5153	38
20	ICHEC-EC-EARTH_UHOH-WRF361H	40	17	47	57	10	50	51	50	23	44	5	24	0,5094	39
63	NCC-NorESM1-M_ETH-COSMO-crCLIM-v1-1	20	1	42	17	47	54	54	46	15	34	44	44	0,5094	40
40	MOHC-HadGEM2-ES_GERICS-REMO2015	4	16	64	20	64	63	68	67	26	5	22	12	0,4941	41
28	ICHEC-EC-EARTH_SMHI-RCA4	60	68	25	11	43	48	11	14	43	61	19	30	0,4918	42
50	MPI-M-MPI-ESM-LR_DMI-HIRHAM5	66	42	7	46	22	10	55	38	10	37	64	38	0,4894	43
38	MOHC-HadGEM2-ES_CNRM-ALADIN63	24	52	26	13	29	7	5	8	70	70	70	74	0,4742	44
22	ICHEC-EC-EARTH_DMI-HIRHAM5	43	21	62	27	34	33	23	57	14	53	40	45	0,4695	45
14	ICHEC-EC-EARTH_GERICS-REMO2015	59	44	23	65	16	51	32	23	20	54	16	54	0,4636	46
61	MPI-M-MPI-ESM-LR_GERICS-REMO2015	6	56	34	5	49	39	41	18	45	55	50	61	0,4613	47
26	ICHEC-EC-EARTH_DMI-HIRHAM5	67	69	36	30	37	55	18	36	17	29	7	62	0,4566	48
6	CNRM-CERFACS_DMI-HIRHAM5	58	61	48	68	52	8	7	43	58	10	14	37	0,4554	49
66	NCC-NorESM1-M_GERICS-REMO2015	14	13	13	21	40	59	47	21	61	58	57	60	0,4554	50
48	MPI-M-MPI-ESM-LR_ETH-COSMO-crCLIM-v1-1	26	19	3	23	4	24	56	40	68	66	67	69	0,4542	51
8	CNRM-CERFACS_KNMI-RACMO22E	21	64	57	63	55	18	22	53	60	9	27	32	0,4354	52
13	ICHEC-EC-EARTH_DMI-HIRHAM5	52	49	44	50	15	41	40	42	28	48	24	52	0,4308	53
47	MPI-M-MPI-ESM-LR_CCLM4-8-17	47	33	17	18	14	26	43	17	69	68	66	68	0,4296	54
69	NCC-NorESM1-M_KNMI-RACMO22E	54	26	40	33	51	17	9	28	46	64	59	59	0,4296	55
67	NCC-NorESM1-M_ICTP-RegCM4-6	48	7	14	66	62	52	31	15	64	57	36	47	0,4143	56
42	MOHC-HadGEM2-ES_IPSL-WRF381P	1	47	31	31	23	23	48	31	66	67	69	73	0,4014	57
65	NCC-NorESM1-M_DMI-HIRHAM5	63	45	46	37	53	47	57	44	12	35	38	35	0,3991	58
7	CNRM-CERFACS_GERICS-REMO2015	27	57	58	62	45	56	53	52	63	16	11	15	0,3955	59
27	ICHEC-EC-EARTH_KNMI-RACMO22E	51	67	60	32	28	60	20	49	34	65	20	39	0,3838	60
71	NCC-NorESM1-M_SMHI-RCA4	55	30	11	14	44	38	49	29	65	62	65	65	0,3815	61
60	MPI-M-MPI-ESM-LR_ETH-COSMO-crCLIM-v1-1	18	63	54	28	32	40	46	26	56	59	53	57	0,3756	62
44	MOHC-HadGEM2-ES_MOHC-HadREM3-GA7-05	13	5	68	19	71	71	70	65	27	36	60	36	0,3650	63
68	NCC-NorESM1-M_IPSL-WRF381P	35	36	16	36	61	58	62	59	53	41	54	58	0,3322	64
46	MOHC-HadGEM2-ES_UHOH-WRF361H	9	6	65	45	65	64	63	64	72	72	72	70	0,2171	65
36	MOHC-HadGEM2-ES_CCLM4-8-17	70	70	70	70	66	68	67	71	41	51	1	25	0,2136	66
43	MOHC-HadGEM2-ES_KNMI-RACMO22E	15	24	67	40	67	66	69	70	67	71	68	66	0,1901	67
45	MOHC-HadGEM2-ES_SMHI-RCA4	22	39	66	22	69	67	66	63	71	69	74	67	0,1843	68
37	MOHC-HadGEM2-ES_ETH-COSMO-crCLIM-v1-1	71	71	71	71	70	70	71	68	38	63	17	41	0,1526	69
41	MOHC-HadGEM2-ES_ICTP-RegCM4-6	36	40	59	47	63	65	64	66	73	73	71	71	0,1455	70
39	MOHC-HadGEM2-ES_DMI-HIRHAM5	28	22	69	55	68	69	65	69	74	74	73	72	0,1338	71

Appendix D

Acronyms

AEMET	Agencia Estatal de Meteorología
AV	Added Value
BMA	Bayesian Model Averaging Technique
CD	Conductivity Discharge
CDO	Climate Data Operators
CEDEX	Centro de Estudios y Experimentación de Obras Públicas
CMIP	WCRP Coupled Model Intercomparison Project
CO2	carbon dioxide
CORDEX	Coordinated Regional Downscaling Experiment
CTP	Comunidad de Trabajo de los Pirineos
D	Relative Probability Difference
DJF	December, January and February
ED	Effective Discharge
EDW	elevation-dependent warming
ET	Evapotranspiration
EURO-CORDEX	European Coordinated Regional Downscaling Experiment
FF	Flushig Floods
GB	Gradient Boosting
GCM	Global Climate Models
GLM	Generalised Linear Model
GLOF	Glacial lake outburst floods
HRU	Hydrological Response Unit
IGA	Indicator of Global Alteration
IHA	Indicators of Hydrological Alteration
IPCC	Intergovernmental Panel on Climate Change
IPE	Instituto Pirenáico de Ecología
JJA	June, July and August
LR	Linear Regression
LULC	Land use/ Land cover
MAM	March, April and May

md	Modified Index of Agreement
MK	Mann–Kendall
ML	Machine Learning
ML-MME	Machine Learning based Multi Model Ensemble
MME	Multi Model Ensemble
OPCC	Observatorio Pirenaico del Cambio Climatico
PDF	Probability Density Function
PET	Potential Evapotranspiration
pr	Precipitation
Q	Runoff
RCM	Regional Climate Models
RCP	Representative Concentration Pathways
RF	Random Forest
RM	Rating Metric
SDG	Sustainable Development Goals
SEM	Simple Ensemble Mean
SON	September, October and November
SROCC	Special Report on the Ocean and Cryosphere in a Changing Climate
SVM	Support Vector Machine
tmax	Maximum temperature
tmin	Minimum temperature
TSS	Taylor Skill Score
WMO	World Meteorological Organization

Bibliography

K.C. Abbaspour, M. Vejdani, and S. Haghighat. SWAT–CUP calibration and uncertainty programs for SWAT. *International Congress on Modelling and Simulation*, 43(3-8):1603–1609, 2007. doi: 10.13031/2013.3000.

Nachiketa Acharya, Nitin Anand Shrivastava, B. K. Panigrahi, and U. C. Mohanty. Development of an artificial neural network based multi-model ensemble to estimate the northeast monsoon rainfall over south peninsular India: An application of extreme learning machine. *Climate Dynamics*, 43(5-6):1303–1310, 2014. ISSN 14320894. doi: 10.1007/s00382-013-1942-2.

Jennifer C. Adam and Dennis P. Lettenmaier. Adjustment of global gridded precipitation for systematic bias. *Journal of Geophysical Research: Atmospheres*, 108(9):1–15, 2003. ISSN 01480227. doi: 10.1029/2002jd002499.

A. Aghakhani Afshar, Y. Hasanzadeh, A. A. Besalatpour, and M. Pourreza-Bilondi. Climate change forecasting in a mountainous data scarce watershed using CMIP5 models under representative concentration pathways. *Theoretical and Applied Climatology*, 129(1-2):683–699, jul 2017. ISSN 14344483. doi: 10.1007/s00704-016-1908-5.

Kamal Ahmed, D. A. Sachindra, Shamsuddin Shahid, Zafar Iqbal, Nadeem Nawaz, and Najeebullah Khan. Multi-model ensemble predictions of precipitation and temperature using machine learning algorithms. *Atmospheric Research*, 236(July 2019):104806, 2020. ISSN 01698095. doi: 10.1016/j.atmosres.2019.104806. URL https://doi.org/10.1016/j.atmosres.2019.104806.

María P. Amblar-Francés, Petra Ramos-Calzado, Jorge Sanchis-Lladó, Alfonso Hernanz-Lázaro, María C. Peral-García, Beatriz Navascués, Marta Dominguez-Alonso, María A. Pastor-Saavedra, and Ernesto Rodríguez-Camino. High resolution climate change projections for the Pyrenees region. *Advances in Science and Research*, 17:191–208, 2020. ISSN 1992-0628. doi: 10.5194/asr-17-191-2020.

Vazken Andréassian. Waters and forests: From historical controversy to scientific debate. *Journal of Hydrology*, 291(1-2):1–27, 2004. ISSN 00221694. doi: 10.1016/j.jhydrol.2003.12.015.

Mazdak Arabi, Rao S. Govindaraju, and Mohamed M. Hantush. A probabilistic approach for analysis of uncertainty in the evaluation of watershed management practices. *Journal of Hydrology*, 333(2-4):459–471, 2007. ISSN 00221694. doi: 10.1016/j.jhydrol.2006.09.012.

Nigel W. Arnell. The effect of climate change on hydrological regimes in Europe: A continental perspective. *Global Environmental Change*, 9(1): 5–23, 1999. ISSN 09593780. doi: 10.1016/S0959-3780(98)00015-6.

J. G. Arnold, D. N. Moriasi, P. W. Gassman, K. C. Abbaspour, M. J. White, R. Srinivasan, C. Santhi, R. D. Harmel, A. Van Griensven, M. W. Van Liew, N. Kannan, and M. K. Jha. SWAT: Model use, calibration, and validation. *Transactions of the ASABE*, 55(4):1491–1508, 2012. ISSN 21510032.

Celina Aznarez, Patricia Jimeno-Sáez, Adrián López-Ballesteros, Juan Pablo Pacheco, and Javier Senent-Aparicio. Analysing the impact of climate change on hydrological ecosystem services in laguna del sauce (Uruguay) using the swat model and remote sensing data. *Remote Sensing*, 13(10), 2021. ISSN 20724292. doi: 10.3390/rs13102014.

Leah A. Bêche, Eric P. McElravy, and Vincent H. Resh. Long-term seasonal variation in the biological traits of benthic-macroinvertebrates in two Mediterranean-climate streams in California, U.S.A. *Freshwater Biology*, 51(1):56–75, 2006. ISSN 00465070. doi: 10.1111/j.1365-2427.2005.01473.x.

Tom Beer. *The Impact of Extreme Weather Events on Food Security*. 2018. ISBN 9783319564685. doi: 10.1007/978-3-319-56469-2_8.

Santiago Beguería, Juan Ignacio López-Moreno, Adrián Lorente, Manuel Seeger, and José M. García-Ruiz. Assessing the effect of climate oscillations and land-use changes on streamflow in the Central Spanish Pyrenees. *Ambio*, 32(4):283–286, 2003. ISSN 00447447. doi: 10.1579/0044-7447-32.4.283.

Martin Beniston. Climatic Change in Mountain Regions: A Review of Possible Impacts. *Climatic Change*, pages 5–31, 2003. doi: 10.1007/978-94-015-1252-7.

Candice Bentéjac, Anna Csörgő, and Gonzalo Martínez-Muñoz. A comparative analysis of gradient boosting algorithms. *Artificial Intelligence Review*, 54:1937–1967, 2021.

Michael R Berthold, Christian Borgelt, Frank Höppner, and Frank Klawonn. *Guide to intelligent data analysis: how to intelligently make sense of real data*. Springer Science & Business Media, 2010.

Nerea Bilbao-Barrenetxea, Patricia Jimeno-Sáez, Francisco José Segura-Méndez, Gerardo Castellanos-Osorio, Adrián López-Ballesteros, Sergio Henrique Faria, and Javier Senent-Aparicio. Declining water resources in the Anduña River Basin of Western Pyrenees: Land abandonment or climate variability? *Journal of Hydrology: Regional Studies*, 53(April):101771, 2024. ISSN 22145818. doi: 10.1016/j.ejrh.2024.101771. URL https://doi.org/10.1016/j.ejrh.2024.101771.

Fredrik Boberg, Peter Berg, Peter Thejll, William J. Gutowski, and Jens H. Christensen. Improved confidence in climate change projections of precipitation evaluated using daily statistics from the PRUDENCE ensemble. *Climate Dynamics*, 32(7-8):1097–1106, 2009. ISSN 09307575. doi: 10.1007/s00382-008-0446-y.

Fredrik Boberg, Peter Berg, Peter Thejll, William J. Gutowski, and Jens H. Christensen. Improved confidence in climate change projections of precipitation further evaluated using daily statistics from ENSEMBLES models. *Climate Dynamics*, 35(7):1509–1520, 2010. ISSN 09307575. doi: 10.1007/s00382-009-0683-8.

J. Boé, L. Terray, E. Martin, and F. Habets. Projected changes in components of the hydrological cycle in French river basins during the 21st century. *Water Resources Research*, 45(8):1–15, 2009. ISSN 00431397. doi: 10.1029/2008WR007437.

Carolina Boix-Fayos, Luc G.J. Boerboom, Ron Janssen, María Martínez-Mena, María Almagro, Pedro Pérez-Cutillas, Joris P.C. Eekhout, Victor Castillo, and Joris de Vente. Mountain ecosystem services affected by land use changes and hydrological control works in Mediterranean catchments. *Ecosystem Services*, 44(June):101136, 2020. ISSN 22120416. doi: 10.1016/j.ecoser.2020.101136. URL https://doi.org/10.1016/j.ecoser.2020.101136.

Christoph Bracher, Susanne Wymann Von Dach, and Carolina Adler. *CDE Working Paper Challenges and Opportunities in Assessing Sustainable Mountain Development Using the UN Sustainable Development Goals A REPORT COMPILED BY THE MOUNTAIN RESEARCH INITIATIVE (MRI), IN COLLABORATION WITH THE CENTRE FOR DEVELOPMENT AND ENVIR*. 2018. ISBN 9783906813738. doi: 10.7892/boris.119737.

S. Brands, S. Herrera, J. Fernández, and J. M. Gutiérrez. How well do CMIP5 Earth System Models simulate present climate conditions in Europe and Africa?: A performance comparison for the downscaling community. *Climate Dynamics*, 41(3-4):803–817, 2013. ISSN 09307575. doi: 10.1007/s00382-013-1742-8.

L. N. Braun, M. Weber, and M. Schulz. Consequences of climate change for runoof from Alpine regions. *Annals of Glaciology*, 31:19–25, 2000. ISSN 02603055. doi: 10.3189/172756400781820165.

Leo Breiman. Random forests. *Machine learning*, 45:5–32, 2001.

Tássia Brighenti, Nadia Bonuma, Fernando Grison, Aline Mota, Masato Kobiyama, and Pedro Chaffe. Two calibration methods for modeling streamflow and suspended sediment with the swat model. *Ecological Engineering*, 127:103–113, 02 2019. doi: 10.1016/j.ecoleng.2018.11.007.

Filippo Calì Quaglia, Silvia Terzago, and Jost von Hardenberg. Temperature and precipitation seasonal forecasts over the Mediterranean region: added value compared to simple forecasting methods. *Climate Dynamics*, 58(7-8):2167–2191, 2022. ISSN 14320894. doi: 10.1007/s00382-021-05895-6.

Rita M. Cardoso and Pedro M.M. Soares. Is there added value in the EURO-CORDEX hindcast temperature simulations? Assessing the added value using climate distributions in Europe. *International Journal of Climatology*, 42(7):4024–4039, 2022. ISSN 10970088. doi: 10.1002/joc.7472.

J A M Careto, P M M Soares, R M Cardoso, S Herrera, and J M Gutiérrez. Added value of EURO-CORDEX high-resolution downscaling over the Iberian Peninsula revisited – Part 2: Max and min temperature. *Geoscientific Model Development*, 15(6):2653–2671, 2022a. doi: 10.5194/gmd-15-2653-2022. URL https://gmd.copernicus.org/articles/15/2653/2022/.

J A M Careto, P M M Soares, R M Cardoso, S Herrera, and J M Gutiérrez. Added value of EURO-CORDEX high-resolution downscaling over the Iberian Peninsula revisited – Part 2: Max and min temperature. *Geoscientific Model Development*, 15(6):2653–2671, 2022b. doi: 10.5194/gmd-15-2653-2022. URL https://gmd.copernicus.org/articles/15/2653/2022/.

João António Martins Careto, Pedro Miguel Matos Soares, Rita Margarida Cardoso, Sixto Herrera, and José Manuel Gutiérrez. Added value of

EURO-CORDEX high-resolution downscaling over the Iberian Peninsula revisited - Part 1: Precipitation. *Geoscientific Model Development*, 15 (6):2635–2652, 2022c. ISSN 19919603. doi: 10.5194/gmd-15-2635-2022.

João António Martins Careto, Pedro Miguel Matos Soares, Rita Margarida Cardoso, Sixto Herrera, and José Manuel Gutiérrez. Added value of EURO-CORDEX high-resolution downscaling over the Iberian Peninsula revisited - Part 1: Precipitation. *Geoscientific Model Development*, 15 (6):2635–2652, 2022d. ISSN 19919603. doi: 10.5194/gmd-15-2635-2022.

Jordi Catalan, Lluís Camarero, Marisol Felip, Sergi Pla, Marc Ventura, Teresa Buchaca, Frederic Bartumeus, Guillermo De Mendoza, Alexandre Miró, Emilio O. Casamayor, Juan Manuel Medina-Sánchez, Montserrat Bacardit, Maddi Altuna, Mireia Bartrons, and Daniel Díaz De Quijano. High mountain lakes: Extreme habitats and witnesses of environmental changes. *Limnetica*, 25(1-2):551–584, 2006. ISSN 02138409. doi: 10.23818/limn.25.38.

Zeyi Chao, Fangling Pu, Yuke Yin, Bin Han, and Xiaoling Chen. Research on real-time local rainfall prediction based on MEMS sensors. *Journal of Sensors*, 2018:1–9, 2018. ISSN 16877268. doi: 10.1155/2018/6184713.

Anne Charmantier and Phillip Gienapp. Climate change and timing of avian breeding and migration: Evolutionary versus plastic changes. *Evolutionary Applications*, 7(1):15–28, 2014. ISSN 17524563. doi: 10.1111/eva.12126.

A. Chavez-Jimenez, B. Lama, L. Garrote, F. Martin-Carrasco, A. Sordo-Ward, and L. Mediero. Characterisation of the Sensitivity of Water Resources Systems to Climate Change. *Water Resources Management*, 27(12): 4237–4258, 2013. ISSN 09204741. doi: 10.1007/s11269-013-0404-2.

Weilin Chen, Zhihong Jiang, and Laurent Li. Probabilistic projections of climate change over China under the SRES A1B scenario using 28 AOGCMs. *Journal of Climate*, 24(17):4741–4756, 2011. ISSN 08948755. doi: 10.1175/2011JCLI4102.1.

Nikolaos Christidis and Peter A. Stott. Human Influence on Seasonal Precipitation in Europe. *Journal of Climate*, 35(15):5215–5231, 2022. ISSN 15200442. doi: 10.1175/JCLI-D-21-0637.1.

James M. Ciarlo, Erika Coppola, Adriano Fantini, Filippo Giorgi, Xue Jie Gao, Yao Tong, Russell H. Glazer, Jose Abraham Torres Alavez, Taleena Sines, Emanuela Pichelli, Francesca Raffaele, Sushant Das, Melissa Bukovsky, Moetasim Ashfaq, Eun Soon Im, Thanh Nguyen-Xuan, Claas Teichmann, Armelle Remedio, Thomas Remke, Katharina Bülow, Torsten Weber, Lars Buntemeyer, Kevin Sieck, Diana Rechid, and Daniela Jacob. A new spatially distributed added value index for regional climate models: the EURO-CORDEX and the CORDEX-CORE highest resolution ensembles. *Climate Dynamics*, 57(5-6):1403–1424, 2021. ISSN 14320894. doi: 10.1007/s00382-020-05400-5.

Adam J Clark. Generation of ensemble mean precipitation forecasts from convection-allowing ensembles. *Weather and Forecasting*, 32(4):1569–1583, 2017.

Andrew F. Colombo, David Etkin, and Bryan W. Karney. Climate variability and the frequency of extreme temperature events for nine sites across Canada: Implications for power usage. *Journal of Climate*, 12(8 PART 2): 2490–2502, 1999. ISSN 08948755. doi: 10.1175/1520-0442(1999)012<2490: cvatfo>2.0.co;2.

Erika Coppola, Francesca Raffaele, Filippo Giorgi, Graziano Giuliani, Gao Xuejie, James M. Ciarlo, Taleena Rae Sines, José Abraham Torres-Alavez, Sushant Das, Fabio di Sante, Emanuela Pichelli, Russell Glazer, Sebastian Karl Müller, Sabina Abba Omar, Moetasim Ashfaq, Melissa Bukovsky, E. S. Im, Daniela Jacob, Claas Teichmann, Armelle Remedio, Thomas Remke, Arne Kriegsmann, Katharina Bülow, Torsten Weber, Lars Buntemeyer, Kevin Sieck, and Diana Rechid. Climate hazard indices projections based on cordex-core, cmip5 and cmip6 ensemble. *Climate Dynamics*, 57:1–91, 09 2021. doi: 10.1007/s00382-021-05640-z.

Jesse Crawford, Kartik Venkataraman, and Juliann Booth. Developing climate model ensembles: A comparative case study. *Journal of Hydrology*, 568(September 2018):160–173, 2019. ISSN 00221694. doi: 10.1016/j.jhydrol.2018.10.054. URL https://doi.org/10.1016/j.jhydrol.2018.10.054.

José María Cuadrat, Roberto Serrano-Notivoli, Ernesto Tejedor, Miguel Ángel Saz, Marc Prohom, Jordi Cunillera, Alba Llabrés, Laura Trapero, Marc Pons, Juan Ignacio López-Moreno, Ramon Copons, Simon Gascoin, Yolanda Luna, Ernesto Rodríguez, Petra Ramos, Pilar Amblar, and Jean-Michel Soubeyroux. Climpy: Climate of the pyrenees (1.0) [data set]. *Zenodo*, 2020a. doi: https://doi.org/10.5281/zenodo.3611127.

José María Cuadrat, Roberto Serrano-Notivoli, Ernesto Tejedor, Miguel Ángel Saz, Marc Prohom, Jordi Cunillera, Alba Llabrés, Laura Trapero, Marc Pons, Juan Ignacio López-Moreno, Ramon Copons, Simon Gascoin, Yolanda Luna, Ernesto Rodríguez, Petra Ramos, Pilar Amblar, and

Jean-Michel Soubeyroux. Climpy: Climate of the pyrenees. *Zenodo*, 2020b.

N. J. Cullen, P. Sirguey, T. Mölg, G. Kaser, M. Winkler, and S. J. Fitzsimons. A century of ice retreat on Kilimanjaro: the mapping reloaded. *The Cryosphere*, 7(2):419–431, 2013. doi: 10.5194/tc-7-419-2013.

A. Dai. Global precipitation and thundertstorm frequencies. Part I: Seasonal and interannual variations. *Journal of Climate*, 14(6):1092–1111, 2001. ISSN 08948755. doi: 10.1175/1520-0442(2001)014<1092:GPATFP>2.0.CO;2.

Aiendrila Dey, Debi Prasad Sahoo, Rohini Kumar, and Renji Remesan. A multimodel ensemble machine learning approach for CMIP6 climate model projections in an Indian River basin. *International Journal of Climatology*, -(June):1–22, 2022. ISSN 10970088. doi: 10.1002/joc.7813.

Alejandro Di and Luca Ramo. Potential for added value in temperature simulated by high-resolution nested RCMs in present climate and in the climate change signal. *Climate Dynamics*, pages 443–464, 2013. doi: 10.1007/s00382-012-1384-2.

Alejandro Di Luca, Daniel Argüeso, Jason P. Evans, Ramón De Elía, and René Laprise. Quantifying the overall added value of dynamical downscaling and the contribution from different spatial scales. *Journal of Geophysical Research*, 121(4):1575–1590, 2016. ISSN 21562202. doi: 10.1002/2015JD024009.

Henry F. Diaz, Martin Grosjean, and Lisa Graumlich. Climate variability and change in high elevation regions: Past, present and future. *Climatic Change*, 59(1-2):1–4, 2003. ISSN 01650009. doi: 10.1023/A:1024416227887.

Tom Dietterich. Overfitting and undercomputing in machine learning. *ACM computing surveys (CSUR)*, 27(3):326–327, 1995.

Laura Dobor and Tomáš Hlásny. Choice of reference climate conditions matters in impact studies: Case of bias-corrected CORDEX data set. *International Journal of Climatology*, 39(4):2022–2040, 2019. ISSN 10970088. doi: 10.1002/joc.5930.

A Escriva-Bou, M. Pulido-Velazquez, and D. Pulido-Velazquez. Economic value of climate change adaptation strategies for water management in spain's jucar basin. *J. Water Res. Plan. ASCE 2017,*, 2:143, 2017.

T. Estrela. Modelos matemáticos para la evaluación de recursos hídricos. *Centro de Estudios Hidrográficos y Experimentación de Obras Públicas. CEDEX.*, 2:55, 1992.

G Evin, S Somot, and B Hingray. Balanced estimate and uncertainty assessment of European climate change using the large EURO-CORDEX regional climate model ensemble. *Earth System Dynamics*, 12(4):1543–1569, 2021. doi: 10.5194/esd-12-1543-2021. URL https://esd.copernicus.org/articles/12/1543/2021/.

Adriano Fantini, Francesca Raffaele, Csaba Torma, Sara Bacer, Erika Coppola, Filippo Giorgi, Bodo Ahrens, Clotilde Dubois, Enrique Sanchez, and Marco Verdecchia. Assessment of multiple daily precipitation statistics in ERA-Interim driven Med-CORDEX and EURO-CORDEX experiments against high resolution observations. *Climate Dynamics*, 51(3):877–900, 2018. ISSN 14320894. doi: 10.1007/s00382-016-3453-4.

FAO. *State of the world's forests 2014: Enhancing the socioeconomic benefits from forests.* 2014. ISBN 978-92-5-108269-0 978-92-5-108270-6.

Simone Fatichi, Enrique R. Vivoni, Fred L. Ogden, Valeriy Y. Ivanov, Benjamin Mirus, David Gochis, Charles W. Downer, Matteo Camporese, Jason H. Davison, Brian Ebel, Norm Jones, Jongho Kim, Giuseppe Mascaro, Richard Niswonger, Pedro Restrepo, Riccardo Rigon, Chaopeng Shen, Mauro Sulis, and David Tarboton. An overview of current applications, challenges, and future trends in distributed process-based models in hydrology. *Journal of Hydrology*, 537:45–60, 2016. ISSN 00221694. doi: 10.1016/j.jhydrol.2016.03.026.

José A. Fernández, Carolina Martínez, and Fernando Magdaleno. Application of indicators of hydrologic alterations in the designation of heavily modified water bodies in Spain. *Environmental Science and Policy*, 16(i): 31–43, 2012. ISSN 14629011. doi: 10.1016/j.envsci.2011.10.004.

Frauke Feser. Enhanced detectability of added value in limited-area model results separated into different spatial scales. *Monthly Weather Review*, 134(8):2180–2190, 2006. ISSN 00270644. doi: 10.1175/MWR3183.1.

Francesc Gallart and Pilar Llorens. Observations on land cover changes and water resources in the headwaters of the Ebro catchment, Iberian Peninsula. *Physics and Chemistry of the Earth*, 29(11-12 SPEC. ISS.):769–773, 2004. ISSN 14747065. doi: 10.1016/j.pce.2004.05.004.

L García-Barrón, J M Camarillo, J Morales, and A Sousa. Temporal analysis (1940–2010) of rainfall aggressiveness in the Iberian Peninsula basins. *Journal of Hydrology*, 525:747–759, 2015. ISSN 0022-1694. doi: https://doi.org/10.1016/j.jhydrol.2015.04.036. URL https://www.sciencedirect.com/science/article/pii/S0022169415002954.

J. M. García-Ruiz, T. Lasanta, L. Ortigosa, P. Ruiz-Flaño, C. Martí-Bono, and C González. Sediment Yield under Different Land Uses in the Spanish Pyrenees . *International Mountain Society*, 15(3):229–240, 1995.

J.M. García Ruiz, S. Beguería, J.I. López-Moreno, A. Lorente Grima, and M. Seeger. Los recursos hídricos superficiales del pirineo aragonés y su evolución reciente. *Geoforma Ediciones*, 192, 2001.

F Giorgi, C Jones, and GR Asrar. Addressing climate information needs at the regional level: the CORDEX framework. *... Organization (WMO) Bulletin*, 58(July):175–183, 2009. URL http://www.euro-cordex.net/uploads/media/Download_01.pdf.

Milan Gocic and Slavisa Trajkovic. Analysis of changes in meteorological variables using Mann-Kendall and Sen's slope estimator statistical tests in Serbia. *Global and Planetary Change*, 100:172–182, 2013. ISSN 09218181. doi: 10.1016/j.gloplacha.2012.10.014. URL http://dx.doi.org/10.1016/j.gloplacha.2012.10.014.

Ivor Growns and Ivars Reinfelds. Environmental flow management using transparency and translucency rules. *Marine and Freshwater Research*, 65 (8):667–673, 2014. ISSN 13231650. doi: 10.1071/MF13192.

Youen Grusson, Xiaoling Sun, Simon Gascoin, Sabine Sauvage, Srinivasan Raghavan, François Anctil, and José Miguel Sáchez-Pérez. Assessing the capability of the SWAT model to simulate snow, snow melt and streamflow dynamics over an alpine watershed. *Journal of Hydrology*, 531:574–588, 2015. ISSN 00221694. doi: 10.1016/j.jhydrol.2015.10.070. URL http://dx.doi.org/10.1016/j.jhydrol.2015.10.070.

Shuchen Guo, Lei Tian, Shuoyu Chen, Jiguang Liang, Jie Tian, Bo Cao, Xuejin Wang, and Chansheng He. Analysis of effects of vegetation cover and elevation on water yield in an alpine basin of the Qilian Mountains in Northwest China by integrating the WRF-Hydro and Budyko framework. *Journal of Hydrology*, 629(July 2023):130580, 2024. ISSN 00221694. doi: 10.1016/j.jhydrol.2023.130580. URL https://doi.org/10.1016/j.jhydrol.2023.130580.

Aditya Gusain, Subimal Ghosh, and Subhankar Karmakar. Added value of cmip6 over cmip5 models in simulating indian summer monsoon rainfall. *Atmospheric Research*, 232:104680, 09 2019. doi: 10.1016/j.atmosres.2019.104680.

J. William Gutowski, Filippo Giorgi, Bertrand Timbal, Anne Frigon, Daniela Jacob, Hyun Suk Kang, Krishnan Raghavan, Boram Lee, Christopher Lennard, Grigory Nikulin, Eleanor O'Rourke, Michel Rixen, Silvina Solman, Tannecia Stephenson, and Fredolin Tangang. WCRP COordinated Regional Downscaling EXperiment (CORDEX): A diagnostic MIP for CMIP6. *Geoscientific Model Development*, 9(11):4087–4095, 2016. ISSN 19919603. doi: 10.5194/gmd-9-4087-2016.

A H Haria and D J Price. Evaporation from Scots pine (Pinus sylvestris) following natural re-colonisation of the Cairngorm mountains, Scotland. *Hydrology and Earth System Sciences*, 4(3):451–461, 2000. doi: 10.5194/hess-4-451-2000. URL https://hess.copernicus.org/articles/4/451/2000/.

Nadja Herger, Gab Abramowitz, Reto Knutti, Oliver Angélil, Karsten Lehmann, and Benjamin M. Sanderson. Selecting a climate model subset to optimise key ensemble properties. *Earth System Dynamics*, 9(1):135–151, 2018. ISSN 21904987. doi: 10.5194/esd-9-135-2018.

S. Herrera, P. M.M. Soares, R. M. Cardoso, and J. M. Gutiérrez. Evaluation of the EURO-CORDEX Regional Climate Models Over the Iberian Peninsula: Observational Uncertainty Analysis. *Journal of Geophysical Research: Atmospheres*, 125(12):1–16, 2020. ISSN 21698996. doi: 10.1029/2020JD032880.

Romain Hugonnet, Robert McNabb, Etienne Berthier, Brian Menounos, Christopher Nuth, Luc Girod, Daniel Farinotti, Matthias Huss, Ines Dussaillant, Fanny Brun, and Andreas Kääb. Accelerated global glacier mass loss in the early twenty-first century. *Nature*, 592(7856):726–731, 2021. ISSN 14764687. doi: 10.1038/s41586-021-03436-z. URL http://dx.doi.org/10.1038/s41586-021-03436-z.

IGN. Plan nacional de ortofotografía aérea., 2017. http://pnoa.ign.es/, (accessed on 3 January 2023). (In Spanish) (In Spanish).

W. W. Immerzeel, A. F. Lutz, M. Andrade, A. Bahl, H. Biemans, T. Bolch, S. Hyde, S. Brumby, B. J. Davies, A. C. Elmore, A. Emmer, M. Feng, A. Fernández, U. Haritashya, J. S. Kargel, M. Koppes, P. D.A. Kraaijenbrink, A. V. Kulkarni, P. A. Mayewski, S. Nepal, P. Pacheco, T. H. Painter, F. Pellicciotti, H. Rajaram, S. Rupper, A. Sinisalo, A. B. Shrestha, D. Viviroli, Y. Wada, C. Xiao, T. Yao, and J. E.M. Baillie. Importance and vulnerability of the world's water towers. *Nature*, 577(7790):364–369, 2020. ISSN 14764687. doi: 10.1038/s41586-019-1822-y. URL http://dx.doi.org/10.1038/s41586-019-1822-y.

IPCC. *Climate Change 2022: Impacts, Adaptation and Vulnerability. Contribution of Working Group II to the Sixth Assessment Report of the Intergovernmental Panel on Climate Change*. Cambridge University Press, Cambridge, UK and New York, NY, USA, 2022. doi: 10.1017/9781009325844.

Francesco A. Isotta, Christoph Frei, Viktor Weilguni, Melita Perčec Tadić, Pierre Lassègues, Bruno Rudolf, Valentina Pavan, Carlo Cacciamani, Gabriele Antolini, Sara M. Ratto, Michela Munari, Stefano Micheletti, Veronica Bonati, Cristian Lussana, Christian Ronchi, Elvio Panettieri, Gianni Marigo, and Gregor Vertačnik. The climate of daily precipitation in the Alps: Development and analysis of a high-resolution grid dataset from pan-Alpine rain-gauge data. *International Journal of Climatology*, 34 (5):1657–1675, 2014. ISSN 10970088. doi: 10.1002/joc.3794.

Jack D. Ives, Rajendra B. Shrestha, and Pradeep K. Mool. Formation of Glacial Lakes in the Hindu Kush-Himalayas and GLOF Risk Assessment. *ICIMOD (Inernational Centre for Integrated Mountain Development)*, page 66, 2010.

Daniela Jacob, Juliane Petersen, Bastian Eggert, Antoinette Alias, Ole Bøssing Christensen, Laurens M. Bouwer, Alain Braun, Augustin Colette, Michel Déqué, Goran Georgievski, Elena Georgopoulou, Andreas Gobiet, Laurent Menut, Grigory Nikulin, Andreas Haensler, Nils Hempelmann, Colin Jones, Klaus Keuler, Sari Kovats, Nico Kröner, Sven Kotlarski, Arne Kriegsmann, Eric Martin, Erik van Meijgaard, Christopher Moseley, Susanne Pfeifer, Swantje Preuschmann, Christine Radermacher, Kai Radtke, Diana Rechid, Mark Rounsevell, Patrick Samuelsson, Samuel Somot, Jean Francois Soussana, Claas Teichmann, Riccardo Valentini, Robert Vautard, Björn Weber, and Pascal Yiou. EURO-CORDEX: New high-resolution climate change projections for European impact research. *Regional Environmental Change*, 14(2):563–578, 2014. ISSN 1436378X. doi: 10.1007/s10113-013-0499-2.

Daniela Jacob, Claas Teichmann, Stefan Sobolowski, Eleni Katragkou, Ivonne Anders, Michal Belda, Rasmus Benestad, Fredrik Boberg, Erasmo Buonomo, Rita M. Cardoso, Ana Casanueva, Ole B. Christensen, Jens Hesselbjerg Christensen, Erika Coppola, Lesley De Cruz, Edouard L. Davin, Andreas Dobler, Marta Domínguez, Rowan Fealy, Jesus Fernandez, Miguel Angel Gaertner, Markel García-Díez, Filippo Giorgi, Andreas Gobiet, Klaus Goergen, Juan José Gómez-Navarro, Juan Jesús González Alemán, Claudia Gutiérrez, José M. Gutiérrez, Ivan Güttler, Andreas Haensler, Tomáš Halenka, Sonia Jerez, Pedro Jiménez-Guerrero, Richard G. Jones, Klaus Keuler, Erik Kjellström, Sebastian

Knist, Sven Kotlarski, Douglas Maraun, Erik van Meijgaard, Paola Mercogliano, Juan Pedro Montávez, Antonio Navarra, Grigory Nikulin, Nathalie de Noblet-Ducoudré, Hans Juergen Panitz, Susanne Pfeifer, Marie Piazza, Emanuela Pichelli, Joni Pekka Pietikäinen, Andreas F. Prein, Swantje Preuschmann, Diana Rechid, Burkhardt Rockel, Raquel Romera, Enrique Sánchez, Kevin Sieck, Pedro M.M. Soares, Samuel Somot, Lidija Srnec, Silje Lund Sørland, Piet Termonia, Heimo Truhetz, Robert Vautard, Kirsten Warrach-Sagi, and Volker Wulfmeyer. Regional climate downscaling over Europe: perspectives from the EURO-CORDEX community. *Regional Environmental Change*, 20(2), 2020. ISSN 1436378X. doi: 10.1007/s10113-020-01606-9.

Inmaculada C. Jiménez-Navarro, Patricia Jimeno-Sáez, Adrián López-Ballesteros, Julio Pérez-Sánchez, and Javier Senent-Aparicio. Impact of climate change on the hydrology of the forested watershed that drains to lake erken in sweden: An analysis using swat+ and cmip6 scenarios. *Forests*, 12(12), 2021. ISSN 19994907. doi: 10.3390/f12121803.

Patricia Jimeno-Sáez, Javier Senent-Aparicio, Julio Pérez-Sánchez, and David Pulido-Velazquez. A comparison of SWAT and ANN models for daily runoff simulation in different climatic zones of peninsular Spain. *Water (Switzerland)*, 10(2), 2018. ISSN 20734441. doi: 10.3390/w10020192.

Patricia Jimeno-Sáez, David Pulido-Velazquez, Antonio-Juan Collados-Lara, Eulogio Pardo-Igúzquiza, Javier Senent-Aparicio, and Leticia Baena-Ruiz. A preliminary assessment of the "undercatching" and the precipitation pattern in an alpine basin. *Water*, 12(4), 2020. ISSN 2073-4441. doi: 10.3390/w12041061. URL https://www.mdpi.com/2073-4441/12/4/1061.

Jorge Jódar, José Antonio Cabrera, Sergio Martos-Rosillo, Ana Ruiz-Constán, Antonio González-Ramón, Luis Javier Lambán, Christian Herrera, and Emilio Custodio. Groundwater discharge in high-mountain watersheds: A valuable resource for downstream semi-arid zones. The case of the Bérchules River in Sierra Nevada (Southern Spain). *Science of The Total Environment*, 593-594:760–772, 2017. ISSN 0048-9697. doi: https://doi.org/10.1016/j.scitotenv.2017.03.190. URL https://www.sciencedirect.com/science/article/pii/S0048969717307131.

C. D. Jones, J. K. Hughes, N. Bellouin, S. C. Hardiman, G. S. Jones, J. Knight, S. Liddicoat, F. M. O'Connor, R. J. Andres, C. Bell, K. O. Boo, A. Bozzo, N. Butchart, P. Cadule, K. D. Corbin, M. Doutriaux-Boucher, P. Friedlingstein, J. Gornall, L. Gray, P. R. Halloran, G. Hurtt, W. J. Ingram, J. F. Lamarque, R. M. Law, M. Meinshausen, S. Osprey, E. J. Palin,

L. Parsons Chini, T. Raddatz, M. G. Sanderson, A. A. Sellar, A. Schurer, P. Valdes, N. Wood, S. Woodward, M. Yoshioka, and M. Zerroukat. The HadGEM2-ES implementation of CMIP5 centennial simulations. *Geoscientific Model Development*, 4(3):543–570, 2011. ISSN 19919603. doi: 10.5194/gmd-4-543-2011.

Dinu Maria Jose, Amala Mary Vincent, and Gowdagere Siddaramaiah Dwarakish. Improving multiple model ensemble predictions of daily precipitation and temperature through machine learning techniques. *Scientific Reports*, 12(1):1–25, 2022. ISSN 20452322. doi: 10.1038/s41598-022-08786-w. URL https://doi.org/10.1038/s41598-022-08786-w.

C. Juez, N. Garijo, E. Nadal-Romero, and S. M. Vicente-Serrano. Wavelet analysis of hydro-climatic time-series and vegetation trends of the Upper Aragón catchment (Central Spanish Pyrenees). *Journal of Hydrology*, 614 (PB):128584, 2022. ISSN 00221694. doi: 10.1016/j.jhydrol.2022.128584. URL https://doi.org/10.1016/j.jhydrol.2022.128584.

Latif Kalin, Sabahattin Isik, Jon E. Schoonover, and B. Graeme Lockaby. Predicting Water Quality in Unmonitored Watersheds Using Artificial Neural Networks. *Journal of Environmental Quality*, 39(4):1429–1440, 2010. ISSN 00472425. doi: 10.2134/jeq2009.0441.

Matti Kämäräinen, Otto Hyvärinen, Andrea Vajda, Grigory Nikulin, Erik van Meijgaard, Claas Teichmann, Daniela Jacob, Hilppa Gregow, and Kirsti Jylhä. Estimates of Present-Day and Future Climatologies of Freezing Rain in Europe Based on CORDEX Regional Climate Models. *Journal of Geophysical Research: Atmospheres*, 123(23):13,291–13,304, 2018. ISSN 21698996. doi: 10.1029/2018JD029131.

Bonnie L. Keeler, Perrine Hamel, Timon McPhearson, Maike H. Hamann, Marie L. Donahue, Kelly A. Meza Prado, Katie K. Arkema, Gregory N. Bratman, Kate A. Brauman, Jacques C. Finlay, Anne D. Guerry, Sarah E. Hobbie, Justin A. Johnson, Graham K. MacDonald, Robert I. McDonald, Nick Neverisky, and Spencer A. Wood. Social-ecological and technological factors moderate the value of urban nature. *Nature Sustainability*, 2 (1):29–38, 2019. ISSN 23989629. doi: 10.1038/s41893-018-0202-1. URL http://dx.doi.org/10.1038/s41893-018-0202-1.

L. Keller, Andreas Paul Zischg, Markus Mosimann, Ole Rössler, Rolf Weingartner, and Olivia Martius. Large ensemble flood loss modelling and uncertainty assessment for future climate conditions for a Swiss prealpine catchment. *Science of the Total Environment*, 693:133400, nov 2019. ISSN 18791026. doi: 10.1016/j.scitotenv.2019.07.206.

Reto Knutti, M. R. Allen, P. Friedlingstein, J. M. Gregory, G. C. Hegerl, G. A. Meehl, M. Meinshausen, J. M. Murphy, G. K. Plattner, S. C.B. Raper, T. F. Stocker, P. A. Stott, H. Teng, and T. M.L. Wigley. A review of uncertainties in global temperature projections over the twenty-first century. *Journal of Climate*, 21(11):2651–2663, 2008. ISSN 08948755. doi: 10.1175/2007JCLI2119.1.

S. Kotlarski, K. Keuler, O. B. Christensen, A. Colette, M. Déqué, A. Gobiet, K. Goergen, D. Jacob, D. Lüthi, E. Van Meijgaard, G. Nikulin, C. Schär, C. Teichmann, R. Vautard, K. Warrach-Sagi, and V. Wulfmeyer. Regional climate modeling on European scales: A joint standard evaluation of the EURO-CORDEX RCM ensemble. *Geoscientific Model Development*, 7(4): 1297–1333, 2014. ISSN 19919603. doi: 10.5194/gmd-7-1297-2014.

Sven Kotlarski, Daniel Lüthi, and Christoph Schär. The elevation dependency of 21st century European climate change: An RCM ensemble perspective. *International Journal of Climatology*, 35(13):3902–3920, 2015. ISSN 10970088. doi: 10.1002/joc.4254.

T. N. Krishnamurti, C. M. Kishtawal, Timothy E. LaRow, David R. Bachiochi, Zhan Zhang, C. Eric Williford, Sulochana Gadgil, and Sajani Surendran. Improved weather and seasonal climate forecasts from multimodel superensemble. *Science*, 285(5433):1548–1550, 1999. ISSN 00368075. doi: 10.1126/science.285.5433.1548.

T. N. Krishnamurti, C. M. Kishtawal, Z. Zhang, T. LaRow, D. Bachiochi, E. Williford, S. Gadgil, and S. Surendran. Multimodel ensemble forecasts for weather and seasonal climate. *Journal of Climate*, 13(23):4196–4216, 2000. ISSN 08948755. doi: 10.1175/1520-0442(2000)013<4196:MEFFWA> 2.0.CO;2.

Valentina Krysanova and Mike White. Aperçu des progrès de l'évaluation des ressources en eau avec SWAT. *Hydrological Sciences Journal*, 60(5): 771–783, 2015. ISSN 21503435. doi: 10.1080/02626667.2015.1029482. URL http://dx.doi.org/10.1080/02626667.2015.1029482.

S. J. Lambert and G. J. Boer. CMIP1 evaluation and intercomparison of coupled climate models. *Climate Dynamics*, 17(2-3):83–106, 2001. ISSN 0930-7575. doi: 10.1007/pl00013736.

Stefano Larsen, Ute Karaus, Cecile Claret, Ferdinand Sporka, Ladislav Hamerlík, and Klement Tockner. Flooding and hydrologic connectivity modulate community assembly in a dynamic river-floodplain ecosystem. *PLoS ONE*, 14(4):1–22, 2019. ISSN 19326203. doi: 10.1371/journal.pone.0213227.

T. Lasanta, J. Arnáez, N. Pascual, P. Ruiz-Flaño, M. P. Errea, and N. Lana-Renault. Space–time process and drivers of land abandonment in Europe. *Catena*, 149:810–823, 2017. ISSN 03418162. doi: 10.1016/j.catena.2016.02.024. URL http://dx.doi.org/10.1016/j.catena.2016.02.024.

T. Lasanta, E. Nadal-Romero, and J. M. García-Ruiz. Clearing shrubland as a strategy to encourage extensive livestock farming in the Mediterranean Mountains. *Geographical Research Letters*, 45(2):487–513, 2019. ISSN 16979540. doi: 10.18172/cig.3616.

Teodoro Lasanta, Estela Nadal-Romero, and José Arnáez. Managing abandoned farmland to control the impact of re-vegetation on the environment. The state of the art in Europe. *Environmental Science and Policy*, 52: 99–109, 2015. ISSN 18736416. doi: 10.1016/j.envsci.2015.05.012.

Marc Lemus-Canovas and Joan Albert Lopez-Bustins. Assessing internal changes in the future structure of dry-hot compound events: The case of the Pyrenees. *Natural Hazards and Earth System Sciences*, 21(6):1721–1738, 2021. ISSN 16849981. doi: 10.5194/nhess-21-1721-2021.

Marc Lemus-Canovas, Joan A. Lopez-Bustins, Laura Trapero, and Javier Martin-Vide. Combining circulation weather types and daily precipitation modelling to derive climatic precipitation regions in the Pyrenees. *Atmospheric Research*, 220(January):181–193, 2019. ISSN 01698095. doi: 10.1016/j.atmosres.2019.01.018. URL https://doi.org/10.1016/j.atmosres.2019.01.018.

N. LeRoy Poff and J. D. Allan. Functional organization of stream fish assemblages in relation to hydrological variability. *Ecology*, 76(2):606–627, 1995. ISSN 00129658. doi: 10.2307/1941217.

Tong Li, Zhihong Jiang, Hervé Le Treut, Laurent Li, Lilong Zhao, and Lingling Ge. Machine learning to optimize climate projection over China with multi-model ensemble simulations. *Environmental Research Letters*, 16(9), 2021. ISSN 17489326. doi: 10.1088/1748-9326/ac1d0c.

Xin Zhong Liang, Kenneth E. Kunkel, Gerald A. Meehl, Richard G. Jones, and Julian X.L. Wang. Regional climate models downscaling analysis of general circulation models present climate biases propagation into future change projections. *Geophysical Research Letters*, 35(8):1–5, 2008. ISSN 00948276. doi: 10.1029/2007GL032849.

Sitian Liu, Julio Pérez-Sánchez, Patricia Jimeno-Sáez, Francisco Javier Alcalá, and Javier Senent-Aparicio. A novel approach to assessing the impacts of dam construction on hydrologic and ecosystem alterations. Case study: Castril river basin, Spain. *Ecohydrology and Hydrobiology*, 22(4): 598–608, 2022. ISSN 20803397. doi: 10.1016/j.ecohyd.2022.08.004. URL https://doi.org/10.1016/j.ecohyd.2022.08.004.

Manel Llena, Estela Nadal-Romero, Javier Zabalza-Martínez, Melani Cortijos-López, and Teodoro Lasanta. Effects of post-abandonment management on surface runoff in a Mediterranean mid-mountain basin. *Catena*, 237(December 2023), 2024. ISSN 03418162. doi: 10.1016/j.catena.2023.107775.

Adrián López-Ballesteros, Javier Senent-Aparicio, Carolina Martínez, and Julio Pérez-Sánchez. Assessment of future hydrologic alteration due to climate change in the Aracthos River basin (NW Greece). *Science of the Total Environment*, 733:139299, 2020. ISSN 18791026. doi: 10.1016/j.scitotenv.2020.139299. URL https://doi.org/10.1016/j.scitotenv.2020.139299.

J. I. López-Moreno and José M. García-Ruiz. Influence of snow accumulation and snowmelt on streamflow in the central Spanish Pyrenees / Influence de l'accumulation et de la fonte de la neige sur les écoulements dans les Pyrénées centrales espagnoles. *Hydrological Sciences Journal*, 49 (5), 2004. ISSN 0262-6667. doi: 10.1623/hysj.49.5.787.55135.

J. I. López-Moreno, M. Beniston, and J. M. García-Ruiz. Environmental change and water management in the Pyrenees: Facts and future perspectives for Mediterranean mountains. *Global and Planetary Change*, 61 (3-4):300–312, 2008. ISSN 09218181. doi: 10.1016/j.gloplacha.2007.10.004.

J. I. López-Moreno, S. M. Vicente-Serrano, E. Moran-Tejeda, J. Zabalza, J. Lorenzo-Lacruz, and J. M. García-Ruiz. Impact of climate evolution and land use changes on water yield in the ebro basin. *Hydrology and Earth System Sciences*, 15(1):311–322, 2011. ISSN 10275606. doi: 10.5194/hess-15-311-2011.

J. Lorenzo-Lacruz, S. M. Vicente-Serrano, J. I. López-Moreno, E. Morán-Tejeda, and J. Zabalza. Recent trends in Iberian streamflows (1945-2005). *Journal of Hydrology*, 414-415:463–475, 2012. ISSN 00221694. doi: 10.1016/j.jhydrol.2011.11.023. URL http://dx.doi.org/10.1016/j.jhydrol.2011.11.023.

Arthur F. Lutz, Herbert W. ter Maat, Hester Biemans, Arun B. Shrestha, Philippus Wester, and Walter W. Immerzeel. Selecting representative climate models for climate change impact studies: an advanced envelope-based selection approach. *International Journal of Climatology*, 36(12): 3988–4005, 2016. ISSN 10970088. doi: 10.1002/joc.4608.

J. I. López-Moreno, S. M. Vicente-Serrano, J. Zabalza, J. Revuelto, M. Gilaberte, C. Azorín-Molina, E. Morán-Tejeda, J. García-Ruiz, and C M. & Tague. Respuesta hidrológica del pirineo central al cambio ambiental proyectado para el siglo xxi. *Pirineos*, 169:160, 2014. doi: http://dx.doi.org/10.3989/Pirineos.2014.169004.

Àngela Manrique-Alba, Santiago Beguería, Antonio J. Molina, María González-Sanchis, Miquel Tomàs-Burguera, Antonio D. del Campo, Michele Colangelo, and J. Julio Camarero. Long-term thinning effects on tree growth, drought response and water use efficiency at two Aleppo pine plantations in Spain. *Science of the Total Environment*, 728:138536, 2020. ISSN 18791026. doi: 10.1016/j.scitotenv.2020.138536. URL https://doi.org/10.1016/j.scitotenv.2020.138536.

P Marcos-Garcia, A Lopez-Nicolas, and M Pulido-Velazquez. Combined use of relative drought indices to analyze climate change impact on meteorological and hydrological droughts in a Mediterranean basin. *Journal of Hydrology*, 554:292–305, 2017. ISSN 0022-1694. doi: https://doi.org/10.1016/j.jhydrol.2017.09.028. URL https://www.sciencedirect.com/science/article/pii/S0022169417306327.

C Martinez and J.A. Fernández. Iahris 2.2 indicators of hydrologic alteration in rivers: Free software. *Ministerio de Medio Ambiente. Universidad Politécnica de Madrid*, 2010.

José Martínez-Fernández, Nilda Sánchez, and Carlos M. Herrero-Jiménez. Recent trends in rivers with near-natural flow regime: The case of the river headwaters in Spain. *Progress in Physical Geography*, 37(5):685–700, 2013. ISSN 03091333. doi: 10.1177/0309133313496834.

C. Martínez Santa-María and Fernández Yuste J.A. Índices de Alteración Hidrológica en Ríos (IAHRIS). Manual de Referencia Metodológica Versión 1. *Ministerio de Medio Ambiente. Universidad Politécnica de Madrid*, pages 1–69, 2008. URL http://www.chduero.es/acciona5/metodologia/iharis.pdf.

C. F. McSweeney, R. G. Jones, R. W. Lee, and D. P. Rowell. Selecting CMIP5 GCMs for downscaling over multiple regions. *Climate Dynamics*, 44(11-12):3237–3260, 2015. ISSN 14320894. doi: 10.1007/s00382-014-2418-8.

Gerald A. Meehl, Francis Zwiers, Jenni Evans, Thomas Knutson, Linda Mearns, and Peter Whetton. Trends in extreme weather and climate events: Issues related to modeling extremes in projections of future climate change. *Bulletin of the American Meteorological Society*, 81(3):

427–436, 2000. ISSN 00030007. doi: 10.1175/1520-0477(2000)081<0427:TIEWAC>2.3.CO;2.

Andrés Mellado-Díaz, Jorge Rubén Sánchez-González, Simone Guareschi, Fernando Magdaleno, and Manuel Toro Velasco. Exploring longitudinal trends and recovery gradients in macroinvertebrate communities and biomonitoring tools along regulated rivers. *Science of the Total Environment*, 695:133774, 2019. ISSN 18791026. doi: 10.1016/j.scitotenv.2019.133774. URL https://doi.org/10.1016/j.scitotenv.2019.133774.

P. A. Minang, M. van Noordwijk, O. E. Freeman, C. Mbow, J. de Leeuw, and Catacutan. Climate-Smart Landscapes: Multifunctionality In Practice. Nairobi, Kenya:World Agroforestry Centre (ICRAF). *World Agroforestry Centre*, page 404, 2015.

Justin R. Minder, Theodore W. Letcher, and S. Mc Kenzie Skiles. An evaluation of high-resolution regional climate model simulations of snow cover and albedo over the rocky mountains, with implications for the simulated snow-albedo feedback. *Journal of Geophysical Research*, 121(15):9069–9088, 2016. ISSN 21562202. doi: 10.1002/2016JD024995.

Eugenio Molina-Navarro, Dennis Trolle, Silvia Martínez-Pérez, Antonio Sastre-Merlín, and Erik Jeppesen. Hydrological and water quality impact assessment of a Mediterranean limno-reservoir under climate change and land use management scenarios. *Journal of Hydrology*, 509:354–366, 2014. ISSN 00221694. doi: 10.1016/j.jhydrol.2013.11.053. URL http://dx.doi.org/10.1016/j.jhydrol.2013.11.053.

Juan Morales-García, Andrés Bueno-Crespo, Fernando Terroso-Sáenz, Francisco Arcas-Túnez, Raquel Martínez-España, and José M. Cecilia. Evaluation of synthetic data generation for intelligent climate control in greenhouses. *Applied Intelligence*, 53(21):24765–24781, 2023. ISSN 15737497. doi: 10.1007/s10489-023-04783-2.

Ana Moreno, Miguel Bartolomé, Juan Ignacio López-Moreno, Jorge Pey, Juan Pablo Corella, Jordi García-Orellana, Carlos Sancho, María Leunda, Graciela Gil-Romera, Penélope González-Sampériz, Carlos Pérez-Mejías, Francisco Navarro, Jaime Otero-García, Javier Lapazaran, Esteban Alonso-González, Cristina Cid, Jerónimo López-Martínez, Belén Oliva-Urcia, Sérgio Henrique Faria, María José Sierra, Rocío Millán, Xavier Querol, Andrés Alastuey, and José M. García-Ruíz. The case of a southern European glacier which survived Roman and medieval warm periods but is disappearing under recent warming. *Cryosphere*, 15(2):1157–1172, 2021. ISSN 19940424. doi: 10.5194/tc-15-1157-2021.

D. N. Moriasi, M. W. Gitau, N. Pai, and P. Daggupati. Hydrologic and water quality models: Performance measures and evaluation criteria. *Transactions of the ASABE*, 58(6):1763–1785, 2015. ISSN 21510032. doi: 10.13031/trans.58.10715.

Daniel Moriasi, Jeff Arnold, Michael Van Liew, Ron Bingner, R.D. Harmel, and Tamie Veith. Model evaluation guidelines for systematic quantification of accuracy in watershed simulations. *Transactions of the ASABE*, 50, 05 2007. doi: 10.13031/2013.23153.

J.M. Murillo and J.A. Navarro. Aplicación del modelo de témez a la determinación de la aportación superficial y subterránea del sistema hidrológico cornisa-vega de granada para su implementación en un modelo de uso conjunto. *Boletín Geológico y Minero*, 122:363–388, 2011. doi: ISSN:0366-0176.

F.O. Nachtergaele, H. Van Velthuizen, L. Verelst, and D. Wiberg. Harmonized world soil database. *IIASA*, version 1.2, 2012. doi: --.

Estela Nadal-Romero, Dhais Peña-Angulo, and David Regues. Rainfall, run-off, and sediment transport dynamics in a humid mountain badland area: Long-term results from a small catchment. *Hydrological Processes*, 32(11):1588–1606, 2018. ISSN 10991085. doi: 10.1002/hyp.11495.

Estela Nadal-Romero, Carmelo Juez, Makki Khorchani, Dhais Peña-Angulo, N. Lana-Renault, D. Regüés, Teodoro Lasanta, and José M. García-Ruiz. *Impacts of Land Abandonment on Flood Mitigation in Mediterranean Mountain Areas*. 05 2021. ISBN 978-3-030-77504-9. doi: 10.1007/698-2021-772.

Robert J. Naiman, Stuart E. Bunn, Christer Nilsson, Geoff E. Petts, Gilles Pinay, and Lisa C. Thompson. Legitimizing fluvial ecosystems as users of water: An overview. *Environmental Management*, 30(4):455–467, 2002. ISSN 0364152X. doi: 10.1007/s00267-002-2734-3.

Christer Nilsson and Magnus Svedmark. Basic principles and ecological consequences of changing water regimes: Riparian plant communities. *Environmental Management*, 30(4):468–480, 2002. ISSN 0364152X. doi: 10.1007/s00267-002-2735-2.

Seok Geun Oh and Myoung Seok Suh. Comparison of projection skills of deterministic ensemble methods using pseudo-simulation data generated from multivariate Gaussian distribution. *Theoretical and Applied Climatology*, 129(1-2):243–262, 2017. ISSN 14344483. doi: 10.1007/s00704-016-1782-1.

OPCC-CTP. *Climate change in the Pyrenees: Impacts, vulnerabilities and adaptation Bases of knowledge for the future climate change adaptation strategy in the Pyrenees*. OPCC-CTP, 2018. ISBN 9788409062683.

Leticia Palazón and Ana Navas. Modeling sediment sources and yields in a Pyrenean catchment draining to a large reservoir (Ésera River, Ebro Basin). *Journal of Soils and Sediments*, 14(9):1612–1625, 2014. ISSN 16147480. doi: 10.1007/s11368-014-0911-7.

Author Palomo and Ignacio Palomo. Climate Change Impacts on Ecosystem Services in High Mountain Areas : A Literature Review Climate Change Impacts on Ecosystem Services in High Mountain Areas : A Literature Review. 37(2):179–187, 2020.

Milan Paluš, Dagmar Novotná, and Petr Tichavský. Shifts of seasons at the European mid-latitudes: Natural fluctuations correlated with the North Atlantic Oscillation. *Geophysical Research Letters*, 32(12):1–4, 2005. ISSN 00948276. doi: 10.1029/2005GL022838.

Christina Papadaki, Konstantinos Soulis, Rafael Muñoz-Mas, Francisco Martinez-Capel, Stamatis Zogaris, Lazaros Ntoanidis, and Elias Dimitriou. Potential impacts of climate change on flow regime and fish habitat in mountain rivers of the south-western Balkans. *Science of the Total Environment*, 540:418–428, 2016. ISSN 18791026. doi: 10.1016/j.scitotenv.2015.06.134. URL http://dx.doi.org/10.1016/j.scitotenv.2015.06.134.

Fernando Pardo, Angel Velasco, and Luis Gil. Tercer Inventario Forestal Nacional 1997-2007: La Tranformación Histórica del Paisaje Forestal en Navarra. *Ministerio de Medio Ambiente, Gobierno de España*, 2:7–19, 2008. doi: --.

V. Pavan and F. J. Doblas-Reyes. Multi-model seasonal hindcasts over the Euro-Atlantic: Skill scores and dynamic features. *Climate Dynamics*, 16 (8):611–625, 2000. ISSN 14320894. doi: 10.1007/s003820000063.

N. Pepin, R. S. Bradley, H. F. Diaz, M. Baraer, E. B. Caceres, N. Forsythe, H. Fowler, G. Greenwood, M. Z. Hashmi, X. D. Liu, J. R. Miller, L. Ning, A. Ohmura, E. Palazzi, I. Rangwala, W. Schöner, I. Severskiy, M. Shahgedanova, M. B. Wang, S. N. Williamson, and D. Q. Yang. Elevation-dependent warming in mountain regions of the world. *Nature Climate Change*, 5(5):424–430, 2015. ISSN 17586798. doi: 10.1038/nclimate2563.

Julio Pérez-Sánchez, Javier Senent-Aparicio, Francisco Segura-Méndez, David Pulido-Velazquez, and Raghavan Srinivasan. Evaluating hydrological models for deriving water resources in peninsular Spain. *Sustainability (Switzerland)*, 11(10):1–36, 2019. ISSN 20711050. doi: 10.3390/su11102872.

Julio Pérez-Sánchez, Javier Senent-Aparicio, Carolina Martínez Santa-María, and Adrián López-Ballesteros. Assessment of ecological and hydro-geomorphological alterations under climate change using SWAT and IAHRIS in the Eo River in Northern Spain. *Water (Switzerland)*, 12 (6), 2020. ISSN 20734441. doi: 10.3390/W12061745.

S. E. Perkins, A. J. Pitman, N. J. Holbrook, and J. McAneney. Evaluation of the AR4 climate models' simulated daily maximum temperature, minimum temperature, and precipitation over Australia using probability density functions. *Journal of Climate*, 20(17):4356–4376, 2007. ISSN 08948755. doi: 10.1175/JCLI4253.1.

C. Piani, G. P. Weedon, M. Best, S. M. Gomes, P. Viterbo, S. Hagemann, and J. O. Haerter. Statistical bias correction of global simulated daily precipitation and temperature for the application of hydrological models. *Journal of Hydrology*, 395(3-4):199–215, 2010. ISSN 00221694. doi: 10.1016/j.jhydrol.2010.10.024. URL http://dx.doi.org/10.1016/j.jhydrol.2010.10.024.

Rafael Poyatos, Jérôme Latron, and Pilar Llorens. Land use and land cover change after agricultural abandonment: The case of a Mediterranean Mountain area (Catalan Pre-Pyrenees). *Mountain Research and Development*, 23(4):362–368, 2003. ISSN 02764741. doi: 10.1659/0276-4741(2003)023[0362:LUALCC]2.0.CO;2.

A. F. Prein, A. Gobiet, H. Truhetz, K. Keuler, K. Goergen, C. Teichmann, C. Fox Maule, E. van Meijgaard, M. Déqué, G. Nikulin, R. Vautard, A. Colette, E. Kjellström, and D. Jacob. Precipitation in the EURO-CORDEX 0.11° and 0.44° simulations: high resolution, high benefits? *Climate Dynamics*, 46(1-2):383–412, 2016. ISSN 14320894. doi: 10.1007/s00382-015-2589-y.

Liying Qiu, Eun Soon Im, Jina Hur, and Kyo Moon Shim. Added value of very high resolution climate simulations over South Korea using WRF modeling system. *Climate Dynamics*, 54(1-2):173–189, 2020. ISSN 14320894. doi: 10.1007/s00382-019-04992-x. URL https://doi.org/10.1007/s00382-019-04992-x.

R Ranzi, M Bochicchio, and B Bacchi. Effects on floods of recent afforestation and urbanisation in the Mella River (Italian Alps). *Hydrology and Earth System Sciences*, 6(2):239–254, 2002. doi: 10.5194/hess-6-239-2002. URL https://hess.copernicus.org/articles/6/239/2002/.

Roberto Ranzi, Paolo Caronna, and Massimo Tomirotti. *Impact of Climatic and Land Use Changes on River Flows in the Southern Alps*, pages 61–83. Springer Singapore, Singapore, 2017. ISBN 978-981-10-2051-3. doi: 10.1007/978-981-10-2051-3-3. URL https://doi.org/10.1007/978-981-10-2051-3-3.

Kabir Rasouli, John Pomeroy, and Paul Whitfield. Hydrological responses of headwater basins to monthly perturbed climate in the north american cordillera. *Journal of Hydrometeorology*, 20, 03 2019a. doi: 10.1175/JHM-D-18-0166.1.

Kabir Rasouli, John W. Pomeroy, and Paul H. Whitfield. Are the effects of vegetation and soil changes as important as climate change impacts on hydrological processes? *Hydrology and Earth System Sciences*, 23(12):4933–4954, 2019b. ISSN 16077938. doi: 10.5194/hess-23-4933-2019.

Alfredo Reder, Mario Raffa, Myriam Montesarchio, and Paola Mercogliano. Performance evaluation of regional climate model simulations at different spatial and temporal scales over the complex orography area of the Alpine region. *Natural Hazards*, 102(1):151–177, 2020. ISSN 15730840. doi: 10.1007/s11069-020-03916-x.

Brian D Richter and Holly E Richter. Society for Conservation Biology Prescribing Flood Regimes to Sustain Riparian Ecosystems along Meandering Rivers Published by : Wiley for Society for Conservation Biology Linked references are available on JSTOR for this article : Prescribing Flood Regim. *Wiley for Society for Conservation Biology*, 14(5):1467–1478, 2000.

Alexandre Rios-Entenza, P.M.M. Soares, Ricardo Trigo, Rita Cardoso, and Gonzalo Miguez-Macho. Moisture recycling in the iberian peninsula from a regional climate simulation: Spatiotemporal analysis and impact on the precipitation regime. *Journal of Geophysical Research: Atmospheres*, 05 2014. doi: 10.1002/2013JD021274.

Luc Roy, Robert Leconte, Franois P. Brissette, and Claude Marche. The impact of climate change on seasonal floods of a Southern Quebec river basin. *Hydrological Processes*, 15(16):3167–3179, 2001. ISSN 08856087. doi: 10.1002/hyp.323.

Alex Ruane and Sonali McDermid. Selection of a representative subset of global climate models that captures the profile of regional changes for integrated climate impacts assessment. *Earth Perspectives*, 4, 12 2017. doi: 10.1186/s40322-017-0036-4.

Markku Rummukainen. Added value in regional climate modeling. *Wiley Interdisciplinary Reviews: Climate Change*, 7(1):145–159, 2016. ISSN 17577799. doi: 10.1002/wcc.378.

Zulfaqar Sa'adi, Shamsuddin Shahid, Eun Sung Chung, and Tarmizi bin Ismail. Projection of spatial and temporal changes of rainfall in Sarawak of Borneo Island using statistical downscaling of CMIP5 models. *Atmospheric Research*, 197(November 2016):446–460, 2017. ISSN 01698095. doi: 10.1016/j.atmosres.2017.08.002. URL https://doi.org/10.1016/j.atmosres.2017.08.002.

D. A. Sachindra, K. Ahmed, Md Mamunur Rashid, S. Shahid, and B. J.C. Perera. Statistical downscaling of precipitation using machine learning techniques. *Atmospheric Research*, 212(September 2017):240–258, 2018. ISSN 01698095. doi: 10.1016/j.atmosres.2018.05.022. URL https://doi.org/10.1016/j.atmosres.2018.05.022.

Saleem A Salman, Shamsuddin Shahid, Tarmizi Ismail, Kamal Ahmed, and Xiao-Jun Wang. Selection of climate models for projection of spatiotemporal changes in temperature of Iraq with uncertainties. *Atmospheric Research*, 213:509–522, 2018. ISSN 0169-8095. doi: https://doi.org/10.1016/j.atmosres.2018.07.008. URL https://www.sciencedirect.com/science/article/pii/S016980951830557X.

Maria Sand, Ragnhild Bieltvedt Skeie, Marit Sandstad, Srinath Krishnan, Gunnar Myhre, Hannah Bryant, Richard Derwent, Didier Hauglustaine, Fabien Paulot, Michael Prather, et al. A multi-model assessment of the global warming potential of hydrogen. *Communications Earth & Environment*, 4(1):203, 2023.

Benjamin M. Sanderson, Reto Knutti, and Peter Caldwell. Addressing interdependency in a multimodel ensemble by interpolation of model properties. *Journal of Climate*, 28(13):5150–5170, 2015. ISSN 08948755. doi: 10.1175/JCLI-D-14-00361.1.

Alba Sanmiguel-Vallelado, Enrique Morán-Tejeda, Esteban Alonso-González, and Juan Ignacio López-Moreno. Effect of snow on mountain river regimes: an example from the Pyrenees. *Frontiers of Earth Science*, 11(3):515–530, 2017. ISSN 20950209. doi: 10.1007/s11707-016-0630-z.

S. Schauwecker, M. Rohrer, D. Acuña, A. Cochachin, L. Dávila, H. Frey, C. Giráldez, J. Gómez, C. Huggel, M. Jacques-Coper, E. Loarte, N. Salzmann, and M. Vuille. Climate trends and glacier retreat in the Cordillera Blanca, Peru, revisited. *Global and Planetary Change*, 119:85–97, 2014. ISSN 09218181. doi: 10.1016/j.gloplacha.2014.05.005. URL http://dx.doi.org/10.1016/j.gloplacha.2014.05.005.

Mikhail A. Semenov and Pierre Stratonovitch. Use of multi-model ensembles from global climate models for assessment of climate change impacts. *Climate Research*, 41(1):1–14, 2010. ISSN 0936577X, 16161572. URL http://www.jstor.org/stable/24870469.

Pranab Kumar Sen. Estimates of the Regression Coefficient Based on Kendall's Tau. *Journal of the American Statistical Association*, 63(324):1379–1389, 1968. doi: 10.1080/01621459.1968.10480934.

Javier Senent-Aparicio, Sitian Liu, Julio Pérez-Sánchez, Adrián López-Ballesteros, and Patricia Jimeno-Sáez. Assessing impacts of climate variability and reforestation activities on water resources in the headwaters of the Segura River Basin (SE Spain). *Sustainability (Switzerland)*, 10(9), 2018a. ISSN 20711050. doi: 10.3390/su10093277.

Javier Senent-Aparicio, Adrián López-Ballesteros, Julio Pérez-Sánchez, Francisco José Segura-Méndez, and David Pulido-Velazquez. Using multiple monthly water balance models to evaluate gridded precipitation products over peninsular spain. *Remote Sensing*, 10(6), 2018b. ISSN 2072-4292. doi: 10.3390/rs10060922. URL https://www.mdpi.com/2072-4292/10/6/922.

Roberto Serrano-Notivoli, Santiago Beguería, Miguel Ángel Saz, Luis Alberto Longares, and Martín de Luis. Spread: a high-resolution daily gridded precipitation dataset for spain–an extreme events frequency and intensity overview. *Earth System Science Data*, 9(2):721–738, 2017. doi: https://doi.org/10.20350/digitalCSIC/7393.

Gerhard Smiatek, Harald Kunstmann, and Alfonso Senatore. EURO-CORDEX regional climate model analysis for the Greater Alpine Region: Performance and expected future change. *Journal of Geophysical Research*, 121(13):7710–7728, 2016. ISSN 21562202. doi: 10.1002/2015JD024727.

Pedro M.M. Soares and Rita M. Cardoso. A simple method to assess the added value using high-resolution climate distributions: Application to the EURO-CORDEX daily precipitation. *International Journal of Climatology*, 38(3):1484–1498, 2018. ISSN 10970088. doi: 10.1002/joc.5261.

M. Soltani and A. Mofidi. Using Mann-Kendall and time series techniques forstatistical analysisof long-term precipitation in gorgan weather station. *World Applied Sciences Journal*, 28(7):902–908, 2013. ISSN 18184952. doi: 10.5829/idosi.wasj.2013.28.07.946.

Abhishekh Srivastava, Richard Grotjahn, and PaulA Ullrich. Evaluation of historical cmip6 model simulations of extreme precipitation over contiguous us regions. *Weather and Climate Extremes*, 29:100268, 06 2020. doi: 10.1016/j.wace.2020.100268.

K Stahl, H Hisdal, J Hannaford, L M Tallaksen, H A J van Lanen, E Sauquet, S Demuth, M Fendekova, and J Jódar. Streamflow trends in Europe: evidence from a dataset of near-natural catchments. *Hydrology and Earth System Sciences*, 14(12):2367–2382, 2010. doi: 10.5194/hess-14-2367-2010. URL https://hess.copernicus.org/articles/14/2367/2010/.

Iris T. Stewart, Daniel R. Cayan, and Michael D. Dettinger. Changes toward earlier streamflow timing across western North America. *Journal of Climate*, 18(8):1136–1155, 2005. ISSN 08948755. doi: 10.1175/JCLI3321.1.

Markus Stoffel, Bartłomiej Wyżga, and Richard A. Marston. Floods in mountain environments: A synthesis. *Geomorphology*, 272:1–9, 2016. ISSN 0169555X. doi: 10.1016/j.geomorph.2016.07.008.

Benjamin T. Stratton, Venakataramana Sridhar, Molly M. Gribb, James P. McNamara, and Balaji Narasimhan. Modeling the spatially varying water balance processes in a Semiarid Mountainous Watershed of Idaho. *Journal of the American Water Resources Association*, 45(6):1390–1408, 2009. ISSN 1093474X. doi: 10.1111/j.1752-1688.2009.00371.x.

Steve Swanson. Indicators of hydrologic alteration. *Bureau of Land Management Resource Notes*, 0(58):2, 2002.

Mou Leong Tan, Philip W. Gassman, Ju Liang, and James M. Haywood. A review of alternative climate products for SWAT modelling: Sources, assessment and future directions. *Science of the Total Environment*, 795: 148915, 2021. ISSN 18791026. doi: 10.1016/j.scitotenv.2021.148915. URL https://doi.org/10.1016/j.scitotenv.2021.148915.

Erich Tasser, Janette Walde, Ulrike Tappeiner, Alexandra Teutsch, and Werner Noggler. Land-use changes and natural reforestation in the Eastern Central Alps. *Agriculture, Ecosystems and Environment*, 118(1):115–129, 2007. ISSN 0167-8809. doi: https://doi.org/10.1016/j.agee.2006.05.004. URL https://www.sciencedirect.com/science/article/pii/S0167880906001575.

Karl E. Taylor, Ronald J. Stouffer, and Gerald A. Meehl. An overview of CMIP5 and the experiment design. *Bulletin of the American Meteorological Society*, 93(4):485–498, 2012. ISSN 00030007. doi: 10.1175/BAMS-D-11-00094.1.

J. Teng, N. J. Potter, F. H.S. Chiew, L. Zhang, B. Wang, J. Vaze, and J. P. Evans. How does bias correction of regional climate model precipitation affect modelled runoff? *Hydrology and Earth System Sciences*, 19(2):711–728, 2015. ISSN 16077938. doi: 10.5194/hess-19-711-2015.

Silvia Terzago, Jost von Hardenberg, Elisa Palazzi, and Antonello Provenzale. Snow water equivalent in the alps as seen by gridded data sets, cmip5 and cordex climate models. *The Cryosphere*, 11(4):1625–1645, 2017. doi: https://doi.org/10.5194/tc-11-1625-2017.

C. W. Thornthwaite. An approach toward a rational classification of climate. *Geographical Review*, 38(1):55–94, 1948. ISSN 00167428. URL http://www.jstor.org/stable/210739.

Csaba Torma, Filippo Giorgi, and Erika Coppola. Added value of regional climate modeling over areas characterized by complex terrain—Precipitation over the Alps. *AGU*, 175(4449):238, 2015. ISSN 00280836. doi: 10.1038/175238c0.

J.R. Témez. Modelo Matemático de Trasformación "Precipitación-Escorrentía". *Asociación de Investigación Industrial Eléctrica (ASINEL)*, 2, 1977.

Mirian Lago Valente, José Miguel Reichert, Rosane Barbosa Lopes Cavalcante, Jean Paolo Gomes Minella, Olivier Evrard, and Raghavan Srinivasan. Afforestation of degraded grasslands reduces sediment transport and may contribute to streamflow regulation in small catchments in the short-run. *Catena*, 204(June 2020), 2021. ISSN 03418162. doi: 10.1016/j.catena.2021.105371.

Erik van Meijgaard and Susanne Crewell. Comparison of model predicted liquid water path with ground-based measurements during CLIWA-NET. *Atmospheric Research*, 75(3):201–226, 2005. ISSN 0169-8095. doi: https://doi.org/10.1016/j.atmosres.2004.12.006.

Robert Vautard, Nikolay Kadygrov, Carley Iles, Fredrik Boberg, Erasmo Buonomo, Katharina Bülow, Erika Coppola, Lola Corre, Erik van Meijgaard, Rita Nogherotto, Marit Sandstad, Clemens Schwingshackl, Samuel Somot, Emma Aalbers, Ole B. Christensen, James M. Ciarlo, Marie Estelle Demory, Filippo Giorgi, Daniela Jacob, Richard G. Jones, Klaus Keuler, Erik Kjellström, Geert Lenderink, Guillaume Levavasseur, Grigory Nikulin, Jana Sillmann, Cosimo Solidoro, Silje Lund Sørland, Christian Steger, Claas Teichmann, Kirsten Warrach-Sagi, and Volker Wulfmeyer. Evaluation of the Large EURO-CORDEX Regional Climate Model Ensemble. *Journal of Geophysical Research: Atmospheres*, 126(17): 1–28, 2021. ISSN 21698996. doi: 10.1029/2019JD032344.

Kartik Venkataraman, Spandana Tummuri, Aldo Medina, and Jordan Perry. 21st century drought outlook for major climate divisions of Texas based on CMIP5 multimodel ensemble: Implications for water resource management. *Journal of Hydrology*, 534:300–316, 2016. ISSN 00221694. doi: 10.1016/j.jhydrol.2016.01.001. URL http://dx.doi.org/10.1016/j.jhydrol.2016.01.001.

S. M. Vicente-Serrano, F. Domínguez-Castro, C. Murphy, D. Peña-Angulo, M. Tomas-Burguera, I. Noguera, J. I. López-Moreno, C. Juez, S. Grainger, L. Eklundh, T. Conradt, C. Azorin-Molina, and A. El Kenawy. Increased Vegetation in Mountainous Headwaters Amplifies Water Stress During Dry Periods. *Geophysical Research Letters*, 48(18):1–10, 2021. ISSN 19448007. doi: 10.1029/2021GL094672.

Sergio M. Vicente-Serrano, Tim R. McVicar, Diego G. Miralles, Yuting Yang, and Miquel Tomas-Burguera. Unraveling the influence of atmospheric evaporative demand on drought and its response to climate change. *Wiley Interdisciplinary Reviews: Climate Change*, 11(2):1–31, 2020. ISSN 17577799. doi: 10.1002/wcc.632.

Daniel Viviroli, Hans H. Dürr, Bruno Messerli, Michel Meybeck, and Rolf Weingartner. Mountains of the world, water towers for humanity: Typology, mapping, and global significance. *Water Resources Research*, 43 (7):1–13, 2007. ISSN 00431397. doi: 10.1029/2006WR005653.

Bin Wang, Lihong Zheng, De Li Liu, Fei Ji, Anthony Clark, and Qiang Yu. Using multi-model ensembles of CMIP5 global climate models to reproduce observed monthly rainfall and temperature with machine learning methods in Australia. *International Journal of Climatology*, 38(13):4891–4902, 2018. ISSN 10970088. doi: 10.1002/joc.5705.

Sanford Weisberg. *Applied linear regression*, volume 528. John Wiley & Sons, 2005.

R. H. White and R. Toumi. The limitations of bias correcting regional climate model inputs. *Geophysical Research Letters*, 40(12):2907–2912, 2013. ISSN 00948276. doi: 10.1002/grl.50612.

Cort J Willmott. ON THE VALIDATION OF MODELS. *Physical Geography*, 2(2):184–194, 1981. doi: 10.1080/02723646.1981.10642213. URL https://doi.org/10.1080/02723646.1981.10642213.

Ellen Wohl, Brian P. Bledsoe, Robert B. Jacobson, N. Leroy Poff, Sara L. Rathburn, David M. Walters, and Andrew C. Wilcox. The natural sediment regime in rivers: Broadening the foundation for ecosystem management. *BioScience*, 65(4):358–371, 2015. ISSN 15253244. doi: 10.1093/biosci/biv002.

Ren Xu, Nengcheng Chen, Yumin Chen, and Zeqiang Chen. Downscaling and Projection of Multi-CMIP5 Precipitation Using Machine Learning Methods in the Upper Han River Basin. *Advances in Meteorology*, 2020, 2020. ISSN 16879317. doi: 10.1155/2020/8680436.

Zhenliang Yin, Qi Feng, Linshan Yang, Xiaohu Wen, Jianhua Si, and Songbing Zou. Long term quantification of climate and land cover change impacts on streamflow in an alpine river catchment, northwestern China. *Sustainability (Switzerland)*, 9(7), 2017. ISSN 20711050. doi: 10.3390/su9071278.

Xue Ying. An overview of overfitting and its solutions. In *Journal of physics: Conference series*, volume 1168, page 022022. IOP Publishing, 2019.

A. Zabaleta, M. Meaurio, J.A. Uriarte, T. Morales, and I. Antigüedad. Hydric vulnerability: recent hydrologic trends in the bay of biscay. *2nd International colloquium on Climate Change in mountain areas PYRADAPT*, 2:72–76, 2017. doi: 10.5194/hess-14-2367-2010. URL https://drive.google.com/file/d/1vBJ2pKzIvF-5X7E4Ij2gCxSekqkoiz-K/view.

Regino Zamora, Antonio J. Pérez-Luque, and Francisco J. Bonet. *Monitoring Global Change in High Mountains*, volume 62. 2017. ISBN 9783319559810. doi: 10.1007/978-3-319-55982-7_16.

Giuseppe Zappa, Len C. Shaffrey, and Kevin I. Hodges. The ability of CMIP5 models to simulate North Atlantic extratropical cyclones. *Journal of Climate*, 26(15):5379–5396, 2013. ISSN 08948755. doi: 10.1175/JCLI-D-12-00501.1.

Zhenzhong Zeng, Zaichun Zhu, Xu Lian, Laurent Z.X. Li, Anping Chen, Xiaogang He, and Shilong Piao. Responses of land evapotranspiration to Earth's greening in CMIP5 Earth System Models. *Environmental Research Letters*, 11(10), 2016. ISSN 17489326. doi: 10.1088/1748-9326/11/10/104006.

Ling Zhang, R. Karthikeyan, Zhongke Bai, and R. Srinivasan. Analysis of streamflow responses to climate variability and land use change in the Loess Plateau region of China. *Catena*, 154:1–11, 2017. ISSN 03418162. doi: 10.1016/j.catena.2017.02.012. URL http://dx.doi.org/10.1016/j.catena.2017.02.012.

Huanhuan Zhu, Zhihong Jiang, Laurent Li, Wei Li, Sheng Jiang, Panyu Zhou, Weihao Zhao, and Tong Li. Intercomparison of multi-model ensemble-processing strategies within a consistent framework for climate projection in china. *Science China Earth Sciences*, 66(9):2125–2141, 2023.

Xueping Zhu, Aoran Zhang, Penglin Wu, Wei Qi, Guangtao Fu, Guangtao Yue, and Xiaoqing Liu. Uncertainty impacts of climate change and downscaling methods on future runoff projections in the Biliu River basin. *Water (Switzerland)*, 11(10):1–17, 2019. ISSN 20734441. doi: 10.3390/w11102130.

X. W. Zhuang, Y. P. Li, G. H. Huang, and J. Liu. Assessment of climate change impacts on watershed in cold-arid region: an integrated multi-GCM-based stochastic weather generator and stepwise cluster analysis method. *Climate Dynamics*, 47(1-2):191–209, 2016. ISSN 14320894. doi: 10.1007/s00382-015-2831-7.

Universidad del País Vasco / Euskal Herriko Unibertsitatea

Zientzia eta Teknologia Fakultatea

Kuaternarioa: Ingurugiro Aldaketak eta Giza Oinatzak Doktoregoa

Doktorego Tesia

Klima Aldaketari buruzko Perspektiba Klimatiko eta Hidrologikoak Pirinioetan: Ikuspegi Integratua

—Euskarazko bertsio murriztua—

Egilea: Nerea Bilbao Barrenetxea

Zuzendariak: Dr. Sérgio Henrique Faria
Dr. Javier Senent-Aparicio

Bilbao, 2024ko Maiatza

Laburpena

Goi–mendietako eskualdeek, beren elementu kriosferikoek, hala nola elurrak, permafrostek eta glaziarrek, gero eta arrisku handiagoa dute klima–aldaketaren aurrean. Eremu horiek, Pirinioak barne, erronka hidroklimatiko handiei aurre egin behar diete. Pirinioek, tesi honen ardatz nagusiak, ezaugarri klimatiko eta hidrologiko bereziak dituzte, eta horiek azterketa zehatza eskatzen dute beren sistema hidroklimatikoak ulertzeko.

Goi–mendiko eskualdeak kritikoak dira ikuspegi ekologiko, sozial eta ekonomikotik, eta klima–aldaketak gehien eragiten dituenetako batzuk dira. Gainazaleko airearen tenperaturaren hazkuntzak, batez ere altitudearen mendeko berotzearen ondorioz, eragin garrantzitsuak ditu elur– eta glaziar–masan, eta mende amaierarako nabarmen txikituko direla aurreikusten da. Elur–estalkiaren eta glaziar–masaren murrizketa horrek eragin zuzena du eskualde horietako ur–baliabideetan, ekosistemetan eta egitura sozioekonomikoetan.

Tesi honen bidez, Pirinioetako eskualdea hobeto ulertu nahi dugu, eta, horretarako, sistema hidroklimatikoaren alderdi kritikoak aztertuko ditugu egungo ingurumen–testuinguruan. Ikerketa hainbat helburu nagusiri erantzuteko egituratuta dago, goi–mendietako eskualdeen nazioarteko ikuspegi orokor batetik hasita, bereziki Pirinioetan zentratuz, eta klima–aldakortasunari, lurzoruaren erabilera–aldaketei eta karakterizazio klimatikoak eta hidrologikoak hobetzeko makinen ikaskuntzaren aplikazioari buruzko ikerketa zehatzen bidez aurrera eginez. Tesia Pirinioetako mendikate osoa eta arroko eskala espezifikoak aztertzeko dago egituratuta, eskualdeko hidrologiaren eta klimaren arteko elkarrekintzei buruzko ikuspegi integrala eskainiz.

1. kapituluan, klima–aldakortasunak eta lurraren erabilera–aldaketek Pirinioetako ziklo hidrologikoan duten eragina aztertzen da. Mendebaldeko Pirinioetan dagoen arro batean egindako analisi kuantitatibo baten bidez, klima aldaketak eta lurraren erabilerak ziklo hidrologikoaren aldaketetan egindako ekarpen indibidualak aztertzen dira kapituluan, muturreko balioak ardatz hartuta. Aurkikuntzek faktore horiek eragin handia dutela ur–emariaren patroi eta prozesu hidrologikoetan azpimarratzen dute, eta eskualdeko baliabide hidrikoen egungo eta etorkizuneko egoerei buruzko ezagutza baliotsuak ematen dituzte.

2. kapituluan, Pirinioetan bereizmen handiko simulazio–produktu klimatikoen gaitasunak eta mugak aztertzen dira. Kapitulu honetan simulazio horien ahuleziak eta indarguneak identifikatzeko eta kuantifikatzeko aukera ematen duen metodologia bat erabiltzen da, muturreko gertaerak

eta emaitzen banaketa espaziala bereziki aztertuz. Ikerketa honek, simulazio horiek eskualdean duten kalitateari buruzko egungo ezagutza nabarmen hobetzen lagundu du.

3. kapituluan, makinen ikaskuntza–planteamenduak kontuan hartu dira, karakterizazio klimatikoak eta hidrologikoak hobetzeko. Makinen ikaskuntzarako algoritmoak eredu klimatikoaren irteeretan aplikatuz, kapitulu honek iragarpen hidrologikoen zehaztasuna hobetzeko helburua du. Teknika aurreratu horiek modelatze–planteamendu tradizionalekin integratzeak berrikuntza metodologiko garrantzitsua dakar hidrologia eta klima ikerketa–eremuan.

Laburbilduz, tesi honek Pirinioetako klima– eta ur–sistemen hainbat alderdiren azterketa zehatza eta sakona eskaintzen du. Modelizazio–teknika aurreratuak, bereizmen handiko simulazioak eta Machine Learning planteamenduak erabiltzeak aurrerapen metodologiko bat suposatzen du, goi–mendietako eskualdeetako ur–baliabideak kudeatzeko gaitasun iragarleetan laguntzen duena. Tesiak espazio–eskala eta ikuspegi metodologiko anitz integratzen ditu, Pirinioetako eskualdeko dinamika konplexuaren ulermen holistiko bat ematen laguntzeko. Tesiaren bertsio hedatua, non helburuak eta ondorioak sakontzen diren, *"Climatic and hydrological Perspectives on Climate Change in the Pyrenees: An Integrated Approach"* izeneko ingelesezko bertsioan kontsulta daiteke.

Aurkibidea

Irudien Aurkibidea

Taulen Aurkibidea

1

Klimaren aldakortasunak eta lurzoruaren erabileraren aldaketak ur baliabideetan duen eragina

Mendiek ezinbesteko eginkizuna betetzen dute ur–geza biltegiratzean, munduko biztanleriaren erdiari ur–baliabideak eskeiniz (Viviroli et al., 2007; Immerzeel et al., 2020). Hala ere, azken hamarkadetan, aldaketa handiak eman dira ziklo hidrologikoa eratzen duten aldagai eta prozesuetan; klima aldagaietan, lur estalduran, elur estalduran eta lurzoruaren propietateetan, esaterako. Zeintzuek ezinbesteko eragina duten ur baliabideen erabilgarritasunean (Arnell, 1999; Beguería et al., 2003; Stewart et al., 2005). Mendi–eskualdeen zahurgarritasuna bereziki nabarmena da Pirinioen kasuan, klima Mediterraneo eta Atlantikoen artean kokatuak, non tenperatura eta prezipitazio–patroietan aldaketa nabariak jasaten ari diren (Amblar-Francés et al., 2020). Era berean, elur–estaldura eta horren metatze eta urtzea zuzenki harremanduta dago Pirinioetako erreken ur–emariarekin (López-Moreno and García-Ruiz, 2004) eta klima aldaketaren testuinguruan ere aldatzen dira. Urteotan klimaren aldakortasunak aldaketak eragin ditu erreketeako ur–emariaren denbora eta kantitatean.

Kapitulu honetan, Pirinioetako eskualdearen ziklo hidrologikoaren, klima–aldaketaren eta lurraren erabilera–aldaketen arteko erlazioak aztertzen ditu (1.1 atala). Hori lortzeko, azterketa kuantitatibo bat egiten du mendebaldeko Pirinioetako arro batean, faktore horiek ziklo hidrologikoaren aldaketan egiten dituzten ekarpen indibidualak ezagutzeko, eta bereziki muturreko balioetan jartzen du arreta (1.3 eta 1.4 atalak). Kapitulu honek, horrela, erregimen hidrologikoaren, klima–aldaketaren eta lurraren erabileraren arteko elkarrekintzei buruzko informazioa ematen du (**2 Helburua**), dinamika horiek hobeto ulertzeko. Ahalegin honen bidez, Pirinioetako erregio hidrologikoaren egungo egoerari eta bilakaerari buruzko ezagutza baliotsuak eskaini nahi dira, **1 Mugarria** betetzen lagunduz.

Lurzoruaren erabilera–aldaketak prozesu hidrologikoetan eragina duten funtzesko aldagaiak dira. 1950. urtetik Pirineo (Poyatos et al., 2003) eta Alpeetako (Ranzi et al., 2002; Tasser et al., 2007) mendi eskualdeek aldaketa nabarmenak izan dituzte lurraren erabileran, hala nola, laborantza lurren uztea eta ondorengo basoberritzea. Altitute ertaineko inguruetan bereziki (hau da, 1600 metrotatik behera kokatutatkoak (García-Ruiz et al., 1995)). basoberritze hori munduan zehar hedatu da azken hiru hamarkadetan (Zeng et al., 2016; FAO, 2014). Basogintza eta nekazaritzarako lurren uzteak eragina izan du ebapotranspirazioan (Haria and Price, 2000; Rasouli et al., 2019a), intertzeptazio eta beste prozesu hidrologikoetan (Beguería et al., 2003). Ikerketa ugarik aldaketa horiek ziklo hidrologikoan eragin ditzaketen aldaketak ikertu dituzte, basoberritzearen ondorioz erreken ur–emariaren murrizketa nabarmenak ematen direla azaleratuz (Rasouli et al., 2019b; Guo et al., 2024; Ranzi et al., 2017), horrek mendiko ekosisteman ekar ditzakeen ondorio potentzialekin (Boix-Fayos et al., 2020). Horretaz gain, lurraren erabileraren aldaketek uholde eta lehorteen erregimenetan eragina dute (Ranzi et al., 2002). Hainbat ikerketek uholdeen arintze potentziala adierazi dute basoberritze praktiken ondorioz (Nadal-Romero et al., 2021; Valente et al., 2021).

1.1 Pirinioetako ziklo hidrologikoan eragina duten faktoreak

Pirinioetako ziklo hidrologikoen aldaketetan faktore horiek duten eragina sakonki ikertu da. López-Moreno et al. (2008)-k isurketa–joera negatiboa ikusi zuen Pirinioetako hainbat arrotan, ebapotranspirazio potentzialaren (PET) areagotzearekin, klima–faktoreen ondorioz isurketa ahalmen murrizketa iradokiz. Hala ere, klima–eragileak ez dira ur–emariaren beherakadaren eragile bakarrak (López-Moreno et al., 2011). Horietaz gain, berotze globalaren ondoriozko elur–estaldura murrizketak ere erregimen hidrologikoetan eragina izan du (López-Moreno and García-Ruiz, 2004; Sanmiguel-Vallelado et al., 2017). Dena den, ikertzaile askok Pirinioetako ur–emariaren beherakada lurraren erabileraren aldaketei egotzi dizkiete (Juez et al., 2022; Lorenzo-Lacruz et al., 2012; Martínez-Fernández et al., 2013).

Horregatik, kapitulu hau, klima–aldakortasunak eta lurraren erabileraren aldaketek ziklo hidrologikoan duten eragina isolatzen eta kuantifikatzen saiatzen da. Ikuspegi analitiko hori askotan erabili izan da, SWAT eredu hidrologikoa aprobetxatuz, funtsa fisikoetan oinarritutako eredu banatua (Senent-Aparicio et al., 2018a; Zhang et al., 2017; Yin et al., 2017). Metodologia hori Iberiar penintsulako hainbat arrotan aplikatu da (Molina-Navarro et al., 2014; Senent-Aparicio et al., 2018a); adibidez, Senent-Aparicio et al. (2018a)-k klima–aldakortasun eta basoberritze ahaleginek Segura ibaiko iturburuetako baliabideetan duten eragina aztertu du. Era berean, Molina-Navarro et al. (2014)-k, klima–aldaketak eta lurraren erabileraren kudeaketak Tajo ibaiaren goiko arroen barruan dagoen Pareja urtegiko ur–isurketetetan dituzten ondorioak ikertu ditu.

Ibaietako Alterazio Hidrologikoaren Adierazleak –IAHRIS, (Martinez and Fernández, 2010)– softwarean jasotako adierazleak lur–uzteak ur–baliabideetan duen eragina aztertzeko erabili dira. Software horrek ur–emariaren hiru elementu nagusien (oiho balioak, uholdeak eta lehortzeak) magnitude, aldakortasun, urtaro eta iraupenari buruzko 22 indize ebaluatzen ditu (Mellado-Díaz et al., 2019). Baliabide hori Espainian garatu da Europako Uren Esparruko Zuzendaritzaren eskakizunak betetzeko. Haren helburua, oso eraldatutzat identifika daitezkeen ur masak identifikatzea; bereziki azken mendean Espainian eraikitako urtegien eraikitze garrantzitsuaren ondorioz (Fernández et al., 2012; Liu et al., 2022). Jatorrizko erabileraz haratago, egile batzuek IAHRIS erabili dute klima–aldaketak ur–baliabideetan duen eragina ebaluatzeko (Aznarez et al., 2021; Jiménez-Navarro et al., 2021; López-Ballesteros et al., 2020; Pérez-Sánchez et al., 2020). Ikerketa hori lur–uzteak ibaietako erregimen hidrologikoetan duen eragina ebaluatzeko adierazle horiek erabiltzen dituen lehena da. Gainera, gure helburua klima–aldakortasunak eta lurraren erabileraren aldaketak erregimen hidrologikoetan duten eragina ebaluatu eta kuantifikatzea da.

1.2 Pirinioetako mendebaldeko Anduña ibaiko arroaren kasuaren ikerketa

Anduña ibaiaren arroa (1.1 irudia) Espainiar Pirinioetako mendilerroaren mendebaldean kokatua dago eta 4728,61 hektareako azalera du. Bertako lurzorua orografikoki konplexua da eta malda gogorrak ditu ezaugarri,

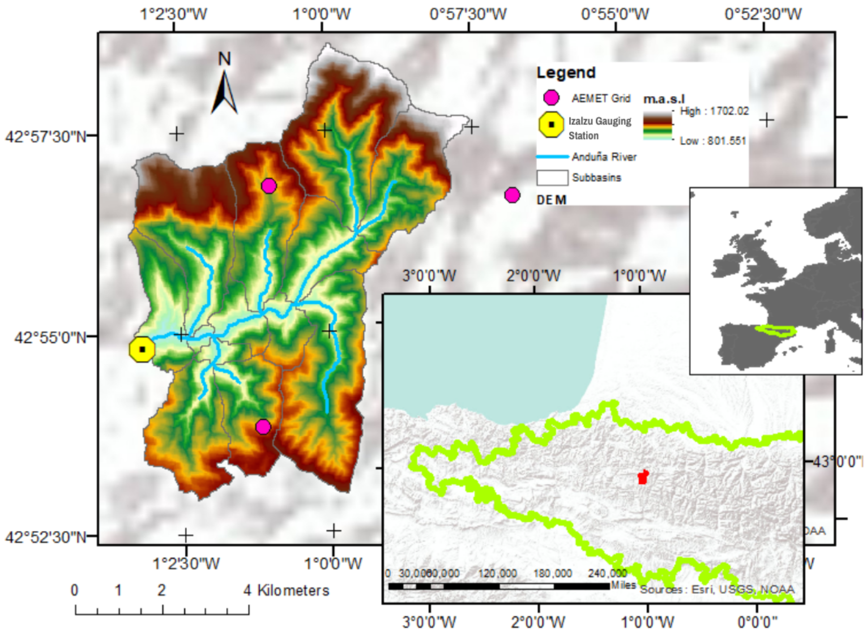

1.1 IRUDIA: a) Pirinioetako eskualdearen kokapen–mapa. b) Anduña ibaiaren arroaren kokapen–mapa. c) Anduña ibaiaren arroaren lur–zoruaren eredu digitala (DEM) eta Anduña ibaiaren neurketa–estazioaren kokapena.

azterketa arroari 801 m-tik 1702 m-rako tarte zabala emanez. Klima nagusiki Atlantikoa da, bi prezipitazio gailur ezberdinekin; udazken eta udaberrian (Amblar-Francés et al., 2020). Inguruak gutxi gorabehera 1750 mm-ko prezipitazioa jasotzen du urtean, bataz beste. Altuera handia dela eta, inguruko eremuekin konparatuz, eskualde honek tenperatura baxuagoak izaten ditu. Izulzako neurketa estazioak 46.2 hm^3-ko erreka–emaria erregistratzen du urtero; erregimen hidrologikoari dagokionez, udako hilabeteetan gutxieneko emaria erregistratzen du eta urtarril eta martxoan gehienezko bi isurketa–gailur ditu. Hori prezipitazio erregimenengatik da, eta udaberriko elur–urtzeen eragina gehituz.

1956tik aurrera, lurraldeko lurraren erabileraren eboluzioa nabarmena izan da. 1950eko hamarkadan, eskualdeko populazioa bereziki nekazaria eta landatarra zen, nekazaritza eta abeltzaintzara zegoen bideratua lurraren erabilera, mekanikazio urriarekin. Euriaz hornitutako laborantza eta abeltzaintza estentsiboak sortutako larre eta sastraka hedapen handiak nagusitu ziren (Pardo et al., 2008). Hala ere, hurrengo hamarkadetan Pirinioetako landa eremuak izan zuen hustutze masiboak inguruko basoberritzea ekarri zuen. Ondorioz, lurraldea basoz osatu zen batez ere (García-Ruiz et al., 1995), konifero eta egur gogorrez osatuak.

1.3 Klima–aldakortasunaren eta lurzoruaren erabilera aldaketen inpaktuak ur–baliabidetan.

1.2 irudiak ikerketa honetan erabilitako metedologiaren fluxu–diagrama aurkezten du, non lehen pausua aldi historikorako aldagai klimatikoen Mann–Kendall joera–analisia egitea izan zen. Ondoren, eguneroko ur–emariaren datuak erabiliz, SWAT eredua garatu, kalibratu eta balioztatu zen. Anduña ibaiaren arroko SWAT eredua A, B eta C eszenatokiak simulatzeko erabili zen. Eszenatoki horiek lurraren erabilera aldaketek eta klimaren aldakortasunak errekaren ur–emarian izan dituen ondorioak simulatu dituzte; 1956-1985 eta 1986-2021 urte tarteetarako. A eszenatokia 1951-1985 urte tarteko klima datuetan eta 1956 lurraren erabileraren mapan oinarritu zen.. Beraz, A eszenatokia izan zen oinarrizko egoera. B eszenatokiak basoberritze prozesuaren aurretik zegoen lurraren erabileraren mapa mantendu zuen eta 1986-2021 urte tarteko klima datuak sartu zituen. Orduan, B eszenatokiak klima–aldakortasunak eragindako aldagai hidrologikoen aldaketari buruzko informazioa eman zuen. Amaitzeko, C eszenatokiak, 1986-2021 urte tarteko klima datuak kontuak hartzeaz gain, 2000. urteko lurraren erabileraren mapa eguneratu zuen. Horregatik, eszenatoki honek lurraren erabileraren aldaketa eta klima aldakortasunaren ondorio bateratuek sorutako aldaketak kontuan hartu zituen.

Ikerketak, ibaiaren aldaketaren zenbatekoa neurtzeko, ziklo hidrologikoaren aldaketak aztertu ditu; isurketa eta PET-an zentratu eta aldaketa hidrologikoaren adierazleak (IHA) erabiliz.

1.3.1 Klima aldagaien joera–analisia

Ikerketa honek denboraldi historikoko tenperatura maximo eta minimoen eta prezipitazioen joerak identifikatzeko, Mann–Kendall proba erabili du. Helburua denbora serieak goranzko edo beheranzko joera esanguratsua erakusten zituen zehaztea zen; joera monotoniko moduan ezagutzen direnak. Test ez–parametriko gisa, edozein banaketarekin funtzionatzen du (hau da, aldagaiak ez du banaketa normalaren suposizioa bete behar). Mann–kendall proba askotan erabili izan da tendentziek denbora serie

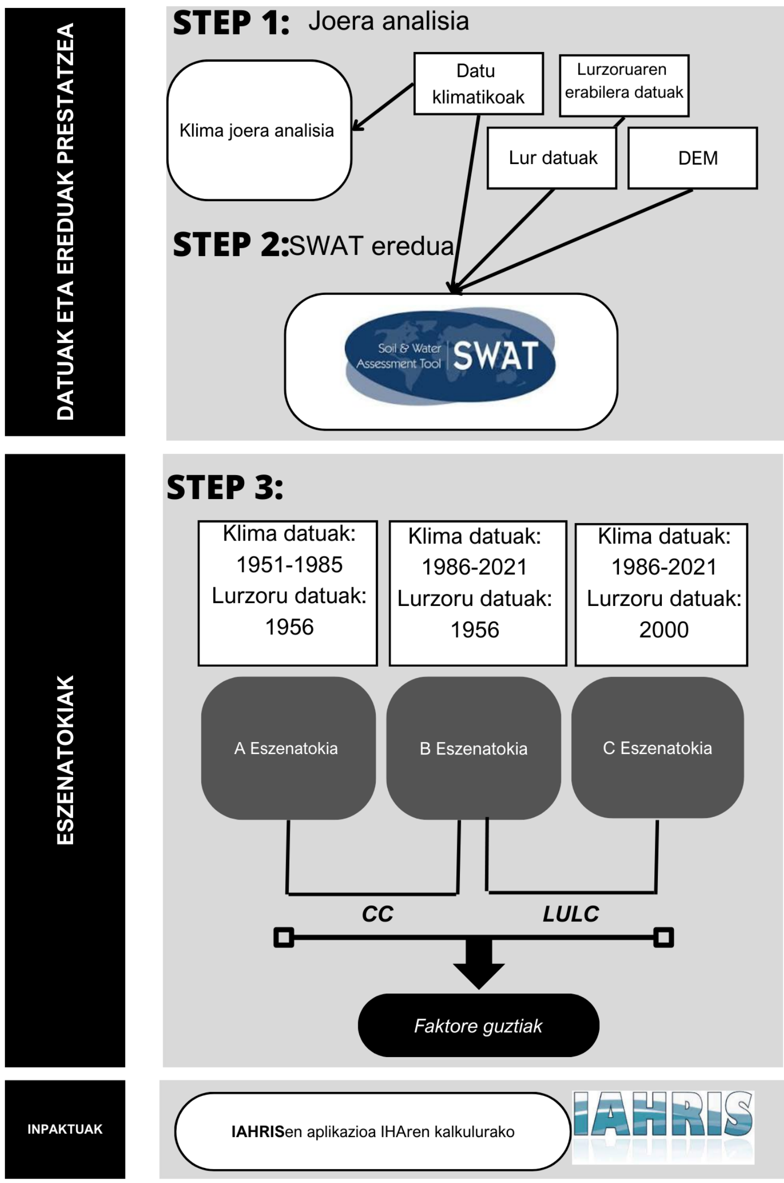

1.2 IRUDIA: 1. Kapituluan egindako azterlanean aplikatutako metodologiaren fluxu–diagrama metereologikoetan duten garrantzia kuantifikatzeko (Gocic and Trajkovic, 2013; Soltani and Mofidi, 2013). Z proba tendentzia esanguratsuen presentzia edo falta ebaluatzeko erabiltzen da; Z–balio negatiboak (positibo) tendentzia negativo (positibo) bati egiten dio erreferentzia. Gainera, Sens maldak (Sen, 1968) joera linealaren malda estimatzen du tendentzien magnitudeari buruzko informazioa emanez, eta, beste neurgailu batzuekin konparatuz, balore atipikoei hain sentikorra izan gabe. N datu pareetarako ematen da adierazpen hau erabiliz:

$$Q_i = median(\frac{x_j - x_k}{j - k}) \ \ for\ i = 1, ..., N \quad (1)$$

non x_j eta x_k j eta k ($j \geq k$) denboran dauden datu–balioak diren, hurrenez hurren. Bi metodoak Pynthon paketeak erabiliz aplikatu dira Mann–Kendall tendentzia–proba ez parametrikoetarako.

1.3.2 SWAT ereduaren deskribapena

SWAT eredu hidrologiko banatua da, aztergai den eskualdeko arroak azpiarro askotan banatu zituena, erantzun hidrologikoko unitateetan (HRU) banatua. Horrela, ereduak ibai–sare eta inguruaren heterogeneotasuna kontuan hartzen ditu (Arnold et al., 2012). HRU bakoitzak lur–estaldua, lurzoru mota eta malda konbinatzen ditu. SWAT eredua, mundu guztian zehar ezaugarri ezberdinak dituzten arroetan, askotan eta arrakastaz aplikatu da (Krysanova and White, 2015).

1.3.2.1 Modelizazio hidrologikorako sarrerako datuak

SWAT eredurako sarrera gisa erabilitako DEM datuek 25 m x 25 m-ko bereizmen espaziala zuten, Espainiako Geografia Insititututik lortuak (IGN, 2017). Harmonized World Soil Map izan zen ikerketa honetan erabilitako lurzoruaren datu multzoa; 1 km x 1km-ko bereizmen espaziala duena. Klimaren eta lurraren erabileraren datuak eszenatokiaren arabera aldatu ziren. Klima datuak, 1951-1985 eta 1986-2020 urte tarteko tenperatura maximo eta minimoa eta prezipitazio datuak biltzen dituena, Espainiako Metereologia Agentziatik (AEMET) lortu dira, 5 km x 5 km-bereizmen espazialarekin eta eguneroko denbora maiztasunarekin. 1956 eta 2000. urteetako lurraren erabileraren mapak erreferentziazko datu gisa erabili ziren bi aldi historikoetarako. Nafarroako Gobernuko datu iturrietatik deskargatu dira. Anduña ibaiaren arroko lur erabileraren sei lur motak ondorengoak izan ziren: lur biluztuak, hosto zabaleko basoak, koniferoz osatutako baso iraunkorrak, baso mistoak, larreak eta zuhaixkak. Amaitzeko, azterketa–arroko isurketen behaketak (Izalzu, 1.1. Irudia), Espainiako Gobernuko Lan Publikoen Azterketa eta Esperimentazio Zentrotik eskuratu ziren (CEDEX web–orrialdea).

1.3.2.2 Ereduaren errendimenduaren kalibrazio, balioztatze eta ebaluazioa

SWAT ereduaren sentikortasun–analisia eta kalibrazioa SWAT–CUP (Abbaspour et al., 2007) programa eta SUFI–2 algoritmoaren ziurgabetasun sekuentziala erabiliz garatu ziren. Tresna honek SWAT erabiltzaileei kalibrazio automatikoak modu eraginkorragoan egiteko aukera ematen die, eta SWAT komunitateak asko erabili du (Arnold et al., 2012). Lehenik eta behin, sentikortasun–analisi global bat egin zen, ur–emarian gehien eragiten duten parametroak identifikatzeko. 500 errepikapenetan aztertutako parametroetatik, 0,005etik beherako p balioak lortzen dituztenak hautatu ziren. Gainera, kalibrazioan elurrarekin lotutako bost parametro aztertu ziren, elurraren dinamikak azterketa–eremuan ziklo hidrologikoan duen eraginagatik (Palazón and Navas, 2014). Ondoren, kalibrazio automatikoa aplikatu zen emaria hobekien erreproduzitu zuten parametroen balioak zehazteko, Kling–Guptaren eraginkortasuna (KGE) funtzio helburutzat hartuta. Guztira, 1.000 simulazio egin ziren, hasieran 500, eta gero beste 500, dohitutako parametroen tarteak erabiliz.

Ereduak kalibrazio eta balioztatze–faseetan duen errendimendua kuantitatiboki ebaluatzeko, hurrengo bost metrikak erabili ziren: Nash–Sutcliffe-ren eraginkortasuna (NSE), errore karratuaren batez besteko erroa (RMSE), ehuneko alborapena (PBIAS), determinazio–koefizientea (R^2) eta KGE, Moriasi et al. (2015)-ek ezarritako ebaluazio–prozedura gomendatuaren arabera. Ereduzko estatistiken emaitzak Kalin et al. (2010)-ek proposatutako irizpideekin ebaluatu ziren. Irizpide horien arabera, emaitzak oso onak, onak, gogobetegarriak eta asegarriak dira.

1.3.3 IHARIS software

Ibaietan ematen diren aldaketak ebaluatzeko metodo ohikoenetako bat IHAk kalkulatzea da (Papadaki et al., 2016; López-Ballesteros et al., 2020). Metodo horrek simulatutako eta oinarrizko eszenatokien arteko aldaketa mailari buruzko informazioa ematen du. Kasu honetan, Anduña ibaiaren arroan klima–aldakortasunak eta lurraren erabilera–aldaketak eragindako aldaketa–maila ebaluatu genuen, eta, horri esker, IHAei faktore bakoitzak egiten dion ekarpena zehaztu ahal izan genuen. Metodo hori IAHRIS

2.2 softwarearen bidez aplikatu zen, 1.1 taulan deskribatutako 24 IHAak barne hartzen dituena. Fluxu–erregimenaren alderdi esanguratsuenetan oinarrituta (magnitudea, maiztasuna, aldakortasuna, urtarokotasuna eta iraupena), IAHRISek muturreko maximoei (uholdeak), gutxieneko muturrekoei (lehorteak) eta ohiko balioei lotutako IHAk ezartzen ditu.

1.1 TAULA: IAHRIS erabiltzen duten IHAen zerrenda.

Erregimenaren osagaiak	Ikuspegia	Adierazlea	Deskribapena
Ohiko balioak	Magnitudea	M1	Urteko bolumenaren magnitudea Hileko bolumenaren magnitudea
		M2	Hilaren bolumenaren magnitudea: 12 balio
		M3	Urteko bolumenaren aldakortasuna
	Aldakortasuna	V1	Hileko bolumenaren aldakortasuna
		V2	Hileko bolumenaren aldakortasuna: 12 balio
		V3	Muturreko aldakortasuna
	urtarokotasuna	E1	Maximoen urtarokotasuna
		E2	Minimoen urtarokotasuna
Muturreko balio maximoak (uholdeak)	Magnitudea	IHA7	Uholde maximoen magnitudea
		IHA8	Isurketa eraginkorraren magnitudea
		IHA9	Eroankortasun–isurketaren magnitudea
		IHA10	Ohiko uholdeen magnitudea
	Variability	IHA11	Uholde maximoen aldakortasuna
		IHA12	Ohiko uholdeen aldakortasuna
	Iraupena	IHA13	Uholdeen iraupena
	Urtarokotasuna	IHA14	Uholdeen urtarokotasuna (1 hilabete bakoitzeko)
Muturreko balio minimoak (lehorteak)	Magnitudea	IHA15	Muturreko lehorteen magnitudea
		IHA16	Ohiko lehorteen magnitudea
	Aldakortasuna	IHA17	Muturreko lehorteen aldakortasuna
		IHA18	Ohiko lehorteen aldakoortasuna
	Iraupena	IHA19	Lehorteen iraupena
		IHA20	Fluxu nuluaren egun kopurua (1 hilabete bakoitzeko)
	Urtarokotasuna	IHA21	Lehorteen urtarokotasuna (1 hilabete bakoitzeko)

IAHRISek 25 parametro erabiltzen ditu IHAren 24 adierazleak kalkulatzeko (1.2 Taula), ibai baten emari–erregimena kuantitatiboki ezaugarritzen dutenak: lau ohiko balioetarako, zortzi uholdeetarako eta zazpi lehorteetarako. 25 parametro horien esparruan, gure ikerketak, uholdeen karakterizaziorako egokiak zirenak aztertu zituen Gure analisia parametro hauetan zentratu zen: urtean zehar eguneko emari maximoen batez bestekoa (Q_c), isurketa eraginkorra (ED), eroankortasun–isurketa (CD), eta uholde garbiketa (FF). ED kontzeptu geomorfikoa da, epe luzera sedimentu gehien garraiatzen dituen fluxua edo fluxu–tartea adierazten duena. Eta CD, berriz, uretako bizitza, materia organikoa, mantenugaiak eta sedimentuak uholde–plano eta ibaertzera garraiatzea ahalbidetzen duen funtsezko adierazlea da. Era berean, FF fluxuen batez besteko kurbari dagokion fluxua da.

Gainera, IHA bakoitzak parametro aldaketa bat azaltzen zuen oinarrizko ezenatoki eta eszenatoki alteraturen artean. Azterketa kasu honetan, A eszenatokitik B eszenatokirako aldakuntza klima–aldakortasunarekin lotuta zegoen, eta A eszenatokitik C eszenatokira, klima–aldakortasunaren eta lurzoruaren erabilera–aldaketaren efektu konbinatuarekin. Aldaketa horiek aurrerantzean "A-B inpaktua" eta "A-C inpaktua" deituko dira, hurrenez hurren. Aldaketa bakoitzerako adierazleak kalkulatu ziren, 0 eta 1 bitarteko balioekin, non 1ek ez zuen inolako asaldurarik adierazten eta 0k gehienezko asaldura adierazten zuen (Swanson, 2002).

1.2 TAULA: IHAak kalkulatzeko parametroen zerrenda.

Erregimenaren osagaiak	Ikuspegia	Parametroa	Deskribapena	Emaitza
Ohiko balioak	Magnitudea eta aldakortasuna	H1	Bataz–bestekoa (hm3)	M1
		H2	Mediana (hm3)	
		H3	Aldakortasun–koefizientea	V1
		H4	Hilaren batez bestekoa (hm3): 12 balioak	M2
		H5	Hileko mediana (hm3): 12 balioak	M3
		H6	Hilaren aldakuntza–koefizientea: 12 balioak	V2
				V3
		H7	Muturreko aldakortasuna (hm3)	V4
	Urtarokotasuna	H8	Hileko gehieneko maiztasun erlatiboa: 12 balio	E1
		H9	Hileko gutxieneko maiztasun erlatiboa: 12 balio	E2
	Aldakortasuna	P4	% 10 eta %90 pertzentilei lotutako batez besteko fluxuen arteko diferentzia	IHA3
Muturreko balio maximoak (uholdeak)	Magnitudea eta maiztasuna	P5	Urtean zehar eguneko gehienezko emarien batez bestekoa	IHA7
		P6	Isurketa eraginkorra	IHA8
		P7	Eroankortasun isurketa	IHA9
		P8	Uholde garbiketa (5% pertzentila)	IHA10
		P9	Urtean zeharreko eguneko gehienezko emarien aldakuntza–koefizientea	IHA11
		P10	Garbiketa uholde seriearen aldakuntza–koefizientea	IHA12
		P11	Urteko egun jarraian % 5 azpiko pertzentilarekin	IHA13
		P12	Hileko batez besteko egun kopurua %5etik gorako pertzentilarekin	IHA14
Muturreko balio minimoak (lehorteak)	Magnitudea eta maiztasuna	P13	Urteko gutxieneko eguneroko emarien batez bestekoa	IHA15
		P14	Lehortearen isuri arrunta (%95 pertzentila)	IHA16
	Aldakortasuna	P15	Urtean zeharreko eguneko gutxieneko emarien aldakuntza–koefizientea	IHA17
	Iraupena	P16	Lehorte arrunten serieen aldakuntza–koefizientea	IHA18
		P17	Urteko egun jarraian %95etik beherako pertzentilarekin	IHA19
		P18	Fluxu nuluarekin hilabeteko batez besteko egun kopurua	IHA20
	Iraupena	P19	Hileko batez besteko egun kopurua %95etik beherako pertzentilarekin	IHA21

IAHRISek hiru izar diagrametan aurkeztu zituen emaitzak: bat ohiko balioentzako, beste bat uholdeentzako eta beste bat lehorteentzako. IAHRISek aldaketa globalari (IGA) buruzko informazioa ematen duen beste adierazle bat lortu zuen, izar diagrametan agertzen diren eszenatoki naturalen eta eraldatuen eremuen arteko azalerari dagokiona.

1.4 Emaitzak

1.4.1 Klima—-aldakortasuna

Mann–Kendall probaren emaitzak eta Sensen malda 1.3 taulan aurkeztu dira. Aldi historikoko tenperatura maximo eta minimoei dagokienez, joera positiboa ikusi genuen urteko hilabete guztietan, 0,001eko konfiantza–mailarekin udako hilabeteetan (ekainean, uztailean eta abuztuan). Urteko joerari ere eusten zaio. Hala ere, ez zen prezipitaziorako joera argirik hauteman, Pirinioetako eskualdean aurretik egindako azterketetan lortutakoekin bat etorriz. Analisi horiek estatistikoki esanguratsuak ez diren 0tik gertuko joerak adierazten dituzte kasu gehienetan (Juez et al., 2022; Lemus-Canovas et al., 2019). Lemus-Canovas et al. (2019)-k, gainera, joera positibo txikiak lortu zituen mendikateko mendebaldeko eskualdean, non gure azterketa–eremua dagoen.

1.3 TAULA: Joeren analisiaren emaitzak. Z proba Mann–Kendall (MK) test estatistikoa da; Qi Sen–en malda estimatzailea da. ** 0,01eko esangura–maila adierazten du, eta ***-k 0,001eko esangura–maila adierazten du

	Prezipitazioa			Tenperatura Maximoa			Tenperatura Minimoa		
	Test Z	Sig.	Q_i	Test Z	Sig.	Q_i	Test Z	Sig.	Q_i
jan	1.350		0.028	2.134		0.019	2.809	**	0.028
feb	0.715		0.012	1.107		0.018	1.817		0.022
mar	0.745		0.012	1.191		0.016	1.995		0.015
apr	0.645		0.008	2.144		0.028	1.936		0.014
may	0.735		0.008	1.698		0.024	1.886		0.016
jun	-0.139		-0.002	3.743	***	0.046	4.070	***	0.027
jul	1.489		0.009	3.703	**	0.041	3.946	***	0.025
aug	0.010		0.000	3.345	***	0.041	4.358	***	0.028
sep	-0.199		-0.002	0.893		0.012	0.655		0.006
oct	0.705		0.012	2.144		0.026	3.018	**	0.025
nov	1.201		0.024	1.152		0.013	2.422		0.022
dec	0.000		0.000	1.102		0.012	1.648		0.015
annual	1.896	**	0.009	4.735	***	0.028	5.490	***	0.021

1.4.2 Lurzoruaren erabileraren aldaketak

LULCren datuak, iraganaldikoak eta oinarrizko eszenatokiarenak,1.4 taulan erakusten dira. 1956ko datuen arabera, azaleraren % 43 baino gehiago larreek estaltzen zuten, eta % 12 baino gehiago sasiek; hiru baso–motek, berriz, % 44 azalera hartzen zuten. 2000. urteko lurraren erabilera–mapak, aldiz, oso bestelako irudia erakusten du: basoak eskualdearen % 73 baino gehiago dira, eta larreak eta sasiak % 30 baino gutxiago. Eraldaketa hori XX. mendeko azken hamarkadetan eskualdean gertatutako aldaketa sozio–ekonomikoen adierazgarri da. Izan ere, landatutako lurrak bertan behera utzi ziren eta horren ondoriozko baso–hedatze prozesua hasi zen, azkenik basoberritutako paisaia sortuz (García-Ruiz et al., 1995; Poyatos et al., 2003; Lasanta et al., 2015, 2017).

1.4 TAULA: Lurraren sei erabilera moten azalera eta estaldura–ehunekoa 1956 eta 2000 urteetarako.

Lur-estalki mota	Eremuaren estaldura km^2 (%)		Aldaketa (%)
	1956	2000	1956–2000
Zoru biluzia	15 (0.3%)	23 (0.5%)	0.23
Baso Hostozabala	1604 (33.2%)	1872 (38.8%)	6.71
Konifero–basoa	334 (6.9%)	1331 (27.5%)	19.62
Baso Mistoa	171 (3.5%)	347 (7.2%)	5.61
Larrea	2101 (43.5%)	1075 (22.3%)	-22.60
Zuhaiskak	607 (12.6%)	183 (3.8%)	-9.88

1.4.3 Ereduraren kalibrazio eta balioztatzea

1.3 atalean aipatu den bezala, sentikortasunaren analisiak ez zituen elurrarekin lotutako parametroak kontuan hartu. Hautatutako parametroak aurreko ikerketetan identifikatutakoekin bat datoz. Parametroen arteko antzekotasun erabakigarriak hurrengo lanetan ikus daitezke: Stratton et al. (2009)-n, non parametro sentikorrak aztertzen diren, elurraren eragina esanguratzua den arro batean, eta Grusson et al. (2015)-k, Pirinioen Frantziako isurialdeko arro bat aztertu zuena. Horiek eta antzeko ezaugarriak dituzten arroen beste azterketa batzuk oinarri hartuta (Palazón and Navas, 2014),1.5 taulan emandako elur–parametroak kalibrazioan gehitu ziren.

Kalibrazio eta balioztatze prozesuetan lortutako NSE balioak (Table1.6) ontzat jo dira Kalin et al. (2010) -k deskribatutako irizpideen arabera. Era berean, PBIAS balioek emaitza oso onak ematen dituzte, ± 25 % azpitik geratzen baitira, eta balio errealak gainestimatzeko joera txiki bat baino

1.5 TAULA: Kalibrazio–parametroen kodeak, deskribapenak, hasierako kalibrazio–tartea eta azken balio optimoak.

Parametroa	Deskribapena	Kalibrazio–eremua	Egokitutako Balioa
Esco	Lurzoruaren lurrunketaren konpentsazio–faktorea	0 – 1	0,7543
Epco	Landareak hartzeko konpentsazio-faktorea	0 – 1	0,7325
Cn_2	SCS hasierako isurketa-kurbaren zenbakiaren II baldintza	±20 %	-19.88
Awc	Eskuragarri dagoen ur-edukiera	±20 %	12.04
Snofall tmp	Elurte-tenperatura (ºC)	-5 – 5	0,491
Snomelt tmp	Elurra urtzeko oinarrizko tenperatura (○C)	-5 – 5	2,465
Snomelt max	Urtean zehar elurra urtze-tasa maximoa (mm ºC-1 day -1)	0 – 10	5,206
Snomelt min	Urtean zehar elurra urtze-tasa minimoa (mm ºC-1 day -1)	0 – 10	1,276
Snomelt lag	Elur-masaren tenperatura atzerapen faktorea	0 – 1	0,973

1.6 TAULA: Kalibrazio eta balioztatze aldietarako eguneroko balio estatistikoak .

Aldia	R^2	NSE	PBIAS	KGE
Kalibrazioa (1992-2004)	0.72	0.51	-12.67	0.55
Balioztatzea (2005-2018)	0.75	0.55	-16.49	0.62

ez dute adierazten. Ereduaren errendimendua ebaluatzeko erabilitako gainerako indizeek ere balio onargarriak eman zituzten: R^2 bi kasuetan 0,70etik gorakoa da, eta KGE, berriz, 0,55etik gorakoa. Aldeko emaitza horiek Anduña ibaiaren arroko SWAT eredua baliozkotzen dute, 1.3 atalean deskribatutako eszenatokietan eguneroko emaria simulatzeko.

1.3 irudiak kalibrazio– eta balioztatze–aldietarako simulatutako eta behatutako hileroko emariaren seriea ematen du. Horrez gain, hileko prezipitazio behatua, eta errendimendua ebaluatzeko estatistika ereduen balioak erakusten ditu. PBIAS negatiboak fluxu baxuen gainestimazioa adierazten du (1.3 Irudia). Hala eta guztiz ere, Moriasi et al. (2015)-k proposatzen du % 25 baino gutxiagoko PBIAS bat onargarria izatea eredu hidrologikoak ebaluatzeko. Tan et al. (2021)-k egindako azken berrikuspenek, SWAT ereduko aplikazioetarako irizpide hau babesten dute, eta Mulliganek (2013) iradokitzen du oinarri fisikoko ereduek, egungo baldintzak zehatz–mehatz simulatuz gero, emaitza onak izango dituztela eszenatokiko baldintzetan. Gainera, Arabi et al. (2007)-k aurkitu du lurraren erabilerako eszenatokiekiko konparazio erlatiboek emaitza koherenteak ematen dituztela ziurgabetasun txikiagoarekin. Horregatik guztiagatik, berezko ziurgabetasunak gorabehera, uste dugu kalibratutako eredua egokia dela gure ikasketa–helburuak lortzeko.

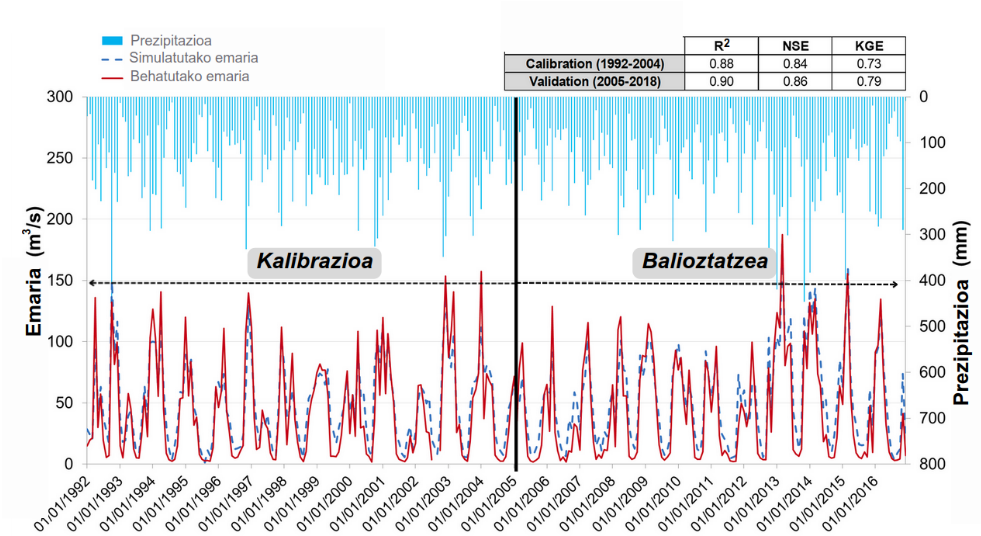

1.3 IRUDIA: Hileroko kalibrazio eta baliozkotze denbora–serieak eta balio estatistikoak.

1.4.4 Lurzoruaren erabilera–aldaketaren eta klima–aldakortasunaren inpaktuak ziklo hidrologikoan

1.7 taulak urteko prezipitazioa, urteko batez besteko emaria eta ebapotranspirazioa (ET) aurkezten ditu, SWAT ereduak simulatua A, B eta C eszenatokietarako. A eta B eszenatokien arteko alderaketatik abiatuta, klima–aldakortasunak ziklo hidrologikoan duen eraginari buruzko informazioa lortu genuen. Horren arabera, prezipitazioak minimikoki handitzen dira, 1.4.1 atalean deskribatutako joera–analisiarekin bat etorriz. Klimaren aldakortasuna, tenperaturen igoerarekin ere erlazionatua, 15,5 mmko ETaren igoera eragin zuen, eta honen ondorioz emariaren 21,8mm-tan gutxitu zen. Klima–aldakortasunaren eta lurzoruaren erabilera–aldaketaren efektu konbinatua A eta C eszenatokiak alderatuz lortu zen, eta horrek ETa 31 mm-tan handitzea eta emaria 36,12 mm murriztea ekarri zuen. Beraz, ETren igoeran faktore bakoitzaren ekarpena % 50 ekoa izan zen. Emariaren beherakadari dagokionez, lurraren erabilera–aldaketaren inpaktuak ia klima–aldakortasuna bezain garrantzitsuak izan ziren, % 41,36 eta % 58,64, hurrenez hurren.

1.7 TAULA: Urteko batez besteko isurketa simulatua, prezipitazioa, PET, ET eta perkolazioa A, B eta C agertokietan (mm).

Eszenatokiak	P	PET	Perkolazioa	ET	Emaria	ET Aldaketa	Emari Aldaketa
A	1718.3	794.3	512.78	576.6	1100.2		
B	1722.2	836.7	481.71	592.1	1079.1	+15.5	-21.2
C	1722.2	836.7	467.23	607.6	1064.1	+31.0	-36.1

1.4.5 Lurraren erabilera–aldaketaren eta klima–aldakortasunaren inpaktuak erregimen hidrologikoaren aldaketetan

IAHRISen emaitzen arabera (1.8 Taula), muturreko gertaera maximoen magnitudea handitu da A eta B eszenatokiak konparatzerakoan. Oro har, klima–aldakortasunak % 40tik gorako hazkundeak eragin zituen Qc, ED eta CD aldagaietan. Aldagai horien aldaketa apur bat arintzen da basoberritzearen ondorioz, eta horrek % 5ean murrizten ditu aldagaien balioak (C eszenatokia), bi faktoreek erregimen hidrologikoan duten eragin konbinatua irudikatuz.

1.8 TAULA: IAHRISen uholde–parametroak A, B eta C agertokietan. Q_c urteko gehienezko eguneko emarien batez bestekoari egiten dio erreferentzia, ED isurketa eraginkorra, CD eroankortasun–isuriari, FF garbiketa–uholdeak eta CVak parametroen aldakortasuna adierazten du.

Eszenatokiak	Q_c	ED	CD	FF	CV(Q_c)	CV(FF)
A	11.21	10.05	13.50	4.31	0.40	0.24
B	15.90	15.30	20.00	4.25	0.44	0.23
C	15.06	14.40	18.80	4.22	0.43	0.23

Uholde–erregimenen aldaketek uholde–lautadako uholdeen maiztasuna eta magnitudea handitzea dakarte, eta eragin zuzena dute hainbat faktorek, hala nola landare–sustraietarako oxigenoaren eskuragarritasunak, funtsezkoa baita ibaiertzeko espezie eta komunitateen konposizioan eta produktibitatean. Era berean, aldaketa horiek eraldatu egin dezakete sedimentuen higadura eta uholde–azaleraren geomorfologia modulatzeaz arduratzen den deklinazioa, eta aldaketa esanguratsuak eragin ditzakete ekosistema riparikoen dinamikan (Richter and Richter, 2000; LeRoy Poff and Allan, 1995).

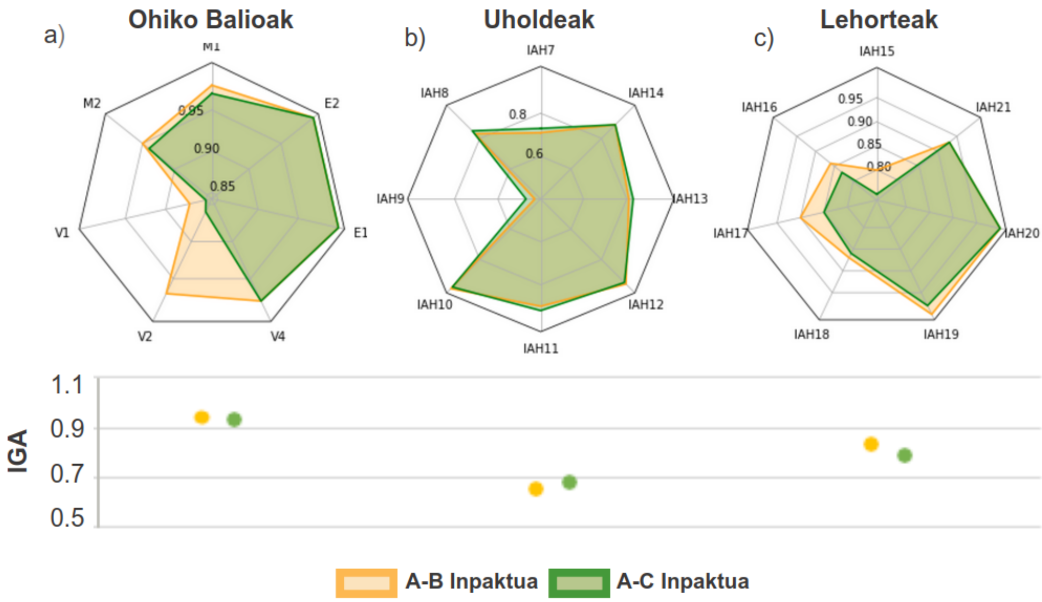

1.4 IRUDIA: IHAen eta IGA balioen izar–diagramak ohiko balioetarako, uholdeetarako eta lehorteetarako A–B eta A–C inpaktuen menpe.

1.4.6 Aldaketa hidrologikoaren adierazleak

1.4 irudiak IGAren eta IHAren izar–diagramen bitartez emaitzak erakusten ditu, ohiko balio, uholde eta lehorteetarako, IAHRIS metodoaren bidez lortuak. Emaitzak bi perturbazio desberdinetarako irudikatzen dira: A-B inpaktuak A eta B eszenatokien arteko asaldurari egiten dio erreferentzia, eta A-C inpaktuak A eta C eszenatokien arteko asaldurari. A-B inpaktuak, orduan, klima–aldakortasunak adierazleen (IHA) aldaketan duen ekarpena islatzen du, eta A-C inpaktuak, berriz, klima–aldakortasunaren eta lurzoruaren erabilera–aldaketen efektu konbinatuek adierazleetan eragindako aldaketari.

IGAren adierazleei dagokienez (1.4 .b Irudia), erregimen hidrikoaren kalitatea gutxitu egin zela ikusi zen, batez ere uholdeetan: IGA 0,65era jaitsi zen klima–aldakortasunaren ondorioz, nahiz eta hori pixka bat arindu zen basoberritze–prozesuari esker, 0,67ra helduz. Ohiko balio eta lehorteetarako, IGAk balio handiagoak adierazi zituen, 0,8tik gorakoak, aldaketa sotilagoa zela adieraziz. Era berean, emaitzek adierazten dute klimaren eta basoberritzearen efektu konbinatuek areagotu egin zutela ohiko balioen eta lehorteen aldaketa, uholdeen emaitzekin alderatuz.

Izar–diagramek (1.4.a. Irudia) aldaketa hidrologikoaren adierazleen emaitzak aurkezten dituzte. Ohiko balioei dagokienez, ez dago uraren erregimenari gehiegi eragiten dion adierazlerik, guztiek 0,80 baino balio handiagoak erakusten baitituzte. Urteko bolumenaren (V1) aldakortasunaren aldaketarik handiena klimaren kausetatik eratorria eta lurraren erabileraren aldaketek areagotua izan zela ikusi genuen. Hala ere, hileroko bolumenaren aldakortasunaren faktore erabakigarria (V2) lurraren erabileraren aldaketa izan zen, adierazlearen balioa 0,86ra jaistea eraginez. Urteko eta urte arteko aldakortasun–aldaketek eragina izan dezakete ekosistema–komunitateen egituran (Bêche et al., 2006). Urteko eta hileko magnitudeari buruzko adierazleek pixka bat behera egin zuten, eta urtarokotasun maximoak eta minimoak 1etik gertuko balioak izan zituzten, asaldura–baldintza minimoak adieraziz. Baldintza horiek mesedegarriak izango lirateke habitat–aniztasunarentzat ezinbestekoak diren prozesuak garatzeko eta ernetzea eta sakabanatzea sustatzeko (Bêche et al., 2006).

Uholdeen erregimena aztertutako erregimenen arteko eraldatuena izan zen. IGAren arabera (1.4.b. Irudia), aldaketa hori klimaren eraginen ondorio izan zen erabat. Aldaketa horiek basoberritzeak arindu zituen apur bat. Adierazlerik kaltetuena konektibitate–fluxuaren maiztasuna izan zen (IHA9; 1.2 Taula), eta hori funtsezkoa da uretako bizitza, materia organikoa, mantenugaiak eta sedimentuak uholde–arriskuko ibai–sistemara garraiatu ahal izateko, bai eta espezieen hazkuntza–etapetarako hezetasun–baldintza egokiak mantentzeko ere (Larsen et al., 2019). Gainera, oso lotuta dago ondorengo dinamikekin, adibidez, bigarren mailako kanalen gaztetzea suspertuz eta urmaelaren ezaugarriak sortuz, zeinek uholde–lautadetako landare eta animalien aniztasuna mantentzen laguntzen duten (Richter and Richter, 2000). Uholde–lautadekiko konektibitatea galtzeak ibaiertzeko habitata etengabe zahartzea dakar, eta arriskuan jartzen du espezieen berritzea (Nilsson and Svedmark, 2002). Uholde maximoen magnitudea (IHA7) izan zen gehien aldatu zen bigarren faktorea, eta isurketa eraginkorraren magnitudea (IHA8) hirugarrena. Aldaketa hauek ere kausa klimatikoek eragin zituzten. Horregatik, ohiko fluxuen birsortze eta goritze zikloei eragingo lieke, eta baita ibaietako geomorfologia (Wohl et al., 2015) eragiten duten sedimentuak eta mugimenduak garraiatzeko prozesuei ere.

Lehorteei dagokienez (1.4.c. Irudia), aldaketa nagusiak magnitudean eta maiztasunean gertatu ziren, eta horiek nabarmenagoak izan ziren

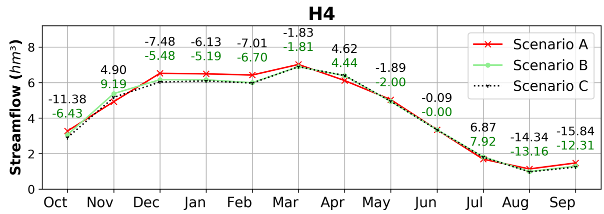

1.5 IRUDIA: Hileroko emariaren batez besteko simulazioak A, B eta C eszenatokietan ehunekotan adierazitako aldaketekin A–B eszenatokirako (berdea) eta A–C eszenatokirako (beltza).

kausa klimatikoen eta basoberritzearen efektu konbinatuekin. Hauek muturreko lehorteen magnitudeari (IHA15), ohiko lehorteen magnitudeari (IHA16) eta muturreko lehorteen aldagarritasunari (IHA17) eragin zieten nagusiki.

1.5 irudiak A, B eta C eszenarioetako hileroko batez besteko fluxu–balioak aurkezten ditu. Beherakadarik esanguratsuenak neguan, udan eta udazkeneko lehen hilabeteetan hauteman ziren. Neguaren beherakada, batez ere, klimaren aldakortasunarekin lotzen zen, landareztatzearen eraginez areagotua. Joera bera gertatu zen udan eta udazkenaren hasieran. Jaitsiera hori tenperaturen igoerarekin lotuta egongo litzateke, 1.3 taulan ilustratua, eta horrek ETren igoera eragingo luke. Basoberritze prozesuak areagotu egingo luke ETren gehikuntza hori, ur–emaria murriztuz.

Hilabete bakoitzeko emari aldakortasuna (H6) 1.6 Irudian agertzen da. Eszenatoki guztietan aldakortasun handiagoa ikusi genuen prezipitazio maila handiko hilabetetan. Martxoan, ekainean eta urrian gorakadak izan ziren klima–aldakortasunaren eraginagatik, eta neguko hilabeteetan, berriz, aldakortasunaren beherakada izan zen. H8 eta H9 parametroek (1.6 irudia), hurrenez hurren, hilabete bakoitzean lortutako gehienezko eta gutxieneko emari–balioen urtarokotasunari buruzko informazioa ematen dute, urteko gehieneko eta gutxieneko hileko ekarpena hilabete horretan egiteko maiztasun edo probabilitate erlatibo gisa. Ikusi genuen apirilean urteko emari maximoa gertatzeko probabilitatea ia bi aldiz handiagoa zela klima–aldakortasunaren eraginaren ondorioz. Era berean, klimaren aldakortasunak minimoen urtarokotasuna aldatu zuen. Beraz, irailean minimoa gertatzeko probabilitatea 0,18tik 0,41era igo zen. Klima–aldakortasunak Anduña ibaiaren arroko erregimen hidrologikoaren maximoa eta minimoa atzeratzea eragin zuen. Erregimen hidrikoaren

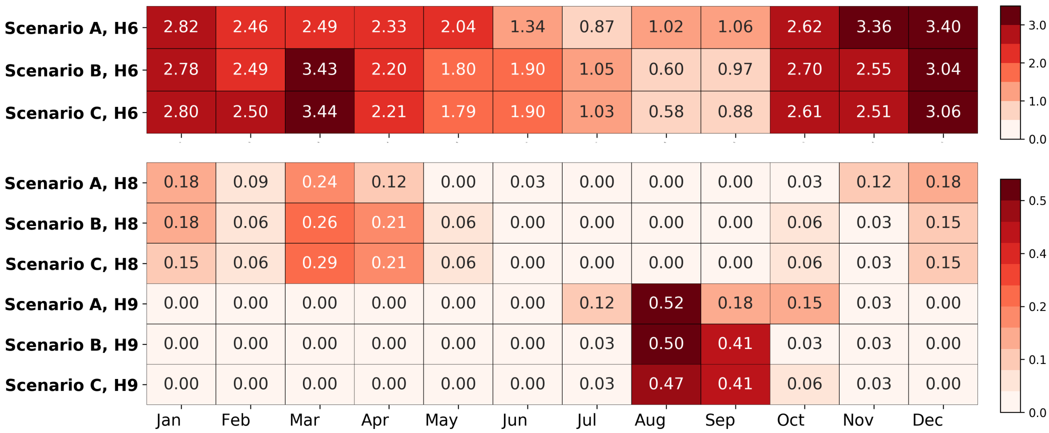

1.6 IRUDIA: IAHRIS parametroen hileko balioak A, B eta C eszenatokietan

urtaro–patroi naturalen aldaketa horiek distortsioak sor ditzakete ibai–funtzionamenduan, ekosistema gisa, espezieen bizi–zikloekiko sinkronia galtzearen ondorioz, besteak beste ugalketa–ereduei, migrazioari, hazkundeari eta garapenari eraginez, eta espezie arrotzen progresioari mesede eginez, azken batean biodibertsitate–galera eraginez (Richter and Richter, 2000; Growns and Reinfelds, 2014).

1.5 Eztabaida

Epe luzeko serieen datuak aztertuta, Anduña ibaiaren arroan ur–emariaren beherakada nabarmena gertatu zen 1951tik 2020ra. Joera hori bat dator Pirinioetako eskualde menditsuan dauden arro anitzetarako dokumentatutako antzeko behaketekin Juez et al. (2022); Vicente-Serrano et al. (2021); López-Moreno et al. (2008). Gainera, Iberiar Penintsulan zehar beste arro natural batzuetan ur–emariaren murrizketa analogoak hauteman dira, batez ere lurraren eraldaketa esanguratsuak jasaten dituztenetan (Lorenzo-Lacruz et al., 2012; Vicente-Serrano et al., 2020).

Gainera, gure analisiak are gehiago kuantifikatzen ditu ur–emariaren beherakada horren oinarrian dauden funtsezko faktoreen ekarpenak, zehazki, klima–aldakortasuna eta lurzoruaren erabilera–aldaketa. Gure aurkikuntzek garrantzi berdina ematen diete bi faktoreei, % 58,6 eta % 41,4ko ekarpenekin, hurrenez hurren. Emaitza horiek López-Moreno et al. (2008)-k planteatutako hipotesia finkatzen dute, ondorengo ikerketetan ere oinarritzen dena; hala nola Juez et al. (2022)-en aburuz, emariaren magnitudearen beherakada ezin zaie faktore klimatikoei bakarrik egotzi, baizik eta Pirinioetako basoberritze–prozesuei partzialki lotuta dago. Gure aurkikuntzak bat datoz Vicente-Serrano et al. (2021) -renekin. Egileek emariaren beheranzko joera nabarmenagoa ikusi zuten, Mediterraneoaren eta Atlantikoaren arteko baldintza klimatiko desberdinei egotzi dakiekeena, baina klimarekin zerikusia ez duten emarien beherakada guztizko murrizketaren % 46 eta % 65 artekoa dela estimatu dute.

Muturreko emarien analisiak faktore klimatikoei egotzitako hazkuntza bat adierazten du, magnitudeari eta maiztasunari dagokienez, arro menditsuetan egindako beste ikerketa batzuen aurkikuntzekin bat datorrena (Roy et al., 2001; Stoffel et al., 2016). Hala eta guztiz ere, erreka–fluxuen gorakada hori leundu egiten da birlandatze–prozesuarekin, zeinak ziklo hidrologikoak prezipitazioei ematen dien erantzuna modulatzen duen, ez bakarrik urteko batez besteko balioetan, eta baita puntako fluxuetan ere (Minang et al., 2015; Ranzi et al., 2002). Basoberritzeak berebiziko garrantzia du uholde–arriskuak murrizteko, lurzoruaren iragazkortasuna indartuz, zuhaitz–sustraien infiltrazioa areagotuz (Keeler et al., 2019) eta baso–kanopioen intertzeptazioa handituz. Faktore horiek guztiek uholdeei lotutako arriskuak murrizten laguntzen dute (Gallart and Llorens, 2004; Andréassian, 2004; Valente et al., 2021). Aitzitik, ohiko eta muturreko gutxieneko emarien kasuan (lehorteak), basoberritzeak erregimen hidrikoaren aldaketak areagotzen ditu, klima–kausekin batera.

Aurreikuspenen arabera, ur–erregimenaren dinamikaren bi faktore erabakigarri horien aldaketek etorkizunean irautea espero da. Zehazki, tenperaturen igoerak eta prezipitazio–patroien aldaketek nabarmen lagunduko dute erregimen hidrikoan gertatzen diren aldaketak areagotzeko. Gainera, laborantza–lurrak uzteko prozesua eta ondoriozko basoberritze prozesua hedatzen jarraitu liteke. Horrez gain, hurrengo urteetan emango den tenperaturen hazkuntzaren ondorioz, baso–mugen goranzko migrazioa geratatuko da (López-Moreno et al., 2008; Beniston, 2003). Efektu horiek baso–estalkia indartuko du, erregimen hidrikoan inpaktuak areagotuz. Klima–aldakortasuna eskualdeko eragileen kontroletik kanpo dagoenez, landarediaren ur–kontsumoa murrizteko lurralde–antolamenduko planak garatzea funtsezkoa da, ziklo hidrologikoaren etorkizuneko inpaktuak arintzeko. Praktika hori baliagarria litzateke lurzoruaren kalitatea hobetzeko (Nadal-Romero et al., 2018) eta baso–suteak prebenitzen laguntzeko (Lasanta et al., 2019). Horrez gain, argaltzea bezalako (Manrique-Alba et al., 2020) sibikultura praktika alternatiboak kontuan hartu behar dira, klima–aldaketaren testuinguruan pinuen basoberritzeak baldintza berrietara egokitzeko eta ziklo hidrologikoa babesteko.

1.6 Ondorioak eta konexioak

Kapitulu honetan, SWAT eredua erabili zen klima–aldakortasunaren eta lurraren ekarpenak kuantifikatzeko; Pirinioetako ibai arro natural baten erregimen hidrologikoan.

SWAT ereduak behar bezala erreproduzitu zuen Anduña ibaiaren arroaren dinamika hidrologikoa, eta honako estatistika hauek lortu zituen balioztatze–aldirako: 0,75eko R2 bat, 0,55eko NSE bat, -16,49ko PBIAS bat eta 0,62ko KGE bat. Emaitza horiek ereduaren errendimendu ona adierazten dute.

Klima–joeraren analisiak agerian utzi zuen udako hilabeteetan joera positibo esanguratsua izan zela tenperatura maximoetan eta minimoetan, eta urtarrilean eta urrian tenperatura minimoetan. Joera esanguratsu hori mantendu egiten da urteko eskalarentzako. Prezipitazioei dagokionez, ez zen joera argirik antzeman hileroko eskalan. Hala ere, prezipitazio hazkuntza txikia ikusten da urtero. Horrez gain, lurraren banaketa goitik behera aldatu zela ikusi zen: larreak eta zuhaixkak nagusi ziren hasieran, eta gero basoak ziren nagusi.

Ingurumen–aldaketa horiek eragina dute ur–baliabideetan. Zehazki, klima–aldakortasunak eta basoberritze prozesuak Anduña ibaiaren arroko urteko batez besteko emaria murriztu dute: klima–aldakortasunaren ekarpena % 58,6koa izanik, eta berdetasun–prozesuari egozten zaion ekarpena, berriz, % 41,1ekoa izanik. Era berean, IAHRISek lortutako emaitzek muturreko gertaera maximoen (uholdeen) magnitudea handitu dela nabarmentzen dute, Qc, ED eta CD aldagaietan % 40ko gehikuntza ikusi baitzen klima–aldakortasunaren ondorioz. Baso–berritzeak aldagai horien aldaketa arindu zuen, % 5 inguru. IHAren arabera, erregimen hidrikoa degradatu egin zen, batez ere uholdeen kasuan. Uholdeen kasuan, degradazioa klima–aldagarritasunak eragiten du, eta basoberritze prozesuaren ondorioz arintzen da. Ohiko balioen eta lehorteen kasuan, klima eta lurraren erabileraren aldaketa konbinatzeak aldaketa handiagoa eragin zuen. Hileroko eskala kontuan hartuta, ur emariaren magnitudean, aldakortasunean eta urtarokotasunean aldaketa bat hauteman zen, nagusiki klima–aldakortasunak eragindakoa.

Kapitulu honek ikuspegi berri eta garrantzitsuak eskaintzen ditu klima–aldaketak eta lurraren erabilera–aldaketek Pirinioetako erregimen hidrologikoan dituzten ondorioei buruz, eta, horrela, **2 Helburua** lortzen eta dinamika horiek eskualdean duten ulermen zientifikoan aurrera egiten laguntzen du. Gainera, 2. kapituluarekin batera, **1. Mugarria** lortzen du, Pirinioetako dinamika hidro–klimatikoa ulertzeko informazio baliotsua eskainiz.

2

Bereizmen handiko klima–simulazioak: abantailak eta mugak orografia–eskualde konplexu batean

Simulazio klimatikoek, hala nola Klima Eredu Globalak (GCM) eta Eskualdeko Klima Ereduak (RCM), ezinbesteko papera betetzen dute egungo baldintza klimatikoen ezagutzan eta etorkizuneko agertoki klimatikoen proiekzioan (Taylor et al., 2012; Jacob et al., 2014; Vautard et al., 2021). GCMek, beren ikuspegi global zabalarekin, eskala handiko prozesu atmosferikoak eta ozeanikoak atzematen dituzte, eta RCMek, berriz, bereizmen espazial finagoa ematen dute, eskualde mailako ebaluazioetarako bereziki baliotsua dena. Simulazio horien bidez, egungo patroi klimatikoei, aldakortasunari eta joerei buruzko pertzepzioak lortzen dira, arrisku eta kalteberatasun klimatikoen ebaluazioa erraztuz. Gainera, berotegi–efektuko gasen emisioen eta beste faktore indargarri batzuen hainbat agertoki simulatuz, GCMk eta RCMk aukera ematen dute klima–aldaketa potentzialak eta horien inpaktuak aurreikusteko eskualde eta sektore ezberdinetan (IPCC, 2022).

Simulazio klimatikoek dinamika klimatikoak era egokian irudikatzeko duten errendimendua eta gaitasuna ulertzea funtsezkoa da modu eraginkorrean erabiltzeko, batez ere eskualde menditsuetan (Torma et al., 2015; Reder et al., 2020; Careto et al., 2022c). Hemen, prozesu mesoeskalar konplexuak eta klima gobernatzen duten kilometro azpiko dinamika klimatikoek oztopo bereziak jartzen dituzte. Eremu hauetan, non irudikapen zehatza erabakigarria den, GCM eta RCM bezalako eredu klimatikoek eskaintzen dituzten ikuspuntuak are baliotsuagoak bihurtzen dira, klima aldaketari aurre egiteko adaptazio estrategiak eta erabaki politikoak eskala espazial anitzetan asmatzen laguntzen bai dituzte.

Kapitulu honetan, Pirinioetako eskualdeko GCM eta RCM simulazioak ebaluatzeari ekiten diogu, aldagai klimatikoen muturreko gertaeren eta haien banaketa espaziala kontuan hartuta. Kapituluak honako hauek bilduko ditu: balio erantsiaren (AV) kontzeptuaren sarrera (2.2 atala), kontuan hartutako aldagaien eta datu–baseen definizioa (2.3 atala), aplikatutako metodologiaren deskribapena (2.4 atala), emaitzen aurkezpena (2.5 atala) eta ondorengo eztabaida (2.6 atala). Analisi integral honek **3. Helburua** du, eta klima–simulazioen abantailak eta mugak ebaluatzen ditu eskualdeko klima ezaugarritzeko, eta, horrela, **2 Mugarria** lortzen laguntzen du, klima–ereduen inguruko ulermenean sakontzea xede duena.

2.1 Balio erantsiaren kontzeptua (AV)

Azken hamarkadetan, bereizmen baxuko ereduek (GCM) eskaintzen duten informazioa bereizmen handiko informazioan bihurtzeko erronkari aurre egiteko, Eskualdeko Klima Ereduak (RCM) garatu dira. RCMek proposatutako ikuspegiak bereizmen handiko ereduak eskala globalean erabiltzeko muga praktikoak gainditu egiten ditu. Azken urteetan, RCMek gero eta garrantzi handiagoa hartu dute. Klima–aldaketaren testuinguruan, bereizmen fineko simulazioen eskaria gero eta handiagoa da, batez ere adaptazio–estrategiak eta inpaktu–ebaluazio azterlanak garatzeko ezinbesteko informazioa ematen dutelako. Hala ere, eredu horien abantailak gorabehera, badira kontuan hartu beharreko mugak (Kotlarski et al., 2014, 2015; Vautard et al., 2021)
.

RCMen ugaritze egoera honetan, CORDEX (Giorgi et al., 2009; Jones et al., 2011; Gutowski et al., 2016) Eskualdeko Klima Erregionalizazioaren Esperimentu Koordinatua sortu zen. Zehazki, Europako eskualdearentzat 70 RCM simulazio baino gehiago egin dira EURO–CORDEX ekimenaren esparruan. Hala ere, GCMetatik datorren informazioa erregionalizatzea konputazionalki oso garestia da. Beraz, ezinbestekoa da, sistema klimatikoa simulatzean, RCMak GCMen aurka erabiltzearen balio erantsia (AV) ebaluatzea .

Horretarako, ikerketa anitzek metodo desberdinak proposatu dituzte AVa hainbat faktoreren arabera kuantifikatzeko; hala nola, aldagaiaren menpekoak, interes–eskualdearen araberakoak eta eskala espazial eta tenporala kontuan hartzen dutenak. Di Luca et al. (2016)-k, esaterako, PAV (Balio erantsi potentziala) metrika proposatu zuten: Metrika horren bitartez RCM-tan ageria den eta GCM simulazioetan presente ez dagoen aldakortasun espaziala aztertzen dute. Metodologia horrek sareko gelaxka bakoitzean analisia egitea baimentzen du. Emaitzek balio erantsi potentzialak (PAV) erakutsi zituzten topografia konplexuko eskualdeetan eta denbora–eskala laburretan, batez ere 3 ordu baino gutxiagokoetan. Metodologia horri esker, gure analisia Probabilitate Banaketa Funtzioaren (PDFaren) segmentu zehatz batera bideratu dezakegu, adibidez, haren isatsetara, batez bestekoan islatuta ez dauden probabilitate txikiko gertaerak aztertzeko aukera emanez. Soares and Cardoso (2018)-ek, Di Luca et al. (2016)-k proposatutako AVren definizioa eta Perkins et al. (2007)-k proposatutako eredu–trebetasunaren definizioa, DAV (Balio Erantsi Banatua) izeneko metriko berri bat sortzeko erabili zuten. DAV metrikak bereizmen handiko simulazioaren balio erantsi normalizatua ematen du, toki horretako behaketa datuak kontuan izanda (Di Luca et al., 2016). Emaitzek AV positiboak erakutsi zituzten Europako eskualde osoan zehar prezipitazio aldagairako. Zehazki, prozesu konbektiboak garrantzitsuak diren lekuetan balio altuagoak lortu ziren, hala nola Alpeetan edo Iberiar Penintsulan. Ildo horretan, Ciarlo et al. (2021)-k PDFen puntuz puntuko analisia aplikatzen dute RCM baten balio erantsia modu espazialean ebaluatzeko. Gainera, aldagai baten ezaugarrien irudikapen integrala eta bere aldakuntza geografikoa kontuan hartzen dituzte. PDF-an oinarritutako AVren kuantifikazioek, prezipitazio aldagaiari dagokionez, banaketaren muturretan (muturreko gertakeretan) AV balio altuagoak lortzen direla adierazten dute.

Emaitza komunak aurkitzen dira literaturan (Feser, 2006; Prein et al., 2016; Fantini et al., 2018; Di Luca et al., 2016; Torma et al., 2015; Ciarlo et al., 2021; Qiu et al., 2020). Lehenik eta behin, AV bereizmen–espazialarekin handitzea ezaugarri topografikoen irudikapen hobearekin lotzen da. Horrek esan nahi du, AVa nabarmen handitu dela topografia konplexua duten eskualdeetan, hala nola, mendialdean edo kostaldean. Bigarrenik, azpimarratzen da AVn hobekuntza nabarmena dagoela RCMak GCMaren sarearen bereizmenera igo direnean ere. Horregatik, RCMren errendimendu hobea prozesu fisikoen irudikapen hobearen ondorio dela esan daiteke, eta ez eskala handiko behartzearen desagregazioaren ondorio. Gainera, guztiek adierazten dute garrantzitsua dela kalitate handiko behaketa–datuak izatea, AV indizea kalkulatzean duten inpaktua dela eta, bereziki adierazgarria banaketaren muturretan (Ciarlo et al., 2021). Behaketen kalitate murriztuak analisi zehatza mugatzen du munduko eskualde askotan.

Pirinioetako mendialdea klima–aldaketaren aurrean bereziki kaltebera den eskualdea da (1. kapitulua), eta funtsezko sektoreetan ditu eraginak, esaterako, uraren kudeaketan edo turismoan (Amblar-Francés et al., 2020). Orain arte, Pirinioak ez dira era bereiztuan aztertu bereizmen altuko edo baxuko modeloak erabiltzearen onurak edo galerak ebaluatzerakoan. Lan honetan, Pirinioetako AVaren ebaluazioa egiten da, eskualde menditsu osoa interesgunetzat hartuz eta RCMen errendimenduan zentratuz GCMen aurrean.

2.2 Behaketa eta simulazio klimatikoak

Azterketa honetan, Ciarlo et al. (2021)-k proposatutako balio erantsiaren metodoa aplikatu zen Pirinioetako eskualdean RCMak edo GCMak erabiltzean aldagai bat adierazten duen irabazia edo galera kuantifikatzeko (41 °N-44 °N, 2.5 °W-3.5°E). Metrika hori sare–puntu bakoitzaren probabilitate–banaketaren funtzioan oinarritzen da (PDF), eta horrek aztertutako eremuaren gaineko balio erantsiaren banaketa espaziala ematen du. Konbinatzen ditu Giorgi et al. (2009) -k deskribatzen duen erregionalizazio espazialaren seinalea eta Rummukainen (2016) -k aipatzen duen korrelazio espazialerako trebetasuna, PDF osoan analisi espaziala egitea baimenduz. Eguneroko prezipitazioa ("pr"), tenperatura maximoa ("tmax") eta tenperatura minimoa ("tmin") aldagaiak aztertu ziren bereizmen handiko behaketa datuak eta simulazio datuak (RCM eta GCM) konparatuz. Gainera, ereduzko simulazioetatik orografia ("orog") aldagaia ere kontuan hartu zen, horrek balio erantsiarekin duen erlazioan sakontzeko helburuarekin.

CLIMPY behaketa datuak, Pirinioak estaltzen dituena (Cuadrat et al., 2020b), erreferentzia gisa hartu zen, 1 km $\times$ 1 km bereizmen espazialarekin eta 1981–2015 ko aldirako. Espainiako, Frantziako eta Andorrako 1.343 estazio meteorologikotako informazioan oinarritutako aldagaien berreraikuntza da. Datu multzo hori CLIMPY proiektuaren esparruan sortu zen eta dagoeneko baliozkotua izan da hainbat ikerlanetan (Amblar-Francés et al., 2020; Lemus-Canovas and Lopez-Bustins, 2021).

EURO–CORDEX simulazio–multzoa ebaluatu genuen (Jacob et al., 2014, 2020), guztira 72 RCM simulazio dituena (2.1 Taula), 0,11 °ko bereizmen espazialarekin. Simulazio hauek 130 urteko aldia hartzen dute eta Kontzentrazio Bide Adierazgarri (RCP) desberdinetarako daude eskuragarri (RCP4.5, RCP8.5 eta RCP2.6). Analisia 2005era arteko simulazio historikoa eta 2005etik aurrerako RCP8.5 simulazioa aztertzean zentratu

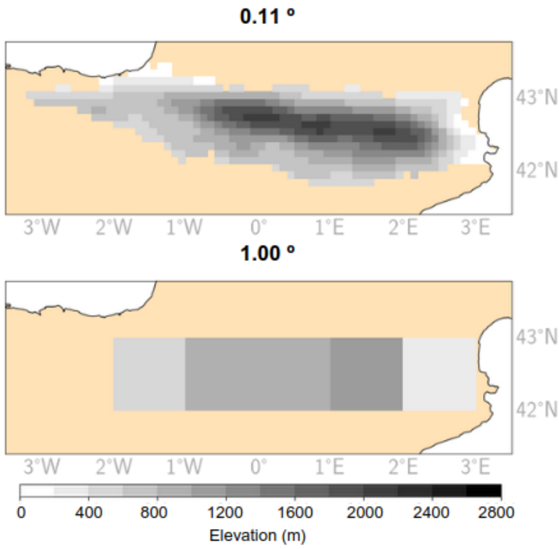

2.1 IRUDIA: Pirineoetako eskualderaren topografia, lan honetan aztertutako bi ebazpenetan: Goiko irudia (0.11°) eta beheko irudia (1.00°)

zen. Simulazio horiek bi eredu motak osatzen dituzte, RCM eta bere gidaria, GCMa (1,00 °ko bereizmenarekin), 12 RCM eta 8 GCMko matrizea osatuz.

Ikerketa honetan, datuak bi sare errektilineotara interpolatu ziren; 0,11 °eta 1,00 ° bereizmenekin, hurrenez hurren RCM eta GCM modeloei dagozkienak. Interpolazioak CDO softwarea erabiliz garatu ziren (CDO, https://code.zmaw.de/projects/cdo). Erresoluzio fineko interpolazioa (0,11 °) *distance–weighted average remapping* metodoarekin aurrera eraman zen (Ciarlo et al., 2021; Fantini et al., 2018; Torma et al., 2015). Metodo horrek, Torma et al. (2015) -k adierazten duen bezala, patroi espazial koherenteenak ematen ditu bereizmen ezberdinetan zehar. Gainera, analisiak ebaluazioa GCMen bereizmen natiboan barne hartzen du. Horretarako, datu guztiak (behaketak eta RCMak barne) 1,00 ° sare batera interpolatu egin dira. Metodologia horrek, Terzago et al. (2017) eta Vautard et al. (2021)-ek nabarmentzen duten bezala, bereizmen espazial horizontalak simulazioaren errendimenduan duen eragina murrizten du. Pauso horretarako *conservative remapping* interpolazio metodoa erabili zen.

2.1 TAULA: Analisirako erabili diren EURO–CORDEX RCM multzoko kideak eta haiei dagozkien gidatze GCMak. 'Aldagaiak' zutabean kide bakoitzarentzat kontuan izan diren aldagaiak biltzen dira.

Erakundea/GCM	Kidea	Kodigoa	RCM	Aldagaiak
CCCma-CanESM2	r1i1p1	1	CLMcom-CCLM4-8-17	pr; tmin; tmax; orog
CCCma/CanESM2	r1i1p1	1	GERICS-REMO2015	pr; tmin; tmax; orog
CNRM-CERFACS/CNRM-CM5	r1i1p1	2	CLMcom-CCLM4-8-17	pr; tmin; tmax
CNRM-CERFACS/CNRM-CM5	r1i1p1	2	CLMcom-ETH	pr; tmin; tmax; orog
CNRM-CERFACS/CNRM-CM5	r1i1p1	2	CNRM-ALADIN63	pr; tmin; tmax; orog
CNRM-CERFACS/CNRM-CM5	r1i1p1	2	DMI-HIRHAM5	pr; tmin; tmax; orog
CNRM-CERFACS/CNRM-CM5	r1i1p1	2	GERICS-REMO2015	pr; tmin; tmax; orog
CNRM-CERFACS/CNRM-CM5	r1i1p1	2	IPSL-WRF381P	pr; tmin; tmax
CNRM-CERFACS/CNRM-CM5	r1i1p1	2	KNMI-RACMO22E	pr; tmin; tmax; orog
CNRM-CERFACS/CNRM-CM5	r1i1p1	2	MOHC-HadREM3-GA7-05	pr; tmin; tmax; orog
CNRM-CERFACS/CNRM-CM5	r1i1p1	2	RMIB-UGent-ALARO-0	pr
CNRM-CERFACS/CNRM-CM5	r1i1p1	2	SMHI-RCA4	pr; tmin; tmax; orog
ICHEC/EC-EARTH	r12i1p1	4	CLMcom-CCLM4-8-17	pr; tmin; tmax; orog
ICHEC/EC-EARTH	r12i1p1	4	CLMcom-ETH	pr; tmin; tmax
ICHEC/EC-EARTH	r12i1p1	4	DMI-HIRHAM5	pr; tmin; tmax; orog
ICHEC/EC-EARTH	r12i1p1	4	GERICS-REMO2015	pr; tmin; tmax; orog
ICHEC/EC-EARTH	r12i1p1	4	ICTP-RegCM4-6	pr; tmin; tmax; orog
ICHEC/EC-EARTH	r12i1p1	4	IPSL-WRF381P	tmin; tmax
ICHEC/EC-EARTH	r12i1p1	4	KNMI-RACMO22E	pr; tmin; tmax; orog
ICHEC/EC-EARTH	r12i1p1	4	MOHC-HadREM3-GA7-05	pr; tmin; tmax; orog
ICHEC/EC-EARTH	r12i1p1	4	SMHI-RCA4	pr; tmin; tmax; orog
ICHEC/EC-EARTH	r12i1p1	4	UHOH-WRF361H	pr; tmin; tmax
ICHEC/EC-EARTH	r1i1p1	3	CLMcom-ETH	pr; tmin; tmax
ICHEC/EC-EARTH	r1i1p1	3	DMI-HIRHAM5	pr; tmin; tmax; orog
ICHEC/EC-EARTH	r1i1p1	3	KNMI-RACMO22E	pr; tmin; tmax; orog
ICHEC/EC-EARTH	r1i1p1	3	SMHI-RCA4	pr; tmin; tmax; orog
IPSL/IPSL-CM5A-MR	r1i1p1	6	DMI-HIRHAM5	pr; tmin; tmax
IPSL/IPSL-CM5A-MR	r1i1p1	6	GERICS-REMO2015	pr; tmin; tmax; orog
IPSL/IPSL-CM5A-MR	r1i1p1	6	IPSL-WRF381P	pr; tmin; tmax
IPSL/IPSL-CM5A-MR	r1i1p1	6	KNMI-RACMO22E	pr; tmin; tmax; orog
IPSL/IPSL-CM5A-MR	r1i1p1	6	SMHI-RCA4	pr; tmin; tmax; orog
MIROC/MIROC5	r1i1p1	7	CLMcom-CCLM4-8-17	pr; tmin; tmax; orog
MIROC/MIROC5	r1i1p1	7	GERICS-REMO2015	pr; tmin; tmax; orog
MIROC/MIROC5	r1i1p1	7	UHOH-WRF361H	pr
MOHC/HadGEM2-ES	r1i1p1	5	CLMcom-CCLM4-8-17	pr; tmin; tmax; orog
MOHC/HadGEM2-ES	r1i1p1	5	CLMcom-ETH	pr; tmin; tmax
MOHC/HadGEM2-ES	r1i1p1	5	CNRM-ALADIN63	pr; tmin; tmax; orog
MOHC/HadGEM2-ES	r1i1p1	5	DMI-HIRHAM5	pr; tmin; tmax; orog
MOHC/HadGEM2-ES	r1i1p1	5	GERICS-REMO2015	pr; tmin; tmax; orog
MOHC/HadGEM2-ES	r1i1p1	5	ICTP-RegCM4-6	pr; tmin; tmax; orog
MOHC/HadGEM2-ES	r1i1p1	5	IPSL-WRF381P	pr; tmin; tmax
MOHC/HadGEM2-ES	r1i1p1	5	KNMI-RACMO22E	pr; tmin; tmax; orog
MOHC/HadGEM2-ES	r1i1p1	5	MOHC-HadREM3-GA7-05	pr; tmin; tmax; orog
MOHC/HadGEM2-ES	r1i1p1	5	SMHI-RCA4	pr; tmin; tmax; orog
MOHC/HadGEM2-ES	r1i1p1	5	UHOH-WRF361H	pr; tmin; tmax
MPI-M/MPI-ESM-LR	r1i1p1	8	CLMcom-CCLM4-8-17	pr; tmin; tmax; orog
MPI-M/MPI-ESM-LR	r1i1p1	8	CLMcom-ETH	pr; tmin; tmax
MPI-M/MPI-ESM-LR	r1i1p1	8	CNRM-ALADIN63	pr; tmin; tmax; orog
MPI-M/MPI-ESM-LR	r1i1p1	8	DMI-HIRHAM5	pr; tmin; tmax; orog
MPI-M/MPI-ESM-LR	r1i1p1	8	ICTP-RegCM4-6	pr; tmin; tmax; orog
MPI-M/MPI-ESM-LR	r1i1p1	8	IPSL-WRF381P	pr; tmin; tmax
MPI-M/MPI-ESM-LR	r1i1p1	8	KNMI-RACMO22E	pr; tmin; tmax; orog
MPI-M/MPI-ESM-LR	r1i1p1	8	MOHC-HadREM3-GA7-05	pr; tmin; tmax; orog
MPI-M/MPI-ESM-LR	r1i1p1	8	MPI-CSC-REMO2009	pr; tmin; tmax
MPI-M/MPI-ESM-LR	r1i1p1	8	SMHI-RCA4	pr; tmin; tmax; orog
MPI-M/MPI-ESM-LR	r1i1p1	8	UHOH-WRF361H	pr; tmin; tmax; orog
MPI-M/MPI-ESM-LR	r2i1p1	9	CLMcom-ETH	pr; tmin; tmax
MPI-M/MPI-ESM-LR	r2i1p1	9	MPI-CSC-REMO2009	pr; tmin; tmax; orog
MPI-M/MPI-ESM-LR	r2i1p1	9	SMHI-RCA4	pr; tmin; tmax; orog
MPI-M/MPI-ESM-LR	r3i1p1	10	CLMcom-ETH	pr; tmin; tmax
MPI-M/MPI-ESM-LR	r3i1p1	10	GERICS-REMO2015	pr; tmin; tmax; orog
MPI-M/MPI-ESM-LR	r3i1p1	10	SMHI-RCA4	tmin; tmax; orog
NCC/NorESM1-M	r1i1p1	11	CLMcom-ETH	pr; tmin; tmax
NCC/NorESM1-M	r1i1p1	11	CNRM-ALADIN63	pr; tmin; tmax; orog
NCC/NorESM1-M	r1i1p1	11	DMI-HIRHAM5	pr; tmin; tmax; orog
NCC/NorESM1-M	r1i1p1	11	GERICS-REMO2015	pr; tmin; tmax; orog
NCC/NorESM1-M	r1i1p1	11	ICTP-RegCM4-6	pr; tmin; tmax; orog
NCC/NorESM1-M	r1i1p1	11	IPSL-WRF381P	pr; tmin; tmax
NCC/NorESM1-M	r1i1p1	11	KNMI-RACMO22E	pr; tmin; tmax; orog
NCC/NorESM1-M	r1i1p1	11	MOHC-HadREM3-GA7-05	pr; tmin; tmax; orog
NCC/NorESM1-M	r1i1p1	11	SMHI-RCA4	pr; tmin; tmax; orog

2.3 Metodologia: Balio erantsiaren (AV) indizea

Sare–puntu bakoitzerako eguneroko gertakarien PDFa kalkulatu zen (prezipitaziorako gertaera lehorrak barne), 1981–2015 aldian, behaketa–datu, RCM eta GCMko aldagai bakoitzeko. Bin tamainaren koherentzia bermatzeko hiru dataseten artean eta aldagai bakoitzeko, bin bat hautatu zen, 1 mm/eguneko prezipitazio aldagaiarentzat, Ciarlo et al. (2021)-n bezala, eta 0,5 °C bin bat tenperatura minimo eta maximoaren aldagaientzat, Perkins et al. (2007) n bezala.

Ondoren, Probabilitate Erlatiboaren Aldea (D_M) Ciarlo et al. (2021) -n definitutako metodologiari jarraituz kalkulatu zen (2.1), behaketen banaketen eta ereduen artean dauden desadostasunei buruzko informazioa ematen duena, GCM edo RCM izan. Hau da, D_M-ko balio handiago (txikiago) batek modeloaren errendimendu txarragoa (hobea) adierazten du.

$$D_M = \frac{\sum_{v=1}^{v_t} |(N_M - N_O)|\Delta v}{\sum_{v=1}^{v_t}(N_O \Delta v)}, \tag{2.1}$$

non N_M eta N_O, hurrenez hurren, bin bakoitzeko ereduen (GCM edo RCM) eta behaketen gertaeren kopurua diren, eta Δv aldagaiaren bin–tamaina adierazten duen. D_M bi balio lortu ziren; D_{RCM} eta D_{GCM}, hurrenez hurren RCM eta GCM simulazioetarako.

Beraz, Balio Erantsiaren Indizea (AV) honela definitzen da Ciarlo et al. (2021)k ematen duen definizioari jarraituz: D_M-ren bi estimazioen arteko aldea, (2.2) -n adierazten den bezala. AV balio positibo (negatibo) batek hobekuntza (okerragotzea) adierazten du RCMren emaitzetan GCMarekin alderatuz, aldagaiaren probabilitate–banaketa adierazterako orduan.

$$AV = D_{GCM} - D_{RCM}. \tag{2.2}$$

Kontuan izan GCMk bin jakin baterako gertaerak simulatzen ez dituenean (adibidez, banaketaren isatsetan, hau da, muturreko balioetan) N_{GCM} zero bada, eta N_O eta N_{RCM} ez. Egoera horretan, D_{GCM} balioa beti 1 izango da, D_{RCM} balioa gainditu ahal izango da, eta horrek nabarmen nahasten du AV kalkulua, AV balio negatibo engainagarriak lortuz. Horregatik, baldintzapeko suposizio bat aplikatzen da: Egoera honetan, N_{GCM} 0 bada bin jakin baterako, N_{RCM} eta N_O ez dira zero, D_{RCM} balioa da bin horretarako. Planteamendu horrek AV indizeari ekarpen positiboa egitea bermatzen du kasu horietan. Alderantzizko baldintza, hau da, N_{GCM} eta

N_O zero ez izatea eta N_{RCM} zero izatea, ez dira kontuan hartu. Ez–egite hori gertaeren guztizkoari buruzko adibide kopuru hutsaletik dator, % 0,01 baino gutxiago baitira.

AV eta altitudearen arteko erlazioak argitzeko, hauen arteko erlazio lineala Pearsonen korrelazio–koefizientearekin kalkulatu zen. % 95-ko Adierazgarritasun–maila, 0,05eko p balioari dagokiona, kontsideratu eta kalkulatu zen: r korrelazio–koefizientea duen lagin jakin baten kasuan, p–balioa da x ausazko lagin baten abs (r ") eta y" populaziotik ateratako abs (r) baino handiagoa edo berdina izateko probabilitatea. Kalkulu hau egiteko, AV matrizea eta RCM kide bakoitzaren orografia hartu ditugu kontuan. Ondorioz, orografiari buruzko informaziorik ez zuten kideak (2.1 Taula) analisitik kanpo geratu ziren.

2.4 Emaitzak

2.4.1 Balio erantsia (AV) PDF osoarentzat

2.2. grafikoak probabilitate erlatiboaren aldea (D_M ;(2.1)) RCM eta GCM multzoen bataz–bestekoetarako erakusten du. Horrez gain, multzo horietarako balio erantsiaren indizea (AV; (2.1)) eraskuten du aztertutako hiru aldagaietarako. Prezipitazioari dagokionez, D_{RCM}k 0,2 eta 0,4 arteko balioak ditu, eskualdean zehar uniformeki banatuta. Aldiz, D_{GCM}k gradiente latitudinala erakusten du, balio handiagoak dituena mendilerroaren hegoaldeko maldan ($\sim\ 0,7$) eta baxuagoak iparraldean (∼0,3). Ondorioz, AV indizeak RCMen errendimendu hobea adierazten du hobekuntza nabarmenarekin hegoaldeko maldaren erdialdean, non GCM multzoak emaitza txarrak lortzen dituen.

Tenperatura minimoari dagokionez, D_{RCM} balio homogeneoak ikusi ziren mendikate ia osoan zehar. Hau ez dator bat D_{GCM} balioekin, 0,8 baino gehiago baita eskualde garaienetan eta hegoaldeko maldaren ekialdean. Ondorioz, GCM multzoak errendimendu desegokia duen eremu hauetan AV maila nabarmen altua ikusten da. Tenperatura maximoaren emaitzek antzeko patroia erakusten dute, baina bereizketa batzuekin. Nahiz eta D_{GCM} altuera handiko eskualdeetan ere handiagoa izan, tenperatura minimoaren kasuan baino lokalizatuagoa dago, eta, orokorrean, GCM multzoaren batez bestekoak tenperatura maximoak minimoak baino zehaztasun handiagoz adierazten dituela iradokitzen du. Tenperatura maximoaren AV balioak erdialdeko balioetara iristen dira, 0 inguruko balioez inguraturik.

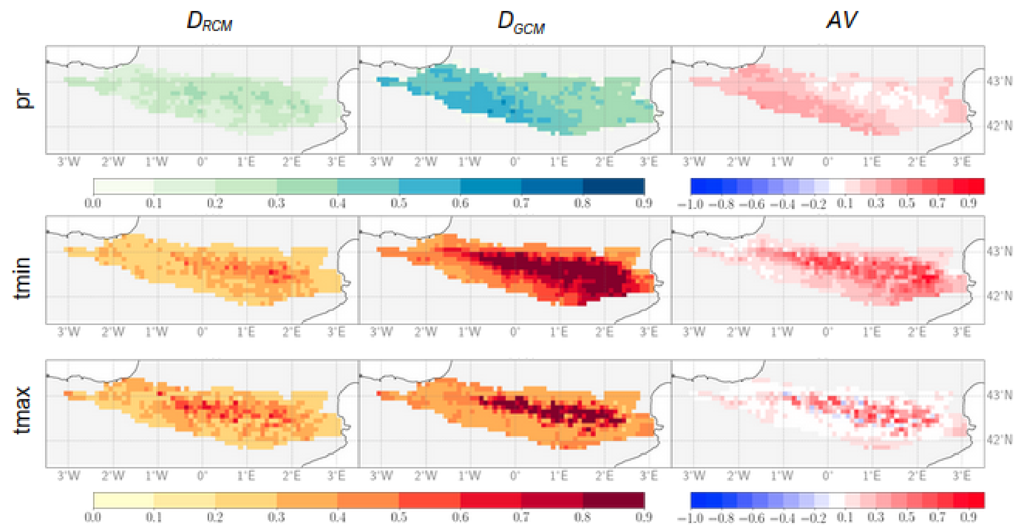

2.2 IRUDIA: Probabilitate erlatiboaren aldea (D_M; (2.1)) RCM-entzat (ezkerreko zutabea) eta GCM-entzat (erdiko zutabea) eta balio erantsia (AV; (2.2); eskuineko zutabean) 0,11 ° bereizmenean, prezipitaziorako (goiko lerroa), tenperatura minimorako (erdiko lerroa) eta tenperatura maximorako (beheko lerroa), CLIMPY erreferentzia gisa erabiliz 1981-2015 aldian.

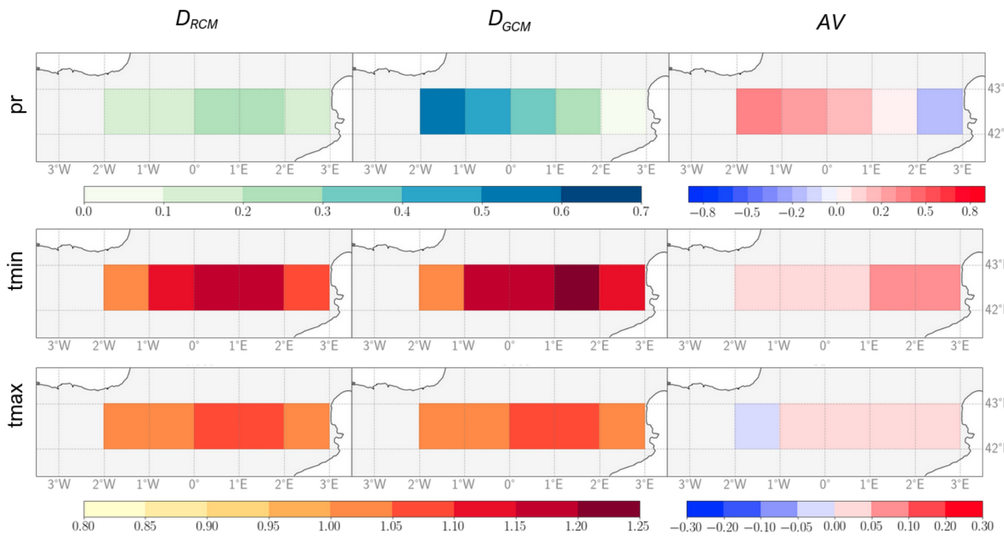

2.3 IRUDIA: Probabilitate erlatiboaren aldea (D_M; (2.1)) RCM-entzat (ezkerreko zutabea) eta GCM-entzat (erdiko zutabea) eta balio erantsia (AV; (2.2); eskuineko zutabean) 1,00 ° bereizmenean, prezipitaziorako (goiko lerroa), tenperatura minimorako (erdiko lerroa) eta tenperatura maximorako (beheko lerroa), CLIMPY erreferentzia gisa erabiliz 1981-2015 aldian.

2.3 irudiak 2.2 irudiarekiko egitura paraleloa erakusten du, nahiz eta datuak GCMren jatorrizko bereizmenera eskalatuta egon (1,00 °). Nabarmenki, D eta AV aurkikuntzak koherenteak dira bi ebazpenetan zehar. Hala ere, bereizmen espazial lodiaren eta Pirinioetako estaldura–eremu txiki samarraren ondorioz, gure analisia bost gelaxkako sare batera mugatzen da. Muga hori gorabehera, lortutako informazioa bat dator 2.2 irudian irudikatutako banaketa espazialarekin. Prezipitazioen kasuan, AVak 1,00 °ko bereizmenean balio maximoak erakusten ditu mendilerroaren mendebaldeko sektorean. Fenomeno hau GCM multzoaren errendimendu txar batekin lotuta dago, D_{GCM} balio altuek erakusten duten bezala. Alderantziz, tmin-ari dagokionez, AV altuena Pirinioen erdialdeko eta ekialdeko eremuan ikusten da, altitude handieneko eskualdeari dagokiona (2.1 Irudia). Azkenik, tmax-ari dagokionez, AV balioak nabarmen txikiagoak dira, mendikatearen beheko altuerako zonaldeetan gertatzen diren balio negatiboen kasuekin.

Multzoaren bataz–besteko azterketatik ateratako ondorioek ez dituzte kontuan hartzen kide bakoitzak emandako seinaleak. B.1–B.3 irudiek 0,11° bereizmenean kide indibidualen AVa aurkezten dute, matrize formatuan, non errenkadek GCMak irudikatzen dituzten eta zutabeek RCMak. Era berean, B.4–B.6 irudiek informazio hori bera ematen dute, baina 1,00°ko bereizmenarekin egindako kalkulurako. Emaitzak koherenteak dira bereizmen fin eta lodientzat. Prezipitazioari dagokionez, AVk GCMrekiko mendekotasun handiagoa erakusten du RCMrekiko baino, Ciarlo et al. (2021) eta Di Luca et al. (2016) aurkikuntzekin lerrokatuz. CanESM (1 kodea), CNRM (2 kodea) eta NCC (11 kodea) eredu–taldeek AV altuena erakusten dute, eta MPIk (8 eta 9 kodeak) bultzatutako ereduek, berriz, AV baxuagoak ematen dituzte, batzuetan balio negatiboak ere erakutsiz, hau da, MPI GCMek (8 eta 9 kodeak) errendimendu bikaina dute Pirinioetan. AVaren banaketa espazialak, kide guztietan, patroi koherente bat jarraitzen du. 2.2 Irudian ikusten da nola, AV balio baxuagoak mendilerroaren altitude handioko eremuetan lortzen diren. Tenperaturari dagokionez, GCMen influentzia ez da hain nabaria AVren emaitzan. Hala ere, tenperatura minimoetan zein maximoetan, CNRMk bultzatutako modeloek (2 kodea) AV txikiagoak erakusten dituzte bi bereizmenetan, eta hori, bereizmen lodiaren kasuan, EC-EARTH GCMrentzat ere agerikoa da (3 eta 4 kodeak). Tenperatura minimoaren kasuan, RCMek AV seinaleari egiten dioten ekarpena bereziki nabarmena da, batez ere RCM RCA4 eta RACMO22E modeloekin, aldagaiaren batez bestekoa irudikatzerako orduan eragin negatiboa baitute. Alderantziz, tenperatura maximoaren kasuan, RCM REMO2019 modeloak AV seinalea modu positiboan itxuratzen du, batez ere 0,11° bereizmenean.

2.4.2 Balio erantsia (AV) pertzentil tarteetan

Bereziki garrantzitsua da PDFaren tarte zehatzetan zentratzea, banaketako isatsetan modeloek nola funtzionatzen duten jakiteko, ezohiko gertaerei lotuta baitaude. 2.4. Irudian AV indizearen irudikatzen da, 0,11 ° bereizmenean, tarteen arabera. Bi ikuspegi hartzen dira kontuan: bata 0 bider 0 bider 0 x tartearen beheko mugatzat, eta bestea 100 bider 100 bider goiko mugatzat. Lehen kasuan 1 eta 100 artean daude, eta bigarrenean 99 eta 0 artean. 2.4 irudiak bi kurba erakusten ditu: lerro laranjak kide guztien batez besteko AV indizea adierazten du pertzentil tartearen arabera, eta laranja–itzalak, berriz, kideen arteko aldakortasuna adierazten du; kurba urdinak, aldiz, multzoaren AV indizearen bilakaera irudikatzen du, 2.2 Irudian azaldu dena, pertzentil tartearen arabera. Lerro urdinak eskualde osorako batez besteko espaziala adierazten du, eta itzal urdinak, berriz, aldakortasun espaziala.

Prezipitazioei dagokienez, AV indizeak gora egiten du pixkanaka 0–x kasuan, PDF banaketaren ezkerreko muturrean AV txikiagoa adieraziz. Muturreko gertaera minimo horiek prezipitazioen gutxieneko balioekin bat datoz (<1mm/egun), gertaera lehorrak barne. Oharpen hau berretsi egiten da X 100 kasuan; orokorrean AV balioak 0–x kasuarekin alderatuta altuagoak baitira. Gainera, 100. pertzentilera hurbildu ahala, AV indizeak gora egiten du. Emaitza horiek iradokitzen dute RCMk zailtasunak aurkitzen dituela PDFko ezkerreko muturrean dauden gertaerak zehatz–mehatz irudikatzeko. 90-100 tartean, AV indizean minimo bat ikusten da, eta ondoren igoera txiki bat. Joera hau hobeto ulertzeko, 2.4 Irudiak kide guztien eta behaketan probabilitate–dentsitatearen funtzioak (PDFak) aurkezten ditu. PDFek frogatzen dute kide guztiek (RCMk eta GCMk) intentsitate baxuko gertaerak gainestimatzen dituztela, *"drizzle"* fenomeno ezagunari lotutako ezaugarria: bai RCMk, bai GCMk, urte osoan zehar dirauten hondoko euri arineko gertaeraren patroia erakusten dute, baina, hala ere, modu desegokian erreproduzitzen dituzte zero prezipitazioko gertakariak (Coppola et al., 2021; Kämäräinen et al., 2018; van Meijgaard and Crewell, 2005). Eguneko 10 mm-ko balioetatik aurrera, 90. pertzentiletik aurrerako tarteari dagokiona, GCMak prezipitazioa gutxiesten hasten dira, RCMek behaketen PDFa nabarmen erreproduzitzen duten bitartean. Inflexio puntua 90. pertzentilaren inguruan gertatzen da, non behaketen kurba GCMen kurbekin gurutzatzen den. Intersekzio honek 2.4.b. Irudiko minimoaren existentzia azaltzen du 90 pertzentilean.

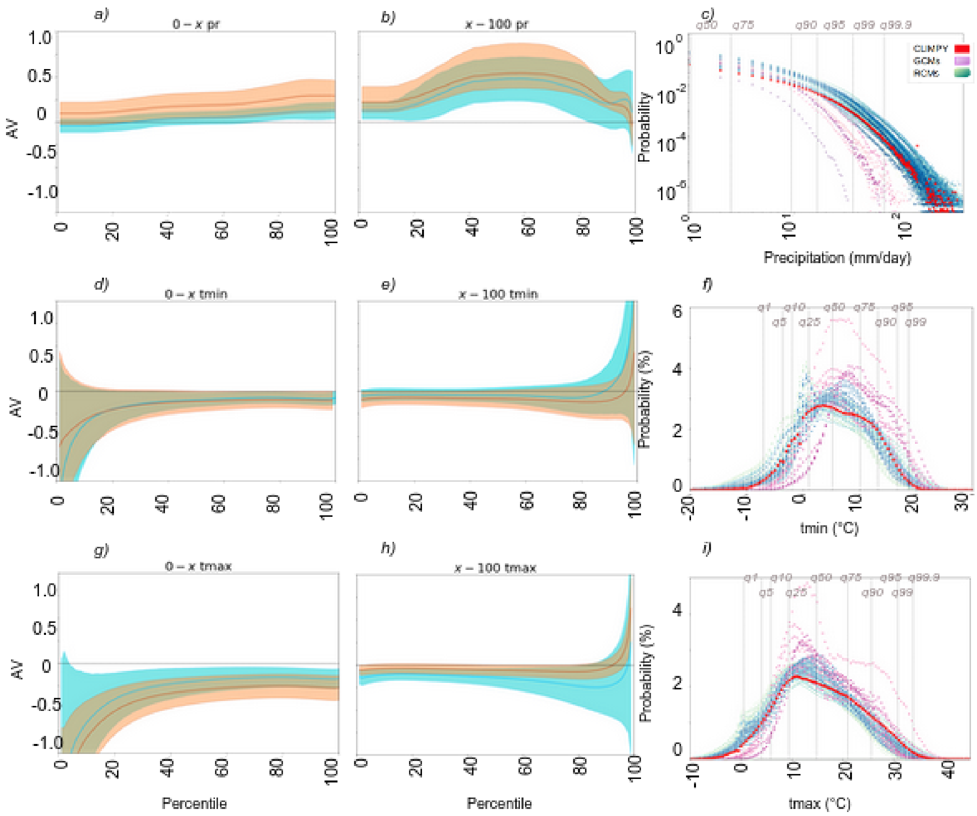

2.4 IRUDIA: Balio erantsiaren indizearen (AV; (2.2)) batez bestekoa eta aldakortasunaren (laranja) eta multzoaren eta haren aldakortasun espazialaren (urdina) eboluzioa, "pr" (a, b), "tmin" (d, e) eta "tmax" (g, h) aldagaietarako, lehen eta bigarren zutabeetan aurkeztuta. Hirugarren zutabeak behaketen PDFak erakusten ditu (gorria), RCMkoak (urdina), eta GCMkoak (arrosa) eta CLIMPYkoak "pr" (c), "tmin" (f) eta "tmax" (i) kasuetarako.

Tenperatura maximoen eta minimoen portaera antzekoa da. 0–x tartean, AV indizeak balio oso baxuak lortzen ditu, eta -0,2 inguruan egonkortzen da x=20 pertzentiletik behera dagoenean bi kasuetan. Eremu laranjek kideen arteko aldakortasuna adierazten dute, $x < 20$-ko tarteetarako aldakaortasun esanguratsua adieraziz. Horrek adierazten du kideek AV balio desberdinak dituztela, balio positiboetatik negatiboetara. Aldakortasun espazialak (urdinez ñabartua) patroi bera jarraitzen du. 0- x tarteetan, non $x < 20$, eremu itzaltsuak zabaltasun handia duen. Laburbilduz, honek iradokitzen du AV indizea tenperatura PDFaren isats minimoan nabarmen aldatuko dela leku espazialaren eta RCM kidearen arabera.

Alderantziz, x-100 tartean, AV indizea handitu egiten da banaketaren eskuineko isatsean, 100. pertzentila kontuan hartzen denean. Emaitza horiek adierazten dute RCM simulazioak balio erantsia ematen diola tenperatura maximoaren eta minimoaren banaketaren eskuineko isatsari, bi tenperaturen gertaera beroei dagokiena. Hala ere, banaketaren ezker isatseko simulazioaren kalitatea gutxitzen du, tenperatura minimoak irudikatzen dituena, gertaera hotzei lotuak.

Tenperaturaren PDFi dagokionez (2.4.f. Irudia; 2.4.i. Irudia), azpimarratzekoa da behaketen antzeko forma dutela, RCMetarako egokitzapenean antzemandako hobekuntzekin. GCMek beti gainestimatzen dituzte maximoak eta gutxietsi egiten dituzte bi tenperaturen minimoak, nahiz eta RCMk maximoen gainestimazioa zuzentzen duen. Hala ere, banaketaren beheko isatsean, RCMek bi tenperaturetarako gertaera minimoen kopurua gainestimatzen dute, AV balio negatiboak sortuz (2.4.d. Irudia; 2.4.g. Irudia).

2.5, 2.6 eta2.7 Irudiek AVaren batez bestekoaren banaketa espazialaren berri ematen dute tarte espezifikoetarako, eta emaitza horiek bat datoz2.4 irudian ikusitako joerekin. Prezipitazioen kasuan (2.5 irudia), AVren pixkanakako hazkuntza dago 0–x tarterako, 2.4 a irudian adierazten den bezala. Gainera, x–100 tarteak AV balio handiagoak erakusten ditu 0–x tartearekin alderatuta, 2.4 b irudian egindako behaketak berretsiz eta AV oso baxu bat adierazten du zero balioen inguruan. AVen banaketa espaziala aztertzean, balio baxuagoak ikusten dira mendilerroko goi–eskualdeetan. X-ek gora egin ahala, AV balio baxuak zabaldu egiten dira, eta batzuetan balio negatiboak lortzen dituzte zenbait eremutan. AV minimo bat gertatzen da 90. pertzentilean, GCM eta RCMen PDFen arteko elkarguneari dagokiona (2.4.c. Irudia).

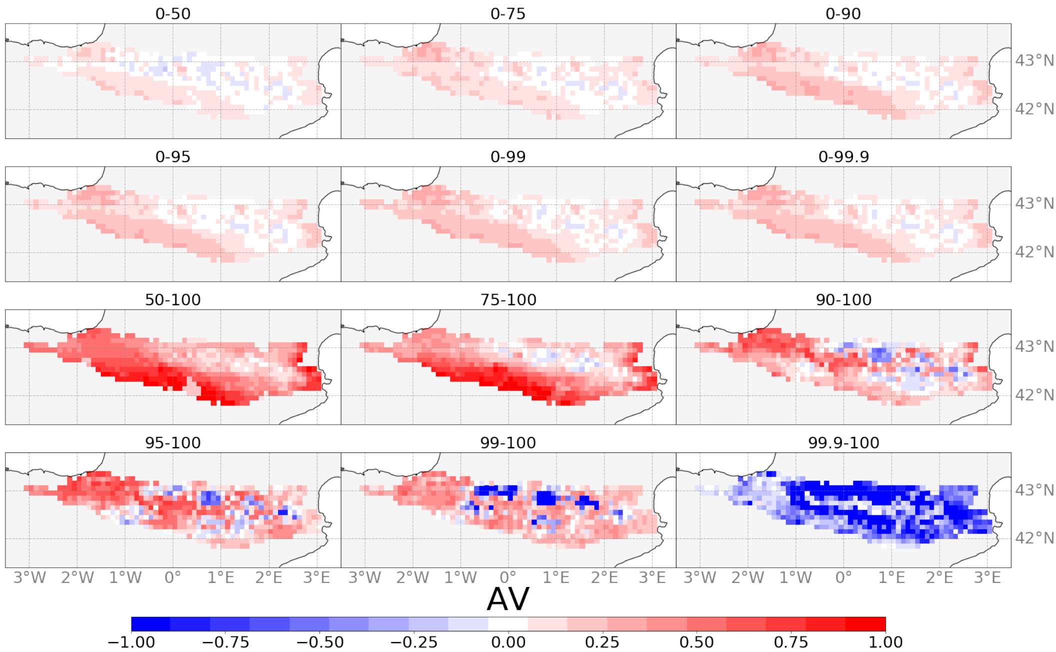

2.5 IRUDIA: Balio erantsiaren indizea (AV, (2.2) ekuazioa) RCM multzoarentzat 0,11 °× 0,11 °, prezipitazio aldagairako, 1981-2015 aldian erreferentzia gisa CLIMPY erabiliz.

Altitude handiko eremuetan AV baxua detektatzearen arrazoia, zonalde horietan prezipitazioen behaketetan dauden gabeziekin lotu daiteke. Goi–mendietako eskualdeetan, Pirinioetan esaterako, behaketa–estazioen dentsitate txikiagoa da nagusi, eskualde menditsu horiek duten urruneko kokapenengatik (Isotta et al., 2014). Honek, neurketa tresnen kalibrazio faltarekin batera, prezipitazioa gutxiestea ekar dezake, batez ere baldintza haizetsu eta elurra nagusi denean, behaketek ez dituzte prezipitazio patroiak zehatz–mehatz irudikatuko garaiera handiko eremuetan (Adam and Lettenmaier, 2003; Torma et al., 2015). Behaketetako alborapen horiek AV indizean eragiteko ahalmena dute, eta, horrela, emaitzen fidagarritasuna mugatzen dute altitude altuetan.

2.5 irudiak, gainera, AV indizearen ezaugarri interesgarri bat erakusten du 99.9–100 tartearen barruan, non AVren beherakada ikusten den eskualde osoan. Fenomeno hau tarte horretan gertatzen den gertaera kopuru txikiagatik azaltzen da, gertaera bakoitza bere magnitudearen arabera binetan sailkatzen delarik. RCMak PDFaren goiko isatsaren irudikapena hobetzen duen arren, gertaera bakan horien magnitudea zehaztasunez aurresaten zailtasunak aurkitzen ditu, behaketekiko bin ezberdinetan kokaraziz. Ondorioz, bin bakoitzean gertaeren maiztasuna konparatzean, AVaren murrizketa eragiten du. Gertaera mota hauen kopuru arbuiagarria kontuan hartuta, horrek ez du eragin nabarmenik PDFaren AV indize orokorrean.

Tenperatura minimo eta maximoen emaitzek, 2.6 eta 2.7 Irudietan aurkeztuak, koherentzia erakusten dute 2.4.c. Irudiarekin. Banaketaren goiko isatsa, gertaera minimoei dagokiena, AV oso baxua erakusten du. AVa etengabe baxu mantentzen da tartearen eboluzioan zehar, baina 90–100 tartera iristen denean, hazkunde esponentzial bat ikusi daiteke, eta balio altuak ematen ditu mendilerroaren erdialdeko eskualdean. AV seinale positibo hau bat dator 2.2 irudian adierazten den banaketa espazialarekin. Funtsean, tenperatura maximo eta minimoetarako lortu diren batez besteko AV balio positiboak banaketaren goiko isatseko AV-ak eragiten du.

Tenperatura minimo eta maximoen AVen eboluzioaren arteko bereizketarik nabarmenena euren hedadura espazialean dago. Tenperatura minimoaren kasuan, AV positiboek eremu handiagoa hartzen dute eta balio altuagoak lortzen dituzte. Alderantziz, tenperatura maximoei lotutako AV positiboak mendikatearen eremu altuenetan kokatuta daude, AV negatiboz inguraturik.

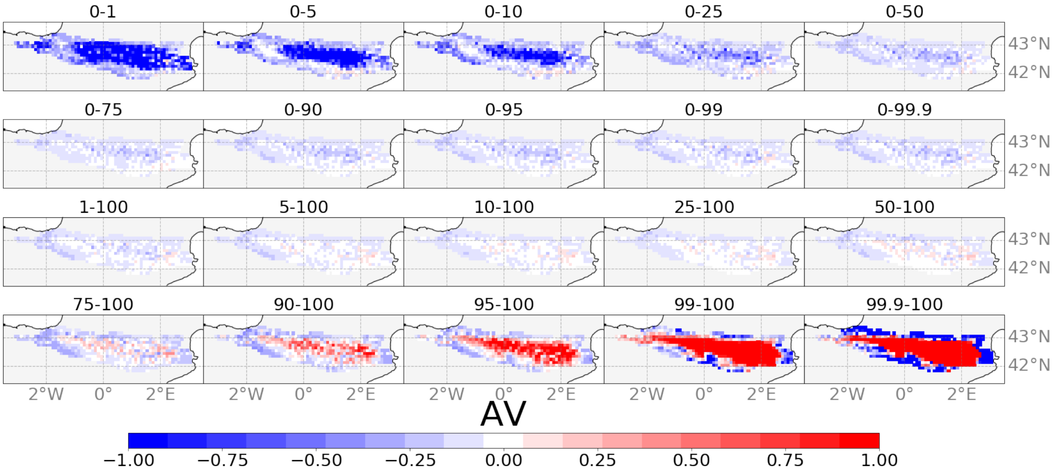

2.6 IRUDIA: Balio erantsiaren indizea (AV, (2.2) ekuazioa) RCM multzoarentzat 0,11 °× 0,11 °, tenperatura minimoaren aldagairako, 1981-2015 aldian erreferentzia gisa CLIMPY erabiliz.

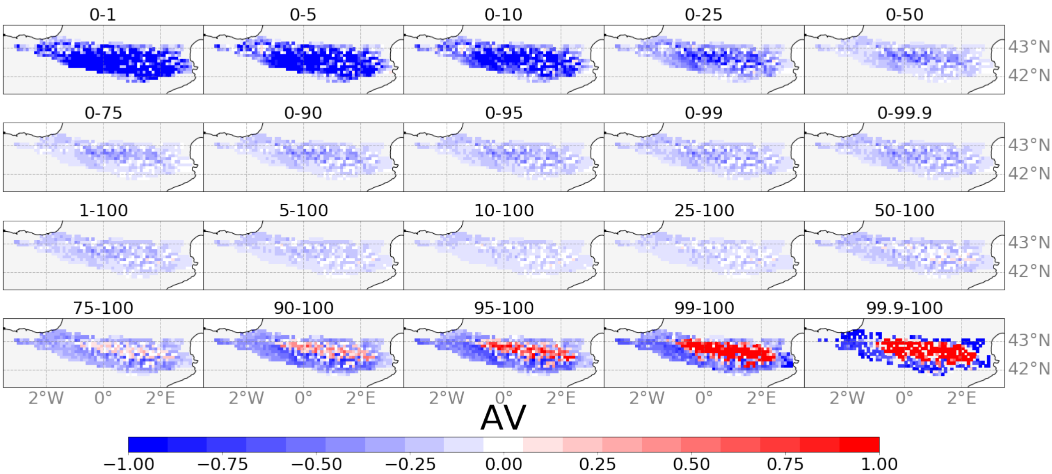

2.7 IRUDIA: Balio erantsiaren indizea (AV, (2.2) ekuazioa) RCM multzoarentzat 0,11 °× 0,11 °, tenperatura maximoaren aldagairako, 1981-2015 aldian erreferentzia gisa CLIMPY erabiliz.

2.4.3 Balio erantsiaren bilakaera orografiarekin

AV indizearen eta altitudearekin arteko itxurazko korrelazioa kontuan hartuta, 2.8 Irudiak AVren batez bestekoaren eta Pireneoetako eskualdeko altitudearen arteko korrelazioan sakontzen du, haien erlazio espazialen azterketa sakonagoa ahalbidetuz. Prezipitazioaren sakabanatze–diagramak (2.8.a. Irudia) erlazio negatiboa erakusten du multzoko bastez besteko AVaren eta altitudearen artean, nahiz eta AV positiboa izaten jarraitzen duen tarte osorako, 2.2 Irudiarekin koherentea. Era berean, prezipitazioak korrelazio negatibo orokortu bat erakusten du ia kide guztietarako (2.8.b. irudia), eta horrek esan nahi du altitudeak gora egin ahala AV indizeak behera egiten duela. Aurkikuntza horiek 2.3.1 eta 2.3.2 ataletan lortutako emaitzekin bat datoz, eta iradokitzen dute eskualde osoan AV nagusiki positiboa den bitartean AVren murrizketa bat dagoela altitude handietan, zein behaketa–datuen kalitatearekin lotuta egon daiteke garaiera horietan. CanESM2k bultzatutako eredu–multzoak (1. kodea) korrelazio–balio positibo nabarmenak erakusten ditu, eta GCM horrek prezipitazioa irudikatzeko ezintasunaren ondorio izan daiteke, RCMak aplikatzean AVa eskualde osoan zehar nabarmen hobetzen baita.

Alderantziz, AVaren eta bi tenperaturen altitudearen arteko erlazioak balio positiboak erakusten ditu, eta horrek AV handiagoa dakar eskualde garaietan. Hala eta guztiz ere, tmax eta tmin aldagaien (2.8.a. Irudia) sakabanatze–diagrametan bereizketa batzuk daude: AVak tmax multzoari dagokionez 0 m-tik 1500 m-ra doan tartean, igoera argirik erakusten ez duen bitartean, 1500 m-tik gora, igoera esanguratsua dago. tminen kasuan, AV eta altitudearen arteko erlazio positiboa konstantea da altitude tarte osorako. Era berean, banako kideen korrelazio–koefizienteak ere orokorrean positiboak dira (2.8.b. Irudia). Behaketa hauek bat datoz 2.6 eta 2.7 irudietan ilustratutako aurkikuntzekin. Hala ere, aipatzekoa da zenbait salbuespenetan korrelazio–koefiziente negatiboak ikusten direla. Zehazki, CNRMk (2. kodea) eta EC-EARTHek (3. eta 4. kodeak) bultzatutako talde ereduan, korrelazio negatibo horiek GCMren errendimendu bikainari egotz dakizkioke, RCMk kasu horietan AV aldagaiaren irudikapena hobetzeko duen gaitasuna mugatzen baitu.

2.9 irudiak AVren eta altitudearen arteko korrelazio–koefizienteen eboluzioa erakusten du, pertzentil tarteen arabera, 2.4 Irudiaren antzeko planteamendu bati jarraituz. Prezipitazioen AVaren eboluzioa konstantea da. Hala ere, tenperaturaren emaitzek ondorio honetara garamatzate: PDF osorako behatutako korrelazio positiboak (2.8 Irudia) banaketaren goiko isatsaren eraginpean daude. Horrek adierazten du RCMak areagotu egiten

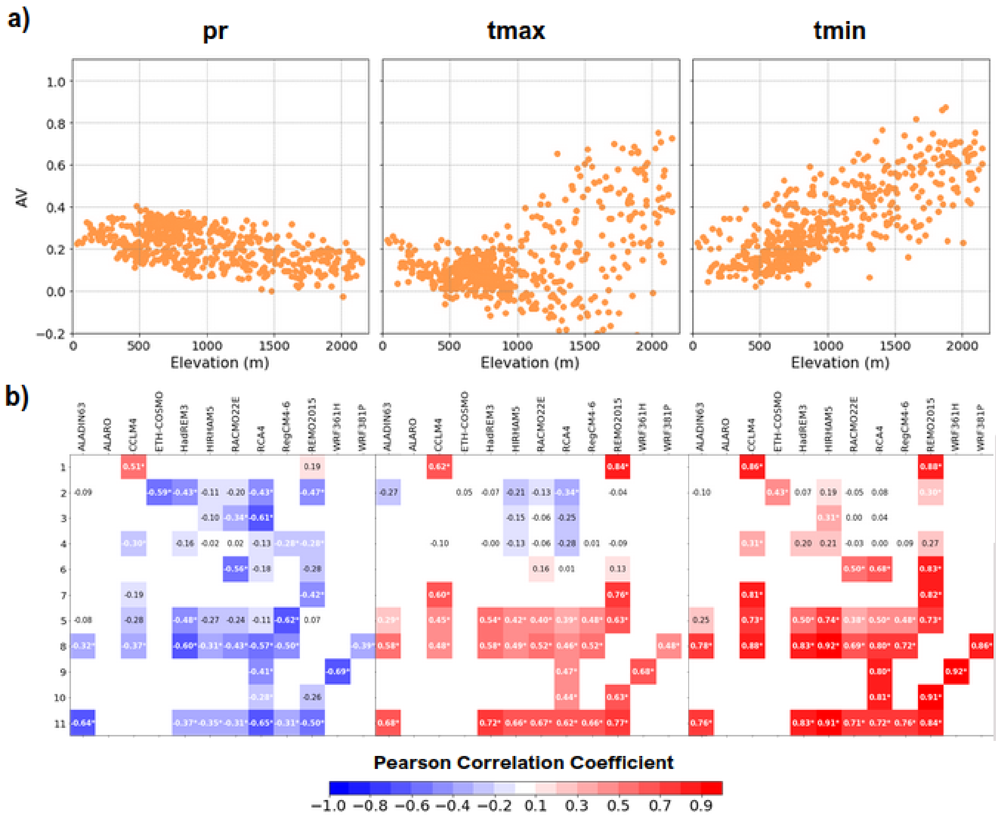

2.8 IRUDIA: a) AV vs. altitudearen sakabanatze–diagramak multzoaren batez bestekorako prezipitazio aldagaietarako, tenperatura maximorako eta tenperatura minimorako b) AVren eta altitudearen arteko korrelazio–koefizienteak kide guztientzat prezipitazioa, tenperatura maximoa eta tenperatura minimoa aldagaiterako. Matrizea RCMek (x ardatza) eta GCMek (y ardatza) osatzen dute, 2.1 taulan definitutako kode gisa adierazita. Izartxoak (*) korrelazio estatistikoki esanguratsua dela adierazten du t Student testaren % 95ean.

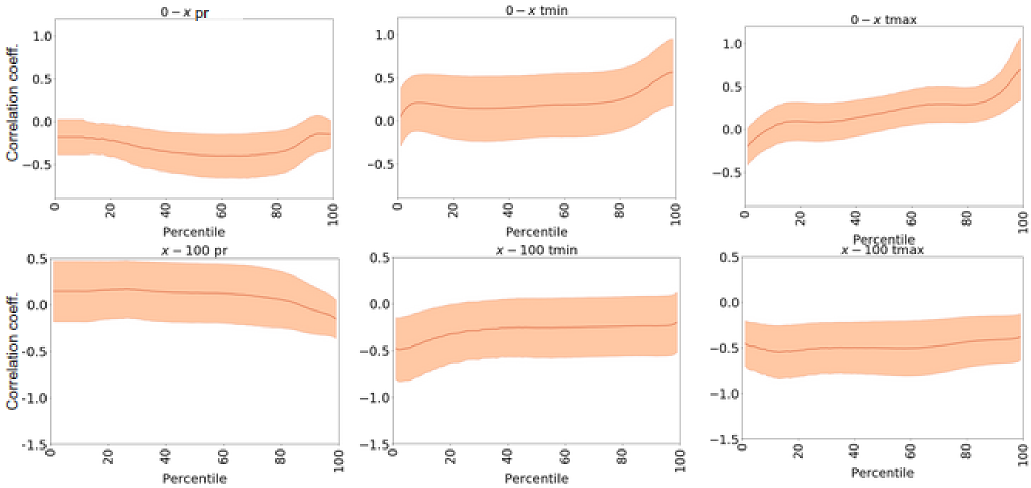

2.9 IRUDIA: AV (AV,(2.2) ekuazioan) indizearen eta CLIMPYren arteko korrelazio–koefizienteen arteko aldagarritasuna, eta "pr", "tmin" eta "tmax" aldagaietarako. X puntu bakoitzak "0–x" (gora) eta "x–100" (behera) bitartekoen korrelazio–koefizientea deskribatzen du. Itzaleko eremuak kideen desbideratze estandarra erakusten du.

duela gertaera beroen irudikapena altitude handiko eskualdeetan. Hala ere, korrelazio–balio negatiboak nabaritu ziren tenperatura–banaketen beheko muturrean. Horrek, beheko isatsetako tenperaturen AV balio baxuekin batera (2.4 d, g Irudia; 2.6 Irudia eta 2.7 Irudia), iradokitzen du RCMek tenperaturen ezkerreko isatsen irudikapen desegokitasuna altitude handiko eskualdeetan dagoela nagusiki.

2.5 Eztabaida

Bereizmen handiko RCMak erabiltzearen balio erantsi positibo argi bat dago, bereizmen lodiko GCMak erabiltzearekiko, batez ere prezipitazioari dagokionez: 0, 11 (2.2) Irudia eta 1,00 °(2.3 Irudia). Aurkikuntza hori bat dator Europa mailako prezipitazioak aztertzen dituzten aldez aurreko ikerketekin, eremu topografikoki konplexuak barne, hala nola Mendilerro Alpinoa eta Iberiar Penintsula, besteak beste (Careto et al., 2022c; Terzago et al., 2017). RCMetan prezipitazio simulazioen hobekuntza topografikoki induzitutako tokiko zirkulazioaren irudikapen hobeari egotz dakioke, (Careto et al., 2022c) bereizmen espaziala handitzearen ondorioz. Era berean, Prein et al. (2016)-k iradokitzen zuen AV positibo hori mendebaldeko haizeen eragina duten eremuetan prezipitazioen irudikapen zehatzagoaren ondorio dela, bereziki nabaria neguko hilabeteetan, non eskala sinoptikoko fluxuak funtzio nagusia baitu Europako sektorean. Hori bat dator AV indizearen hazkundea erakusten duten gure emaitzekin, bereziki Pirinioen mendebaldean, non Ozeano Atlantikotik datozen mendebaldeko perturbazioek neguko prezipitazioei gehien laguntzen dieten.

Era berean, tenperatura maximoen eta minimoen kasuan, AV positibo bat identifikatzen da RCMak erabiltzean, batez ere Pirinioetako eremu garaienetan bi bereizmenetan (2.2 Irudia eta 2.3 Irudia). Zehazki, AV positibo zabalago bat ikusten da tenperatura minimoen kasuan tenperatura minimoekin alderatuz, Cardoso and Soares (2022)-k ateratako ondorioekin bat etorriz, zeinek AV positibo handiagoak aurkitu zituzten Europan tenperatura minimorako tenperatura maximorako baino. Tenperatura minimoetarako AV balio altuak GCMek orografikoki eragindako tenperatura minimoen desitxuratze potentzialari egotz dakizkioke, zeinak automatikoki zuzentzen baitira ezaugarri topografikoak zehaztasun handiagoz kontuan hartuz bereizmenaren handiagotzearen bidez (Perkins et al., 2007). Izan ere, Di and Ramo (2013)-k ezarri zuen RCMk Ipar Amerikako eskualdean, batez ere topografia konplexua duten eremuetan, ematen duen 2-mko tenperaturaren balio erantsi potentziala zuzenean egotzi ahal izango litzaiokeela orografikoki eragindako interakzio sinpleen % 65 baino gehiagori. Hau, zehazki, tenperaturaren eta altitudearen arteko korrelazio orokorrari dagokio. Horrela, elebazio–gradienteen irudikapen zehatzagoak nabarmen hobetuko lituzke GCMen tenperatura patroiak, baita eskala fineko prozesu atmosferikorik ez dagoenean ere. Ondorioz, zehazteke dago zenbateraino arindu daitekeen lortutako AVa, bereizmen handiko azaleraren eta bereizmen baxuko tenperatura maximo eta minimoen arteko erlazio sinpleak kontuan hartuta. Gainera, Cardoso and Soares (2022)-k iradokitzen du Iberiar Penintsulako tenperatura maximoetarako AV balio positiboak prezipitazio eta elurraren irudikapen hobetuekin lotzen direla, batez ere elurrik gabeko gainazalak hobeto irudikatzeari dagokionez.

Garrantzitsua da nabarmentzea aldaera esanguratsuak daudela banako kideen seinaleetan (B.1–B.6 irudiak) bi ebazpenetan, AVak GCMarekiko duen funtsezko menpekotasuna adierazten dutenak. Jokabide honek azpimarratzen du GCM gidariaren kalitateak RCMren gaitasuna muga dezakeela aldagaiaren irudikapena hobetzeko. Prezipitazioaren kasuan, MPI-ESM-LR ereduaren errendimendu bikainak (8 eta 9 kodeak;

Brands et al. (2013)) AV balioak jaistea dakar. Hala ere, EC-EARTH GCM-rako (3 eta 4 kodeak), prezipitazio irudikapen onak ezaugarri dituena (D_{GCM}= 0,32 eta 0,29 hurrenez hurren 0,11 ° bereizmenean), beherakadak AV balio esanguratsuak ematen jarraitzen du. Ohar honek iradokitzen du AV eta ereduaren arteko harremanak eratzen dituzten beste faktore eragingarri batzuk daudela. Faktore horietako batek ekaitz–ibilbideen kokapen zehatza edo eskasarekin erlazionatuta egon daiteke. RCMak prezipitazioen karakterizazioa hobetuko du, betiere GCMk ekaitz–iinlbideen kokapena zehatz identifikatzen badu. Hala ere, GCMk ez badu lortzen, RCMren AV potentziala mugatua izan daiteke. Izan ere, Zappa et al. (2013)-k nabarmentzen du EC-EARTH GCMrako (3 eta 4 kodeak) ekaitz–pista zuzen kokatzearen garrantzia. Alderantziz, HadGEM GCMk (5 kodea) D_{GCM}(0,27) EC-EARTHren antzeko balioak ditu, baina RCMak ez dakar ezaugarri aldakor hoberik, eta horrek AV txikiagoa dakar. Desadostasun hau modeloak udako hilabeteetan ekaitz–ibilbideen kokapen txarrari egotzi dakioke (Zappa et al., 2013) azterketa–eremuaren longitudeetan. Era berean, tenperatura minimoetan zein maximoetan, errendimendu hobea duten GCMek, hala nola CNRM-CM5 (Code 2; McSweeney et al. (2015)), RCMak erabiliz lortutako AVa murrizten dute. Hau da, D_{GCM} baxu batek, GCMren irudikapen aldakor hobea adierazten duenak, RCMren ahalmena mugatzen du irudikapen hori hobetzeko, eta horrek AV gutxituak eragiten ditu. RCMen bereizmen altuko simulazioek testuinguru honetan ekarri dituen hobekuntzen izaera ñabarra gorabehera, zenbait kasutan egokiak izaten jarraitzen dute. Adibidez, 0,11 °bereizmenerako, CNRM+CLMcom-ETH ereduan, D_{GCM} balio baxuak eta konparagarriak behatzen dira, bai tmax eta tmin aldagaietarako, 0,31 eta 0,33, hurrenez hurren. Hala eta guztiz ere, tmaxerako beherakadaren AVa ia zero (-0,007) den bitartean, tmin-erako 0,12 da, irudikapen aldagarrian hobekuntza nabarmena esan nahi duelarik. Era berean, EC-EARTH GCMak 0,41 inguruko Dgcm balioak erakusten ditu tenperaturaren bi aldagaietarako eta RCM RCA4ak tmax irudikapena 0,03 hobetzea lortzen du, tmin-erako AVa zerora hurbiltzen den bitartean.

Erabilitako metodologiak aukera ematen du AV sakonago aztertzeko probabilitate–dentsitatearen funtzioaren tarte desberdinen bidez (PDF). Ikusten da GCM guztiek modu koherentean gutxiesten dituztela prezipitazio handiko gertaerak, eta, aldi berean, prezipitazio arinezko gertaeren gainirudikapen bat erakusten dutela (2.4.c. Irudia), Perkins et al. (2007) k ere azpimarratu zuen bezala. RCMk 90eko pertzentiletik gorako gertaeren irudikapena nabarmen hobetzea lortzen du, AVren eboluzioak X–100 kasuan bereziki nabaria izanik (2.4.b. Irudia). Hala ere, eguneko 10 mm baino gutxiagoko prezipitazio tasetarako, RCMk behaketek baino prezipitazio balio handiagoak erregistratzen ditu, behaketen PDFaren eta RCMen PDFen arteko intersekzioa eraginez. Intersekzio hau agerian geratzen da, baita ere, 2.4.b. Irudian, AV-an (Ciarlo et al., 2021) minimo bat agertzen delarik. Ondorioz, RCMk euri–jasa arinak eta gertaera lehorrak irudikatzean zailtasunak aurkitzen dituzte (Boberg et al., 2009, 2010; Soares and Cardoso, 2018; Careto et al., 2022c). Garrantzitsua da aitortzea, nahiz eta prezipitazio minimoak erreproduzitzeko muga horiek egon, ez dutela eragin nabarmenik izango erabateko prezipitazioaren ezaugarrietan. Izan ere, horrelako gertaerek, normalean, gutxieneko ekarpena egiten diote prezipitazio kopuru orokorrari (Dai, 2001).

Maila espazialean (2.5 Irudia), AV baliorik baxuenak pertzentil–tarte ezberdinetarako (0–50, 0–75, 0–90) mendilerroaren ekialde–muturrean kontzentratzen dira, klima Mediterraneoa (Lemus-Canovas et al., 2019) ezaugarri duena, non uraren birziklapenak, lurraren hezetasun–atmosferaren birelikaduraren bidez, funtzio kritikoa betetzen duen, batez ere, udako prezipitazioetan.

AV tenperaturarako PDF tarteen ekarpenen azterketa sakonagoak adierazten du PDF ia osoaren AVa zerotik gertu dagoen bitartean, tenperaturaren PDF muturrak direla seinalea eratzen dutenak. GCMk muturreko gertaera maximoak gehiegi estimatzeko joera du, isatsaren beheko gertaerak gutxiesten dituen bitartean (2.4.f. Irudia, 2.4.i. Irudia), Perkins et al. (2007)-ren aurkikuntzekin bat etorriz. RCMak nabarmen hobetzen du isatsaren goiko muturren irudikapena, bai tenperatura maximoetan, bai minimoetan, batez ere Pirinioetako erdialdeko eskualdean, altitude handiagoek ezaugarritzen dutena. Gainera, onura handiagoak ikusten dira tenperatura minimoetan, tenperatura maximoen aldean (Cardoso and Soares, 2022). Alderantziz, bi tenperaturetan beheranzko isatsen irudikapenak behera egin du oro har, eta horrek adierazten du RCMen simulazioak eragin negatiboa duela muturreko minimoak simulatzean. Gainera, zailtasunak sortzen dira izozte–tenperaturak era zehatzean adierazteko (2.4.f. Irudia, 2.4.i. Irudia), eta horrek tenperatura maximoak eta minimoak 0 °C inguruan gainestimatzea dakar, Careto et al. (2022a)-k ere adierazten duen bezala. RCMren gabezia hauek elurraren dinamika eta bere elkarrekintzak simulatzeko arazoekin lotzen dira, elur–albedoaren feedbackean eta gainazaleko fluxuen banaketan eraginez. Elur–estaldura irudikatzeko alborapen horiek elurrezko albedo simulatuetan eta azaleko tenperaturetan eragin ditzakete (Minder et al., 2016). Muturreko tenperatura minimoetan dauden alborapen horiek AV balio negatibo gisa agertzen dira PDFaren ezkerreko muturrean bi tenperaturetarako, Pirinio osoan zehar hedatuz. Tenperatura maximo eta minimoei dagokien balio erantsiaren beste alderdi esanguratsu bat banaketaren muturreko isatsetan kide arteko aldakortasuna egotea da. Aldakortasun hau oso lotuta dago GCMk tenperatura dinamika eta patroiak simulatzeko duen gaitasunarekin.

Aurkikuntzek, gainera, AV balioen eta Pirinioetako orografiaren arteko korrelazio esanguratsuak erakusten dituzte, altitudearen garrantzia simulazio klimatikoen errendimendua ebaluatzerakoan azpimarratuz (Reder et al., 2020). Korrelazio–balio negatiboek AV negatiboa adierazten dute bereziki garaiera handiko eskualdeetan, puntu hauetan behaketen kalitate mugatua adierazten ditzakena (Torma et al., 2015). Tenperaturari dagokionez, banaketaren eskuineko isatsean korrelazio positiboa dago, eta horrek adierazten du AV balio altuak altitude handiko eskualdeetan kontzentratzen direla gertaera beroetan. Alderantziz, ezkerreko isatsaren korrelazio negatibo batek iradokitzen du, gertaera hotzetarako, altuagoak diren eskualdeek AV balio txikiagoak aurkezten dituztela.

2.6 Ondorioak eta konexioak

Kapitulu honek Eskualdeko Eredu Klimatikoak (RCM) Klima eredu globalekin (GCM) alderatzen ditu Pirinioetako eremuan; prezipitazio, tenperatura minimo eta tenperatura maximoetarako ematen duten balio erantsiaren ebaluazio integrala aurkeztuz. Analisi hori egiteko, CLIMPY behaketa datu–basea erabili zen erreferentzia gisa. Analisiak balio erantsiaren banaketa espazialean zein aztertutako aldagaien Probabilitatearen Banaketa Funtzioaren (PDF) tarteek balio erantsi orokorrari egiten dioten ekarpenean sakontzen du. Kapitulu honek **3 Helburua** lortzea errazten du, eta horrek simulazio klimatikoetan dauden indarguneak eta mugak identifikatzea dakar. Gainera, **Mugarria 2** betetzen laguntzen du, etorkizuneko klima–aldaketak aurreikusteko erabiltzen diren tresna prediktiboen azterketa sakona eginez.

Lortutako emaitzek hobekuntza nabarmena azpimarratzen dute, RCMen bidez mendikatearen erdialdean eta hego–mendebaldean prezipitazioa zehatz erreproduzituz. Azpimarratzekoa da eskualde horietan mendebaldeko perturbazioek eragina dutela, eta horiek funtsezko zeregina dutela prezipitazioen erregimena eratzeko. Batez besteko tenperatura maximoek eta minimoek ere balio erantsi positiboak dituzte, bereziki nabariak Pirinioetako garaiera handietan. Eta bereizmen espazialaren fintzearekin zerikusia dute.

Ereduetako multzoko kideek balio erantsiari egindako ekarpenak aztertuta, GCMren simulazioaren kalitatearekiko mendekotasun handia dagoela ikusi daiteke. Mendekotasun horrek esan nahi du GCMek RCMen ahalmena mugatzen dutela aldagai horien irudikapena eraginkortasunez hobetzeko.

Prezipitazioa PDF tarteen bidez aztertuz gero, beherapen dinamikoak 90eko muga gainditzen duten prezipitazio–gertaerak hobeto irudikatzen dituela ikusten da, eta prezipitazio–tasa txikiagoak behar bezala irudikatzeko oztopoak daudela, bereziki klima mediterraneoa nagusi den ekialdeko eskualdean. Prezipitazio–tasa baxuen gainestimazioa, RCM ereduen bidez, hezetasunaren eta atmosferaren arteko feedbacka bidezko uraren birziklapenaren irudikapen desegokiaren ondorio izan daiteke. Balio erantsi negatiboak Pirinioetako goi–eskualdeetan erregistratzen dira, behaketa–datuen gabeziei egotziz.

Tenperatura–tarteei dagokienez, AVan ikusitako beherakada bereziki nabarmentzen da muturretan. Muturreko gertaera horiek ere aldakortasun espazial handia eta kide artekoa erakusten dute. RCMren arabera, GCMen aldean, lurralde altuenetan gertakari beroak harrapatzeko gaitasun hobea dago. Alderantziz, muturreko hotzak (PDFen ezkerreko isatsak) irudikatzeko RCMaren eraginkortasuna mugatua dago, batez ere elurraren dinamikak eragin handiagoa duen eremu garaietan.

Aurkikuntza horiek RCMen ekarpen esanguratsuak azpimarratzen dituzte: prezipitazioa, tenperatura minimoa eta tenperatura maximoaren aldagaiak zehaztasunez ezaugarritzeko. Hala ere, ezinbestekoa da mugak onartzea, RCMren datuen erabilera arduratsua errazteko aldi historikoan. Gainera, aldi historikoaren azterketa batetik lortutako informazio hori baliotsua da eredu klimatikoen etorkizuneko proiekzioak aplikatzerakoan. Liang et al. (2008)-k aipatzen du RCMen zein GCMen simulazio historikoan agertzen diren joera nagusiak sistematikoki hedatzen direla, etorkizuneko klima proiektatuan eskualde–eskalan. Horren arabera, azterlan honek adierazitako RCMen indarguneak eta ahuleziak etorkizuneko agertokietarako ere erreproduzituko dira. Horregatik, abantaila/muga horiek ezagutzea funtsezkoa da datu horiek hobeto aplikatzeko, etorkizunean arriskuak kudeatzeko estrategiak eta egokitze–planak garatu eta aplikatzerakoan. Muga horiek RCMko gertaera lehor eta hotzen erreprodukzio eskasean dira nabariak. Lehenengoa, Pirinioen barruko eskualde mediterraneoetako prezipitazio–ereduetan ebapotranspirazioak duen eraginaren interpretazio okerrarekin lotu daiteke. Azken hori, batez ere, RCM ereduek elur dinamikaren simulazioan duten gabeziari egotzi behar zaio. Erronka honek garrantzi berezia hartzen du Pirinioetako eskualde garaietan, non elurraren dinamikak eragin handia duen.

3

Klima eta Hidrologia Karakterizazioa Hobetzeko Makina Ikaskuntzaren Planteamenduak

Etorkizuneko klima zehatz–mehatz ezaugarritzea garrantzi erabakigarria du baliabide hidrikoen plangintza eta kudeaketarako epe ertain eta luzera, klima–aldaketaren testuinguruan (IPCC, 2022). Klima Eredu Globalak (GCM) eta Eskualdeko Klima Ereduak (RCM) (Jacob et al., 2014; Giorgi et al., 2009) tresna indartsu gisa agertu diren bitartean klima iragarpenerako (Semenov and Stratonovitch, 2010), oraindik ere muga batzuk erakusten dituzte eskala txikiko prozesuek definitutako eskualdeko klimak irudikatzerakoan (Torma et al., 2015), 4. kapituluan aztertzen den bezala. Horregatik, gabezia eta ziurgabetasun horiek arintzeko teknika berriak garatzea ezinbestekoa da. Kapitulu honetan, Machine Learning-en errotutako ikuspegi berritzaile bat aztertzen da eredu anitzeko multzoak eraikitzeko (Multi Model Ensemble), **4. Helburuarekin** lerrokatuz. Kapitulu honek, 4. kapituluarekin batera, tesiaren **2. Mugarria** osatzen du.

Lehenik eta behin, kapituluak eredu anitzeko multzoen kontzeptuak aurkezten dizkigu (3.1 atala). Ondoren, azterketa fluxua zedarritzen du, erabilitako aldagai eta datu–baseekin batera (3.2 atala). Ondoren, metodologia argitzen du, Machine Learning algoritmoen garapenean eta eredu hidrologikoaren aplikazioan sustraitua (3.3 atala), emaitzen analisi eta eztabaidarekin amaitu aurretik (3.4 atala).

3.1 Klima simulazioko Eredu Anitzeko Multzoak (MME)

RCMk GCMen aldean abantaila argiak dituen arren eskualdeko klimaren ezaugarri nagusiak atzemateko orduan (4. kapitulua) (Kotlarski et al., 2014; Ciarlo et al., 2021), berezko ziurgabetasunek bere horretan diraute. Ziurgabetasun horiek egiturazko desberdintasunak biltzen dituzte bai GCM eta bai RCM modeloetan (Knutti et al., 2008), downscaling teknika bera (Zhu et al., 2019), prozezu fisikoak azaltzeko erabiltzen diren ereduen parametrizazioak (Chen et al., 2011), eta hasierako baldintzak, beste faktore batzuen artean (Knutti et al., 2008; Dey et al., 2022). Gainera, arro–eskalan egindako ikerketetan, hala nola klima–aldaketak ur–baliabideetan dituen inpaktuak aztertzen dituztenetan, desoreka–eskala bat gertatzen da, eta horrek, batzuetan, ebatzi gabeko dinamika klimatikoak eragiten ditu, RCMren ebazpen ahalmenetatik haratago. Ondorioz, ziurgabetasun horiek RCMen arteko klima–aldaketaren proiekzioetan desadostasun nabarmenak sor ditzakete, baita emisio–agertoki berdinak aztertzen direnean ere (Ruane and McDermid, 2017). Horrek, irudikapen klimatikoari mugak ezartzen dizkion eskalako desegokitasunarekin batera, oztopatu egiten du datu horien erabilera eraginkorra arro–eskalako plangintzarako eta ur–baliabideen kudeaketarako (Venkataraman et al., 2016).

Inpaktu–ereduak erabiltzen dituzten ikerlari eta profesionalek metodo ugari erabiltzen dituzte ziurgabetasun eta akats horiei aurre egiteko, konplexutasun–espektro zabal bat hartuz. Metodo horiek (Crawford et al., 2019; Xu et al., 2020) azterketa–eremuaren barruan errendimendu handieneko simulazioak identifikatzetik (Dobor and Hlásny, 2019; Teng et al., 2015; Piani et al., 2010) behaketa–datuak dituzten alborapenak zuzentzeko teknikak erabiltzera eta Eredu Anitzeko Multzoak (MME) (Calì Quaglia et al., 2022; Salman et al., 2018) garatzera hedatzen dira. Alborapenak zuzentzeko metodoak funtsezkoak izan dira simulazioei datxezkien errore sistematikoak zuzentzeko (Piani et al., 2010). Hala ere, askotan ez dira hain eraginkorrak alborapen ez–egonkorrei aurre egiteko (White and Toumi, 2013; Wang et al., 2018). Eredu klimatikoen ziurgabetasunari aurre egiteko etorkizun oparoa MMEen garapenean datza, ziurgabetasunak arintzeko eta proiekzio klimatikoetan konfiantza areagotzeko ahalmena baitute (Pavan and Doblas-Reyes, 2000; Lutz et al., 2016; Sanderson et al., 2015; Keller et al., 2019). MMEak bi taldetan sailkatzen dira: SEM (Simple Ensemble Mean) eta WEM (Weighted Ensemble Mean). Lehen planteamenduan, taldeko kide guztiei pisu berdinak esleitzen zaizkie uniformeki, eta WEM metodoan, aldiz, kide bakoitzari pisu ezberdin bat esleitzen zaio, iraganeko baldintza klimatikoen erreplikazioan duen trebetasunak zehaztua (Oh and Suh, 2017; Ahmed et al., 2020). SEM, bere sinpletasunagatik ezaguna, normalean erabiltzen den metodo bat da, banakako kideek (Lambert and Boer, 2001) baino errendimendu hobea ematen duena. Hala ere, muga batzuekin dator. Eredu askok eredu–parametroak eta osagaiak partekatzen dituzte, eta horrek interdependentziak sor ditzake simulazio klimatikoen artean (Sanderson et al., 2015). Interdependentzia hori kontuan hartzen ez bada, baliteke eredu engainagarria izatea, zehaztasuna murriztea eta ziurgabetasunaren estimazio okerra egitea (Herger et al., 2018). Gainera, baliteke SEMa aplikazio guztietarako egokia ez izatea, informazioaren espazio– eta denbora–aldakortasuna nabarmen gutxitzen baitu banako kideekin eta behaketa–datuekin alderatuz gero (Wang et al., 2018).

Aldiz, WEM metodoek erakutsi dute gaitasuna dutela banakako kideen artean errore sistematikoen eragina arintzeko eta are multzoaren ahalmen prediktiboak indartzeko (Krishnamurti et al., 1999, 2000). Machine Learning algoritmoen erabilera Multi–Model Ensemble (ML–MME) bat sortzeko, simulazio klimatikoan agertzen ari den teknika bat da (Zhu et al., 2023; Sand et al., 2023). Algoritmo horiek potentzial handia dute simulazio klimatikoen emaitzak hobetzeko, batez ere erantzun–aldagaien eta prediktiboen arteko linealtasunik ezari aurre egiteko dituen abantailei dagokienez (Ahmed et al., 2020; Sachindra et al., 2018; Xu et al., 2020). Krishnamurti et al. (1999)k MMEren aurrekari bat ezarri zuten, 850 hPa haizearen abiadura eta zortzi zirkulazio–eredu orokorren (GCM) prezipitazio simulazioak hobetzeko erregresio–teknika anitzetan oinarritutakoa. Wang et al. (2018) lau Machine Learning (ML) teknika erabili zituen MMEak garatzeko hileko batez besteko tenperatura eta prezipitazio aldagaientzat, 33 CMIP5 GCM kontuan hartuta eta jakinarazi zuen Random Forestek (RF) eta Support Vector Makinek (SVM) hobekuntza nabarmena erakutsi zutela batez besteko multzoarekiko. Emaitza hauek Sa'adi et al. (2017) k jakinarazitako emaitzekin bat dator, kasu honetan berriz, General Linear Model (GLM) bat erabili zuten MMEren fabrikaziorako. Ildo horretako emaitzak jakinarazi dira Iraken hileko batez besteko tenperatura simulatzeko(Salman et al., 2018), edo hileko prezipitazioa erreproduzitzeko Pakistanen (Ahmed et al., 2020), Golkoko Arroan eta Ipar Amerikan (Crawford et al., 2019). Eguneroko eskalako azterketek ere ML–MME tekniken aldeko emaitzak erakusten dituzte (Jose et al., 2022). Era berean, Dey et al. (2022) k hobekuntza nabarmenak lortu zituen klima–aldagai horien karakterizazioan CMIP6 GCMen datuekin.

Gure ikerketan, ikuspegi berri bat proposatzen dugu ML–MME metodo batzuk RCMei lehen aldiz aplikatuz. Metodo horiek eredu hidrologiko bati aplikatu zitzaizkion. Machine–Learning teknikak oinarritutako emaitzak SEM metodoarekin konparatu genituen, hileko prezipitazioa (pr), eguneko tenperatura maximoaren hileko batez bestekoa (tmax) eta eguneko tenperatura minimoaren hileko batez bestekoa (tmin) aztertuz. Zehazki, ML–MME teknikek Erregresio Lineala (LR), Gradient Boosting (GB) eta Random Forest (RF) hartzen zituzten. Ikerketa hau bereziki azpimarragarria da, eskualde topografiko konplexu batean aplikatzen baitugu, zeinak gure ikerketari berritasun geruza bat gehitzen baitio simulaziorako dituen erronkak kontuan hartuta (Torma et al., 2015; Reder et al., 2020). Lehenik eta behin, RCMen rankinga garatu da, iraganeko klima ezaugarritzeko duten trebetasunean oinarrituta, eta RCM kopuru optimoa zehaztu da ML–MMEetan sartzeko. Hiru aldagaietarako azken ML–MMEak definitu ondoren, hileroko serieak xehetasunez aztertu ziren klimaren behaketekin alderatuz. ML–MMEek arro–eskalako inpaktu–azterketen aplikazioan duten erabilgarritasun praktikoa argitzeko, Temez eredu hidrologikorako sarrera–datu gisa erabili genituen, bai aldi historikoetarako, bai etorkizuneko proiekzio klimatikoetarako, azterketa–eremuaren barruan.

3.2 Datuak eta azterketa eremua

EURO–CORDEX multzoa (Jacob et al., 2014, 2020) aztertu genuen, guztira 72 RCM simulazioekin (C.1 taula) $0,11° \times 0,11°$ (2.2 atalean azalduta). CLIMPY behaketa–datuak (Cuadrat et al., 2020a; Serrano-Notivoli et al., 2017) erreferentzia gisa erabili dira, 1 km $\times$ 1 km-ko bereizmen espazialarekin, egunero 1980–2015 aldia betez (datuen azalpen zehatzagoa 2.2 atalean aurki daiteke). Simulazioen eta behaketen datuak behar bezala alderatzeko, biek sare–espazial berean egon behar dute. Horretarako, interpolazio bilinear bat egin da $0,11° \times 0,11°$-ko bereizmena duen sare–errektilineo batera.

Esca ibaiaren arroa mendebaldeko Pirinioetan dago, Espainiako ipar–ekialdean, eta 425 km ^{2}-ko azalera hartzen du, hau da, datu klimatikoen lau gelaxka. Gradiente altitudinal handi batek ezaugarritzen du arroko punturik altuenaren altuera 2.100 metrokoa dela, eta punturik baxuena, berriz, itsas mailatik 595 metrora dagoena. Ezaugarri orografikoek nabarmen zailtzen dute arro mota honetako dinamika klimatikoa simulatzea (Kotlarski et al., 2014; Smiatek et al., 2016) Horregatik, bereziki problematikoak dira etorkizuneko klima eta hidrologiarekin lotutako inpaktuak zehatz–mehatz iragartzeko (Fatichi et al., 2016). Garrantzitsua da zailtasun horiek gainditzeko ahaleginak egitea, batez ere Esca ibaiaren arroa bezalako kasuetan, funtsezko ibaiadarra baita Esako urtegia elikatzeko, mendebaldeko Pirinioetako urtegirik garrantzitsuena. Esca ibaiaren emariei buruzko datuak Espainiako Ikerketa Hidrografikoen Zentroaren (CEDEX) web orrian (https://ceh.cedex.es/anuarioaforos/default.asp) daude eskuragarri, non datuak 2017ko irailera eguneratzen diren.

pr, tmax eta tmin aldagaien hautespena bi kontsiderazioetan dago oinarrituta. Lehenik eta behin, haien erabilgarritasuna CLIMPY datu basean (Cuadrat et al., 2020a). Bigarrenik, aldagai horiek funtsezkoak direlako sistema klimatikoa ezaugarritzeko, aldez aurretiko azterketa hauetan azpimarratzen den bezala: (Meehl et al., 2000; Perkins et al., 2007; Careto et al., 2022d,b), eta zeregin erabakigarria dute hainbat sistema hidrologiko, biologiko eta industrialetan eragiteko (Colombo et al., 1999; Coppola et al., 2021).

3.3 Metodologia

Azterketa horrek metodologia espezifiko bat jarraitzen du, hainbat fasetan sailkatu ahal dena: (1) aztertutako hiru aldagaien –tmax, tmin, eta pr– errendimenduaren araberako RCM rankinga egin zen urtaro eskalan (3.3.1 atala), (2) SEMak eta ML–MMEak eraiki ziren (3.3.2 atala) eta (3) RCMen zenbaki optimoa aukeratu zen MMEak osatzeko (3.3.3 atala). (4) Behin betiko MMEak ebaluatu ziren (3.3.4 atala). Gero (5) aldagai klimatikoek fluxuen karakterizazioan duten eragina ebaluatzeko, MME horiek erabili ditugu Temez eredu hidrologikoaren sarrerako datu gisa (3.3.5 atala). Azkenik, (6) klima–aldaketaren inpaktua ebaluatzeko ML–MME emaitzak aplikatzeko adibide argigarri gisa, behin betiko ML–MME algoritmoak aplikatu ziren RCP8.5 emisio–agertokiko klima–proiekzioetan.

Deskribatutako 1., 2., 3. eta 4. urratsetan proposatutako metodologiak datuen analisi–prozesu tipikoen eskema jarraitzen du (Berthold et al., 2010), 3.1 irudian aurkeztua. Metodologia hautaketa–prozesu berezi batekin hasten da. Prozesu horren helburua da zarata eragiten duten ezaugarriak (RCMak) ezabatzea datasetetik, horrela iragarpen–eredu egonkor eta fidagarri baten garapena bermatzeko. Horrek esan nahi du, RCM rankinga egin behar dela eta ondoren *filter–busper* teknika bat aplikatu behar dela ezaugarri egokienak identifikatzeko. RCM optimoak hautatzean, hainbat ML modelo sortzen dira haien hiperparametroak optimizatuz, baliozkotze gurutzatuaren bidez. Ondoren, tmax, tmin eta pr MMEak sortzen dira garatutako ML algoritmoak erabiliz. MME hauei errendimendu estatistikoaren ebaluazioa egin zitzaien.

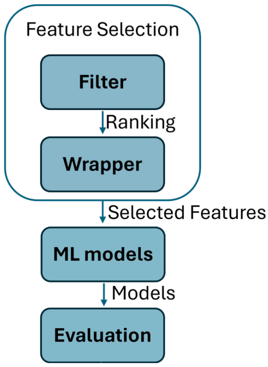

3.1 IRUDIA: 3. kapituluan egindako lanean jarraitutako datuen analisi–prozesuaren faseen eskema.

3.3.1 RCMen sailkapena

Datuen analisiaren barruan, lehenengo faseetako bat datuen aurretiazko tratamendua da. Adibide honetan, ezaugarrien aukeraketa bat aplikatu zen RCM rankinga sortzeko eta iragarpen–eredu fidagarri bat lortzeko informazio garrantzitsuena zutenak aukeratzeko. Erabilitako prozedura *filter–wrapper* prozezua da, eta bi zati ditu: iragazki–zatia (filter) eta bilgarri–zatia (wrapper). Hasiera batean, sailkapen bat sortu zen neurri kuantitatibo bat erabiliz (filter), eta, ondoren, garrantzitsuenak hautatu ziren (wrapper, 3.3 atala). Honela, RCMak beren errendimenduaren arabera sailkatzeko prozedura hau aplikatu zen, behaketa–datuetan oinarrituta: pr, tmax eta tmin denbora–serieak aztertutako eremuko klima atlantikoaren adierazgarri diren lau urtaroetan banatu ziren, hau da, negua (DJF), udaberria (MAM), uda (JJA) eta udazkena (SON). Aldagai eta urtaro bakoitzerako TSS (Taylor Skill Score,Taylor (2001)) metrika kalkulatu zen (filter–indizea). TSSak RCM bakoitzak pr, tmax eta tmin aldagaiak simulatzeko duen gaitasunaren neurri kuantitatibo bat ematen du. Klima–aldagai jakin baten behaketekiko RCMen desbideratze estandarraren korrelazioan eta proportzioan oinarritzen da:

$$\mathrm{TSS} = \frac{4(1+R)^4}{(\sigma_f + 1/\sigma_f)^2 (1+R_0)^4}\,, \tag{3.1}$$

non σ_f RCMen eta behaketen arteko desbideratze estandarra den, r Pearsonen korrelazio–koefizienteari den eta R_0 korrelazioaren balio maximoa adierazten duen, hau da, 1. TSS 0 eta 1 artekoa da. Balio handiago batek simulazio errendimendu hobea adierazten du, eta balio txikiago batek, berriz, errendimendu okerragoa. TSSren emaitzetan oinarrituta, 12 sailkapen lortu ziren, bat aldagai eta urtaro bakoitzeko, eta horiek kontuan hartu ziren RM (Ahmed et al., 2020) metrika kalkulatzeko.:

$$\mathrm{RM} = 1 - \frac{1}{nm} \sum_{i=1}^{n} \mathrm{rank}_i \ , \tag{3.2}$$

non n eta m RCM eta urtaro kopurua adierazten duten, hurrenez hurren, eta $rank_i$, berriz, i^{th} denboraldiko kideari dagokion rankingaren zenbakiari dagokion. Azkenik, RCMko kideak RMren arabera ordenatu ziren. Horri esker, RCM ereduen rankinga lortu dugu, hoberenetik txarrenera ordenatuta, aztertutako arroko behaketa–datuei dagokienez duten errendimenduaren arabera.

3.3.2 SEM eta ML–MME algoritmoen garapena

RCMen rankinga garatu ondoren, MMEren egitura eta ezaugarriak diseinatu dira. Lehenik eta behin, ML–MME algoritmoak formulatzean, funtsezkoa da aldagaien urtaroko dinamika kontuan hartzea. Kontsiderazio honek algoritmoek aldagarritasun ereduak bereizteko duten gaitasuna indartzen du. Urte barneko tenperaturaren dinamika nabaria dela eta, latitude erdiko eskualdean, urtaroak modu independentean kontsideratzea erabaki dugu, zehazki tmin eta tmax, ML–MME algoritmoak eraikitzean (Morales-García et al., 2023; Ahmed et al., 2020). Beste alde batetik, prezipitazioarekin, estrategia alternatibo bati ekin diogu: aldagai horren konplexutasuna eta azken hamarkadetan Europako latitude ertainetan (Christidis and Stott, 2022; Paluš et al., 2005) urteko zikloan ikusitako aldaketak kontuan hartuta, urtaro–eredu argiak ezartzea zeregin korapilatsuagoa da. Urtaroetan soilik oinarritutako ML algoritmoak diseinatzea planteamendu okerra da, algoritmoek aldagaiaren portaera zehatz atzematea oztopatuz.

Datuen konplexutasun eta desoreka horri aurre egiteko, hileko prezipitazio–gertaerak kontuan hartzea erabaki dugu, bi azpitaldetan sailkatuz Chao et al. (2018): behaketa–datuen arabera 80 th pertzentiltik gorakoak eta haren azpitik daudenak. Prezipitazioa bi datu–base ezberdinetan bereiziz, aldagaiaren aldakortasuna murriztu zen, ML modeloek lortutako emaitzetan zehaztasun handiagoa lortuz. Oinarri horri jarraituz, ML–MME teknika bakoitzak lau algoritmo sortu ditu tmax eta tmin kasuetarako, urtaro bakoitzari dagozkionak. Gainera, bi algoritmo sortu dira prezipitaziorako: bata 0–80 tarteko gertaeretarako eta bestea

80-100 tarteko gertaeretarako.

Metodo ezberdinak erabili ziren MME hileroko eskalan eraikitzeko, alde batetik SEM, eta bestetik hiru ML teknika: RF, GB eta LR. MME garatzeko lehen teknika SEM da, normalean eta oso erabilia MME kalkulatzeko (Clark, 2017). Gainerako hiru teknikak landuagoak dira eta ML erregresio ereduetan oinarritzen dira. Hiru teknika hauek jarraian zehazten dira:

- Random Forest (RF). RF makina bidezko ikasketa teknika bat da, eta bere oinarria zuhaitz iragarleen konbinazio bat da, halako moldez non zuhaitz bakoitza modu independentean eta banaketa berdinarekin probatutako ausazko bektore baten balioen mende baitago. Zuhaitz–bilketaren funtsezko eraldaketa bat da, korrelaziorik gabeko zuhaitz–multzo handi bat eraiki eta gero haien batez bestekoa egiten duena. Baso ausazko bat sortzeko algoritmoaBreiman (2001) -k garatu zuen. Datu–multzo zaratatsu baten barruan bariantza murrizteko erabili ohi den multzoa ikasteko metodoa da. RF metodoak aldakuntza kontrolatua duten erabaki–zuhaitzen bilduma bat eraikitzeko hautespena ausaz egozteko eta *"bagging"* ideia konbinatzen du. Atributuen azpimultzo ausazko baten hautaketa, ausazko subespazioaren metodoaren adibide bat da, diskriminazio estokastikoa egiteko modu bat (Breiman, 2001).

- Gradient Boosting (GB). GB makina bidezko ikaskuntza teknika bat da, erregresio analisian eta sailkapen estatistikoan oinarritutako teknika. *"Boosting"* teknika zenbait sailkapengile ahulen emaitzak konbinatzean datza, sailkatzaile sendo bat lortzeko. Sailkatzaile ahul hauei gehitzen direnean, euren iragarpenen zehaztasunaren arabera pisu ezberdinak esleitzen zaizkie. Sailkapengile ahul bat gehitu ondoren, datuak pisuaren egitura aldatzen du: gaizki sailkatutako kasuek pisua irabazten dute eta zuzen sailkatutakoek pisua galtzen dute. Horrela, sailkapengile indartsuek indar handiagoz erreparatzen diete sailkapengile ahulek gaizki sailkatutako kasuei. GB teknikak iragarpen–eredu bat sortzen du, iragarpen ahuleko ereduetan oinarritua, normalean zuhaitz erabakigarrietan oinarritua. GB iragarpen eredu multzo bat eskaintzen duen multzo bat da, iragarpen egoki bat ondorioztatzen duena, kasu batzuetan RF teknikaren emaitzak gaindituz (Bentéjac et al., 2021).

- Linear Regression (LR). LR gainbegiratuko ikaskuntza algoritmo bat da, makinen ikaskuntzan eta estatistikan erabiltzen dena. Bere bertsiorik sinpleenean, datu multzo jarraitu baten joera adieraziko duen lerro bat kalkulatzen du. LR aldagai eskalako dependente baten eta aldagai esplikatzaile baten edo gehiagoren arteko erlazioa eredutzat har daiteke. LR teknikak errore koadratikoaren funtzio baten kostua minimizatu behar du, eta koefiziente horiek lerro optimoarekin bat etorriko dira. Hainbat metodo daude kostua murrizteko. Ohikoena bertsio bektoriala eta ekuazio normala erabiltzea da, emaitza zuzena emango duena. (Weisberg, 2005).

Machine–Learning tekniken hiperparametroak hautatzeko, sareta bat erabili da, balidazio gurutzatuaren bidez, parametro guztiak arakatzeko eta, horrela, onenak hautatzeko.

3.3.3 RCMen hautaketa

RCM rankinga amaitu eta MMEren ezaugarriak zehaztu ondoren, aldagai bakoitzerako (tmax, tmin eta pr) MMEak sortzean kontuan hartu beharreko RCM kopuru onena hautatzeko prozesuari ekin zitzaion. Prozesu hau 3.1 Irudian aurkezten den wrapper–prozesuaren zatia da. MMEak RM-n oinarritutako RCM rankinga 1etik 40ra kontuan hartuta garatu ziren (5.1. taula). Hasiera batean, rankingan 1 postuko RCMa bakarrik erabili zen MMEri sarrerak emateko. Ondoren, 2. postuko RCMak gehitu ziren, eta ondoren RCMen sarrera inkrementala 3, 4, 5... 40 postuekin garatu zen. Metodo hau, top–ranked approach delakoa (Ahmed et al., 2020), errendimendu handieneko RCMrekin hasi zen (1. postua) eta ondorengo RCMekin egin zuen aurrera, euren RM-ko rankingaren goranzko ordenan.

MMEko irteeren errendimenduaren ebaluazioa, RCM kopuru aldakorrekin sortua, berreraikitako denbora–seriean egin da. MMEk lortutako emaitzen berreraikitze hau 3.2. atalean deskribatutako urtaroetan (tmax, tmin) edo pertzentil tarteetan (pr) banatutako datuak denbora–serie bihurtuz egin da.

Ebaluazio metrika Akordioaren Indize Aldatua izan zen (*md* ,(3.3)), Sen (1968)-k proposatua eta ondoren (Ahmed et al., 2020) asko aplikatu dena. 0 eta 1 artekoa da, eta eredua hobeto egokitzen denean balio altuagoak aurkezten ditu.

$$md = 1 - \frac{\sum_{i=1}^{n} (x_{\text{obs},i} - x_{\text{sim},i})^j}{\sum_{i=1}^{n} (|x_{\text{sim},i} - \bar{x}_{\text{obs}}| + |x_{\text{obs},i} - \bar{x}_{\text{obs}}|)^j} \,, \tag{3.3}$$

non $x_{\text{sim},i}$ eta $x_{\text{obs},i}$ i. data puntua diren simulatutako eta behatutako klima aldagaiko datu–seriean, hurrrenez hurren. Kalkulua sareko lau puntuetan aplikatu da.

Prozedura honi jarraituz RCM guztiak MMEn sartzen dira. Ondoren, ebaketa–puntua RCMetan egiten da, *md* metrikak okertzen hasten denean edo *overfitting* arazo bat behatzen denean. Horrek adierazten du RCM horretatik aurrera beste RCMek ematen duten informazioa zaratatsua dela onuragarria baino gehiago.

3.3.4 SEM eta ML–MME algoritmoen ebaluazioa

Hautaketa fasea amaitu eta behin betiko MMEak eraiki ondoren, ebaluazioa egin zen. Datuak entrenamendu (*training*) eta proba (*testing*) faseetan banatu ziren, datuen % 80 eta % 20 hurrenez hurren, kronologikoki banatuta. Beraz, entrenamendu–faseak 1980-2006 aldia hartu zuen, eta proba–faseak, berriz, 2007-2015 aldia. Bereziki, sare–espazialeko lau gelaxketako datuak sartu dira algoritmoak elikatzeko. Gainera, ebaluazioa denbora–serieen antzekotasunen karakterizazioan erabili ohi diren hiru metrika gehigarrirekin egin zen: determinazio–koefizientea (R^2), bataz besteko errore koadratikoa (RMSE), eta erroaren batez besteko portzentajezko errorea (RMSEPE).

3.3.5 ML–MME datuak Temezen eredu hidrologikoan aplikazioa

Temez eredua (Témez, 1977), Espainiako arro hidrografiko askotan aplikatu izan da (Pérez-Sánchez et al., 2019; Escriva-Bou et al., 2017; Chavez-Jimenez et al., 2013; García-Barrón et al., 2015; Jódar et al., 2017; Marcos-Garcia et al., 2017; Senent-Aparicio et al., 2018b) eta arroen simulazio–eredu agregatuen kategorian sartzen da (Estrela, 1992). Euriteak hasten direnetik ibaietara isurketa hasi arte, Temez ereduak sistema hidrologiko baten barruan interkonektatutako prozesuen bidez kudeatzen ditu hezetasun–balantzeak. Temez eredurako sarrera–aldagaiek hileko batez besteko prezipitazio espaziala arro osorako eta Evapotranspirazio potentziala (ETP) barne hartzen dituzte. Kapitulu honek duen hileko datu klimatikoetan duen fokuaren ildoa jarraituz, ETP Thornthwaite metodoa erabiliz zehaztu zen (Thornthwaite, 1948).

Eredu hidrologikoaren emaitzak ikerketa hidrologikoan onartutako lau ebaluazio irizpideren arabera ebaluatu genituen (Jimeno-Sáez et al., 2018). Irizpide horien artean Nash–Sutcliffe Efficiency koefizientea (NSE), ehuneko alborapena (PBIAS), Pearson korrelazio–koefizientea (r) eta Kling–Gupta Efficiency koefizientea (KGE) daude.

Proposatutako lau ML–MME teknikak ebaluatu ondoren, algoritmoak RCP8.5 emisio–agertokirako etorkizuneko klima–proiekzioei aplikatu zitzaizkien epe luzera, eta etorkizuneko ibaiaren ur–emaria simulatzeko sarrera–datu gisa erabili ziren.

3.4 Emaitzak eta eztabaida

3.4.1 RCMren sailkapena

C.1 taulak RCM sailkapenak aurkezten ditu TSSen arabera DJF, MAM, JJA eta SON urtaroetan zehar tmin, tmax eta pr aldagaietarako. Azpimarratzekoa da urtaroen eta aldagaien artean aldakortasun nabarmenak sortzen direla. Zenbait kasutan, RCM bat nabarmentzen da aldagai bat urtaro batean simulatzerakoan bikain egiten duelako, eta RCM berak, alidz, beste aldagai bat beste urtaro batean simulatzerakoan sailkapenaren beheko muturrean aurkitzen da. Kasu zehatz bat IPSL-RCA4 da (33 kodea), SON eta JJAn prezipitazioa simulatzeko sailkapenaren goiko postuetan dagoena, baita tenperatura maximoa SONen simulatzerakoan ere. Hala ere, eraginkortasun eza erakusten du RCMko beste kide batzuekin alderatuta DJF eta MAM -ko prezipitazioak simulatzean (Kotlarski et al., 2014).

Oharpen nabarmen bat GCM gidariaren ekarpen handia da sailkapen–postuan, eta hori bat dator Vautard et al. (2021) -k dioenarekin, zeinak aldagai batzuk GCMek zehaztutako eskala handiko muga–baldintzek baldintzatzen dituztela ezarri baitzuen. Adibidez, MPI-ESM–LR GCMk bultzatzen duten RCM kideek, koherentziaz lortzen dituzte RM balio altuenak (C.1. taula), errendimendu orokor handiagoa adieraziz. Hau Brands et al. (2013)ren aurkikuntzekin lerrokatzen da, GCM honek Europako latitude ertainetan prezipitazioa simulatzeko duen gaitasun bikaina azpimarratuz. RCMren errendimendu txar batek, ordea, simulazioan ere eragin nabarmena izan dezake, MPI gidari izan arren sailkapenean postu eskasak dituzten 60 eta 48 modeloen kasuan bezala. Era berean, CNRM–CM5 gidaria duten RCMak ere goi mailakoak dira, tenperatura (McSweeney et al., 2015) behar bezala ezaugarritzeko gai direlako. Alderantziz, baldintza klimatikoen simulazioan gabeziak dituen

GCM batek eragin negatiboa du RCMren rankingean. Horren adibide, MOHC–HadGEM2 GCM -a da, zeinak alborapen handiak erakusten baititu klima–aldagaien irudikapenean. Ondorioz, MOHC–HadGEM2k gidari gisa duten RCMak beheragoko posizioak lortzen dituzte aldagai eta urtaro guztietan.

3.4.2 RCMen kopuru optimoaren hautaketa

ML–MMEren ikasketa–kurbaren azterketa egin genuen, analisi sakonagoetan kontuan hartu beharreko RCM kopuru optimoa zehazteko. Lehen deskribatutako Machine–Learning teknika guztiak kontsideratu dira RCM kopurua hautatzeko.

3.2 irudian adierazten den bezala, behaketak oinarri hartuta kalkulatutako *md*balioak, SEM eta ML–MMEak eraikitzeko erabilitako RCM kopuruaren kontra irudikatu dira. RCMak sartzeko ordena *top–ranked approach*-a jarraitzen du (Ahmed et al., 2020). Nabarmentzekoa da hiru RCM baino gutxiago kontuan hartzerakoan, *md* balioek igoera nabarmena izan dutela hasieran, eta hortik aurrera joera asintotikoa egonkortzen dela ML teknika, aldagai eta aldi guztietan. Salbuespen bat ikusten da GBrekin, non, RCM kopuru jakin batetik haratago (pr 16, tmax 35 eta tmin 25), *md* balioak 1 baliora hurbiltzen diren. Honek *overfitting*-a adierazten du (Ying, 2019; Dietterich, 1995).

Aldagai indibidualak hurbilagotik aztertzerakoan, prezipitaziorako SEM eta ML–MMEren emaitzek ezberdintasun handiak dituztela nabarmentzen da. SEMek 0,4 *md* inguruko balioak erregistratzen ditu, eta ML–MME teknikek, berriz, 0,6 eta 0,8 arteko balioak ematen dituzte (GBren *overfitting* kasua alde batera utzita). Tenperatura–aldagaiei dagokienez, hasierako *md* handiagoa da, 0,6 gutxi gorabehera, eta horrek adierazten du RCMek gaitasun handiagoa dutela hileko tenperatura–dinamikak errepikatzeko, prezipitazioekin alderatuta. Horren arrazoi nagusia prezipitazio dinamikari datxekion konplexutasun handiagoa da, zeinak erronkak planteatzen baititu zenbakizko ereduek aldagaiaren dinamikak zehatz–mehatz simulatzeko (Perkins et al., 2007; Aghakhani Afshar et al., 2017). Simulazio–muga hauek RCMetan ere aurkitzen dira (Vautard et al., 2021; Herrera et al., 2020; Kotlarski et al., 2014). Tenperatura–aldagaietan ML–MMErekin hobekuntzak ikusten diren arren, *md* balioen kontrastea ez da hain nabarmena prezipitazioarekin alderatzen badugu, batez ere tenperatura minimoari dagokionez.

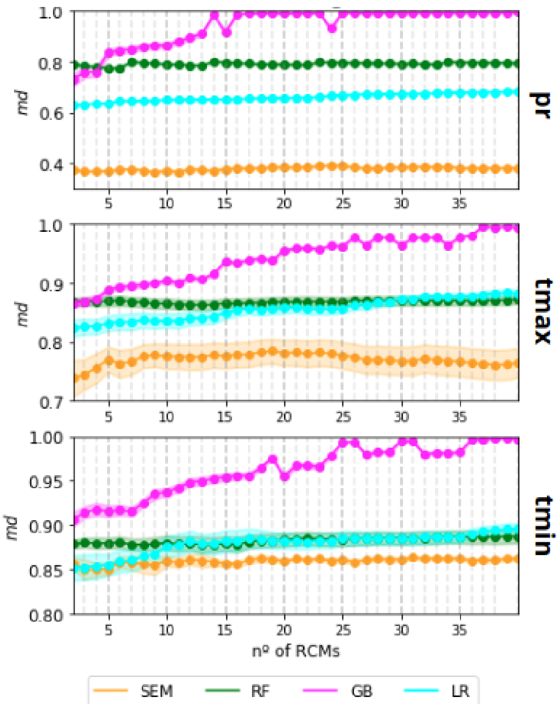

3.2 IRUDIA: *md* vs. RCM kopurua prezipitaziorako (pr), tenperaturara maximorako (tmax) eta tenperaturara minimorako (tmin). Eremu itzaltsuak sare–espazialeko lau gelaxken desbideratze estandarra adierazten du.

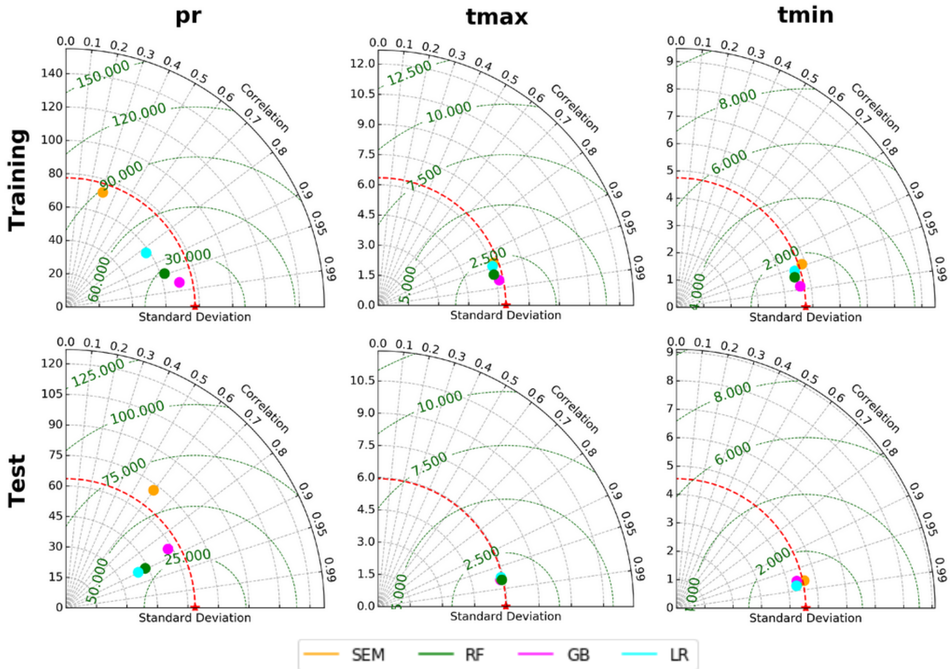

3.3 IRUDIA: Prezipitazio (pr), tenperatura maximoa (tmax) eta tenperatura minimoa (tmin) aldagaien batez besteko espazialaren Taylor diagramak entrenamendu–adirako (1980–2006) eta proba–aldirako (2007–2015).

RCM kopuruari buruzko hobekuntzen eboluzioa aztertu ondoren, eta hasierako aurreratzearen ondoren geldialdi fase bat behatu ondoren, guztira zazpi RCM sartzea erabaki genuen. Erabaki hau, gainera, *overfitting* kasuak saihesteko aplikatu zen, GBn tmin aldagaiaren kasuan konkretuki. Aldi berean, ereduaren konplexutasunaren eta errendimendu prediktiboaren arteko oreka mantentzeko xedearekin aurrera eraman da. Erabilitako ereduen kopurua bat dator Dey et al. (2022)-ren aurkikuntzekin, zeinek, hautaketa aurreko prozesu baten ondoren, 5 eredu sartu zituzten euren analisian. Era berean, Ahmed et al. (2020) -k emaitza alderagarriak lortu zituen prezipitazioen analisian, errendimendu handia erakusten duten 7-10 ereduek sortutako datuen arabera.

3.4.3 SEM eta ML–MMEen ebaluazioa

3.3, 3.4 eta3.5 Irudiek SEM eta ML–MME emaitzen ebaluazioa eskaintzen dute pr, tmax eta tmin aldagaietarako CLIMPY behaketak oinarri hartuta.

Emaitzen argitasuna bermatzeko, batez besteko espazialaren ebaluazioan zentratu ginen. Azpimarratzekoa da 3.3 irudiko lehen zutabean Taylorren diagramak, bai entrenamendu– eta bai proba–aldietan prezipitazioari dagokionez, ML–MME aplikatzetik eratorritako hobekuntza nabarmenak adierazten dituela SEMekin alderatuta. ML–MME metodoen artean, RF eta LR metodoek emaitza alderagarriak erakusten dituzte, eta GBk, berriz, emaitzarik onenak lortzen ditu urteko eskalan, bai entrenamendu, bai proba–aldietarako.

Tenperaturen batez besteko espazialari dagokionez, Taylorren diagramek ez dute hobekuntza nabarmenik erakusten. Bai tmin eta bai tmax-en SEMek dagoeneko erakusten dute azterketa–eremuko hileko tenperaturen irudikapen bikaina, neurri estatistikoen arabera. Hori azaltzeko kontuan hartu beharrekoa da hautatutako RCMak kalitate handiko simulazioak direla (C.1. taula). Ondorioz, RCMren simulazioaren kalitatearen abiapuntu apartak muga dezake ML–MMEk eskain lezakeen hobetzeko ahalmen potentziala.

Prezipitazioen errendimendua zehatzago aztertzeko, 3.4 Irudiak SEM eta ML–MMEren batez besteko emaitza espazialen serieak aurkezten ditu hilero. ML–MME guztiek SEMekin alderatuta izan duten hobekuntza nabaria da. SEMek zero inguruko R^2-a, RMSE altua eta 0,5etik beherako *md*-a erakutsi zuen bi aldietan. ML–MME teknika guztiek, aldiz, errendimendu nabarmen hobetua erakusten dute, hileroko prezipitazio ereduak simulatzeko gaitasun handiagoa dutela adieraziz. Nabarmentzekoa da GBk lortu dituela emaitzarik onenak *md*, 0,88 eta 0,75eko balioekin, hurrenez hurren, entrenamendu eta proba aldietarako. RF, ordea, ez dago oso atzean, R^2 = 0,80ko balioak erregistratuz proba aldirako, GBren 0,75 baino gehiago. Nahiz eta LRk RMSE balio handiagoak erakutsi (44 mm/hilabete inguru) eta prezipitazio minimoak eta maximoak detektatzeko gaitasun txikiagoa izan, LRn oinarritutako ML–MMEak, nabarmen hobetzen du azterketa–eremuaren prezipitazioaren irudikapena SEMekin alderatuta. Emaitza horiek bat datoz zenbait ikerketetan lortutakoekin (Acharya et al., 2014; Salman et al., 2018; Li et al., 2021). Adibidez, Dey et al. (2022) ML-n oinarritutako MMEren metodoak garatu ziren CMIP6rako Indiako ibaiaren arro batean, RF-n oinarritutako ML–MMEk errendimendu hobea erakutsi zuela SEMekin alderatuta. Ildo beretik, Jose et al. (2022) -k RF proposatu zuen Indiaren gaineko ML eredurik egokiena MME sortzeko eta antzemandako aldagai klimatikoak simulatzeko, ibai tropikalen arro batean. Arroen eskaletan egindako ikerketez gain, eskala espazial zabalagoetan ere aplikatu dira ML–MME hurbilketak. Hori da Wang et al. (2018) SEM, BMA (Bayesian Model Averaging teknika), RF, eta SVM aplikatu

3.4 IRUDIA: Spatially averaged observed precipitation and simulated precipitation time series and evaluation metrics (SEM and ML–MME) for the training (1980–2006) and test (2007–2015) periods. Batez besteko prezipitazio behatua eta prezipitazio simulatuaren denbora–serieak eta ebaluazio–metrikak (SEM eta ML–MME) entrenamendu–aldietarako (1980–2006) eta proba–aldietarako (2007–2015).

lituztenen kasua CMIP5 datuekin Australia eskualdean, ondorioztatuz RF eta SVMk emaitza hobeak izan zitzaketela SEM eta BMArekin alderatuta.

3.5 irudiak SEM, ML–MME eta banakako zazpi RCMen ebaluazio zehatza eskaintzen du, bai urteko eskalan, bai urtarokoan. Aipagarria da SEMa ML–MME teknikekin alderatzean, hobekuntza orokortu bat ikusten dela, batez ere prezipitaziorako. Adibidez, DJF urtaroan, RCM indibidualentzako *md* balio baxuenak erregistratzen dituenak (0,2 inguru), hobekuntza nabarmena ikusten du ML–MME teknikekin, RF eta LRren kasuan *md* -a 0,55era igoz, eta GBren kasuan 0,70tik gora. Hobekuntza hori koherentea da urtaro guztietan, eta mantentzen da urteko datuetarako ere. Era berean, R^2eta RMSEk hobekuntza nabarmenak dituzte. R^2koefizientea, RCM eta urtaro jakin batzuetarako batzuetan 0ra jaisten dena, orain, modu koherentean, 0,6tik gora mantentzen da urtaro guztietan eta ML–MME tekniketan, 0,8ko urteko balioetara iritsiz. RMSEPE, zatiki gisa adierazia, zenbait RCM indibidualetan 3 baino gehiago dena, ML–MME kasu guztietan 1etik behera dago. Prezipitazioen karakterizazioan izandako hobekuntza nabarmen eta esanguratsu horrek, bai urtaroari dagokionez, bai urteko eskalari dagokionez, aztertutako eskualdean aztertutako hiru metrikek erakusten dutenez, abantaila kualitatibo esanguratsua ematen du ML–MMEk, RCMko kide indibidualetatik lortutako emaitzekin alderatuta. Hobekuntza horrek, onura garrantzitsuak ekar ditzake lurralde–antolamenduan, uraren eta nekazaritzaren kudeaketan eta klima–arriskurako prestakuntzan, besteak beste.

Tenperaturari dagokionez, nahiz eta urtaroen hobekuntza nabarmenik ez izan R^2 eta *md* -etan, urteko balioek gora egiten dute bai tmax eta bai tmin aldagaietarako. Hala ere, simulazioaren kalitatearen hobekuntza, urtaroen eskalan ere, RMSEren balioen beherakada gisa agertzen da. RCM indibidualek 2,0 $C°$ eta 5,2 $C°$arteko RMSE balioak erakusten dituzte tmax aldagaiarentzako. ML–MME teknikak aplikatu ondoren, RMSEa izugarri murrizten da, 0,8 $C°$ eta 3 $C°$ arteko balioekin. Jokabide paralelo bat ikusten da tmin-entzat. Tenperaturaren adierazpenaren hobekuntza horrek interes berezia du aztertutako azterketa–eremu moduko leku batean, non elurraren eta elurraren urtze–prozesuak faktore giltzarriak diren tenperatura dinamikak definitzerako orduan, eragin handia izanez eskualdearen kudeaketan.

Aztertutako kasu bakoitzean, MMEk modu koherentean gainditzen ditu banakako kideen simulazioak, baita eraginkortasun txikieneko MMEk, SEMek, kontuan hartzen dituenean ere. Behaketa hau MMEk banakako errendimendua hobetzeko eta klima–datuen ziurgabetasuna

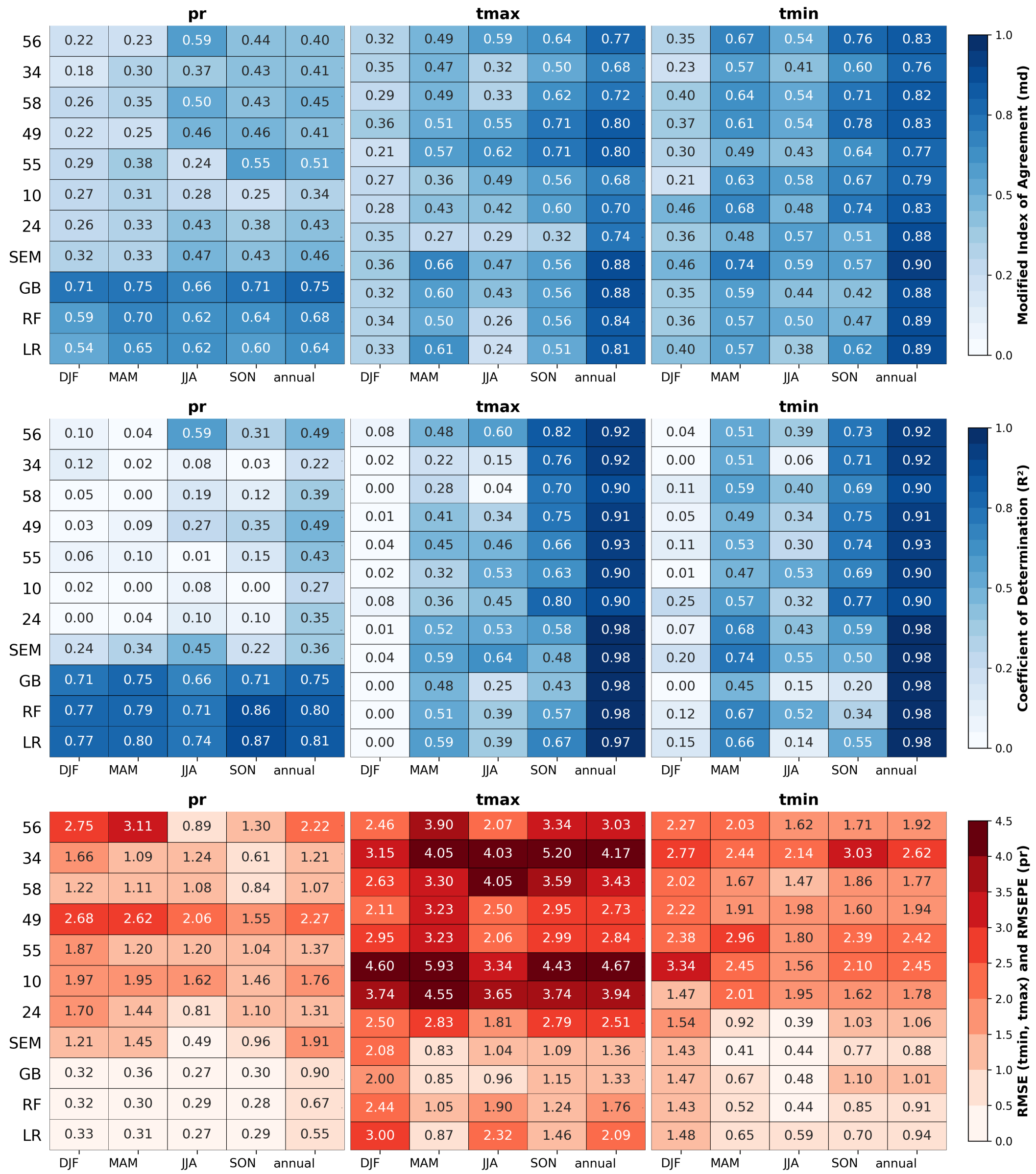

3.5 IRUDIA: *md* , R^2, RMSE (tmax, tmin) eta RMSEPE (pr) metrikak erakusten dituzten bero–mapak, behaketen konparaziotik lortuak, SEM, ML–MME eta RCM indibidualentzako, proba–aldian (2007–2015).

murrizteko duen gaitasuna azpimarratzen duten ikerketa askoetako ondorioekin bat egiten du. Analisi aipagarrienak India (Gusain et al., 2019), USA(Srivastava et al., 2020), Txina (Zhuang et al., 2016) eta

Europa (Evin et al., 2021) bezalako eskualdetan garatu dira. Gainera, gure emaitzek adierazten dute ML–MMEk SEMek baino errendimendu handiagoa duela, batez ere prezipitazioaren kasuan, 3.4 eta3.5 irudietan adierazten den bezala. Aurkikuntza honek ML–MMEren garrantzia azpimarratzen du arro–eskalan. ML–MMEk SEMarekin alderatuz duen errendimendu hobeagoa ML metodoei egotzi ahal zaie; metodo horiek eredu klimatikoaren irteeren eta behatzeko dataseten arteko korrelazio ez–linealak eta dimentsio handikoak jorratzeko gaitasunari hain zuzen (Dey et al., 2022). Gainera, Li et al. (2021) k nabarmentzen duen bezala, ML–MME algoritmoek informazio zehatza harrapatu ahal izango lukete eskala lokaletan, ML–MME algoritmoen eraikuntzari buruzko bereizmen handiko behaketak erantsita.

Ikerketa honetan, arrakastaz integratzen ditugu EURO–CORDEX RCMak, azterketa–eremurako bereizmen espazial handiena duten simulazio klimatikoak, ML algoritmo matematikoen indarguneekin. Konbinazio honek etorkizun handia izan ditzake eskala baxuko proiekzio klimatikoetan ziurgabetasuna murrizteko. Hurrengo atalean (3.4.4 atala), ML–MME algoritmoen irteerak erabiltzen ditugu Esca ibaiaren arroan eredu hidrologiko bat elikatzeko.

3.4.4 SEM eta ML–MME datu klimatikoen aplikazioa Temez eredu hidrologikoan

3.4.4.1 Temez ereduaren konfigurazioa

Eredu hidrologikoa konfiguratzeko, simulazio–aldia bi fasetan banatu zen: kalibrazio–aldia, 1981etik 2000ra artekoa, eta ondorengo baliozkotze–aldia, 2001etik 2014ra bitartekoa. Beroketa urte bat ezarri zen Temez ereduan egoera egonkor bat lortzeko. Kalibrazioa lau parametro giltzarri doitzean oinarritu da: $H_{\max}$(lurzorua biltegiratzeko gehienezko gaitasuna) C(soberako abiadura–koefizientea) $I_{\max}$(infiltrazio maximoa) eta α(lurpeko uren ekarpen–koefizientea). Lehenengo bi parametroek lurzoruaren biltegiratzeari buruzko informazioa kontrolatzen dute, hirugarrenak lurrazaleko jariatzea eta lurpeko uren jariatzea bereizten ditu, eta laugarrenak lur azpiko drainatzea (Murillo and Navarro, 2011) modulatzen du. 3.1 Taulak, 3.4 atalean deskribatutako metrikak aurkezten ditu, simulazio hidrologikoaren ebaluazio integrala aurkeztuz.

According to what was established by Moriasi et al. (2007) and Brighenti et al. (2019), the performance of the model both in the calibration and validation period is satisfactory since the results of NSE and KGE

3.1 TAULA: Kalibrazioaren (1981–2000) eta balidazioaren (2001–2014) emaitzak Temez eredu hidrologikorako. Aurkeztutako estatistikak hauek dira: Nash–Sutcliffe Efficiency koefizientea (NSE), Pearson korrelazio koefizientea (r), Batez besteko errore koadratikoa (RMSE), Kling–Gupta Efficiency koefizientea (KGE) eta Ehuneko Alborapen koefizientea (PBIAS).

	NSE	r	RMSE	KGE	PBIAS
Kalibrazioa	0.63	0.85	13.27	0.78	-12.76
Balioztatzea	0.67	0.83	13.08	0.82	7.21

exceed 0.5 and the PBIAS reaches its maximum in the calibration period with -12.76 %, remaining below the ±25 %.

3.4.4.2 SEM eta ML–MME sarrerako datuetarako korronte–fluxuaren ebaluazioa

Temez eredu kalibratu eta balioztatutik abiatuta, ondoren deskribatutako simulazioak garatu dira klima datuen inpaktua ebaluatzeko. Datu horiek zehazki aztertu dira 4.3 atalean, ur–emariaren aldagaiaren karakterizazioan. Lehenik eta behin, hileroko emariaren simulazioa garatu da Temez eredua elikatuz prezipitazio behaketetako datuekin eta tmax eta tmin behaketetatik eratorritako ETParekin. Sarrera dato hauekin lortutako emaitzak $Q_{\text{sim-OBS}}$ gisa izendatu dira. Ildo beretik jarraituz, lau emari simulazio gehiago garatu ziren, ondoren $Q_{\text{sim-SEM}}$, $Q_{\text{sim-GB}}$, $Q_{\text{sim-LR}}$eta $Q_{\text{sim-RF}}$ gisa identifikatuak. Simulazio bakoitzean MME tekniketatik eratorritako sarrera datuak sartu ziren: SEM, GB, LR eta RF, hurrenez hurren. Azalpena errazteko, beste termino bat gehitu da simulatutako fluxuek osatutako taldeari erreferentzia egiten diona, ML–MMEtik eratorritako datu klimatikoak erabiliz: $Q_{\text{sim-ML-MME}}$.

3.2 taulak ML–MME algoritmoen entrenamendu-aldirako (1980–2006) eta proba–aldirako (2007–2015) deskribatutako simulazioen estatistikak aurkezten ditu. Aldi zehatz horiek aukeratzearen arrazoia azterlanaren helburuarekin bat dator, ML–MME tekniken bidez irudikapen klimatikoa hobetzeko eta hobekuntza horiek ur–emariaren karaketerizazioan zenbateraino eragiten duten ebaluatzeko xedea duena. Klima–aldagaien eta emariaren azterketa–aldiek bat etortzeak ikerketaren koherentzia hobetzen du. 3.2 taulan azaldutako estatistiken analisitik hurrengo puntuak ondorioztatzen dira: $Q_{\text{sim-SEM}}$k bi aldietarako emaitza desegokiak lortzen dituen bitartean, ML–MMEk fluxuaren irudikapena nabarmen hobetzea lortzen du. Azpimarratzekoak dira bai $Q_{\text{sim-RF}}$eta $Q_{\text{sim-GB}}$-ren estatistikak, zeintzuk $Q_{\text{sim-OBS}}$ emaitzen oso parekoak diren. Izan ere, NSE 0,60tik gora mantentzen da entrenamendu aldirako, eta $r$balioak 0,74tik gorakoak dira bi aldietan. $Q_{\text{sim-LR}}$simulazioak, ona bada ere, emaitza apalagoak ematen ditu PBIAS eta NSE eta KGE balio txikiagoekin. Emaitza horiek esan nahi dute ML–MMEk klima–aldagaiak irudikatzeko egiten dituen hobekuntzek ur–emariaren karakterizaziora hedatu egiten direla, azken hauek nabarmen hobetuz, bai entrenamendu–aldian, bai proba–aldian.

3.2 TAULA: Simulazioen vs. behaketen estatistikoak ur–emari aldagairako entrenamendu (1980–2006) eta proba (2007–2015) aldietarako. Aurkeztutako estatistikak hauek dira: Nash–Sutcliffe Efizientzia koefizientea (NSE), Pearson korrelazio–koefizientea (r), Batez besteko errore kuadratikoa (RMSE) eta Kling–Gupta Efizientzia koefizientea (KGE).

	Entrenamendu–aldia				Proba–aldia			
	NSE	r	RMSE	KGE	NSE	r	RMSE	KGE
$Q_{\text{sim-OBS}}$	0.67	0.85	12.55	0.81	0.60	0.82	15.00	0.78
$Q_{\text{sim-SEM}}$	-1.84	0.59	36.59	-0.27	-1.97	0.58	40.95	-0.36
$Q_{\text{sim-GB}}$	0.69	0.85	12.08	0.81	0.48	0.74	17.13	0.73
$Q_{\text{sim-LR}}$	0.56	0.77	14.48	0.69	0.52	0.74	16.42	0.61
$Q_{\text{sim-RF}}$	0.66	0.83	12.59	0.76	0.61	0.80	14.86	0.63

Simulazio hidrologikoen errendimenduaren ebaluazioan gehiago sakontzeko, urteko zikloa irudikatu dugu 3.5 Irudian hurrengo simulazioetarako: $Q_{\text{sim-ML–MME}}$ lau ML tekniketarako, gehi $Q_{\text{sim-OBS}}$eta Q_{OBS}. Azken honek behatutako emariei egiten dio erreferentzia. Ikusten denez, entrenamendu–aldian (1980–2006), ur–emariaren urteko zikloak bi maximo ditu urtarrilean eta maiatzean, eta minimo bat abuztuan eta irailean. Urte barneko dinamika hau Temez eredu kalibratu eta baliozkotuak erreproduzitzen du $Q_{\text{sim-OBS}}$ simulazioan ageri denez. $Q_{\text{sim-MME}}$-ri arreta jartzen badiogu, ikusiko dugu Q_{SEM}-k urteko zikloa ezaugarritzeko gai ez den bitartean, urteko fluxuaren gainestimazio orokor bat aurkeztuz, $Q_{\text{sim-MME}}$ -k Esca ibaiaren ziklo hidrologikoa zehatz–mehatz erreproduzitzen duela. Proba–aldiaren urteko zikloak (2007–2015) entrenamendu–aldiarekiko ezberdintasun batzuk aurkezten ditu, batez ere udaberriko maximoan, nabarmenagoa baita,60 hm² -ra helduz. Temez ereduak ($Q_{\text{sim-OBS}}$) zailtasun gehiago ditu aldi honetarako ziklo hidrologikoa simulatzeko, nahiz eta gutxi gorabehera ezaugarritzea

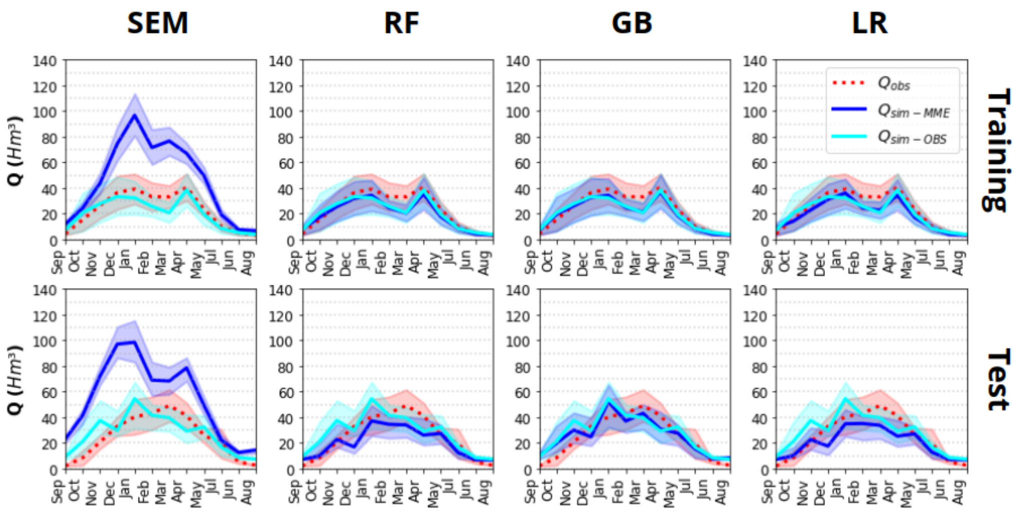

3.6 IRUDIA: Urteko ur–emariaren zikloa, entrenamendu (1980–2006) eta proba (2007–2015) aldietarako. Ur–emariaren behaketa datuetarako emaitzak erakusten dira (Q_{OBS}), hala nola Temez ereduaren bidez simulatutako ur–emaria CLIMPY-ko klima–behaketen sarrera–datuekin ($Q_{\text{sim-OBS}}$) eta Temez–simulatutako emaria SEM eta ML–MMEs-en sarrera–datuekin ($Q_{\text{sim-MME}}$). Itzalpeko eremuak streamflow emaitzen urteko aldakortasuna adierazten du.

lortzen duen. $Q_{\text{sim-ML–MME}}$simulazioek zehatz–mehatz erreproduzitzen dute $Q_{\text{sim-OBS}}$zikloa, batez ere $Q_{\text{sim-GB}}$. $Q_{\text{sim-SEM}}$k, ordea, errendimendu eskasa erakusten du. Funtsean, $Q_{\text{sim-ML–MME}}$k, $Q_{\text{sim-OBS}}$simulazioan atzematen den urte arteko dinamika erreproduzitzen dute, horrela frogatuz ML–MME tekniken aplikaziotik eratorritako irudikapen klimatikoan lortutako hobekuntzek eragin positiboa dutela ziklo hidrologikoaren karakterizazioan. Bestalde, garrantzitsua da nabarmentzea ur–emariaren behaketetatik (Q_{OBS}) eta simulazioetatik eratorritako desberdintasunak Temez modeloak emandako akatsei egozten zaizkiela, ziurrenik (Jimeno-Sáez et al., 2020) eredu hidrologikoak elur metaketa eta urtze prozesuak faltsutzearekin zerikusia dutenak.

3.4.5 Klima–aldagaien eta aldagai hidrologikoen etorkizuneko proiekzioak

Beraz, orain arte frogatu da ML–MME tekniken erabilerak aldagai klimatikoen irudikapena hobetzeaz gain, nabarmen hobetu duela azterketa–eremuko aldi historikoan karakterizazio hidrologikoaren zehaztasuna. Ildo berean, metodologia bera etorkizunerako RCP8.5 emisio–agertokirako aplikatzen badugu, ML–MME ereduen proiekzioek SEM-en datuak baino informazio errealistagoa eskain ditzakete (Liang et al., 2008).

3.7. irudiak aztertutako aldagaien — pr, tmax, tmin eta Q — urteko zikloak irudikatzen ditu, bi aldi ezberdinetarako: historikoa (1986–2015) eta epe luzerako etorkizuna (2065–2095). Irudi honek ML–MME tekniken simulazio datuak aldi historikoko behaketa datuekin alderatzen ditu. Analisi konparatiboak erakusten du ML–MME teknikek hobeto ezaugarritzen dituztela dinamika klimatikoak SEMekin alderatuta. Zehazki, SEMek DJF eta MAMen prezipitazioa gehiegi estimatzeko joera duen bitartean, ML–MMEk zehatzago atzematen ditu urte arteko dinamikak, apirilean eta azaroan bi maximo eta ekainetik abuztura arteko minimo bat agertzen direlarik (Lemus-Canovas et al., 2019). Era berean, ML–MME teknikek zehatzago erreplikatzen dituzte urte arteko tenperatura–aldaketak. Gainera, ML–MME teknikek modu positiboan eragiten dute Temez ereduaren duen ur–emariaren zikloaren urteko estimazioan. Izan ere, SEMez elikatutako simulazioek gainestimazio nabarmenak erakusten dituzte, 4.4 atalean aipatu den bezala. RF–MME, GB–MME eta LRMEk, berriz, errendimendu esanguratsuki handiagoa erakusten dute.

Emaitza horiek eta 4.3. eta 4.4. ataletan aztertutakoek adierazten dute ML–MME teknikek informazio errealistagoa ematen dutela SEMek baino, baita RCP8.5 emisio–agertokiaren proiekzioetarako ere. RF eta GB kontuan hartzen baditugu, ikusten dugu, proiekzio horien arabera, prezipitazioak behera egingo duela urtean zehar, DJF eta MAM izan ezik, urtaro hauetan prezipitazio kantitatea gora eginez, eta horrela urte arteko prezipitazio patroiak aldatuko dira. Aldi berean, tenperaturak modu orokorrean igotzea espero da (Amblar-Francés et al., 2020; Lemus-Canovas and Lopez-Bustins, 2021), tenperatura minimoen haskuntza handiak erregistratuz martxoan eta apirilean zehar. Litekeena da urte arteko dinamikan egindako aldaketa horiek ziklo hidrologikoa birmoldatzea, eta horrek udako minimo nabarmenagoak ekarriko ditu. Gainera, ur–emariaren kantitatea areagotu egingo da otsailean eta martxoan, RF eta GBk proiektatu bezala eta Pirinioetako hainbat ibaitan lortutako emaitzen ildotik (López-Moreno et al., 2014; García Ruiz et al., 2001; Stahl et al.,

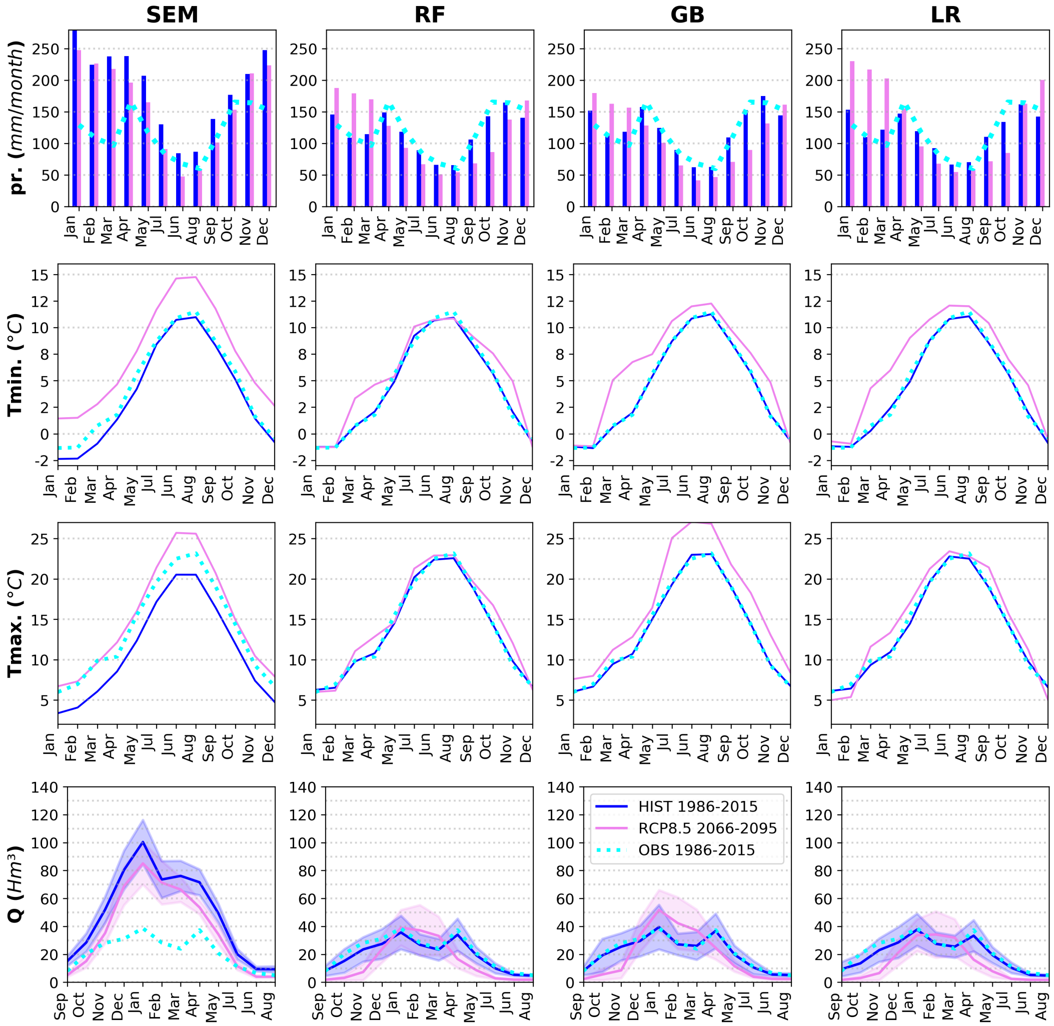

3.7 IRUDIA: pr, tmin, tmax eta Q aldagaien urteko zikloak, aldi historiko eta epe–luzeko etrokizuneko aldirako (RCP8.5), 1986–2015, 2066–2095, hurrenez hurren. Qaldagaiaren itzalpeko eremuak emaitzen urteko aldakortasuna adierazten du.

2010; Zabaleta et al., 2017; Boé et al., 2009; OPCC-CTP, 2018). Temez eredu hidrologikoaren sinpletasunak, hileroko eskalako analisiarekin batera, gure ondorioak informazio ikuspegietara mugatzen dituen arren, ML–MME teknikak eguneko–eskalako eredu hidrologiko konplexuagoetan integratzeko ahalmena ere nabarmentzen du, horrela, klima–aldaketaren testuinguruan baliabide zehatzagoak, plangintza eta egokitzapen estrategiak erraztu ditzaketen proiekzioak garatzeko bidea erraztuz.

3.5 Ondorioak eta konekzioak

Kapitulu honetan, Machine–Learning algoritmoak inplementatu genituen Eredu Anitzeko Multzoak (MME) garatzeko Esca ibaiaren arroaren barruan, Pirinioetako goi mendialdeko eskualdean. Planteamendu horrek **4. Helburua** betetzea ahalbidetzen du Machine Learningen oinarritutako teknika berriak aztertzen eta proposatzen dituelako, klima eta hidrologia ezaugarritzea hobetzeko. Gainera, 2. kapituluarekin batera, **2. Mugarria** betetzen laguntzen du, klima–aldaketa aurreikusteko dauden tresna iragarleen analisian sakontzen.

3. kapituluan egindako analisiaren bidez, RCMen sailkapen integrala garatu zen, aldagai eta urtaro indibidualetan zehar errendimenduan aldakortasun nabarmena azaleratuz, MPI-ek bultzatutako RCMek sailkapenean postu altuak lortuz. MMEren eraikuntzarako RCM kopuru onena zehazteko, *top–ranked approach*-ean oinarritutako prozedura aurrera eraman zen. Zazpi RCM hautatu ziren errendimendu–kurben analisia kontuan hartuz, behin betiko MMEak osatuz.

Hobekuntza nabarmenak ikusi ziren prezipitazioaren irudikapenean, bai urteko eskalan, bai urtarokoan, Machine–Learningean (ML) oinarritutako MMEetan. Tenperaturetan lortutako emaitzak ML-an oinarritutako MMEak erabiliz urtaroen eskalan finagoak badira ere, hobekuntza nabarmena ikusten da RMSEren urteko balioetan. Simulazio hidrologikoek, Random Forest, Linear Regression eta Gradient Boosting sistemetan oinarritutako aldagai klimatikoen MMESak erabiliz, klimaren behaketek elikatutakoen pareko emaitzak eman zituzten, SEM eta RCM bakarretan oinarritutako simulazioak nabarmen gaindituz. Gure emaitzek funtsezko bi aurkikuntza erakusten dituzte. Lehenik eta behin, azpimarratzen dute ikasketa automatikoko teknikek duten potentziala MMEak eraikitzean aldagai klimatikoen karakterizazioa hobetzeko. Bigarrenik, ML–MME horiek eredu hidrologikoen sarrera–datu gisa erabiltzearen abantailak nabarmentzen dituzte.

Gainera, gure metodologiak moldakortasun handia erakutsi zuen, RCP8.5 agertokiaren araberako proiekzio klimatikoei algoritmoak aplikatuz, metodo tradizionalak baino informazio errealistagoa eskainiz, eta, horrela, klima–irteeretan ziurgabetasuna murrizteko aukera emanez , klima–aldaketaren testuinguruan egokitzapena eta arro eskalako inpaktu–azterketak planifikatzeko. Ekarpen horrek garrantzi eta berritasun berezia du topografia konplexua ezaugarri duen eskualde batean, hala nola Pirinioetako goi mendialdeko eskualdean, non etorkizuneko aldaketak iragartzea zeregin konplexua izateaz gain, ezinbestekoa baita eskualdearen klima–aldaketara egokitzeko.

Bibliography

K.C. Abbaspour, M. Vejdani, and S. Haghighat. SWAT–CUP calibration and uncertainty programs for SWAT. *International Congress on Modelling and Simulation*, 43(3-8):1603–1609, 2007. doi: 10.13031/2013.3000.

Nachiketa Acharya, Nitin Anand Shrivastava, B. K. Panigrahi, and U. C. Mohanty. Development of an artificial neural network based multi-model ensemble to estimate the northeast monsoon rainfall over south peninsular India: An application of extreme learning machine. *Climate Dynamics*, 43(5-6):1303–1310, 2014. ISSN 14320894. doi: 10.1007/s00382-013-1942-2.

Jennifer C. Adam and Dennis P. Lettenmaier. Adjustment of global gridded precipitation for systematic bias. *Journal of Geophysical Research: Atmospheres*, 108(9):1–15, 2003. ISSN 01480227. doi: 10.1029/2002jd002499.

A. Aghakhani Afshar, Y. Hasanzadeh, A. A. Besalatpour, and M. Pourreza-Bilondi. Climate change forecasting in a mountainous data scarce watershed using CMIP5 models under representative concentration pathways. *Theoretical and Applied Climatology*, 129(1-2):683–699, jul 2017. ISSN 14344483. doi: 10.1007/s00704-016-1908-5.

Kamal Ahmed, D. A. Sachindra, Shamsuddin Shahid, Zafar Iqbal, Nadeem Nawaz, and Najeebullah Khan. Multi-model ensemble predictions of precipitation and temperature using machine learning algorithms. *Atmospheric Research*, 236(July 2019):104806, 2020. ISSN 01698095. doi: 10.1016/j.atmosres.2019.104806. URL `https://doi.org/10.1016/j.atmosres.2019.104806`.

María P. Amblar-Francés, Petra Ramos-Calzado, Jorge Sanchis-Lladó, Alfonso Hernanz-Lázaro, María C. Peral-García, Beatriz Navascués, Marta Dominguez-Alonso, María A. Pastor-Saavedra, and Ernesto Rodríguez-Camino. High resolution climate change projections for the Pyrenees region. *Advances in Science and Research*, 17:191–208, 2020. ISSN 1992-0628. doi: 10.5194/asr-17-191-2020.

Vazken Andréassian. Waters and forests: From historical controversy to scientific debate. *Journal of Hydrology*, 291(1-2):1–27, 2004. ISSN 00221694. doi: 10.1016/j.jhydrol.2003.12.015.

Mazdak Arabi, Rao S. Govindaraju, and Mohamed M. Hantush. A probabilistic approach for analysis of uncertainty in the evaluation of watershed management practices. *Journal of Hydrology*, 333(2-4):459–471, 2007. ISSN 00221694. doi: 10.1016/j.jhydrol.2006.09.012.

Nigel W. Arnell. The effect of climate change on hydrological regimes in Europe: A continental perspective. *Global Environmental Change*, 9(1): 5–23, 1999. ISSN 09593780. doi: 10.1016/S0959-3780(98)00015-6.

J. G. Arnold, D. N. Moriasi, P. W. Gassman, K. C. Abbaspour, M. J. White, R. Srinivasan, C. Santhi, R. D. Harmel, A. Van Griensven, M. W. Van Liew, N. Kannan, and M. K. Jha. SWAT: Model use, calibration, and validation. *Transactions of the ASABE*, 55(4):1491–1508, 2012. ISSN 21510032.

Celina Aznarez, Patricia Jimeno-Sáez, Adrián López-Ballesteros, Juan Pablo Pacheco, and Javier Senent-Aparicio. Analysing the impact of climate change on hydrological ecosystem services in laguna del sauce (Uruguay) using the swat model and remote sensing data. *Remote Sensing*, 13(10), 2021. ISSN 20724292. doi: 10.3390/rs13102014.

Leah A. Bêche, Eric P. McElravy, and Vincent H. Resh. Long-term seasonal variation in the biological traits of benthic-macroinvertebrates in two Mediterranean-climate streams in California, U.S.A. *Freshwater Biology*, 51(1):56–75, 2006. ISSN 00465070. doi: 10.1111/j.1365-2427.2005.01473.x.

Santiago Beguería, Juan Ignacio López-Moreno, Adrián Lorente, Manuel Seeger, and José M. García-Ruiz. Assessing the effect of climate oscillations and land-use changes on streamflow in the Central Spanish Pyrenees. *Ambio*, 32(4):283–286, 2003. ISSN 00447447. doi: 10.1579/0044-7447-32.4.283.

Martin Beniston. Climatic Change in Mountain Regions: A Review of Possible Impacts. *Climatic Change*, pages 5–31, 2003. doi: 10.1007/978-94-015-1252-7.

Candice Bentéjac, Anna Csörgő, and Gonzalo Martínez-Muñoz. A comparative analysis of gradient boosting algorithms. *Artificial Intelligence Review*, 54:1937–1967, 2021.

Michael R Berthold, Christian Borgelt, Frank Höppner, and Frank Klawonn. *Guide to intelligent data analysis: how to intelligently make sense of real data*. Springer Science & Business Media, 2010.

Fredrik Boberg, Peter Berg, Peter Thejll, William J. Gutowski, and Jens H. Christensen. Improved confidence in climate change projections of precipitation evaluated using daily statistics from the PRUDENCE ensemble. *Climate Dynamics*, 32(7-8):1097–1106, 2009. ISSN 09307575. doi: 10.1007/s00382-008-0446-y.

Fredrik Boberg, Peter Berg, Peter Thejll, William J. Gutowski, and Jens H. Christensen. Improved confidence in climate change projections of precipitation further evaluated using daily statistics from ENSEMBLES models. *Climate Dynamics*, 35(7):1509–1520, 2010. ISSN 09307575. doi: 10.1007/s00382-009-0683-8.

J. Boé, L. Terray, E. Martin, and F. Habets. Projected changes in components of the hydrological cycle in French river basins during the 21st century. *Water Resources Research*, 45(8):1–15, 2009. ISSN 00431397. doi: 10.1029/2008WR007437.

Carolina Boix-Fayos, Luc G.J. Boerboom, Ron Janssen, María Martínez-Mena, María Almagro, Pedro Pérez-Cutillas, Joris P.C. Eekhout, Victor Castillo, and Joris de Vente. Mountain ecosystem services affected by land use changes and hydrological control works in Mediterranean catchments. *Ecosystem Services*, 44(June):101136, 2020. ISSN 22120416. doi: 10.1016/j.ecoser.2020.101136. URL https://doi.org/10.1016/j.ecoser.2020.101136.

S. Brands, S. Herrera, J. Fernández, and J. M. Gutiérrez. How well do CMIP5 Earth System Models simulate present climate conditions in Europe and Africa?: A performance comparison for the downscaling community. *Climate Dynamics*, 41(3-4):803–817, 2013. ISSN 09307575. doi: 10.1007/s00382-013-1742-8.

Leo Breiman. Random forests. *Machine learning*, 45:5–32, 2001.

Tássia Brighenti, Nadia Bonuma, Fernando Grison, Aline Mota, Masato Kobiyama, and Pedro Chaffe. Two calibration methods for modeling streamflow and suspended sediment with the swat model. *Ecological Engineering*, 127:103–113, 02 2019. doi: 10.1016/j.ecoleng.2018.11.007.

Filippo Calì Quaglia, Silvia Terzago, and Jost von Hardenberg. Temperature and precipitation seasonal forecasts over the Mediterranean region: added value compared to simple forecasting methods. *Climate Dynamics*, 58(7-8):2167–2191, 2022. ISSN 14320894. doi: 10.1007/s00382-021-05895-6.

Rita M. Cardoso and Pedro M.M. Soares. Is there added value in the EURO-CORDEX hindcast temperature simulations? Assessing the added value using climate distributions in Europe. *International Journal of Climatology*, 42(7):4024–4039, 2022. ISSN 10970088. doi: 10.1002/joc.7472.

J A M Careto, P M M Soares, R M Cardoso, S Herrera, and J M Gutiérrez. Added value of EURO-CORDEX high-resolution downscaling over the Iberian Peninsula revisited – Part 2: Max and min temperature. *Geoscientific Model Development*, 15(6):2653–2671, 2022a. doi: 10.5194/gmd-15-2653-2022. URL https://gmd.copernicus.org/articles/15/2653/2022/.

J A M Careto, P M M Soares, R M Cardoso, S Herrera, and J M Gutiérrez. Added value of EURO-CORDEX high-resolution downscaling over the Iberian Peninsula revisited – Part 2: Max and min temperature. *Geoscientific Model Development*, 15(6):2653–2671, 2022b. doi: 10.5194/gmd-15-2653-2022. URL https://gmd.copernicus.org/articles/15/2653/2022/.

João António Martins Careto, Pedro Miguel Matos Soares, Rita Margarida Cardoso, Sixto Herrera, and José Manuel Gutiérrez. Added value of EURO-CORDEX high-resolution downscaling over the Iberian Peninsula revisited - Part 1: Precipitation. *Geoscientific Model Development*, 15 (6):2635–2652, 2022c. ISSN 19919603. doi: 10.5194/gmd-15-2635-2022.

João António Martins Careto, Pedro Miguel Matos Soares, Rita Margarida Cardoso, Sixto Herrera, and José Manuel Gutiérrez. Added value of EURO-CORDEX high-resolution downscaling over the Iberian Peninsula revisited - Part 1: Precipitation. *Geoscientific Model Development*, 15 (6):2635–2652, 2022d. ISSN 19919603. doi: 10.5194/gmd-15-2635-2022.

Zeyi Chao, Fangling Pu, Yuke Yin, Bin Han, and Xiaoling Chen. Research on real-time local rainfall prediction based on MEMS sensors. *Journal of Sensors*, 2018:1–9, 2018. ISSN 16877268. doi: 10.1155/2018/6184713.

A. Chavez-Jimenez, B. Lama, L. Garrote, F. Martin-Carrasco, A. Sordo-Ward, and L. Mediero. Characterisation of the Sensitivity of Water Resources Systems to Climate Change. *Water Resources Management*, 27(12): 4237–4258, 2013. ISSN 09204741. doi: 10.1007/s11269-013-0404-2.

Weilin Chen, Zhihong Jiang, and Laurent Li. Probabilistic projections of climate change over China under the SRES A1B scenario using 28 AOGCMs. *Journal of Climate*, 24(17):4741–4756, 2011. ISSN 08948755. doi: 10.1175/2011JCLI4102.1.

Nikolaos Christidis and Peter A. Stott. Human Influence on Seasonal Precipitation in Europe. *Journal of Climate*, 35(15):5215–5231, 2022. ISSN 15200442. doi: 10.1175/JCLI-D-21-0637.1.

James M. Ciarlo, Erika Coppola, Adriano Fantini, Filippo Giorgi, Xue Jie Gao, Yao Tong, Russell H. Glazer, Jose Abraham Torres Alavez, Taleena Sines, Emanuela Pichelli, Francesca Raffaele, Sushant Das, Melissa Bukovsky, Moetasim Ashfaq, Eun Soon Im, Thanh Nguyen-Xuan, Claas Teichmann, Armelle Remedio, Thomas Remke, Katharina Bülow, Torsten Weber, Lars Buntemeyer, Kevin Sieck, Diana Rechid, and Daniela Jacob. A new spatially distributed added value index for regional climate models: the EURO-CORDEX and the CORDEX-CORE highest resolution ensembles. *Climate Dynamics*, 57(5-6):1403–1424, 2021. ISSN 14320894. doi: 10.1007/s00382-020-05400-5.

Adam J Clark. Generation of ensemble mean precipitation forecasts from convection-allowing ensembles. *Weather and Forecasting*, 32(4):1569–1583, 2017.

Andrew F. Colombo, David Etkin, and Bryan W. Karney. Climate variability and the frequency of extreme temperature events for nine sites across Canada: Implications for power usage. *Journal of Climate*, 12(8 PART 2): 2490–2502, 1999. ISSN 08948755. doi: 10.1175/1520-0442(1999)012<2490: cvatfo>2.0.co;2.

Erika Coppola, Francesca Raffaele, Filippo Giorgi, Graziano Giuliani, Gao Xuejie, James M. Ciarlo, Taleena Rae Sines, José Abraham Torres-Alavez, Sushant Das, Fabio di Sante, Emanuela Pichelli, Russell Glazer, Sebastian Karl Müller, Sabina Abba Omar, Moetasim Ashfaq, Melissa Bukovsky, E. S. Im, Daniela Jacob, Claas Teichmann, Armelle Remedio, Thomas Remke, Arne Kriegsmann, Katharina Bülow, Torsten Weber, Lars Buntemeyer, Kevin Sieck, and Diana Rechid. Climate hazard indices projections based on cordex-core, cmip5 and cmip6 ensemble. *Climate Dynamics*, 57:1–91, 09 2021. doi: 10.1007/s00382-021-05640-z.

Jesse Crawford, Kartik Venkataraman, and Juliann Booth. Developing climate model ensembles: A comparative case study. *Journal of Hydrology*, 568(September 2018):160–173, 2019. ISSN 00221694. doi: 10.1016/j.jhydrol.2018.10.054. URL https://doi.org/10.1016/j.jhydrol.2018.10.054.

José María Cuadrat, Roberto Serrano-Notivoli, Ernesto Tejedor, Miguel Ángel Saz, Marc Prohom, Jordi Cunillera, Alba Llabrés, Laura Trapero, Marc Pons, Juan Ignacio López-Moreno, Ramon Copons, Simon Gascoin, Yolanda Luna, Ernesto Rodríguez, Petra Ramos, Pilar Amblar, and

Jean-Michel Soubeyroux. Climpy: Climate of the pyrenees (1.0) [data set]. *Zenodo*, 2020a. doi: https://doi.org/10.5281/zenodo.3611127.

José María Cuadrat, Roberto Serrano-Notivoli, Ernesto Tejedor, Miguel Ángel Saz, Marc Prohom, Jordi Cunillera, Alba Llabrés, Laura Trapero, Marc Pons, Juan Ignacio López-Moreno, Ramon Copons, Simon Gascoin, Yolanda Luna, Ernesto Rodríguez, Petra Ramos, Pilar Amblar, and Jean-Michel Soubeyroux. Climpy: Climate of the pyrenees. *Zenodo*, 2020b.

A. Dai. Global precipitation and thundertstorm frequencies. Part I: Seasonal and interannual variations. *Journal of Climate*, 14(6):1092–1111, 2001. ISSN 08948755. doi: 10.1175/1520-0442(2001)014<1092:GPATFP> 2.0.CO;2.

Aiendrila Dey, Debi Prasad Sahoo, Rohini Kumar, and Renji Remesan. A multimodel ensemble machine learning approach for CMIP6 climate model projections in an Indian River basin. *International Journal of Climatology*, -(June):1–22, 2022. ISSN 10970088. doi: 10.1002/joc.7813.

Alejandro Di and Luca Ramo. Potential for added value in temperature simulated by high-resolution nested RCMs in present climate and in the climate change signal. *Climate Dynamics*, pages 443–464, 2013. doi: 10.1007/s00382-012-1384-2.

Alejandro Di Luca, Daniel Argüeso, Jason P. Evans, Ramón De Elía, and René Laprise. Quantifying the overall added value of dynamical downscaling and the contribution from different spatial scales. *Journal of Geophysical Research*, 121(4):1575–1590, 2016. ISSN 21562202. doi: 10.1002/2015JD024009.

Tom Dietterich. Overfitting and undercomputing in machine learning. *ACM computing surveys (CSUR)*, 27(3):326–327, 1995.

Laura Dobor and Tomáš Hlásny. Choice of reference climate conditions matters in impact studies: Case of bias-corrected CORDEX data set. *International Journal of Climatology*, 39(4):2022–2040, 2019. ISSN 10970088. doi: 10.1002/joc.5930.

A Escriva-Bou, M. Pulido-Velazquez, and D. Pulido-Velazquez. Economic value of climate change adaptation strategies for water management in spain's jucar basin. *J. Water Res. Plan. ASCE 2017,*, 2:143, 2017.

T. Estrela. Modelos matemáticos para la evaluación de recursos hídricos. *Centro de Estudios Hidrográficos y Experimentación de Obras Públicas. CEDEX.*, 2:55, 1992.

G Evin, S Somot, and B Hingray. Balanced estimate and uncertainty assessment of European climate change using the large EURO-CORDEX regional climate model ensemble. *Earth System Dynamics*, 12(4):1543–1569, 2021. doi: 10.5194/esd-12-1543-2021. URL https://esd.copernicus.org/articles/12/1543/2021/.

Adriano Fantini, Francesca Raffaele, Csaba Torma, Sara Bacer, Erika Coppola, Filippo Giorgi, Bodo Ahrens, Clotilde Dubois, Enrique Sanchez, and Marco Verdecchia. Assessment of multiple daily precipitation statistics in ERA-Interim driven Med-CORDEX and EURO-CORDEX experiments against high resolution observations. *Climate Dynamics*, 51(3):877–900, 2018. ISSN 14320894. doi: 10.1007/s00382-016-3453-4.

FAO. *State of the world's forests 2014: Enhancing the socioeconomic benefits from forests.* 2014. ISBN 978-92-5-108269-0 978-92-5-108270-6.

Simone Fatichi, Enrique R. Vivoni, Fred L. Ogden, Valeriy Y. Ivanov, Benjamin Mirus, David Gochis, Charles W. Downer, Matteo Camporese, Jason H. Davison, Brian Ebel, Norm Jones, Jongho Kim, Giuseppe Mascaro, Richard Niswonger, Pedro Restrepo, Riccardo Rigon, Chaopeng Shen, Mauro Sulis, and David Tarboton. An overview of current applications, challenges, and future trends in distributed process-based models in hydrology. *Journal of Hydrology*, 537:45–60, 2016. ISSN 00221694. doi: 10.1016/j.jhydrol.2016.03.026.

José A. Fernández, Carolina Martínez, and Fernando Magdaleno. Application of indicators of hydrologic alterations in the designation of heavily modified water bodies in Spain. *Environmental Science and Policy*, 16(i): 31–43, 2012. ISSN 14629011. doi: 10.1016/j.envsci.2011.10.004.

Frauke Feser. Enhanced detectability of added value in limited-area model results separated into different spatial scales. *Monthly Weather Review*, 134(8):2180–2190, 2006. ISSN 00270644. doi: 10.1175/MWR3183.1.

Francesc Gallart and Pilar Llorens. Observations on land cover changes and water resources in the headwaters of the Ebro catchment, Iberian Peninsula. *Physics and Chemistry of the Earth*, 29(11-12 SPEC. ISS.):769–773, 2004. ISSN 14747065. doi: 10.1016/j.pce.2004.05.004.

L García-Barrón, J M Camarillo, J Morales, and A Sousa. Temporal analysis (1940–2010) of rainfall aggressiveness in the Iberian Peninsula basins. *Journal of Hydrology*, 525:747–759, 2015. ISSN 0022-1694. doi: https://doi.org/10.1016/j.jhydrol.2015.04.036. URL https://www.sciencedirect.com/science/article/pii/S0022169415002954.

J. M. García-Ruiz, T. Lasanta, L. Ortigosa, P. Ruiz-Flaño, C. Martí-Bono, and C González. Sediment Yield under Different Land Uses in the Spanish Pyrenees . *International Mountain Society*, 15(3):229–240, 1995.

J.M. García Ruiz, S. Beguería, J.I. López-Moreno, A. Lorente Grima, and M. Seeger. Los recursos hídricos superficiales del pirineo aragonés y su evolución reciente. *Geoforma Ediciones*, 192, 2001.

F Giorgi, C Jones, and GR Asrar. Addressing climate information needs at the regional level: the CORDEX framework. *... Organization (WMO) Bulletin*, 58(July):175–183, 2009. URL http://www.euro-cordex.net/uploads/media/Download_01.pdf.

Milan Gocic and Slavisa Trajkovic. Analysis of changes in meteorological variables using Mann-Kendall and Sen's slope estimator statistical tests in Serbia. *Global and Planetary Change*, 100:172–182, 2013. ISSN 09218181. doi: 10.1016/j.gloplacha.2012.10.014. URL http://dx.doi.org/10.1016/j.gloplacha.2012.10.014.

Ivor Growns and Ivars Reinfelds. Environmental flow management using transparency and translucency rules. *Marine and Freshwater Research*, 65 (8):667–673, 2014. ISSN 13231650. doi: 10.1071/MF13192.

Youen Grusson, Xiaoling Sun, Simon Gascoin, Sabine Sauvage, Srinivasan Raghavan, François Anctil, and José Miguel Sáchez-Pérez. Assessing the capability of the SWAT model to simulate snow, snow melt and streamflow dynamics over an alpine watershed. *Journal of Hydrology*, 531:574–588, 2015. ISSN 00221694. doi: 10.1016/j.jhydrol.2015.10.070. URL http://dx.doi.org/10.1016/j.jhydrol.2015.10.070.

Shuchen Guo, Lei Tian, Shuoyu Chen, Jiguang Liang, Jie Tian, Bo Cao, Xuejin Wang, and Chansheng He. Analysis of effects of vegetation cover and elevation on water yield in an alpine basin of the Qilian Mountains in Northwest China by integrating the WRF-Hydro and Budyko framework. *Journal of Hydrology*, 629(July 2023):130580, 2024. ISSN 00221694. doi: 10.1016/j.jhydrol.2023.130580. URL https://doi.org/10.1016/j.jhydrol.2023.130580.

Aditya Gusain, Subimal Ghosh, and Subhankar Karmakar. Added value of cmip6 over cmip5 models in simulating indian summer monsoon rainfall. *Atmospheric Research*, 232:104680, 09 2019. doi: 10.1016/j.atmosres.2019.104680.

J. William Gutowski, Filippo Giorgi, Bertrand Timbal, Anne Frigon, Daniela Jacob, Hyun Suk Kang, Krishnan Raghavan, Boram Lee, Christopher Lennard, Grigory Nikulin, Eleanor O'Rourke, Michel Rixen, Silvina Solman, Tannecia Stephenson, and Fredolin Tangang. WCRP COordinated Regional Downscaling EXperiment (CORDEX): A diagnostic MIP for CMIP6. *Geoscientific Model Development*, 9(11):4087–4095, 2016. ISSN 19919603. doi: 10.5194/gmd-9-4087-2016.

A H Haria and D J Price. Evaporation from Scots pine (Pinus sylvestris) following natural re-colonisation of the Cairngorm mountains, Scotland. *Hydrology and Earth System Sciences*, 4(3):451–461, 2000. doi: 10.5194/hess-4-451-2000. URL https://hess.copernicus.org/articles/4/451/2000/.

Nadja Herger, Gab Abramowitz, Reto Knutti, Oliver Angélil, Karsten Lehmann, and Benjamin M. Sanderson. Selecting a climate model subset to optimise key ensemble properties. *Earth System Dynamics*, 9(1): 135–151, 2018. ISSN 21904987. doi: 10.5194/esd-9-135-2018.

S. Herrera, P. M.M. Soares, R. M. Cardoso, and J. M. Gutiérrez. Evaluation of the EURO-CORDEX Regional Climate Models Over the Iberian Peninsula: Observational Uncertainty Analysis. *Journal of Geophysical Research: Atmospheres*, 125(12):1–16, 2020. ISSN 21698996. doi: 10.1029/2020JD032880.

IGN. Plan nacional de ortofotografía aérea., 2017. http://pnoa.ign.es/, (accessed on 3 January 2023). (In Spanish) (In Spanish).

W. W. Immerzeel, A. F. Lutz, M. Andrade, A. Bahl, H. Biemans, T. Bolch, S. Hyde, S. Brumby, B. J. Davies, A. C. Elmore, A. Emmer, M. Feng, A. Fernández, U. Haritashya, J. S. Kargel, M. Koppes, P. D.A. Kraaijenbrink, A. V. Kulkarni, P. A. Mayewski, S. Nepal, P. Pacheco, T. H. Painter, F. Pellicciotti, H. Rajaram, S. Rupper, A. Sinisalo, A. B. Shrestha, D. Viviroli, Y. Wada, C. Xiao, T. Yao, and J. E.M. Baillie. Importance and vulnerability of the world's water towers. *Nature*, 577(7790):364–369, 2020. ISSN 14764687. doi: 10.1038/s41586-019-1822-y. URL http://dx.doi.org/10.1038/s41586-019-1822-y.

IPCC. *Climate Change 2022: Impacts, Adaptation and Vulnerability. Contribution of Working Group II to the Sixth Assessment Report of the Intergovernmental Panel on Climate Change*. Cambridge University Press, Cambridge, UK and New York, NY, USA, 2022. doi: 10.1017/9781009325844.

Francesco A. Isotta, Christoph Frei, Viktor Weilguni, Melita Perčec Tadić, Pierre Lassègues, Bruno Rudolf, Valentina Pavan, Carlo Cacciamani, Gabriele Antolini, Sara M. Ratto, Michela Munari, Stefano Micheletti, Veronica Bonati, Cristian Lussana, Christian Ronchi, Elvio Panettieri, Gianni Marigo, and Gregor Vertačnik. The climate of daily precipitation in the Alps: Development and analysis of a high-resolution grid dataset from pan-Alpine rain-gauge data. *International Journal of Climatology*, 34 (5):1657–1675, 2014. ISSN 10970088. doi: 10.1002/joc.3794.

Daniela Jacob, Juliane Petersen, Bastian Eggert, Antoinette Alias, Ole Bøssing Christensen, Laurens M. Bouwer, Alain Braun, Augustin Colette, Michel Déqué, Goran Georgievski, Elena Georgopoulou, Andreas Gobiet, Laurent Menut, Grigory Nikulin, Andreas Haensler, Nils Hempelmann, Colin Jones, Klaus Keuler, Sari Kovats, Nico Kröner, Sven Kotlarski, Arne Kriegsmann, Eric Martin, Erik van Meijgaard, Christopher Moseley, Susanne Pfeifer, Swantje Preuschmann, Christine Radermacher, Kai Radtke, Diana Rechid, Mark Rounsevell, Patrick Samuelsson, Samuel Somot, Jean Francois Soussana, Claas Teichmann, Riccardo Valentini, Robert Vautard, Björn Weber, and Pascal Yiou. EURO-CORDEX: New high-resolution climate change projections for European impact research. *Regional Environmental Change*, 14(2):563–578, 2014. ISSN 1436378X. doi: 10.1007/s10113-013-0499-2.

Daniela Jacob, Claas Teichmann, Stefan Sobolowski, Eleni Katragkou, Ivonne Anders, Michal Belda, Rasmus Benestad, Fredrik Boberg, Erasmo Buonomo, Rita M. Cardoso, Ana Casanueva, Ole B. Christensen, Jens Hesselbjerg Christensen, Erika Coppola, Lesley De Cruz, Edouard L. Davin, Andreas Dobler, Marta Domínguez, Rowan Fealy, Jesus Fernandez, Miguel Angel Gaertner, Markel García-Díez, Filippo Giorgi, Andreas Gobiet, Klaus Goergen, Juan José Gómez-Navarro, Juan Jesús González Alemán, Claudia Gutiérrez, José M. Gutiérrez, Ivan Güttler, Andreas Haensler, Tomáš Halenka, Sonia Jerez, Pedro Jiménez-Guerrero, Richard G. Jones, Klaus Keuler, Erik Kjellström, Sebastian Knist, Sven Kotlarski, Douglas Maraun, Erik van Meijgaard, Paola Mercogliano, Juan Pedro Montávez, Antonio Navarra, Grigory Nikulin, Nathalie de Noblet-Ducoudré, Hans Juergen Panitz, Susanne Pfeifer, Marie Piazza, Emanuela Pichelli, Joni Pekka Pietikäinen, Andreas F. Prein, Swantje Preuschmann, Diana Rechid, Burkhardt Rockel, Raquel Romera, Enrique Sánchez, Kevin Sieck, Pedro M.M. Soares, Samuel Somot, Lidija Srnec, Silje Lund Sørland, Piet Termonia, Heimo Truhetz, Robert Vautard, Kirsten Warrach-Sagi, and Volker Wulfmeyer. Regional climate downscaling over Europe: perspectives from the EURO-CORDEX community. *Regional Environmental Change*, 20(2), 2020. ISSN 1436378X. doi: 10.1007/s10113-020-01606-9.

Inmaculada C. Jiménez-Navarro, Patricia Jimeno-Sáez, Adrián López-Ballesteros, Julio Pérez-Sánchez, and Javier Senent-Aparicio. Impact of climate change on the hydrology of the forested watershed that drains to lake erken in sweden: An analysis using swat+ and cmip6 scenarios. *Forests*, 12(12), 2021. ISSN 19994907. doi: 10.3390/f12121803.

Patricia Jimeno-Sáez, Javier Senent-Aparicio, Julio Pérez-Sánchez, and David Pulido-Velazquez. A comparison of SWAT and ANN models for daily runoff simulation in different climatic zones of peninsular Spain. *Water (Switzerland)*, 10(2), 2018. ISSN 20734441. doi: 10.3390/w10020192.

Patricia Jimeno-Sáez, David Pulido-Velazquez, Antonio-Juan Collados-Lara, Eulogio Pardo-Igúzquiza, Javier Senent-Aparicio, and Leticia Baena-Ruiz. A preliminary assessment of the "undercatching" and the precipitation pattern in an alpine basin. *Water*, 12(4), 2020. ISSN 2073-4441. doi: 10.3390/w12041061. URL https://www.mdpi.com/2073-4441/12/4/1061.

Jorge Jódar, José Antonio Cabrera, Sergio Martos-Rosillo, Ana Ruiz-Constán, Antonio González-Ramón, Luis Javier Lambán, Christian Herrera, and Emilio Custodio. Groundwater discharge in high-mountain watersheds: A valuable resource for downstream semi-arid zones. The case of the Bérchules River in Sierra Nevada (Southern Spain). *Science of The Total Environment*, 593-594:760–772, 2017. ISSN 0048-9697. doi: https://doi.org/10.1016/j.scitotenv.2017.03.190. URL https://www.sciencedirect.com/science/article/pii/S0048969717307131.

C. D. Jones, J. K. Hughes, N. Bellouin, S. C. Hardiman, G. S. Jones, J. Knight, S. Liddicoat, F. M. O'Connor, R. J. Andres, C. Bell, K. O. Boo, A. Bozzo, N. Butchart, P. Cadule, K. D. Corbin, M. Doutriaux-Boucher, P. Friedlingstein, J. Gornall, L. Gray, P. R. Halloran, G. Hurtt, W. J. Ingram, J. F. Lamarque, R. M. Law, M. Meinshausen, S. Osprey, E. J. Palin, L. Parsons Chini, T. Raddatz, M. G. Sanderson, A. A. Sellar, A. Schurer, P. Valdes, N. Wood, S. Woodward, M. Yoshioka, and M. Zerroukat. The HadGEM2-ES implementation of CMIP5 centennial simulations. *Geoscientific Model Development*, 4(3):543–570, 2011. ISSN 19919603. doi: 10.5194/gmd-4-543-2011.

Dinu Maria Jose, Amala Mary Vincent, and Gowdagere Siddaramaiah Dwarakish. Improving multiple model ensemble predictions of daily precipitation and temperature through machine learning techniques. *Scientific Reports*, 12(1):1–25, 2022. ISSN 20452322. doi: 10.1038/s41598-022-08786-w. URL https://doi.org/10.1038/s41598-022-08786-w.

C. Juez, N. Garijo, E. Nadal-Romero, and S. M. Vicente-Serrano. Wavelet analysis of hydro-climatic time-series and vegetation trends of the Upper Aragón catchment (Central Spanish Pyrenees). *Journal of Hydrology*, 614 (PB):128584, 2022. ISSN 00221694. doi: 10.1016/j.jhydrol.2022.128584. URL https://doi.org/10.1016/j.jhydrol.2022.128584.

Latif Kalin, Sabahattin Isik, Jon E. Schoonover, and B. Graeme Lockaby. Predicting Water Quality in Unmonitored Watersheds Using Artificial Neural Networks. *Journal of Environmental Quality*, 39(4):1429–1440, 2010. ISSN 00472425. doi: 10.2134/jeq2009.0441.

Matti Kämäräinen, Otto Hyvärinen, Andrea Vajda, Grigory Nikulin, Erik van Meijgaard, Claas Teichmann, Daniela Jacob, Hilppa Gregow, and Kirsti Jylhä. Estimates of Present-Day and Future Climatologies of Freezing Rain in Europe Based on CORDEX Regional Climate Models. *Journal of Geophysical Research: Atmospheres*, 123(23):13,291–13,304, 2018. ISSN 21698996. doi: 10.1029/2018JD029131.

Bonnie L. Keeler, Perrine Hamel, Timon McPhearson, Maike H. Hamann, Marie L. Donahue, Kelly A. Meza Prado, Katie K. Arkema, Gregory N. Bratman, Kate A. Brauman, Jacques C. Finlay, Anne D. Guerry, Sarah E. Hobbie, Justin A. Johnson, Graham K. MacDonald, Robert I. McDonald, Nick Neverisky, and Spencer A. Wood. Social-ecological and technological factors moderate the value of urban nature. *Nature Sustainability*, 2 (1):29–38, 2019. ISSN 23989629. doi: 10.1038/s41893-018-0202-1. URL http://dx.doi.org/10.1038/s41893-018-0202-1.

L. Keller, Andreas Paul Zischg, Markus Mosimann, Ole Rössler, Rolf Weingartner, and Olivia Martius. Large ensemble flood loss modelling and uncertainty assessment for future climate conditions for a Swiss prealpine catchment. *Science of the Total Environment*, 693:133400, nov 2019. ISSN 18791026. doi: 10.1016/j.scitotenv.2019.07.206.

Reto Knutti, M. R. Allen, P. Friedlingstein, J. M. Gregory, G. C. Hegerl, G. A. Meehl, M. Meinshausen, J. M. Murphy, G. K. Plattner, S. C.B. Raper, T. F. Stocker, P. A. Stott, H. Teng, and T. M.L. Wigley. A review of uncertainties in global temperature projections over the twenty-first century. *Journal of Climate*, 21(11):2651–2663, 2008. ISSN 08948755. doi: 10.1175/2007JCLI2119.1.

S. Kotlarski, K. Keuler, O. B. Christensen, A. Colette, M. Déqué, A. Gobiet, K. Goergen, D. Jacob, D. Lüthi, E. Van Meijgaard, G. Nikulin, C. Schär, C. Teichmann, R. Vautard, K. Warrach-Sagi, and V. Wulfmeyer. Regional climate modeling on European scales: A joint standard evaluation of the

EURO-CORDEX RCM ensemble. *Geoscientific Model Development*, 7(4): 1297–1333, 2014. ISSN 19919603. doi: 10.5194/gmd-7-1297-2014.

Sven Kotlarski, Daniel Lüthi, and Christoph Schär. The elevation dependency of 21st century European climate change: An RCM ensemble perspective. *International Journal of Climatology*, 35(13):3902–3920, 2015. ISSN 10970088. doi: 10.1002/joc.4254.

T. N. Krishnamurti, C. M. Kishtawal, Timothy E. LaRow, David R. Bachiochi, Zhan Zhang, C. Eric Williford, Sulochana Gadgil, and Sajani Surendran. Improved weather and seasonal climate forecasts from multimodel superensemble. *Science*, 285(5433):1548–1550, 1999. ISSN 00368075. doi: 10.1126/science.285.5433.1548.

T. N. Krishnamurti, C. M. Kishtawal, Z. Zhang, T. LaRow, D. Bachiochi, E. Williford, S. Gadgil, and S. Surendran. Multimodel ensemble forecasts for weather and seasonal climate. *Journal of Climate*, 13(23):4196–4216, 2000. ISSN 08948755. doi: 10.1175/1520-0442(2000)013<4196:MEFFWA> 2.0.CO;2.

Valentina Krysanova and Mike White. Aperçu des progrès de l'évaluation des ressources en eau avec SWAT. *Hydrological Sciences Journal*, 60(5): 771–783, 2015. ISSN 21503435. doi: 10.1080/02626667.2015.1029482. URL http://dx.doi.org/10.1080/02626667.2015.1029482.

S. J. Lambert and G. J. Boer. CMIP1 evaluation and intercomparison of coupled climate models. *Climate Dynamics*, 17(2-3):83–106, 2001. ISSN 0930-7575. doi: 10.1007/pl00013736.

Stefano Larsen, Ute Karaus, Cecile Claret, Ferdinand Sporka, Ladislav Hamerlík, and Klement Tockner. Flooding and hydrologic connectivity modulate community assembly in a dynamic river-floodplain ecosystem. *PLoS ONE*, 14(4):1–22, 2019. ISSN 19326203. doi: 10.1371/journal.pone.0213227.

T. Lasanta, J. Arnáez, N. Pascual, P. Ruiz-Flaño, M. P. Errea, and N. Lana-Renault. Space–time process and drivers of land abandonment in Europe. *Catena*, 149:810–823, 2017. ISSN 03418162. doi: 10.1016/j.catena.2016.02.024. URL http://dx.doi.org/10.1016/j.catena.2016.02.024.

T. Lasanta, E. Nadal-Romero, and J. M. García-Ruiz. Clearing shrubland as a strategy to encourage extensive livestock farming in the Mediterranean Mountains. *Geographical Research Letters*, 45(2):487–513, 2019. ISSN 16979540. doi: 10.18172/cig.3616.

Teodoro Lasanta, Estela Nadal-Romero, and José Arnáez. Managing abandoned farmland to control the impact of re-vegetation on the environment. The state of the art in Europe. *Environmental Science and Policy*, 52: 99–109, 2015. ISSN 18736416. doi: 10.1016/j.envsci.2015.05.012.

Marc Lemus-Canovas and Joan Albert Lopez-Bustins. Assessing internal changes in the future structure of dry-hot compound events: The case of the Pyrenees. *Natural Hazards and Earth System Sciences*, 21(6):1721–1738, 2021. ISSN 16849981. doi: 10.5194/nhess-21-1721-2021.

Marc Lemus-Canovas, Joan A. Lopez-Bustins, Laura Trapero, and Javier Martin-Vide. Combining circulation weather types and daily precipitation modelling to derive climatic precipitation regions in the Pyrenees. *Atmospheric Research*, 220(January):181–193, 2019. ISSN 01698095. doi: 10.1016/j.atmosres.2019.01.018. URL https://doi.org/10.1016/j.atmosres.2019.01.018.

N. LeRoy Poff and J. D. Allan. Functional organization of stream fish assemblages in relation to hydrological variability. *Ecology*, 76(2):606–627, 1995. ISSN 00129658. doi: 10.2307/1941217.

Tong Li, Zhihong Jiang, Hervé Le Treut, Laurent Li, Lilong Zhao, and Lingling Ge. Machine learning to optimize climate projection over China with multi-model ensemble simulations. *Environmental Research Letters*, 16(9), 2021. ISSN 17489326. doi: 10.1088/1748-9326/ac1d0c.

Xin Zhong Liang, Kenneth E. Kunkel, Gerald A. Meehl, Richard G. Jones, and Julian X.L. Wang. Regional climate models downscaling analysis of general circulation models present climate biases propagation into future change projections. *Geophysical Research Letters*, 35(8):1–5, 2008. ISSN 00948276. doi: 10.1029/2007GL032849.

Sitian Liu, Julio Pérez-Sánchez, Patricia Jimeno-Sáez, Francisco Javier Alcalá, and Javier Senent-Aparicio. A novel approach to assessing the impacts of dam construction on hydrologic and ecosystem alterations. Case study: Castril river basin, Spain. *Ecohydrology and Hydrobiology*, 22(4): 598–608, 2022. ISSN 20803397. doi: 10.1016/j.ecohyd.2022.08.004. URL https://doi.org/10.1016/j.ecohyd.2022.08.004.

Adrián López-Ballesteros, Javier Senent-Aparicio, Carolina Martínez, and Julio Pérez-Sánchez. Assessment of future hydrologic alteration due to climate change in the Aracthos River basin (NW Greece). *Science of the Total Environment*, 733:139299, 2020. ISSN 18791026. doi: 10.1016/j.scitotenv.2020.139299. URL https://doi.org/10.1016/j.scitotenv.2020.139299.

J. I. López-Moreno and José M. García-Ruiz. Influence of snow accumulation and snowmelt on streamflow in the central Spanish Pyrenees / Influence de l'accumulation et de la fonte de la neige sur les écoulements dans les Pyrénées centrales espagnoles. *Hydrological Sciences Journal*, 49 (5), 2004. ISSN 0262-6667. doi: 10.1623/hysj.49.5.787.55135.

J. I. López-Moreno, M. Beniston, and J. M. García-Ruiz. Environmental change and water management in the Pyrenees: Facts and future perspectives for Mediterranean mountains. *Global and Planetary Change*, 61 (3-4):300–312, 2008. ISSN 09218181. doi: 10.1016/j.gloplacha.2007.10.004.

J. I. López-Moreno, S. M. Vicente-Serrano, E. Moran-Tejeda, J. Zabalza, J. Lorenzo-Lacruz, and J. M. García-Ruiz. Impact of climate evolution and land use changes on water yield in the ebro basin. *Hydrology and Earth System Sciences*, 15(1):311–322, 2011. ISSN 10275606. doi: 10.5194/hess-15-311-2011.

J. Lorenzo-Lacruz, S. M. Vicente-Serrano, J. I. López-Moreno, E. Morán-Tejeda, and J. Zabalza. Recent trends in Iberian streamflows (1945-2005). *Journal of Hydrology*, 414-415:463–475, 2012. ISSN 00221694. doi: 10.1016/j.jhydrol.2011.11.023. URL http://dx.doi.org/10.1016/j.jhydrol.2011.11.023.

Arthur F. Lutz, Herbert W. ter Maat, Hester Biemans, Arun B. Shrestha, Philippus Wester, and Walter W. Immerzeel. Selecting representative climate models for climate change impact studies: an advanced envelope-based selection approach. *International Journal of Climatology*, 36(12): 3988–4005, 2016. ISSN 10970088. doi: 10.1002/joc.4608.

J. I. López-Moreno, S. M. Vicente-Serrano, J. Zabalza, J. Revuelto, M. Gilaberte, C. Azorín-Molina, E. Morán-Tejeda, J. García-Ruiz, and C M. & Tague. Respuesta hidrológica del pirineo central al cambio ambiental proyectado para el siglo xxi. *Pirineos*, 169:160, 2014. doi: http://dx.doi.org/10.3989/Pirineos.2014.169004.

Àngela Manrique-Alba, Santiago Beguería, Antonio J. Molina, María González-Sanchis, Miquel Tomàs-Burguera, Antonio D. del Campo, Michele Colangelo, and J. Julio Camarero. Long-term thinning effects on tree growth, drought response and water use efficiency at two Aleppo pine plantations in Spain. *Science of the Total Environment*, 728:138536, 2020. ISSN 18791026. doi: 10.1016/j.scitotenv.2020.138536. URL https://doi.org/10.1016/j.scitotenv.2020.138536.

P Marcos-Garcia, A Lopez-Nicolas, and M Pulido-Velazquez. Combined use of relative drought indices to analyze climate change impact on meteorological and hydrological droughts in a Mediterranean basin. *Journal of Hydrology*, 554:292–305, 2017. ISSN 0022-1694. doi: https://doi.org/10.1016/j.jhydrol.2017.09.028. URL https://www.sciencedirect.com/science/article/pii/S0022169417306327.

C Martinez and J.A. Fernández. Iahris 2.2 indicators of hydrologic alteration in rivers: Free software. *Ministerio de Medio Ambiente. Universidad Politécnica de Madrid*, 2010.

José Martínez-Fernández, Nilda Sánchez, and Carlos M. Herrero-Jiménez. Recent trends in rivers with near-natural flow regime: The case of the river headwaters in Spain. *Progress in Physical Geography*, 37(5):685–700, 2013. ISSN 03091333. doi: 10.1177/0309133313496834.

C. F. McSweeney, R. G. Jones, R. W. Lee, and D. P. Rowell. Selecting CMIP5 GCMs for downscaling over multiple regions. *Climate Dynamics*, 44(11-12):3237–3260, 2015. ISSN 14320894. doi: 10.1007/s00382-014-2418-8.

Gerald A. Meehl, Francis Zwiers, Jenni Evans, Thomas Knutson, Linda Mearns, and Peter Whetton. Trends in extreme weather and climate events: Issues related to modeling extremes in projections of future climate change. *Bulletin of the American Meteorological Society*, 81(3):427–436, 2000. ISSN 00030007. doi: 10.1175/1520-0477(2000)081<0427:TIEWAC>2.3.CO;2.

Andrés Mellado-Díaz, Jorge Rubén Sánchez-González, Simone Guareschi, Fernando Magdaleno, and Manuel Toro Velasco. Exploring longitudinal trends and recovery gradients in macroinvertebrate communities and biomonitoring tools along regulated rivers. *Science of the Total Environment*, 695:133774, 2019. ISSN 18791026. doi: 10.1016/j.scitotenv.2019.133774. URL https://doi.org/10.1016/j.scitotenv.2019.133774.

P. A. Minang, M. van Noordwijk, O. E. Freeman, C. Mbow, J. de Leeuw, and Catacutan. Climate-Smart Landscapes: Multifunctionality In Practice. Nairobi, Kenya:World Agroforestry Centre (ICRAF). *World Agroforestry Centre*, page 404, 2015.

Justin R. Minder, Theodore W. Letcher, and S. Mc Kenzie Skiles. An evaluation of high-resolution regional climate model simulations of snow cover and albedo over the rocky mountains, with implications for the simulated snow-albedo feedback. *Journal of Geophysical Research*, 121(15):9069–9088, 2016. ISSN 21562202. doi: 10.1002/2016JD024995.

Eugenio Molina-Navarro, Dennis Trolle, Silvia Martínez-Pérez, Antonio Sastre-Merlín, and Erik Jeppesen. Hydrological and water quality impact assessment of a Mediterranean limno-reservoir under climate change and land use management scenarios. *Journal of Hydrology*, 509: 354–366, 2014. ISSN 00221694. doi: 10.1016/j.jhydrol.2013.11.053. URL http://dx.doi.org/10.1016/j.jhydrol.2013.11.053.

Juan Morales-García, Andrés Bueno-Crespo, Fernando Terroso-Sáenz, Francisco Arcas-Túnez, Raquel Martínez-España, and José M. Cecilia. Evaluation of synthetic data generation for intelligent climate control in greenhouses. *Applied Intelligence*, 53(21):24765–24781, 2023. ISSN 15737497. doi: 10.1007/s10489-023-04783-2.

D. N. Moriasi, M. W. Gitau, N. Pai, and P. Daggupati. Hydrologic and water quality models: Performance measures and evaluation criteria. *Transactions of the ASABE*, 58(6):1763–1785, 2015. ISSN 21510032. doi: 10.13031/trans.58.10715.

Daniel Moriasi, Jeff Arnold, Michael Van Liew, Ron Bingner, R.D. Harmel, and Tamie Veith. Model evaluation guidelines for systematic quantification of accuracy in watershed simulations. *Transactions of the ASABE*, 50, 05 2007. doi: 10.13031/2013.23153.

J.M. Murillo and J.A. Navarro. Aplicación del modelo de témez a la determinación de la aportación superficial y subterránea del sistema hidrológico cornisa-vega de granada para su implementación en un modelo de uso conjunto. *Boletín Geológico y Minero*, 122:363–388, 2011. doi: ISSN:0366-0176.

Estela Nadal-Romero, Dhais Peña-Angulo, and David Regues. Rainfall, run-off, and sediment transport dynamics in a humid mountain badland area: Long-term results from a small catchment. *Hydrological Processes*, 32(11):1588–1606, 2018. ISSN 10991085. doi: 10.1002/hyp.11495.

Estela Nadal-Romero, Carmelo Juez, Makki Khorchani, Dhais Peña-Angulo, N. Lana-Renault, D. Regüés, Teodoro Lasanta, and José M. García-Ruiz. *Impacts of Land Abandonment on Flood Mitigation in Mediterranean Mountain Areas*. 05 2021. ISBN 978-3-030-77504-9. doi: 10.1007/698-2021-772.

Christer Nilsson and Magnus Svedmark. Basic principles and ecological consequences of changing water regimes: Riparian plant communities. *Environmental Management*, 30(4):468–480, 2002. ISSN 0364152X. doi: 10.1007/s00267-002-2735-2.

Seok Geun Oh and Myoung Seok Suh. Comparison of projection skills of deterministic ensemble methods using pseudo-simulation data generated from multivariate Gaussian distribution. *Theoretical and Applied Climatology*, 129(1-2):243–262, 2017. ISSN 14344483. doi: 10.1007/s00704-016-1782-1.

OPCC-CTP. *Climate change in the Pyrenees: Impacts, vulnerabilities and adaptation Bases of knowledge for the future climate change adaptation strategy in the Pyrenees*. OPCC-CTP, 2018. ISBN 9788409062683.

Leticia Palazón and Ana Navas. Modeling sediment sources and yields in a Pyrenean catchment draining to a large reservoir (Ésera River, Ebro Basin). *Journal of Soils and Sediments*, 14(9):1612–1625, 2014. ISSN 16147480. doi: 10.1007/s11368-014-0911-7.

Milan Paluš, Dagmar Novotná, and Petr Tichavský. Shifts of seasons at the European mid-latitudes: Natural fluctuations correlated with the North Atlantic Oscillation. *Geophysical Research Letters*, 32(12):1–4, 2005. ISSN 00948276. doi: 10.1029/2005GL022838.

Christina Papadaki, Konstantinos Soulis, Rafael Muñoz-Mas, Francisco Martinez-Capel, Stamatis Zogaris, Lazaros Ntoanidis, and Elias Dimitriou. Potential impacts of climate change on flow regime and fish habitat in mountain rivers of the south-western Balkans. *Science of the Total Environment*, 540:418–428, 2016. ISSN 18791026. doi: 10.1016/j.scitotenv.2015.06.134. URL http://dx.doi.org/10.1016/j.scitotenv.2015.06.134.

Fernando Pardo, Angel Velasco, and Luis Gil. Tercer Inventario Forestal Nacional 1997-2007: La Tranformación Histórica del Paisaje Forestal en Navarra. *Ministerio de Medio Ambiente, Gobierno de España*, 2:7–19, 2008. doi: --.

V. Pavan and F. J. Doblas-Reyes. Multi-model seasonal hindcasts over the Euro-Atlantic: Skill scores and dynamic features. *Climate Dynamics*, 16(8):611–625, 2000. ISSN 14320894. doi: 10.1007/s003820000063.

Julio Pérez-Sánchez, Javier Senent-Aparicio, Francisco Segura-Méndez, David Pulido-Velazquez, and Raghavan Srinivasan. Evaluating hydrological models for deriving water resources in peninsular Spain. *Sustainability (Switzerland)*, 11(10):1–36, 2019. ISSN 20711050. doi: 10.3390/su11102872.

Julio Pérez-Sánchez, Javier Senent-Aparicio, Carolina Martínez Santa-María, and Adrián López-Ballesteros. Assessment of ecological and hydro-geomorphological alterations under climate change using SWAT and IAHRIS in the Eo River in Northern Spain. *Water (Switzerland)*, 12 (6), 2020. ISSN 20734441. doi: 10.3390/W12061745.

S. E. Perkins, A. J. Pitman, N. J. Holbrook, and J. McAneney. Evaluation of the AR4 climate models' simulated daily maximum temperature, minimum temperature, and precipitation over Australia using probability density functions. *Journal of Climate*, 20(17):4356–4376, 2007. ISSN 08948755. doi: 10.1175/JCLI4253.1.

C. Piani, G. P. Weedon, M. Best, S. M. Gomes, P. Viterbo, S. Hagemann, and J. O. Haerter. Statistical bias correction of global simulated daily precipitation and temperature for the application of hydrological models. *Journal of Hydrology*, 395(3-4):199–215, 2010. ISSN 00221694. doi: 10.1016/j.jhydrol.2010.10.024. URL http://dx.doi.org/10.1016/j.jhydrol.2010.10.024.

Rafael Poyatos, Jérôme Latron, and Pilar Llorens. Land use and land cover change after agricultural abandonment: The case of a Mediterranean Mountain area (Catalan Pre-Pyrenees). *Mountain Research and Development*, 23(4):362–368, 2003. ISSN 02764741. doi: 10.1659/0276-4741(2003)023[0362:LUALCC]2.0.CO;2.

A. F. Prein, A. Gobiet, H. Truhetz, K. Keuler, K. Goergen, C. Teichmann, C. Fox Maule, E. van Meijgaard, M. Déqué, G. Nikulin, R. Vautard, A. Colette, E. Kjellström, and D. Jacob. Precipitation in the EURO-CORDEX 0.11° and 0.44° simulations: high resolution, high benefits? *Climate Dynamics*, 46(1-2):383–412, 2016. ISSN 14320894. doi: 10.1007/s00382-015-2589-y.

Liying Qiu, Eun Soon Im, Jina Hur, and Kyo Moon Shim. Added value of very high resolution climate simulations over South Korea using WRF modeling system. *Climate Dynamics*, 54(1-2):173–189, 2020. ISSN 14320894. doi: 10.1007/s00382-019-04992-x. URL https://doi.org/10.1007/s00382-019-04992-x.

R Ranzi, M Bochicchio, and B Bacchi. Effects on floods of recent afforestation and urbanisation in the Mella River (Italian Alps). *Hydrology and Earth System Sciences*, 6(2):239–254, 2002. doi: 10.5194/hess-6-239-2002. URL https://hess.copernicus.org/articles/6/239/2002/.

Roberto Ranzi, Paolo Caronna, and Massimo Tomirotti. *Impact of Climatic and Land Use Changes on River Flows in the Southern Alps*, pages

61–83. Springer Singapore, Singapore, 2017. ISBN 978-981-10-2051-3. doi: 10.1007/978-981-10-2051-3-3. URL https://doi.org/10.1007/978-981-10-2051-3-3.

Kabir Rasouli, John Pomeroy, and Paul Whitfield. Hydrological responses of headwater basins to monthly perturbed climate in the north american cordillera. *Journal of Hydrometeorology*, 20, 03 2019a. doi: 10.1175/JHM-D-18-0166.1.

Kabir Rasouli, John W. Pomeroy, and Paul H. Whitfield. Are the effects of vegetation and soil changes as important as climate change impacts on hydrological processes? *Hydrology and Earth System Sciences*, 23(12): 4933–4954, 2019b. ISSN 16077938. doi: 10.5194/hess-23-4933-2019.

Alfredo Reder, Mario Raffa, Myriam Montesarchio, and Paola Mercogliano. Performance evaluation of regional climate model simulations at different spatial and temporal scales over the complex orography area of the Alpine region. *Natural Hazards*, 102(1):151–177, 2020. ISSN 15730840. doi: 10.1007/s11069-020-03916-x.

Brian D Richter and Holly E Richter. Society for Conservation Biology Prescribing Flood Regimes to Sustain Riparian Ecosystems along Meandering Rivers Published by : Wiley for Society for Conservation Biology Linked references are available on JSTOR for this article : Prescribing Flood Regim. *Wiley for Society for Conservation Biology*, 14(5):1467–1478, 2000.

Luc Roy, Robert Leconte, Franois P. Brissette, and Claude Marche. The impact of climate change on seasonal floods of a Southern Quebec river basin. *Hydrological Processes*, 15(16):3167–3179, 2001. ISSN 08856087. doi: 10.1002/hyp.323.

Alex Ruane and Sonali McDermid. Selection of a representative subset of global climate models that captures the profile of regional changes for integrated climate impacts assessment. *Earth Perspectives*, 4, 12 2017. doi: 10.1186/s40322-017-0036-4.

Markku Rummukainen. Added value in regional climate modeling. *Wiley Interdisciplinary Reviews: Climate Change*, 7(1):145–159, 2016. ISSN 17577799. doi: 10.1002/wcc.378.

Zulfaqar Sa'adi, Shamsuddin Shahid, Eun Sung Chung, and Tarmizi bin Ismail. Projection of spatial and temporal changes of rainfall in Sarawak of Borneo Island using statistical downscaling of CMIP5 models. *Atmospheric Research*, 197(November 2016):446–460, 2017. ISSN 01698095.

doi: 10.1016/j.atmosres.2017.08.002. URL https://doi.org/10.1016/j.atmosres.2017.08.002.

D. A. Sachindra, K. Ahmed, Md Mamunur Rashid, S. Shahid, and B. J.C. Perera. Statistical downscaling of precipitation using machine learning techniques. *Atmospheric Research*, 212(September 2017):240–258, 2018. ISSN 01698095. doi: 10.1016/j.atmosres.2018.05.022. URL https://doi.org/10.1016/j.atmosres.2018.05.022.

Saleem A Salman, Shamsuddin Shahid, Tarmizi Ismail, Kamal Ahmed, and Xiao-Jun Wang. Selection of climate models for projection of spatiotemporal changes in temperature of Iraq with uncertainties. *Atmospheric Research*, 213:509–522, 2018. ISSN 0169-8095. doi: https://doi.org/10.1016/j.atmosres.2018.07.008. URL https://www.sciencedirect.com/science/article/pii/S016980951830557X.

Maria Sand, Ragnhild Bieltvedt Skeie, Marit Sandstad, Srinath Krishnan, Gunnar Myhre, Hannah Bryant, Richard Derwent, Didier Hauglustaine, Fabien Paulot, Michael Prather, et al. A multi-model assessment of the global warming potential of hydrogen. *Communications Earth & Environment*, 4(1):203, 2023.

Benjamin M. Sanderson, Reto Knutti, and Peter Caldwell. Addressing interdependency in a multimodel ensemble by interpolation of model properties. *Journal of Climate*, 28(13):5150–5170, 2015. ISSN 08948755. doi: 10.1175/JCLI-D-14-00361.1.

Alba Sanmiguel-Vallelado, Enrique Morán-Tejeda, Esteban Alonso-González, and Juan Ignacio López-Moreno. Effect of snow on mountain river regimes: an example from the Pyrenees. *Frontiers of Earth Science*, 11(3):515–530, 2017. ISSN 20950209. doi: 10.1007/s11707-016-0630-z.

Mikhail A. Semenov and Pierre Stratonovitch. Use of multi-model ensembles from global climate models for assessment of climate change impacts. *Climate Research*, 41(1):1–14, 2010. ISSN 0936577X, 16161572. URL http://www.jstor.org/stable/24870469.

Pranab Kumar Sen. Estimates of the Regression Coefficient Based on Kendall's Tau. *Journal of the American Statistical Association*, 63(324):1379–1389, 1968. doi: 10.1080/01621459.1968.10480934.

Javier Senent-Aparicio, Sitian Liu, Julio Pérez-Sánchez, Adrián López-Ballesteros, and Patricia Jimeno-Sáez. Assessing impacts of climate variability and reforestation activities on water resources in the headwaters of the Segura River Basin (SE Spain). *Sustainability (Switzerland)*, 10(9), 2018a. ISSN 20711050. doi: 10.3390/su10093277.

Javier Senent-Aparicio, Adrián López-Ballesteros, Julio Pérez-Sánchez, Francisco José Segura-Méndez, and David Pulido-Velazquez. Using multiple monthly water balance models to evaluate gridded precipitation products over peninsular spain. *Remote Sensing*, 10(6), 2018b. ISSN 2072-4292. doi: 10.3390/rs10060922. URL https://www.mdpi.com/2072-4292/10/6/922.

Roberto Serrano-Notivoli, Santiago Beguería, Miguel Ángel Saz, Luis Alberto Longares, and Martín de Luis. Spread: a high-resolution daily gridded precipitation dataset for spain–an extreme events frequency and intensity overview. *Earth System Science Data*, 9(2):721–738, 2017. doi: https://doi.org/10.20350/digitalCSIC/7393.

Gerhard Smiatek, Harald Kunstmann, and Alfonso Senatore. EURO-CORDEX regional climate model analysis for the Greater Alpine Region: Performance and expected future change. *Journal of Geophysical Research*, 121(13):7710–7728, 2016. ISSN 21562202. doi: 10.1002/2015JD024727.

Pedro M.M. Soares and Rita M. Cardoso. A simple method to assess the added value using high-resolution climate distributions: Application to the EURO-CORDEX daily precipitation. *International Journal of Climatology*, 38(3):1484–1498, 2018. ISSN 10970088. doi: 10.1002/joc.5261.

M. Soltani and A. Mofidi. Using Mann-Kendall and time series techniques forstatistical analysisof long-term precipitation in gorgan weather station. *World Applied Sciences Journal*, 28(7):902–908, 2013. ISSN 18184952. doi: 10.5829/idosi.wasj.2013.28.07.946.

Abhishekh Srivastava, Richard Grotjahn, and PaulA Ullrich. Evaluation of historical cmip6 model simulations of extreme precipitation over contiguous us regions. *Weather and Climate Extremes*, 29:100268, 06 2020. doi: 10.1016/j.wace.2020.100268.

K Stahl, H Hisdal, J Hannaford, L M Tallaksen, H A J van Lanen, E Sauquet, S Demuth, M Fendekova, and J Jódar. Streamflow trends in Europe: evidence from a dataset of near-natural catchments. *Hydrology and Earth System Sciences*, 14(12):2367–2382, 2010. doi: 10.5194/hess-14-2367-2010. URL https://hess.copernicus.org/articles/14/2367/2010/.

Iris T. Stewart, Daniel R. Cayan, and Michael D. Dettinger. Changes toward earlier streamflow timing across western North America. *Journal of Climate*, 18(8):1136–1155, 2005. ISSN 08948755. doi: 10.1175/JCLI3321.1.

Markus Stoffel, Bartłomiej Wyżga, and Richard A. Marston. Floods in mountain environments: A synthesis. *Geomorphology*, 272:1–9, 2016. ISSN 0169555X. doi: 10.1016/j.geomorph.2016.07.008.

Benjamin T. Stratton, Venakataramana Sridhar, Molly M. Gribb, James P. McNamara, and Balaji Narasimhan. Modeling the spatially varying water balance processes in a Semiarid Mountainous Watershed of Idaho. *Journal of the American Water Resources Association*, 45(6):1390–1408, 2009. ISSN 1093474X. doi: 10.1111/j.1752-1688.2009.00371.x.

Steve Swanson. Indicators of hydrologic alteration. *Bureau of Land Management Resource Notes*, 0(58):2, 2002.

Mou Leong Tan, Philip W. Gassman, Ju Liang, and James M. Haywood. A review of alternative climate products for SWAT modelling: Sources, assessment and future directions. *Science of the Total Environment*, 795: 148915, 2021. ISSN 18791026. doi: 10.1016/j.scitotenv.2021.148915. URL https://doi.org/10.1016/j.scitotenv.2021.148915.

Erich Tasser, Janette Walde, Ulrike Tappeiner, Alexandra Teutsch, and Werner Noggler. Land-use changes and natural reforestation in the Eastern Central Alps. *Agriculture, Ecosystems and Environment*, 118(1):115–129, 2007. ISSN 0167-8809. doi: https://doi.org/10.1016/j.agee.2006.05.004. URL https://www.sciencedirect.com/science/article/pii/S0167880906001575.

Karl E Taylor. in a Single Diagram. *Jorunal of Geophysical Research*, 106: 7183–7192, 2001.

Karl E. Taylor, Ronald J. Stouffer, and Gerald A. Meehl. An overview of CMIP5 and the experiment design. *Bulletin of the American Meteorological Society*, 93(4):485–498, 2012. ISSN 00030007. doi: 10.1175/BAMS-D-11-00094.1.

J. Teng, N. J. Potter, F. H.S. Chiew, L. Zhang, B. Wang, J. Vaze, and J. P. Evans. How does bias correction of regional climate model precipitation affect modelled runoff? *Hydrology and Earth System Sciences*, 19(2):711–728, 2015. ISSN 16077938. doi: 10.5194/hess-19-711-2015.

Silvia Terzago, Jost von Hardenberg, Elisa Palazzi, and Antonello Provenzale. Snow water equivalent in the alps as seen by gridded data sets, cmip5 and cordex climate models. *The Cryosphere*, 11(4):1625–1645, 2017. doi: https://doi.org/10.5194/tc-11-1625-2017.

C. W. Thornthwaite. An approach toward a rational classification of climate. *Geographical Review*, 38(1):55–94, 1948. ISSN 00167428. URL http://www.jstor.org/stable/210739.

Csaba Torma, Filippo Giorgi, and Erika Coppola. Added value of regional climate modeling over areas characterized by complex terrain—Precipitation over the Alps. *AGU*, 175(4449):238, 2015. ISSN 00280836. doi: 10.1038/175238c0.

J.R. Témez. Modelo Matemático de Trasformación "Precipitación-Escorrentía". *Asociación de Investigación Industrial Eléctrica (ASINEL)*, 2, 1977.

Mirian Lago Valente, José Miguel Reichert, Rosane Barbosa Lopes Cavalcante, Jean Paolo Gomes Minella, Olivier Evrard, and Raghavan Srinivasan. Afforestation of degraded grasslands reduces sediment transport and may contribute to streamflow regulation in small catchments in the short-run. *Catena*, 204(June 2020), 2021. ISSN 03418162. doi: 10.1016/j.catena.2021.105371.

Erik van Meijgaard and Susanne Crewell. Comparison of model predicted liquid water path with ground-based measurements during CLIWA-NET. *Atmospheric Research*, 75(3):201–226, 2005. ISSN 0169-8095. doi: https://doi.org/10.1016/j.atmosres.2004.12.006.

Robert Vautard, Nikolay Kadygrov, Carley Iles, Fredrik Boberg, Erasmo Buonomo, Katharina Bülow, Erika Coppola, Lola Corre, Erik van Meijgaard, Rita Nogherotto, Marit Sandstad, Clemens Schwingshackl, Samuel Somot, Emma Aalbers, Ole B. Christensen, James M. Ciarlo, Marie Estelle Demory, Filippo Giorgi, Daniela Jacob, Richard G. Jones, Klaus Keuler, Erik Kjellström, Geert Lenderink, Guillaume Levavasseur, Grigory Nikulin, Jana Sillmann, Cosimo Solidoro, Silje Lund Sørland, Christian Steger, Claas Teichmann, Kirsten Warrach-Sagi, and Volker Wulfmeyer. Evaluation of the Large EURO-CORDEX Regional Climate Model Ensemble. *Journal of Geophysical Research: Atmospheres*, 126(17): 1–28, 2021. ISSN 21698996. doi: 10.1029/2019JD032344.

Kartik Venkataraman, Spandana Tummuri, Aldo Medina, and Jordan Perry. 21st century drought outlook for major climate divisions of Texas based on CMIP5 multimodel ensemble: Implications for water resource management. *Journal of Hydrology*, 534:300–316, 2016. ISSN 00221694. doi: 10.1016/j.jhydrol.2016.01.001. URL http://dx.doi.org/10.1016/j.jhydrol.2016.01.001.

S. M. Vicente-Serrano, F. Domínguez-Castro, C. Murphy, D. Peña-Angulo, M. Tomas-Burguera, I. Noguera, J. I. López-Moreno, C. Juez, S. Grainger, L. Eklundh, T. Conradt, C. Azorin-Molina, and A. El Kenawy. Increased

Vegetation in Mountainous Headwaters Amplifies Water Stress During Dry Periods. *Geophysical Research Letters*, 48(18):1–10, 2021. ISSN 19448007. doi: 10.1029/2021GL094672.

Sergio M. Vicente-Serrano, Tim R. McVicar, Diego G. Miralles, Yuting Yang, and Miquel Tomas-Burguera. Unraveling the influence of atmospheric evaporative demand on drought and its response to climate change. *Wiley Interdisciplinary Reviews: Climate Change*, 11(2):1–31, 2020. ISSN 17577799. doi: 10.1002/wcc.632.

Daniel Viviroli, Hans H. Dürr, Bruno Messerli, Michel Meybeck, and Rolf Weingartner. Mountains of the world, water towers for humanity: Typology, mapping, and global significance. *Water Resources Research*, 43 (7):1–13, 2007. ISSN 00431397. doi: 10.1029/2006WR005653.

Bin Wang, Lihong Zheng, De Li Liu, Fei Ji, Anthony Clark, and Qiang Yu. Using multi-model ensembles of CMIP5 global climate models to reproduce observed monthly rainfall and temperature with machine learning methods in Australia. *International Journal of Climatology*, 38(13):4891–4902, 2018. ISSN 10970088. doi: 10.1002/joc.5705.

Sanford Weisberg. *Applied linear regression*, volume 528. John Wiley & Sons, 2005.

R. H. White and R. Toumi. The limitations of bias correcting regional climate model inputs. *Geophysical Research Letters*, 40(12):2907–2912, 2013. ISSN 00948276. doi: 10.1002/grl.50612.

Ellen Wohl, Brian P. Bledsoe, Robert B. Jacobson, N. Leroy Poff, Sara L. Rathburn, David M. Walters, and Andrew C. Wilcox. The natural sediment regime in rivers: Broadening the foundation for ecosystem management. *BioScience*, 65(4):358–371, 2015. ISSN 15253244. doi: 10.1093/biosci/biv002.

Ren Xu, Nengcheng Chen, Yumin Chen, and Zeqiang Chen. Downscaling and Projection of Multi-CMIP5 Precipitation Using Machine Learning Methods in the Upper Han River Basin. *Advances in Meteorology*, 2020, 2020. ISSN 16879317. doi: 10.1155/2020/8680436.

Zhenliang Yin, Qi Feng, Linshan Yang, Xiaohu Wen, Jianhua Si, and Songbing Zou. Long term quantification of climate and land cover change impacts on streamflow in an alpine river catchment, northwestern China. *Sustainability (Switzerland)*, 9(7), 2017. ISSN 20711050. doi: 10.3390/su9071278.

Xue Ying. An overview of overfitting and its solutions. In *Journal of physics: Conference series*, volume 1168, page 022022. IOP Publishing, 2019.

A. Zabaleta, M. Meaurio, J.A. Uriarte, T. Morales, and I. Antigüedad. Hydric vulnerability: recent hydrologic trends in the bay of biscay. *2nd International colloquium on Climate Change in mountain areas PYRADAPT*, 2:72–76, 2017. doi: 10.5194/hess-14-2367-2010. URL https://drive.google.com/file/d/1vBJ2pKzIvF-5X7E4Ij2gCxSekqkoiz-K/view.

Giuseppe Zappa, Len C. Shaffrey, and Kevin I. Hodges. The ability of CMIP5 models to simulate North Atlantic extratropical cyclones. *Journal of Climate*, 26(15):5379–5396, 2013. ISSN 08948755. doi: 10.1175/JCLI-D-12-00501.1.

Zhenzhong Zeng, Zaichun Zhu, Xu Lian, Laurent Z.X. Li, Anping Chen, Xiaogang He, and Shilong Piao. Responses of land evapotranspiration to Earth's greening in CMIP5 Earth System Models. *Environmental Research Letters*, 11(10), 2016. ISSN 17489326. doi: 10.1088/1748-9326/11/10/104006.

Ling Zhang, R. Karthikeyan, Zhongke Bai, and R. Srinivasan. Analysis of streamflow responses to climate variability and land use change in the Loess Plateau region of China. *Catena*, 154:1–11, 2017. ISSN 03418162. doi: 10.1016/j.catena.2017.02.012. URL http://dx.doi.org/10.1016/j.catena.2017.02.012.

Huanhuan Zhu, Zhihong Jiang, Laurent Li, Wei Li, Sheng Jiang, Panyu Zhou, Weihao Zhao, and Tong Li. Intercomparison of multi-model ensemble-processing strategies within a consistent framework for climate projection in china. *Science China Earth Sciences*, 66(9):2125–2141, 2023.

Xueping Zhu, Aoran Zhang, Penglin Wu, Wei Qi, Guangtao Fu, Guangtao Yue, and Xiaoqing Liu. Uncertainty impacts of climate change and downscaling methods on future runoff projections in the Biliu River basin. *Water (Switzerland)*, 11(10):1–17, 2019. ISSN 20734441. doi: 10.3390/w11102130.

X. W. Zhuang, Y. P. Li, G. H. Huang, and J. Liu. Assessment of climate change impacts on watershed in cold-arid region: an integrated multi-GCM-based stochastic weather generator and stepwise cluster analysis method. *Climate Dynamics*, 47(1-2):191–209, 2016. ISSN 14320894. doi: 10.1007/s00382-015-2831-7.